STRUCTURAL, ISOTOPIC, AND KINEMATIC ANALYSIS OF ECLOGITE-FACIES SHEAR ZONES AND ASSOCIATED STRUCTURES, LOFOTEN, NORTH NORWAY

Except where reference is made to the work of others, the work described in this thesis is my own or was done in collaboration with my advisory committee. This thesis does not include proprietary or classified information.

_____

Gabriel Philip Kassos

Certificate of Approval:

_____	_____
Willis E. Hames Professor Geology and Geography	Mark G. Steltenpohl, Chair Professor Geology and Geography
_____	_____
Lorraine W. Wolf Professor Geology and Geography	Joe F. Pittman Interim Dean Graduate School

STRUCTURAL, ISOTOPIC, AND KINEMATIC ANALYSIS OF ECLOGITE-FACIES SHEAR ZONES AND ASSOCIATED STRUCTURES, LOFOTEN, NORTH NORWAY

Gabriel Kassos

A Thesis

Submitted to

the Graduate Faculty of

Auburn University

in Partial Fulfillment of the

Requirements for the

Degree of

Master of Science

Auburn, Alabama
August 9, 2008

STRUCTURAL, ISOTOPIC, AND KINEMATIC ANALYSIS OF ECLOGITE-FACIES SHEAR ZONES AND ASSOCIATED STRUCTURES, LOFOTEN, NORTH NORWAY

Gabriel P. Kassos

Permission is granted to Auburn University to make copies of this thesis at its discretion, upon request of individuals or institutions and at their expense. The author reserves all publication rights.

_____
Signature of Author

_____
Date of Graduation

THESIS ABSTRACT

STRUCTURAL, ISOTOPIC, AND KINEMATIC ANALYSIS OF ECLOGITE-FACIES SHEAR ZONES AND ASSOCIATED STRUCTURES, LOFOTEN, NORTH NORWAY

Gabriel P. Kassos

Master of Science, August 9, 2008
(B.S., Auburn University, 2002)

205 Typed Pages

Directed by Mark G. Steltenpohl

Three variably retrograded, fluid-mediated eclogite occurrences on Flakstadøy, in the Lofoten archipelago of north Norway, display two structurally-controlled styles that are rheological inverses: competent lenses and crystal-plastic shear zones. Lenses of eclogite at Myrland and Storvatnet formed from mafic enclaves and were stretched and rotated in a semi-rigid state within amphibolite-facies shear zones generated during uplift. Post-eclogite shearing almost completely obliterated any primary eclogite-facies deformational fabrics, leaving these retro-eclogites disconnected from their lower-crustal paleostress fields. Amphibolite-facies shear zones encapsulating the eclogite lenses do, however, preserve the paleostress record of their early uplift. Shear zones at Nusfjord are

the rheological inverse of the lens types because eclogite was the weak unit, serving as the locus of crystal-plastic deformation. These are true eclogite-facies shear zones where minerals in the gabbronorite host rocks are progressively transformed into eclogite-facies minerals only within the shear zone boundaries, thus, preserving their lower-crustal paleostress fields. The proximity of these three occurrences and their vastly different deformational styles suggests that additional factors beyond lithology control shear zone formation in the lower crust.

Structural, petrological, and isotopic information allow insights into deformation and exhumation of the deep-continental crust now exposed in the northern Caledonides. U/Pb analyses of zircon and xenotime from a syenogranite dike that cuts retro-eclogite are reported. The dike intruded its mafic host at 1800 ± 5 Ma and was eclogitized together with it at 478 ± 41 Ma, which places eclogitization early in the Caledonian Orogeny. The east-west orientation of σ_1 determined from the Nusfjord eclogite shear zones parallels that observed for Caledonian thrust translation upon mainland Norway. Omphacite breakdown textures imply rapid isothermal decompression during initial uplift, followed by slow uplift. Near-vertical σ_2 at all three occurrences implies continued compressive stress during initial uplift. Emplacement of the overlying Leknes Group at 469-461 Ma implies Lofoten basement resided in the lower crust for at least 17 million years. Cooling dates from hornblende from a retro-eclogite at Nusfjord and muscovites from throughout Lofoten imply the residence of retro-eclogites in the middle crust for 101-190 m.y., which resulted in a high degree of retrogression relative to eclogites from the Bergen Arcs and Western Gneiss Region in southern Norway.

ACKNOWLEDGEMENTS

The author would like to thank several people including: Dr. Arild Andresen for invaluable field and logistical assistance; Dr. Emma Rehnstrøm for conducting geochronologic work; the faculty and staff of the Auburn University Department of Geology and Geography, in particular Dr. Mark Steltenpohl, for their patience during completion of this thesis; Kelli Hardesty and Jennifer Glidewell for assistance during final preparation of this thesis; and Mrs. Jennifer Hansom (Kassos) for her unceasing encouragement.

Style manual or journal used:

Geological Society of America Bulletin

Computer software used:

Microsoft Office 2007 Suite including Word, PowerPoint & Excel

Rockware

Stereonet freeware provided by Rick Allmendinger. Available at http://www.geo.cornell.edu/geology/faculty/RWA/programs.html

Adobe Illustrator 10

Magma

TABLE OF CONTENTS

LIST OF FIGURES x

LIST OF TABLES xxvi

INTRODUCTION 1

METHODS 6

GEOLOGIC SETTING 9

MYRLAND ECLOGITE LOCALITY 11

Overview 11

Lithologic Units 15

Retrograde Eclogite 15

Amphibolite 28

Monzodioritic Orthogneiss 31

Felsic Injections 34

Structures 44

Structural Fabrics 44

Mesoscopic Structures 48

Mineral, Chemical, and Volume Changes in the Myrland Shear Zone 61

Geochronology 69

Interpretations and Conclusions 76

NUSFJORD ECLOGITE LOCALITY 78

Overview 78

Lithologic Units 80

Gabbronorite 80

Basalt Injections....83
Eclogite....83
Structures....84
Mesoscopic Structures....84
Rheological Observations....99
Interpretations and Conclusions....115
STORVATNET ECLOGITE LOCALITY....120
Overview....120
Lithologic Units....122
Anorthosite....122
Troctolite....123
Porphyritic Norite....123
Retro-Eclogite....124
Garnet-Bearing Amphibolite....138
Leucocratic Veins and Mobilized Rocks....140
Structures....143
Interpretations and Conclusions....157
DISCUSSION AND CONCLUSIONS....162
REFERENCES....167

LIST OF FIGURES

Figure 1. Early Carboniferous reconstruction of the northern Caledonides illustrating relative positions of Norway and Greenland, the position of Lofoten within the orogen (box), known eclogite localities throughout Norway and Greenland, and place names used in the text. Figure from Steltenpohl et al. (2006) 2

Figure 2. Geologic interpretation along the Ofoten-Lofoten transect. Upper cross-section shows general geologic features. Lower cross-section shows metamorphic conditions within basement rocks. Abbreviations: um-unmetamorphosed; chl-chlorite zone; bt-biotite zone; gt-garnet zone; ky-kyanite zone; gran-granulite facies; SL-sea level; GSZ-Gullesfjorden shear zone; AT-Austerfjord thrust. See Figure 1 for location. Figure from Steltenpohl et al. (2004) 3

Figure 3. Geologic map of Flakstadøy and surrounding area. See Figure 2 for location. UTM coordinates for each retro-eclogite locality are presented in the text. Figure from Steltenpohl et al. (2006) 5

Figure 4. Geologic map of Myrland eclogite locality. UTM coordinates in text marked with red star. A) Location of photo in Figure 14 and boudin in Figure 19. B) Location of samples ML-42 and AA03-03 and photos in Figures 18 and 22. C) Location of fold in Figure 16b 12

Figure 5. Felsic dike located several hundred meters east of the retro-eclogite lenses at Myrland. Although rubble obscures much of the intervening outcrop, this felsic vein is likely of the same generation as that illustrated in Figure 4. Cliff face is ~70 m high..14

Figure 6. Photomicrograph of sample ML-13B. Plane-polarized light. FOV = 5 mm....16

Figure 7. Backscatter electron image of relict garnet neomineralized to amphibole and plagioclase but with original garnet shape preserved (outlined in red). Garnet (gt) is the brightest mineral, followed by amphibole (amph), and plagioclase (plag). Points analyzed by electron microprobe are shown with light blue dots. Microprobe results are shown in Figures 9 and 10 and Table 1 18

Figure 8. Two thin sections from sample ML-13. Note the clusters of small garnets and the plagioclase haloes separating amphibole from other minerals. Short dimension is 2 cm. A) ML-13A is cut perpendicular to foliation and parallel to elongation lineation. B) ML-13B is cut parallel to foliation and elongation lineation.....19

Figure 9. Garnet species concentrations for the garnet presented in Figure 7.....20

Figure 10. Py-Grs-Alm ternary diagram illustrating the chemical evolution from core to rim of the garnet from sample ML-13B presented in Figure 7. Py = pyrope; Grs = grossular; Alm = almandine.....21

Figure 11. $X_{(Mg)}$ vs. Si diagram of the compositions of two analyzed amphibole grains according to the classification scheme of Leake (1978). Myrland sample ML-13B and Storvatnet sample SR-19 are from this report. Sample SK-1 is from the Skagen eclogite locality on Flakstadøy (Figure 3) described by Markl and Bucher (1997) and Steltenpohl et al. (2006).....23

Figure 12. Photomicrograph of biotite and muscovite clusters within retrogressed eclogite. Note the irregular habit of biotite and the tabular habit of muscovite. Sample ML-13B. Plane-polarized light. FOV = 5 mm.....27

Figure 13. Scans of thin sections from amphibolite at the Myrland locality. Schistosity parallels long dimension. Short dimension is 2 cm. A) Biotite-amphibolite sample ML-17. B) Biotite-amphibolite sample ML-27. C) Garnet-amphibolite sample ML-28 30

Figure 14. Monzodioritic orthogneiss (right) darkens significantly as the amphibolite (far left) is approached. Field of view is ~4 m at bottom of photo. Location A on Figure 4 32

Figure 15. Upper half of the Q-A-P-F diagram (LeMaitre, 1989) on which the CIPW norm compositions of Myrland samples ML-35, 36, 37, 38 and 42 are plotted (Table 7). 38

Figure 16. A. Isoclinally folded, sheared, and foliated felsic vein. Note axial planar foliation parallels that of country rock. B. Highly contorted and folded felsic vein. Early generation isoclines, F_1 (red), with axial-planar schistosity, are deformed by a later-phase fold, F_2 (blue), which has resulted in a Ramsay type III "fish hook" interference pattern. (Location C on Figure 4) 40

Figure 17. Steeply dipping (to the left in photo), tops-north, distributed ductile shear zone cutting and displacing a felsic vein located ~4 m south of amphibolite/orthogneiss contact at Myrland. Shear zones are < 2 cm thick. View is to the west. Hammer is ~35 cm long.....41

Figure 18. Thin, fine-grained felsic vein at location B on Figure 4. See geochemistry sample ML-42 in Tables 5, 6, and 7, and in Figure 15. Sample AA03-3 was also sampled for U-Pb geochronology from this location. Hammer is ~35 cm long.....42

Figure 19. Pegmatitic boudin, ~90 cm long, at location A on Figure 4.....43

Figure 20. Thin section scans of retro-eclogite samples from the Myrland locality. All are cut parallel to elongation lineation and perpendicular to foliation. Schistosity, S_2, parallels long dimension of slides. Delicate dark and light banding, S_1, (yellow boxes) is clearly folded and transposed into the predominant schistosity, S_2. Phases visible are amphibole (dark and light green), garnet (red and pink), plagioclase (clear), and biotite (brown). A) Sample ML-5. B) Sample ML-6. C) Sample ML-13A 46

Figure 21. Thin (1-4 cm thick), cross-cutting mylonite shears along the margins of the Myrland eclogite zone, located several meters to the west of the area depicted in Figure 4. First shear zone (red) dips to the south with tops-down displacement. Second shear zone (blue) dips shallowly to the north with tops-north displacement. View is to the west 49

Figure 22. Nose of the northwest retro-eclogite lens at Myrland depicted in Figure 4 (Location B). Amphibolite foliation wraps around the lens. Felsic vein cuts through the center of the lens. View is to the northwest 50

Figure 23. Lower-hemisphere stereographic contour plot of elongation lineations in retro-eclogite at the Myrland locality. Point maxima indicate lineations plunge moderately to the east and shallowly to the southeast. Legend denotes measurement density per 1% area. N = 31.....51

Figure 24. Lower-hemisphere stereographic contour plot of poles to foliations measured in retro-eclogite lenses at the Myrland locality. Point maxima are clustered in the northeast and southwest quadrants. β-axis (black dot) of visual best-fit great circle of poles to planes defined by the point maxima is oriented S28°E, 08°. Legend denotes measurement density per 1% area. N = 70 52

Figure 25. Lower-hemisphere stereographic contour plot of poles to schistosity in amphibolite at the Myrland locality. Point maxima are loosely concentrated in the southwestern quadrant. Legend denotes measurement density per 1% area. N = 150 .54

Figure 26. Lower-hemisphere stereographic contour plot of elongation and mineral lineations in amphibolite measured at the Myrland eclogite locality. Point maxima are concentrated in the southeast quadrant. Legend denotes measurement density per 1 % area. N = 63.....55

Figure 27. Photo mosaic that shows mylonite progression and geochemical sample locations from the Myrland shear zone. Hammer is ~35 cm long. View is vertical with mylonite foliation oriented N~77°W, ~60°NE. Location is ~50 m northwest of the eclogite pods in Figure 4.....58

Figure 28. Lower-hemisphere stereographic projection of poles to Myrland shear zone mylonitic foliation (N = 6) and elongation lineation (N = 1) 59

Figure 29. Isocon diagram comparing geochemical data for strongly sheared and relatively unsheared samples ML-35/36 and ML-38, respectively. Units are weight percent for oxides and mg/kg for trace elements. Concentrations are multiplied as shown, using methods reported by Grant (1986).....64

Figure 30. Isocon diagram comparing geochemical data from ML-31 (retrograded eclogite) and ML-38 (unsheared monzodioritic orthogneiss). Multiple possible isocon lines are possible. Only the isocon with the steepest slope is depicted 67

Figure 31. Upper discordia intercept for zircon grains 73

Figure 32. Upper discordia intercepts for zircon and xenotime grains 75

Figure 33. Geologic map of the Nusfjord eclogite locality. Shear zones are designated I-IV to be consistent with Kullerud et al. (2001). Topographic base map (1:5000) obtained from Statens Kartverk, Norway. UTM coordinates in text marked with red star 79

Figure 34. Photograph of the northern half of shear zone II. Retro-eclogite is at the top, deformed gabbronorite shoulder is in the center, and undeformed host gabbronorite is on the bottom. Red line is shear boundary in gabbronorite. Green line marks the gabbronorite-eclogite contact. Notice the asymptotic shearing in the deformed shoulder, indicating left-slip displacement. Horizontal FOV = ~50 cm 81

Figure 35. Lower-hemisphere stereographic projection of one elongation lineation and poles to eleven shear zone foliation measurements 82

Figure 36. Photograph of paired S-C fabrics in the eclogitized shoulder of shear zone II. View is vertical. S-plane – yellow. C-plane – red 85

Figure 37. Lower-hemisphere stereographic projection of poles to S- and C-planes, slip lines, principal stress axes, and elongation lineation from the Nusfjord locality. Slip lines: SZ I – N56°W, 58°; SZ III – N53°W, 33°, and S56°E, 11°. Principal stress axes: σ_1 = S57°W, 20°; σ_2 = S75°E, 61°; σ_3 =N26°W, 20 86

Figure 38. Photograph of a steeply plunging, intrafolial, 'S' fold of the mylonitic foliation from the southeastern portion of shear zone I. The white layer marking the fold is a feldspar ribbon 88

Figure 39. Photograph of steeply plunging, rootless fold of the mylonitic foliation within shear zone I that does not show a clear sense of shear. Other nearby folds, however, are asymmetric and clearly indicate left-slip vergence.....89

Figure 40. Photomicrograph of a tops-left, σ-type garnet porphyroclast from sample NFA-2 under cross-polarized light and a ¼ wave plate. Note the subtle color saturation difference. Crystal faces are moderately well preserved. Biotite in pressure shadow is a late retrogressive feature. Note also the amphibole tail in the lower right. Horizontal FOV = 2.1 mm 90

Figure 41. Photomicrograph of sample NFA-10. Weak LPO in plagioclase and strain shadow (upper left of garnet) indicate left-lateral shear sense. Horizontal FOV = 5.5 mm. A) Plane-polarized light. Euhedral 1st generation garnets with rim of 2nd generation growth. B) Cross-polarized light with the ¼ wave plate inserted. Plagioclase has a uniform LPO except in vicinity of the relict garnet clast 91

Figure 42. Photomicrograph of omphacite retrograded to diopside in sample NFA-8. Lamellar exsolution along twin planes with 1st order white and yellow birefringence are omphacite; those with 1st order blue and purple birefringence are diopside. Blue-grey bleb in the upper right of this pyroxene is plagioclase. S-plane – green. C-plane – red. C', or extensional shear band – yellow.....92

Figure 43. Photomicrograph of a hypersthene grain rotated sinistrally into the C-plane, consistent with LPO in plagioclase. A) Plane-polarized light. C-plane – yellow. S-plane – green. B) Cross-polarized light. FOV = 2.75 mm.....93

Figure 44. Photomicrograph of broken, displaced garnet in sample NFA-2. Sense of displacement (antithetic, tops-down to right) is consistent with overall left-slip kinematic plan. A rim of 2nd generation garnet surrounds both 1st generation cores. Fracture sets marked by yellow lines. A) Plane-polarized light. B) Cross-polarized light. Horizontal FOV = 5.5 mm.....94

Figure 45. Broken and displaced clinopyroxene grain from sample NFA-8. Grain is cut into three pieces. Sense of displacement (synthetic, tops-down the left) is consistent with overall left-slip kinematic plan. Plane-polarized light.....95

Figure 46. Photomicrograph of a part of a plagioclase ribbon from sample NFA-2. Note the preferred grain shape orientation and the strong LPO indicating left-slip shear. Horizontal FOV = 2.75 mm. A) Plane-polarized light. B) Cross-polarized light through a 1-wavelength plate.....96

Figure 46. Parallel, stranded and mineralized fracture sets at Nusfjord.....98

Figure 48. Photomicrograph mosaic of a garnet 'stringer' (train of black grains along the longitudinal center of mosaic B composed of small, 2nd generation euhedral garnet crystals recrystallized from plastically deformed 1st generation garnet. Stringers are oriented parallel with long direction of mosaic. A) Plane-polarized light. B) Cross-polarized light.....102

Figure 49. Photomicrograph mosaic of a garnet stringer in sample NFA-8. Stringer extends from garnet concentration (in yellow), interpreted to be a first generation garnet recrystallized and partially destroyed during retrogression. Second generation garnets are concentrated along the margins of plagioclase ribbons. Viewed under plane-polarized light 103

Figure 50. Photomicrograph of sample NFA-9 (shear zone interior). A) Plane-polarized light. Note cloudy core and clear rims of anhedral garnets. B) Cross-polarized light. Horizontal FOV = 2.75 mm……105

Figure 51. Photomicrograph of rotated garnet porphyroclasts from sample NFA-2. Viewed under plane-polarized light. Horizontal FOV = 5 mm 106

Figure 52. Photomicrograph of one well-developed and one poorly developed fracture set in a relict 1st generation garnet with no rim from sample NFA-17. The dominant fracture set is inclined moderately to the right; the subordinate set is inclined shallowly to the left. Plane-polarized light. Horizontal FOV = 5.5 mm 107

Figure 53. LPO, grain size reduction, and grain shape preferred orientation along fractures in a plagioclase grain from host rock sample NF-11 located near the eclogitized shear zones. Viewed under cross-polarized light with the ¼ wave plate inserted. Horizontal FOV = 2.75 mm 109

Figure 54. Primary eclogite-facies omphacite σ-clast in sample NFA-10. Lower third of grain is altered to amphibole. Horizontal FOV = 2.75 mm. A) Plane-polarized light. B) Cross-polarized light. Omphacite σ-clast outlined in yellow 110

Figure 55. Breakdown of omphacite in sample NFA-8. Hypersthene is first replaced by omphacite, and followed by diopside. Horizontal FOV = 2.75 mm. A) Plane-polarized light. B) Cross-polarized light.....111

Figure 56. Near-complete replacement of omphacite by diopside and plagioclase in sample NFA-8. Omphacite is low-birefringence, sub-horizontally oriented lamellae in the diopside grain. Horizontal FOV = 2.75 mm. A) Plane-polarized light. B) Cross-polarized light 112

Figure 57. Photomicrograph of symplectic intergrowth (Symp) of plagioclase and amphibole within an embayment in garnet (Gt). From sample NFA-17. Plane-polarized light. Horizontal FOV = 2.75 mm.....114

Figure 58. Zoisite in sample NFA-6A is aligned roughly parallel with the eclogite S-plane (yellow). Horizontal FOV = 2.75 mm. A) Plane-polarized light. B) Cross-polarized light 116

Figure 59. Photomicrograph of zoisite in sample NFA-6A. Subgrain formation indicates formation prior to or during shearing. Cross-polarized light. Horizontal FOV = 2.75 mm 117

Figure 60. Geologic outcrop map of the Storvatnet eclogite locality created on a 1:5000 topographic base map (Statens Kartverk, Norway). A) Location of eclogite-derived leucocratic veins in Figure 74. B) Location of shear zone in Figure 79. C) Location of paired S-C planes from Figure 81. UTM coordinates in text marked by red star.....121

Figure 61. Porphyritic norite ~800 m from eclogitized zone. Light colored grains are plagioclase. Hammer is ~35 cm long.....125

Figure 62. Photomicrograph of garnet crystal faces preserved along contact with amphibole in sample SR-24 from the Storvatnet locality. Horizontal FOV = 2.75 mm. A) Plane-polarized light. B) Cross-polarized light 126

Figure 63. Mantle of fine grained amphibole (core-mantle structure) surrounding relict omphacite from sample SR-22. Note fairly high birefringence. A) Plane-polarized light. B) Cross-polarized light. Horizontal FOV = 5.5 mm.....127

Figure 64. Relict omphacite theta clast surrounded by fine grained tails of dynamically recrystallized amphibole. Note low birefringence. Plagioclase and amphibole flow banding wraps around omphacite clast. Horizontal FOV = 5.5 mm. A) Plane-polarized light. B) Cross-polarized light.....128

Figure 65. Photomicrograph of amphibole + plagioclase + opaques symplectite (Symp) formed from inclusions in garnet in Storvatnet area sample SVM-1. Gt = Garnet; Op = opaque minerals. Horizontal FOV = 2.75 mm. A) Plane-polarized light. B) Cross-polarized light 130

Figure 66. Scans of two thin sections from Storvatnet sample SR-22. Foliation was not clear, therefore, these two thin sections were cut perpendicular to each other and parallel to elongation lineation. Plastic flow structure wraps around undeformed, but retrograded garnet. The flow structure is defined predominantly by the fine grained, dynamically recrystallized plagioclase. Short dimension of slide is 2 cm 131

Figure 67. Photomicrograph of a highly degraded, inclusion filled, first generation garnet from Storvatnet area sample SR-21. Included material consists of amphibole, plagioclase, and opaque minerals. Horizontal FOV = 2.75 mm. A) Plane-polarized light. B) Cross-polarized light.....132

Figure 68. Photomicrograph of a first generation garnet from sample SR-22 with two fracture sets. The dominant fracture set is oriented roughly vertical in this photo. The subordinate set is oriented roughly 50 °Clockwise from vertical. Inclusions are opaques with plagioclase rims. Plane-polarized light. Horizontal FOV = 5.5 mm 133

Figure 69. Garnet halo formed around amphibole grains. The garnet has numerous tiny inclusions and is radially fractured. Amphibole color is pale green-blue to clear. A thin corona of very fine-grained amphibole/plagioclase symplectite (Symp) exists between the garnet and the larger amphiboles. Horizontal FOV = 2.75 mm. A) Plane light. B) Cross-polarized light.....134

Figure 70. Photomicrograph of a garnet halo around fine grained amphibole, plagioclase, and opaque minerals. Note the inclusion density increasing outwards within the garnet rim. Horizontal FOV = 2.75 mm. A) Plane-polarized light. B) Cross-polarized light.... 135

Figure 71. Scans of thin sections of retro-eclogite from the Storvatnet locality illustrating garnet in an amoeboid or 'reef' habit, which requires recrystallization after deformation. The paucity of plagioclase likely restricted dynamic flow in this rock. Short dimension of slide is 2 cm. A) Sample SR-24. B) Sample SVM-1 137

Figure 72. Photomicrograph of a pyroxene pseudomorph that has retained its original grain shape though it is now completely altered to amphibole and plagioclase. Note also the symplectite (Symp) rim around the garnet in the lower left corner. Horizontal FOV =2.75 mm. A) Plane –polarized light. B) Cross-polarized light 139

Figure 73. Diffuse, mobilized, monzodioritic to anorthositic 'sweat out' blebs within eclogite. Hammer is ~35 cm long. Hammer head is ~10 cm wide. A) Volume of mobilized material increases downwards in photograph. B) Mobilized material is roughly volumetrically equal to eclogite in this photograph 141

Figure 74. Photos depicting the contact between retro-eclogite and leucocratic injections. All were taken at location A on Figure 60 (samples SR-25 and SR-30). A) Retro-eclogite on left, injection on right. Contact is vertical and gradational over 1 - 2 cm. B) Retro-eclogite on left, injection on right. Contact is vertical and sharp. C) Injection on left, retro-eclogite on right. Contact is roughly vertical. Several small-scale off-shoot injections into retro-eclogite are present. D) Injection on left, retro-eclogite on right. Contact is vertical and sharp. Note the presence of biotite in the injection.....142

Figure 75. Upper half of a Q-A-P-F diagram (LeMaitre, 1989) on which the CIPW norm composition of Storvatnet samples SR-25 and SR-30 are plotted.....146

Figure 76. Lower-hemisphere stereographic projection of poles to foliation in retro-eclogite, anorthositic country rocks, and anorthositic and monzo-dioritic injections. Data are clustered mostly in the western and northwestern quadrants, and to a lesser extent in the northeastern quadrant. N = 55.....148

Figure 77. Lower-hemisphere contour diagram of foliation data in Figure 76. Point maximum is located at N79°W, 38°, which indicates an average foliation plane at N12°E, 44°SE. Legend denotes measurement density per 1 % area. N = 55 149

Figure 78. Lower-hemisphere stereographic projection of contoured elongation lineations in retro-eclogite at the Storvatnet locality. The maximum is located at S05°E, 45°. Legend denotes measurement density per 1 % area. N = 28 150

Figure 79. Tops-northeast, plastic shear in eclogite observed at Storvatnet (location B on Figure 60). Movement sense if left-lateral with a minor reverse component. View is to the east. Note fabric swept up from the shear to the upper left. White blebs in this fabric are elongated plagioclase clusters. Hammer head is ~10 cm wide.....151

Figure 80. Lower-hemisphere stereographic reconstruction of the slip line at the shear zone observed at location B on Figure 60 using S-planes swept into the C-plane. The slip line is oriented S16°W, 13°, which generally agrees with the measured elongation lineations 152

Figure 81. Lower-hemisphere stereographic reconstruction of slip lines from paired S-C planes measured at location C on Figure 60. Slip lines are oriented S77°E, 12°, N77°E, 14°, and N90°E, 14 154

Figure 82. Lower-hemisphere stereographic reconstruction of principal stress axes based on conjugate shear fracture criteria. Orientations for principal stress axes are: σ_1 = N22°W, 01°; σ_2 = N69°E, 28°; and σ_3 = S68°W, 60°. Elongation lineations in retro-eclogite from Figure 78 and slip lines determined in Figures 80 and 81 are also presented for comparison. Arrows indicate relative movement sense. (a) right-lateral strike-slip movement with minor normal component. (b) left-lateral strike-slip movement with minor reverse component.....155

Figure 83. Strongly mylonitized and folded anorthosite in float blocks found at the southeastern corner of the Storvatnet eclogite locality depicted in Figure 60. Folds are defined by mylonitic foliation. Coins are ~2 cm in diameter. A) Ultramylonite with sheath fold geometries. B) Tight to isoclinal, intrafolial folds 156

Figure 84. Brittle structures at Storvatnet most likely are pressure-release joints. Three sets, representative of dominant brittle sets in this area, are visible here. View is to the east. Hammer is ~35 cm long. Set (1) Moderately inclined to the right of the photo. This is the dominant set in the Storvatnet area, corresponding to the point maximum shown in the northwestern quadrant of Figure 85. Set (2) Moderately inclined to the left of the photo. Set (3) Sub-horizontally oriented. The orientation of sets 2 and 3 is variable across the mapped area resulting in poles to fractures being spread across all areas except the southeast quadrant of Figure 85 158

Figure 85. Lower-hemisphere contour diagram of poles to brittle fractures. A point maximum is located at N52°W 50°, indicating that the dominant brittle fracture set is oriented N38°E, 40°SE. Subordinate fracture sets loosely congregate in the northwest and northeast quadrants. Legend denotes measurement density per 1 % area. N = 63 159

LIST OF TABLES

Table 1. Microprobe data and calculations for garnet from sample ML-13B presented in Figure 7 22

Table 2. Microprobe data for amphiboles in sample ML-13B (Figure 8.....24

Table 3. Microprobe data from plagioclase feldspar in sample ML-13B (Figure 8).....26

Table 4. Table of point count data for sheared and unsheared orthogneiss samples (n = 400 for each sample). Abbreviations after Siivola and Schmid (2007). Fsp denotes feldspar which could not be differentiated between Pc and Kfs using optical microscopy. (Refer to Figure 27 for sample locations) 33

Table 5. Geochemical major oxide weight percent data for samples collected from the Myrland shear zone, retro-eclogite, and felsic dike. Samples ML-35 and 36 were averaged as described in the text. See Figures 4, 18, and 27 for sample locations 35

Table 6. Geochemical trace element data (mg/kg) for samples collected from the Myrland shear zone, retro-eclogite, and felsic dike. Samples ML-35 and 36 were averaged as described in the text. See Figures 4, 18, and 27 for sample locations 36

Table 7. CIPW norm values and data normalized for use on the Q-A-P-F diagram (Figure 15) for samples ML-35, 36, 37, 38, and 42 from the Myrland locality 37

Table 8. Measured densities of geochemical samples (location shown in Figure 27), plus a representative retrograde eclogite sample, ML-31 62

Table 9. Data for comparison of felsic injection with the calculated mass lost during the hypothetical transition from monzodioritic orthogneiss to eclogite 68

Table 10. Data for comparison of felsic injection with calculated mass lost in ultramylonitized relative to unsheared monzodioritic orthogneiss.....70

Table 11. Table containing details for grains analyzed for U/Pb dating 72

Table 12. Major oxide weight percent and trace element geochemical data for samples SR-25 and SR-30, collected from the eclogite partial-melt injections shown in Figure 74 144

Table 13. CIPW norm data for eclogite-derived leucocratic injections at the Storvatnet locality 145

INTRODUCTION

The geological history of rocks underlying the Lofoten islands (Figure 1) has historically been poorly understood due to lack of documented Caledonian fabrics and structures. Suggested tectonic models for the evolution of Lofoten have included the islands as a tectonic window beneath Caledonian allochthons (Talwani and Eldholm, 1977; Tull, 1977) and as a micro-continent beached onto Baltica (Hakkinen, 1977; Griffin and Taylor, 1978; Griffin et al., 1978; Tull, 1978). Most workers now agree that Lofoten and the Western Gneiss Region of southern Norway (Figure 1) represent a continuous section of the Baltic basement (Hodges et al., 1982; Olesen et al., 1997). Lofoten basement rocks are the tectonically lowest exposed unit in the crustal column described by Steltenpohl et al. (2004) (Figure 2). The lack of obvious Caledonian fabrics is interpreted to be the result of anhydrous conditions in the granulite-facies crust (Bartley, 1982a, 1984; Hodges et al., 1982; Olesen et al., 1997). Limited Cl-rich fluid encroachment (Kullerud, 1996; Kullerud et al., 2001) into these dry rocks allowed fabric development and formation of prograde, eclogite-facies metamorphic assemblages (Markl and Bucher, 1997). Fabric development is limited to shear zones that are reported to have nucleated mostly around mafic enclaves (Markl and Bucher, 1997). Similar eclogite-facies shear zones have been reported from southern Norway in the Bergen Arcs (e.g., Austrheim, 1987; Boundy et al., 1992; Austrheim et al., 1996) (Figure 1).

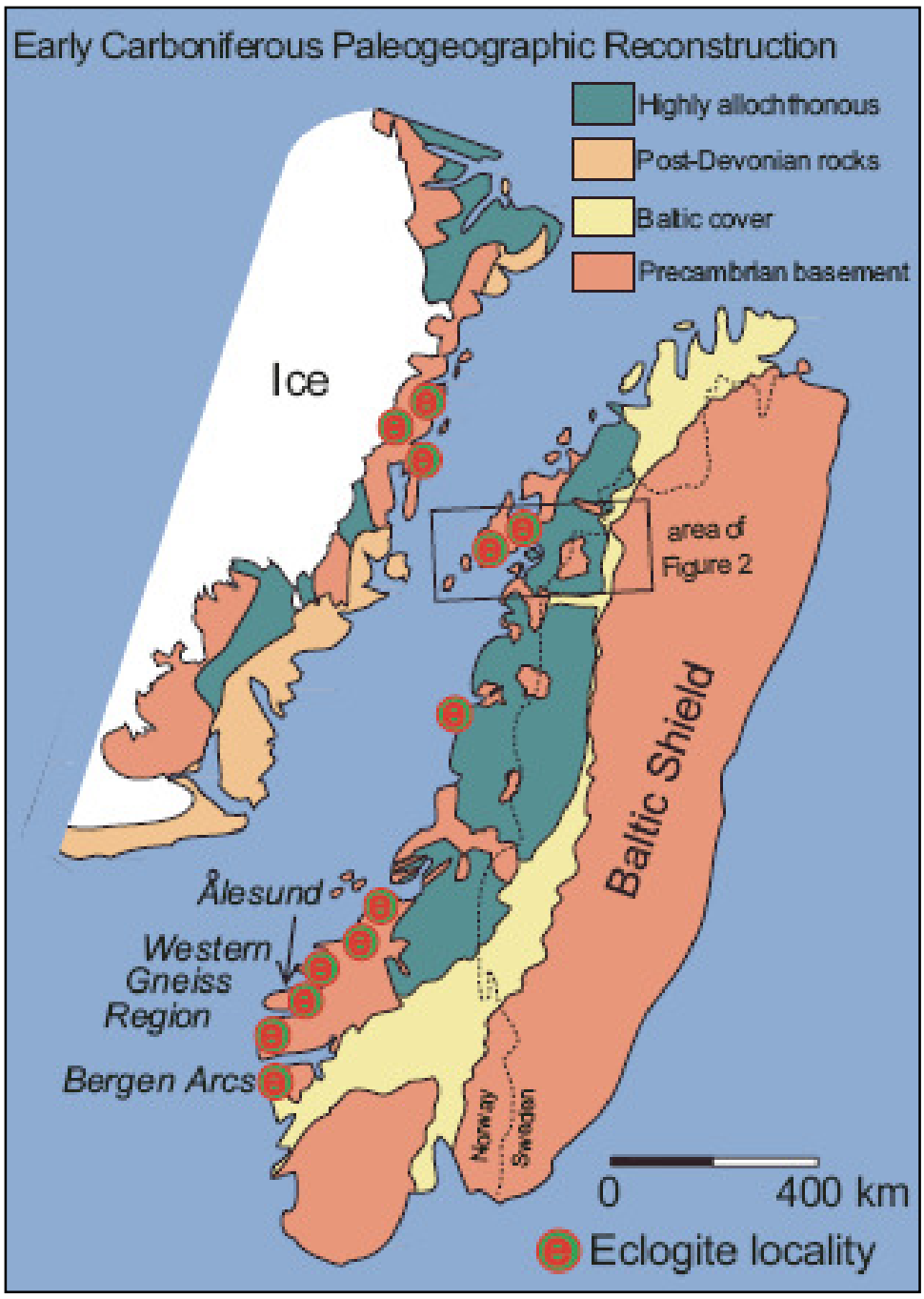

Figure 1: Early Carboniferous reconstruction of the northern Caledonides illustrating relative positions of Norway and Greenland, the position of Lofoten within the orogen (box), known eclogite localities throughout Norway and Greenland, and place names used in the text. Figure from Steltenpohl et al. (2006).

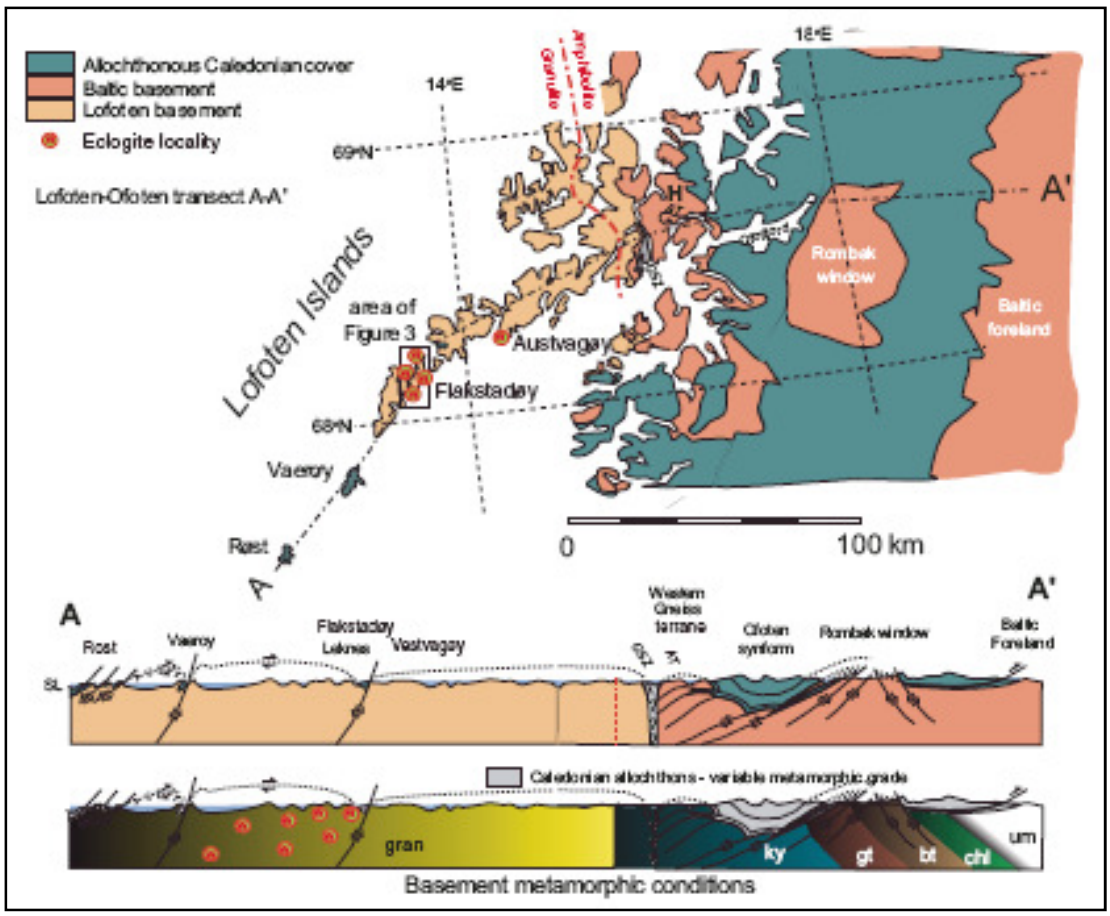

Figure 2: Geologic interpretation along the Ofoten-Lofoten transect. Upper cross-section shows general geologic features. Lower cross-section shows metamorphic conditions within basement rocks. Abbreviations: um-unmetamorphosed; chl-chlorite zone; bt-biotite zone; gt-garnet zone; ky-kyanite zone; gran-granulite facies; SL-sea level; GSZ-Gullesfjorden shear zone; AT-Austerfjord thrust. See Figure 1 for location. Figure from Steltenpohl et al. (2004).

Structural and petrological observations are herein reported from three eclogite-shear zones on Flakstadøy in the Lofoten archipelago: Myrland, Nusfjord, and Storvatnet (Figures 2 and 3). Sheared eclogite at these localities have been investigated in varying detail for petrological reasons, mainly to characterize mineral assemblages and pressure-temperature conditions of eclogitization (Kullerud, 1992, 1996; Kullerud and Erambert, 1999; Kullerud et al., 2001; Markl and Bucher, 1997). No structural investigation has been reported for these important shear zones, however, which is the primary objective of the present study. In addition, due to previous focus in the literature on the conditions of eclogitization, little information is known about the variable, amphibolite-facies retrogressive overprint. The conditions and structural context of this retrogression, however, is crucial to understanding post-Caledonian exhumation of the eclogites.

The timing of eclogitization in rocks of Flakstadøy is also poorly constrained. Markl and Bucher (1997), relying on age relations established in Griffin et al. (1978), suggested that eclogitization occurred during Proterozoic. Steltenpohl et al. (2003) reported a 433 Ma $^{40}Ar/^{39}Ar$ cooling date on hornblende from a retrograde eclogite on Flakstadøy that places a minimum age of eclogitization. Though the latter authors reported that this date combines with field relations to suggest Caledonian eclogitization, the precise time of the event remains undetermined. U/Pb age dates are, therefore, reported for zircon and xenotime separated from a felsic vein within eclogitized mafic rocks on Flakstadøy. This vein cuts, but is also deformed by the eclogite shear foliation and so provides time constraints for emplacement of the igneous host rocks, eclogitization, and vein crystallization.

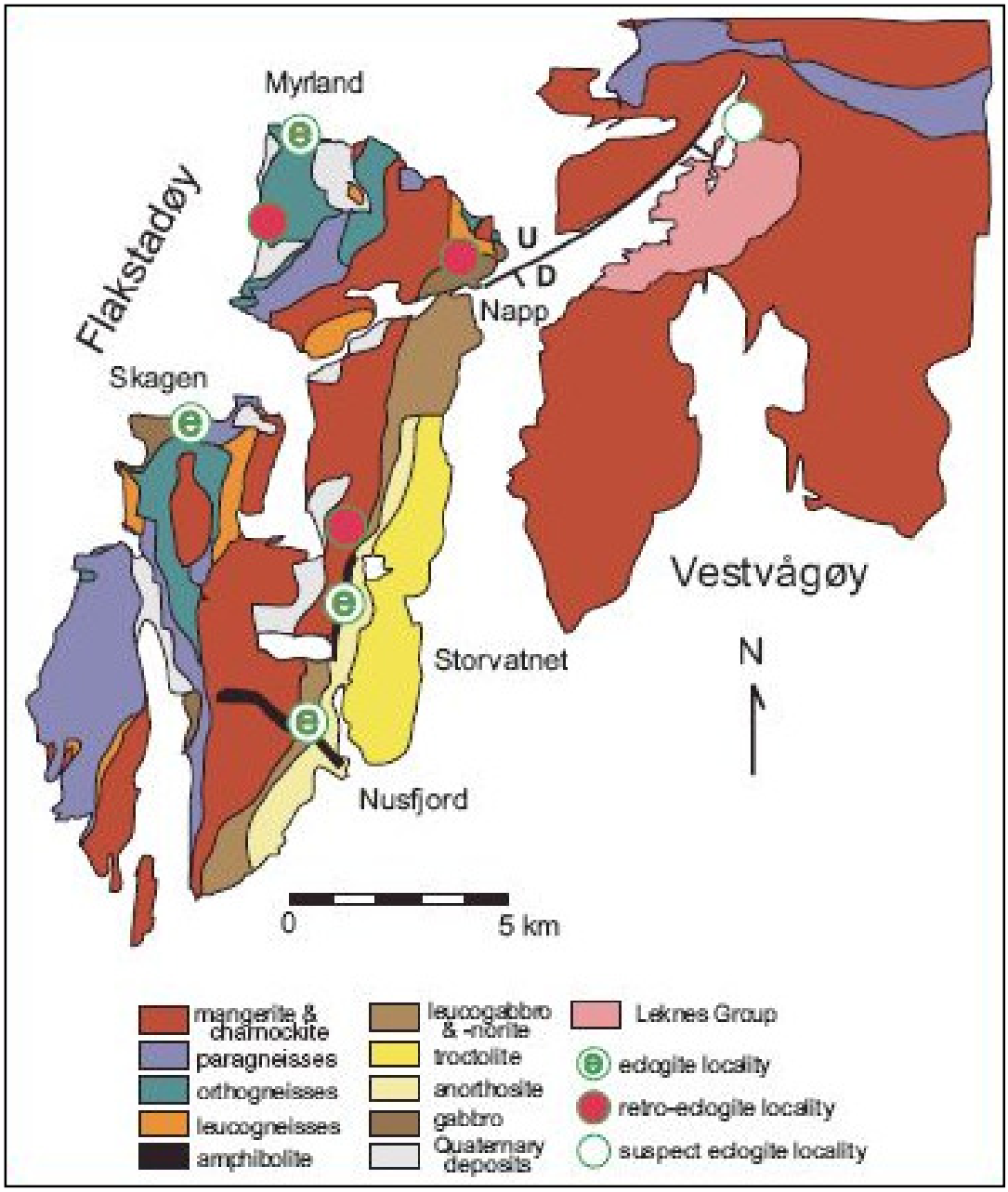

Figure 3: Geologic map of Flakstadøy and surrounding area. See Figure 2 for location. UTM coordinates for each retro-eclogite locality are presented in the text. Figure from Steltenpohl et al. (2006).

METHODS

Field investigation of the Myrland, Nusfjord, and Storvatnet eclogite localities (Figure 3) was conducted during three months in the summer of 2003. Field work consisted of detailed geologic mapping of each site, collection of structural data including metamorphic and shear-related foliation and lineation measurements, and oriented sample collection. Standard field methods were employed. Each locality required different mapping techniques that are described individually below.

The Myrland eclogite occurrence (Figure 3) is too small to effectively map on a topographic base map. A large-scale geologic composite map was created by sketching 2m x 2m grid squares (276 total squares). Sketches were drawn at a 1:10 scale and later scanned and digitally stitched together. The final map was created using Adobe Illustrator®. Density values for geochemical samples were obtained by measuring the mass on a digital scale and volume via displacement of water in a graduated cylinder after soaking the samples in water for 48 hours to remove air bubbles.

Kullerud et al. (2001) had already produced a simple geological map documenting the location of the eclogite shear zones at the Nusfjord locality (Figure 3). As such, the primary function of the map presented below is to add a newly-discovered shear zone to previously published data.

Outcrop at the Storvatnet locality (Figure 3) is limited, being extensively covered with vegetation, rubble, and lichen (as previously noted in Romey, 1971). Mapping of this area was accomplished by detailed outcrop mapping on an enlarged 1:5,000 scale topographic base map. After all exposed rock was mapped and transferred to the base map Adobe Illustrator® was used to create a digital map of inferred eclogite locations.

Petrographic analysis was conducted using a Nikon® petrographic microscope at Auburn University. Microstructural analysis was conducted using a combination of the above-mentioned microscope and also high-resolution scanning and digital enlargement of thin section images.

Geochemical data for individual minerals were obtained using electron microprobe facilities at the University of Georgia and the University of Alabama, both of which use identical JEOL JXA 8600 SEM Superprobes. Bulk geochemical samples were commercially analyzed for major oxides and trace elements using ICP. The 'isocon' method utilized in the Myrland chapter follows the procedure outlined in Grant (1986).

Stereographic projections were created using a number of programs including Rockware® and software provided by Rick Allmendinger of Cornell University, as well as digitization of manually drawn stereoplots using Microsoft PowerPoint®.

CIPW norms were calculated using Magma® software, available as freeware. CIPW norm data were plotted on ternary diagrams using Rockware®.

Mineral separation and U-Pb isotopic studies were done by Dr. Emma Rehnstrøm at the Department of Geosciences, University of Oslo. Zircon and xenotime were analyzed using isotope dilution thermal ionization mass spectrometry (ID-TIMS)

following Krogh (1973). The sample was crushed, ground and separated on a water-shaking table, with a magnetic separator and heavy liquids. Mineral fractions were handpicked and most fractions air-abraded (Krogh, 1982). The grains were washed in dilute nitric acid and rinsed with water and acetone. The fractions were spiked with a mixed $^{205}Pb/^{235}U$ spike and then dissolved in Teflon bombs. Zircon fractions weighing over 3 µg and the xenotime fraction were subjected to chemical separation following the procedures outlined by Corfu and Noble (1992) and Corfu and Stone (1998). U and Pb isotopic ratios were measured on a Finnigan MAT 262 mass spectrometer in static mode using Faraday cups, and for small samples, in dynamic mode with an ion-counting secondary electron multiplier (SEM). Pb and U ratios were corrected for 0.1%/AMU fractionation with an additional bias correction for the SEM measurements. The correction for initial lead composition was made using compositions modeled by Stacey and Kramers (1975), and the resulting isotopic ratios were analyzed with the ISOPLOT program of Ludwig (1999).

GEOLOGIC SETTING

The Lofoten archipelago is part of a continuous crustal column exposed roughly parallel to latitude 67.5° N across northern Scandinavia (Steltenpohl et al., 2004) (Figure 2). This column ranges from unmetamorphosed rocks in the Swedish foreland to chlorite-grade on the eastern side of the Rombak window, through the Barrovian series to the amphibolite/granulite isograd on Hinnøy, and finally to isolated eclogite facies localities exposed on Austvagøy and Flakstadøy. The geologic evolution of Lofoten began before 2.7 Ga, when Archean plutonic rocks intruded a supracrustal sequence preserved as rafts and xenoliths. These were migmatized at 2.3 Ga. Supracrustals were deposited at 2.1 Ga and mangeritic and charnockitic plutons were emplaced at 1.8 to 1.7 Ga under granulite-facies conditions (Giffin et al., 1978). Amphibolite-facies metasedimentary rocks of the Leknes Group were thrust over the Lofoten basement (Klein, 1997). Thrust-emplacement and associated amphibolite-facies metamorphism (600 °C, 6 kbar; Klein et al., 1999) of the Leknes Group has been constrained to between 469 ± 3 Ma and 461 ± 1 Ma (Corfu, 2004a).

Flakstadøy (Figures 2 and 3) is underlain primarily by basement rocks of the anorthosite-mangerite-charnockite-granite (AMCG) suite of Griffin et al. (1978). The eastern third of the island is a series of north-northeast striking and eastward-dipping mafic igneous units, the “Flakstadøy Basic Complex” of Romey (1971). From top down,

this complex comprises anorthosite, troctolite, and gabbronorite (Romey, 1971; Markl and Bucher, 1997). Both gradational and sharp contacts have been observed between these units. Pegmatites within gabbro units in the basic complex yield upper intercept ages, interpreted to be the ages of crystallization, of 1793 ± 4 Ma and 1789 ± 2 Ma (Corfu, 2004b). To the west of the basic complex is a large, steeply-dipping to vertical mangerite pluton (Romey, 1971). The mangerite ranges from <1 km wide at the southern tip of the island to >4 km wide in the center of the island and is the single most abundant unit. Mangerite was emplaced at 1800 ± 2 Ma (Corfu, 2004b). The western third of Flakstadøy is predominately ortho- and paragneisses that are folded and dip sub-vertically (Romey, 1971). Eclogites are observed in all three major divisions (Wade, 1985; Kullerud, 1992; Markl and Bucher, 1997).

MYRLAND ECLOGITE LOCALITY

Overview

The northern tip of the island Flakstadøy is underlain by granulite-facies intrusive mangeritic orthogneiss (Markl and Bucher, 1997). A small package of garnet-bearing amphibolite occurs in the mangerite and is exposed on the northern shoreline of the island west of the village at Myrland (Figures 3 and 4; UTM: 33W, 431123 E, 7562550 N). The garnet amphibolite has been interpreted as retrograded eclogite (Markl and Bucher, 1997). Two distinctly different amphibolites exist; a fine-grained, weakly foliated, green-gray, garnet amphibolite that is enclosed by a medium- to coarse-grained, strongly foliated, salt and pepper, biotite-garnet amphibolite. Eclogitic assemblages in rocks at this exposure are variably retrograded to amphibolite-facies assemblages, but the eclogitic nature (including green color, weathering pattern, rock hardness, and garnet content) of the interior amphibolite is preserved. More importantly, these retrograded eclogites contain a symplectite composed of low-Na clinopyroxene, amphibole, and albite, which Markl and Bucher (1997) state is proof that the rocks passed through eclogite-facies conditions. For clarity in this report, the interior amphibolite will be referred to as retrograde eclogite or retro-eclogite.

A wide, crystal-plastic shear zone has cut across the package of mafic rocks as well as the adjacent host rocks. The shear zone, herein called the Myrland shear zone, clearly separates the granulite-facies orthogneiss from the package of at least four

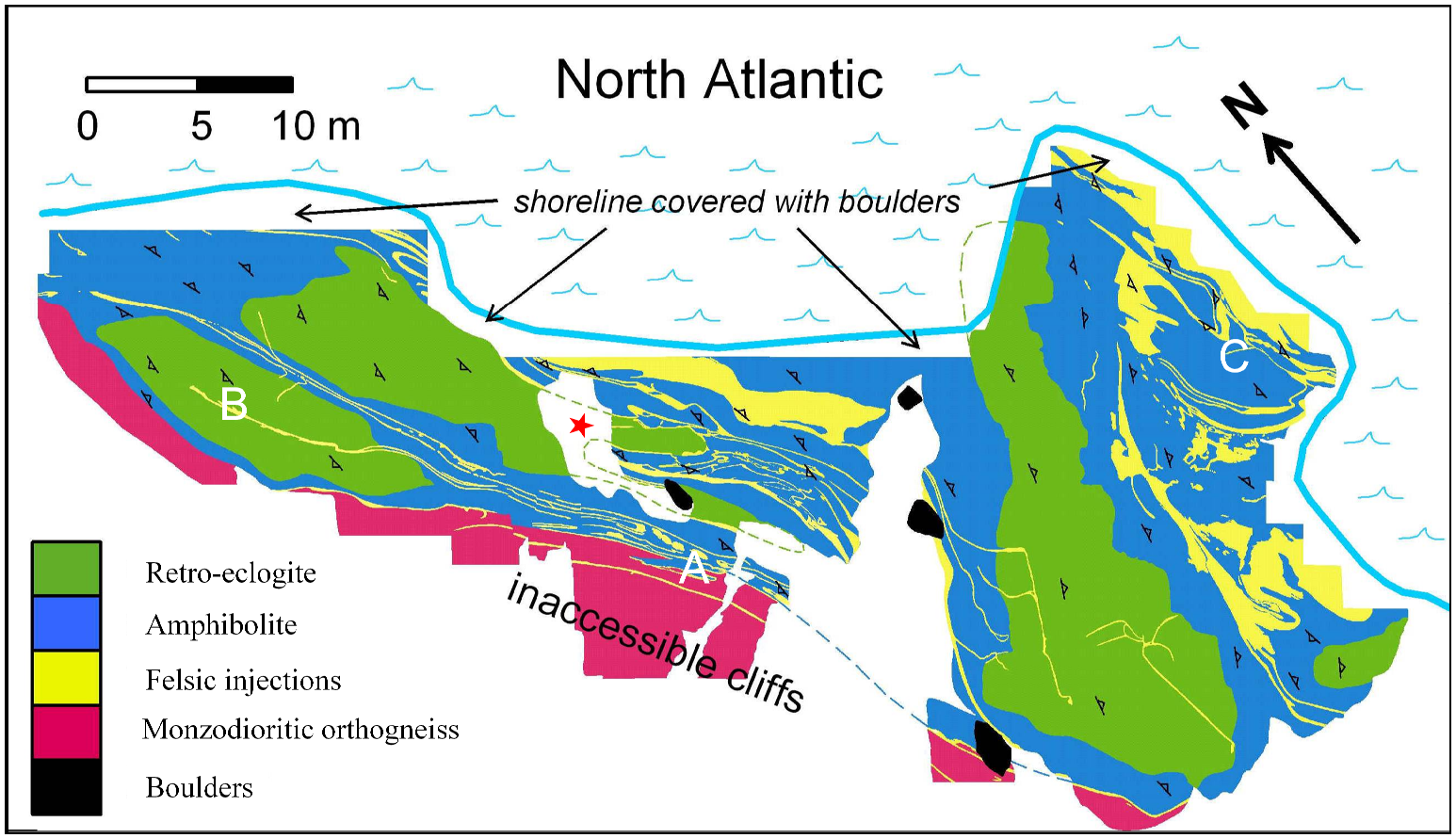

Figure 4: Geologic map of Myrland eclogite locality. UTM coordinates in text marked with red star. A) Location of photo in Figure 14 and boudin in Figure 19. B) Location of samples ML-42 and AA03-03 and photos in Figures 18 and 22. C) Location of fold in Figure 16b.

retrograded eclogite-facies mafic lenses. The exposed retrograde eclogite is continuously exposed although several meters of outcrop directly along the shoreline are variably obscured by boulders and a crust of organic oceanic deposits.

The shoreline on the northeast side of the outcrop is completely covered with boulders and steep cliffs bound the southwest edge. Retrograde eclogite lenses are ~15-20 meters in apparent length and 3-6 meters in apparent width. Approximately 5 meters of topographical relief prevents identification of the geometry of the bodies in the vertical dimension.

Cores of the retro-eclogite lenses show minimal signs of deformation, but they acquire a progressively stronger foliation toward their boundaries with the encapsulating amphibolite. The thickness of this transition from retro-eclogite to garnet-amphibolite varies from tens of centimeters to meters. Corresponding with this progression is an increase in biotite and a decrease in garnet.

The contact between orthogneiss and amphibolite is sharp and distinct. Felsic material commonly separates the orthogneiss from the amphibolite. The local orthogneiss body is foliated; the foliation intensity progressively increases as the margin with the lenses is approached across a distance of ~5-10 m. A felsic dike extends well beyond the zone containing the eclogites (Figure 5).

Figure 5: Felsic dike located several hundred meters east of the retro-eclogite lenses at Myrland. Although rubble obscures much of the intervening outcrop, this felsic vein is likely of the same generation as that illustrated in Figure 4. Cliff face is ~70 m high.

Lithologic Units

Retrograded Eclogite

Although the mineralogy clearly documents this unit as an amphibolite, past workers have interpreted it as a retrograded eclogite (Markl and Bucher, 1997). This interpretation is based on distinctive symplectites of low-Na clinopyroxene and Na-rich plagioclase as retrogressive reaction products formed during the breakdown of omphacite. In order to avoid confusion and to better describe the retrogressive history, this unit is here referred to as either retrograde eclogite or retro-eclogite.

Retro-eclogite has a greenish-gray color and is more distinctly green in the lens interior. Garnets are abundant and small (1-2 mm maximum diameter). White-colored bands are visible to the naked eye but individual crystals, or a characteristic crystal habit, are not discernable. No other minerals can be easily identified by the unaided eye. Thin-section analysis reveals that retrograde eclogite mineralogy includes predominately green amphibole, almandine garnet and plagioclase feldspar (the previously mentioned white bands) (Figure 6). Minor minerals include biotite, sphene, epidote/clinozoisite, quartz, and opaques. These grains are predominantly anhedral and form an interlobate, inequigranular to seriate texture (scheme from Passchier and Trouw, 1998, p. 46, after Moore, 1970).

Relict omphacite was not identified at the Myrland locality during this study. It has been variably replaced by symplectites consisting of low-Na clinopyroxene and

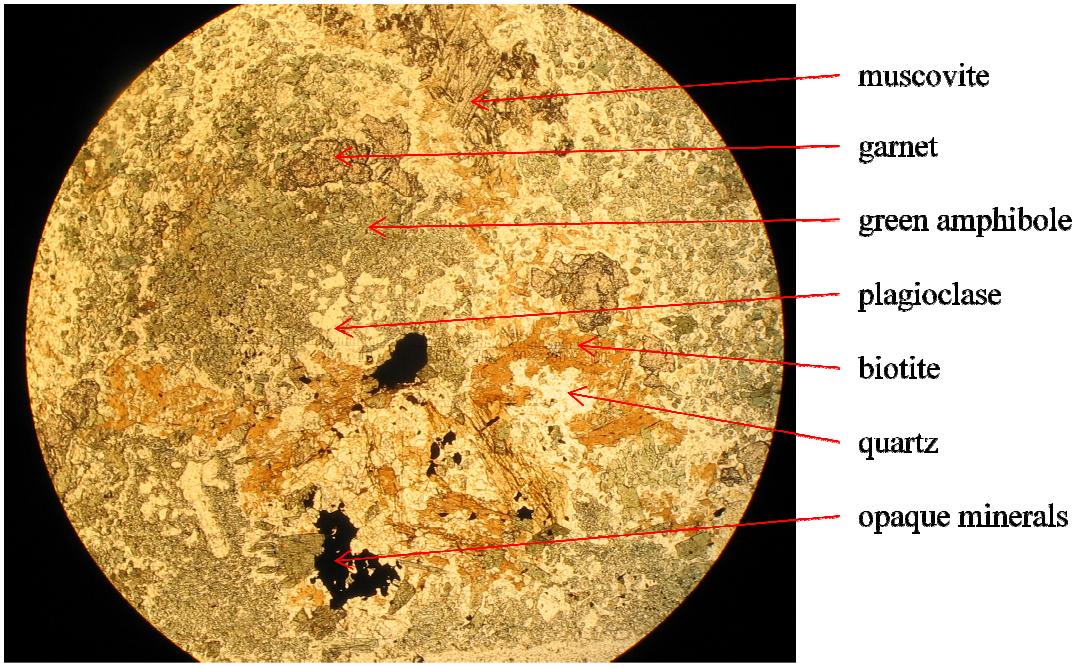

Figure 6: Photomicrograph of sample ML-13B. Plane-polarized light. FOV = 5 mm.

albite/andesine (± amphibole). Given the importance of the preserved assemblages for identifying the retrogressive character, each phase is described in detail below.

Garnet is variably abundant in the retro-eclogite (~10% - ~30%, visual estimation). Crystal rims have been degraded and replaced by amphibole and plagioclase leaving the cores with an eroded, amoeboid texture (Figure 7). Garnets are pale red to pink. Cores range from inclusion-free to inclusion-rich. Inclusions are predominantly quartz and aluminum silicate (kyanite).

Three points in a garnet core from sample ML-13B (Figures 7 and 8B) were analyzed with an electron microprobe: center, rim, and an intermediate point (Figures 9 and 10, Table 1). Almandine and spessartine concentrations increase and pyrope concentrations decrease from core to rim. Grossular remains relatively constant. The same data trends were noted by Markl and Bucher (1997) for their sample GM 63. Figures 9 and 10 indicate retrograde replacement of pyrope with almandine. This reflects replacement of Mg with Fe. The original eclogitic garnet composition is likely to be closest to that of the remaining garnet cores ($alm_{54.2}$, $py_{32.3}$, $gro_{12.0}$, $sp_{1.5}$).

Amphibole is the most abundant mineral in the retro-eclogite. These grains range from light to dark green and give the rock its dull green color. Grains are anhedral (Figure 6), except in the case of mineral replacement (Figure 7). Two amphiboles from sample ML-13B were microprobed yielding edenitic hornblende and ferroan pargasitic hornblende compositions (Figure 11, Table 2). These results are consistent with previous reports on amphiboles from retrograde eclogites in Lofoten (Kullerud, 1996; Markl and

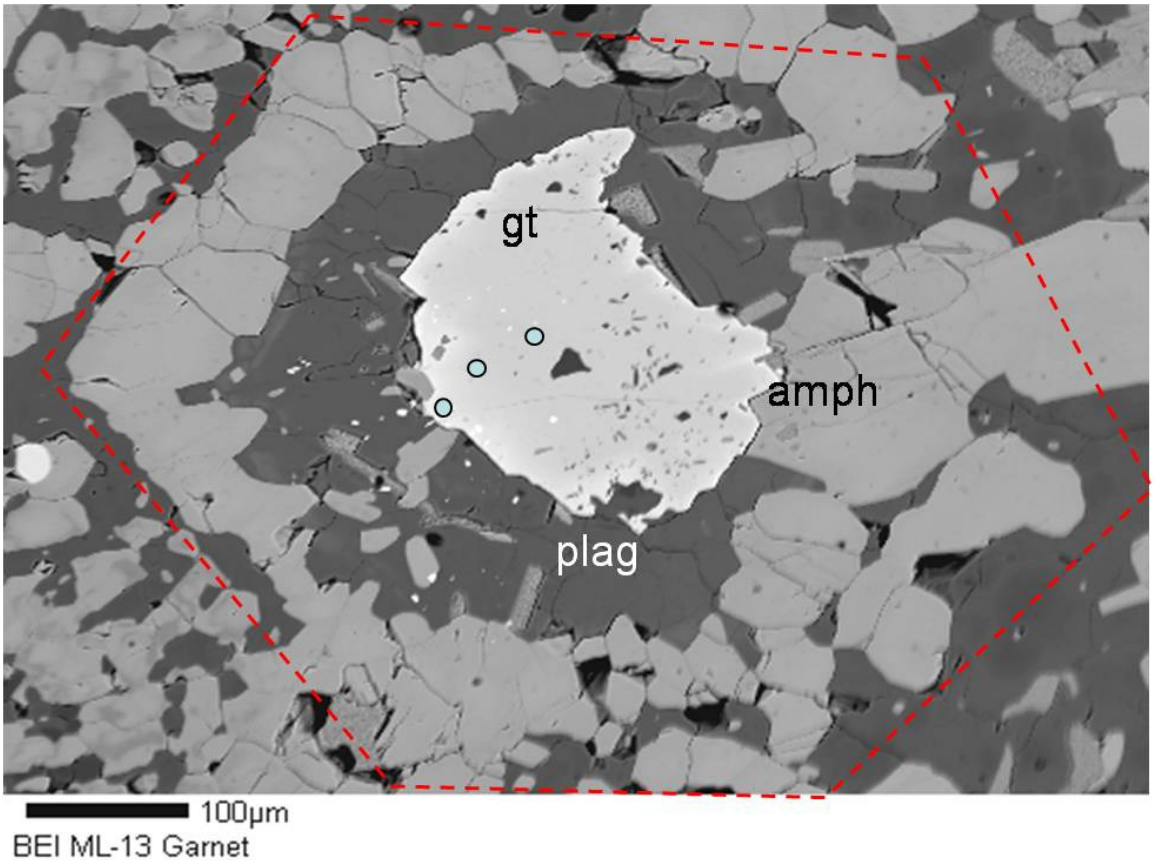

Figure 7: Backscatter electron image of relict garnet neomineralized to amphibole and plagioclase but with original garnet shape preserved (outlined in red). Garnet (gt) is the brightest mineral, followed by amphibole (amph), and plagioclase (plag). Points analyzed by electron microprobe are shown with light blue dots. Microprobe results are shown in Figures 9 and 10 and Table 1.

A.

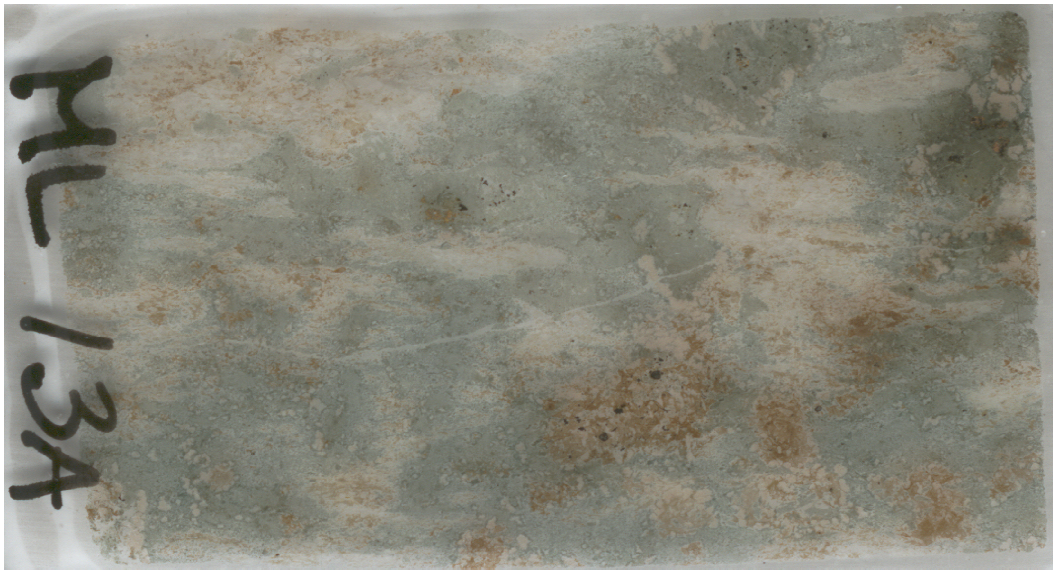

B.

Figure 8: Two thin sections from sample ML-13. Note the clusters of small garnets and the plagioclase haloes separating amphibole from other minerals. Short dimension is 2 cm. A) ML-13A is cut perpendicular to foliation and parallel to elongation lineation. B) ML-13B is cut parallel to foliation and elongation lineation.

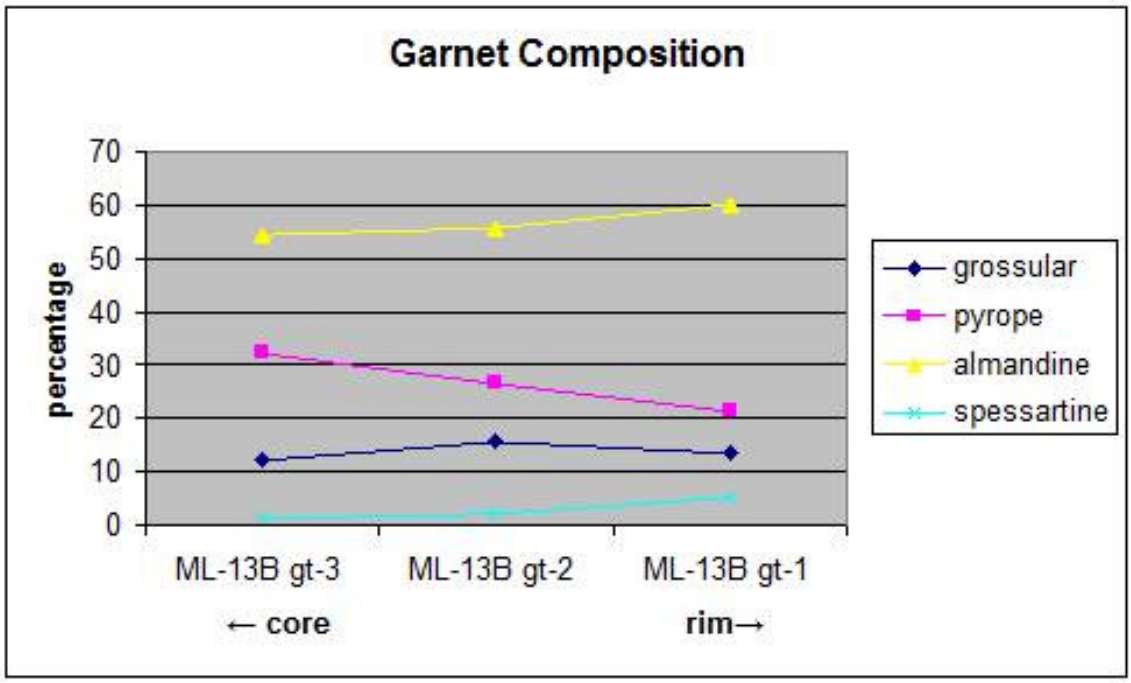

Figure 9: Garnet species concentrations for the garnet presented in Figure 7.

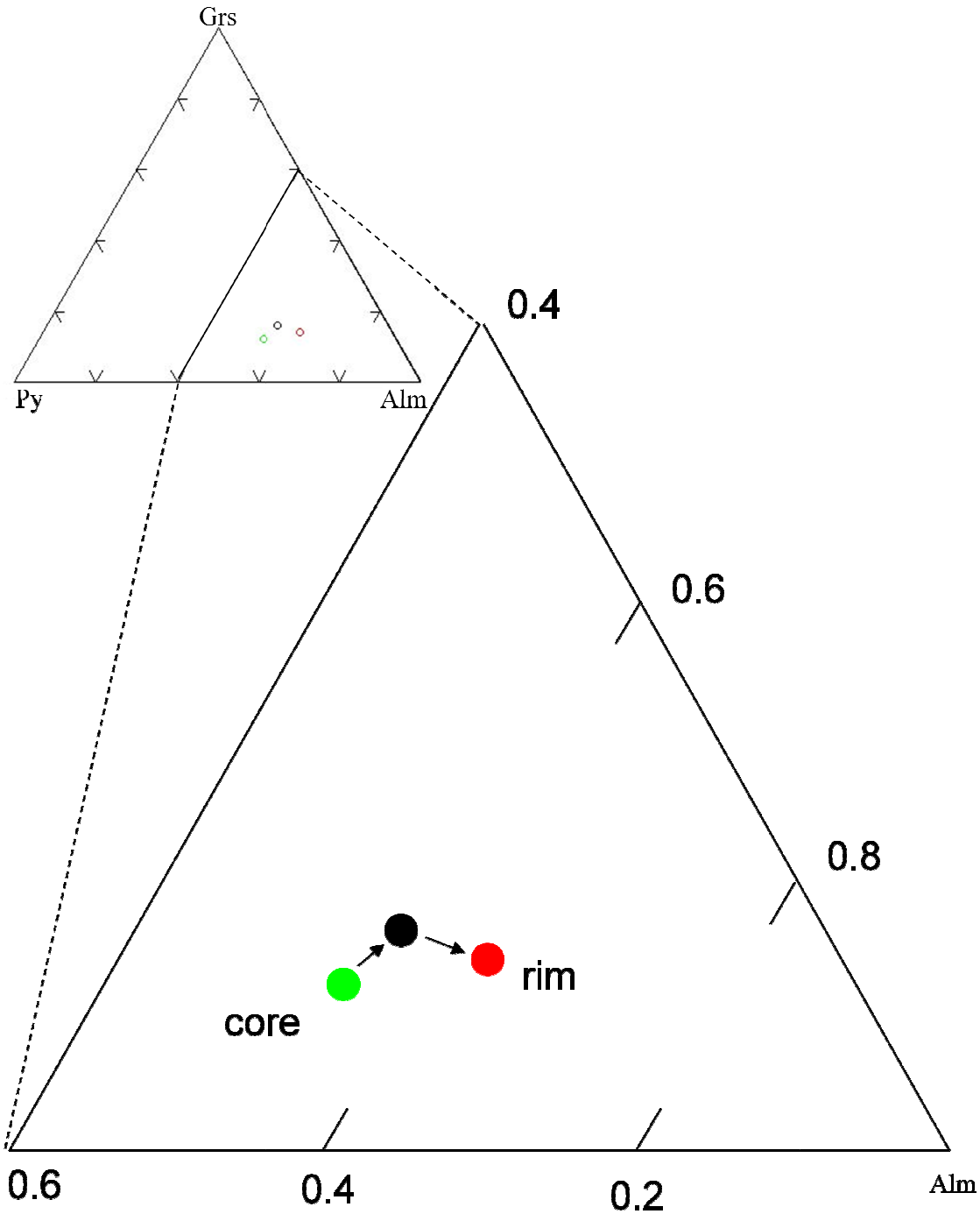

Figure 10: Py-Grs-Alm ternary diagram illustrating the chemical evolution from core to rim of the garnet from sample ML-13B presented in Figure 7. Py = pyrope; Grs = grossular; Alm = almandine.

Major Oxide	ML-13B gt-1 (rim)	ML-13B gt-2	ML-13B gt-3 (core)
SiO_2	37.860	38.750	39.130
TiO_2	0.126	0.051	0.047
Al_2O_3	21.760	21.920	22.070
MgO	5.470	7.180	8.210
FeO	27.290	26.710	24.570
CaO	4.780	5.840	4.250
MnO	2.260	1.061	0.669
Cr_2O_3	0.000	0.000	0.034

atoms per formula unit	ML-13B gt-1 (rim)	ML-13B gt-2	ML-13B gt-3 (core)
Si	5.962	5.941	6.047
Ti	0.015	0.006	0.005
Al	4.039	3.961	4.020
Mg	1.284	1.641	1.891
Fe	3.594	3.425	3.176
Ca	0.807	0.959	0.704
Mn	0.301	0.138	0.088
Cr	0.000	0.000	0.004
sum	16.003	16.072	15.935

Garnet Species %	ML-13B gt-1 (rim)	ML-13B gt-2	ML-13B gt-3 (core)
grossular	13.474	15.567	12.013
pyrope	21.451	26.626	32.286
almandine	60.040	55.571	54.207
spessartine	5.036	2.236	1.494
total	100.000	100.000	100.000

Table 1: Microprobe data and calculations for garnet from sample ML-13B presented in Figure 7.

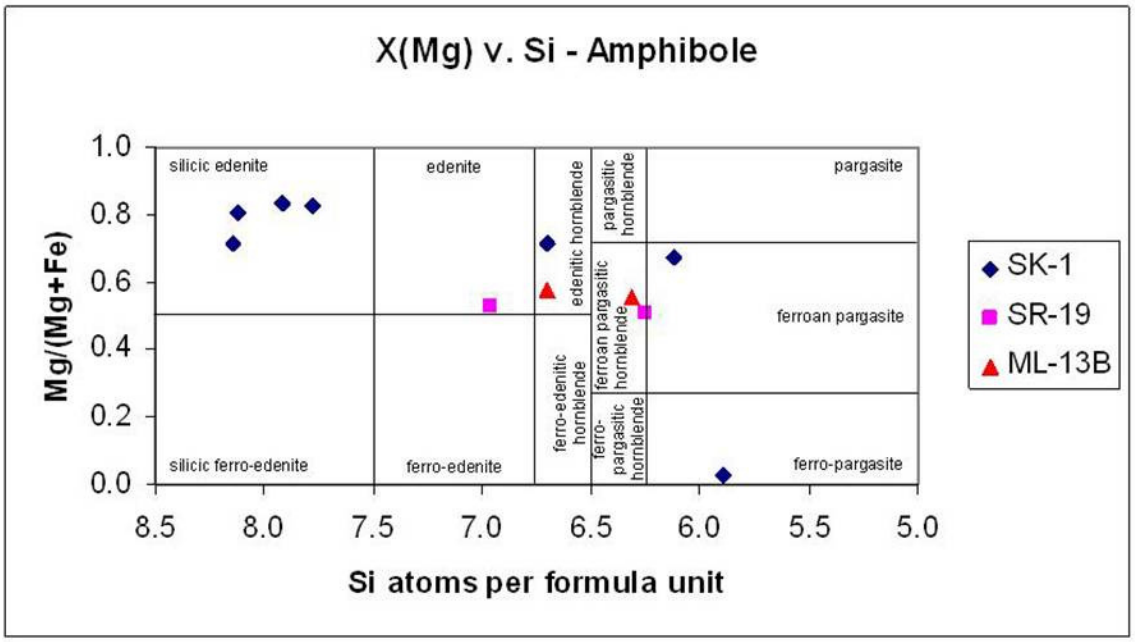

Figure 11: $X_{(Mg)}$ vs. Si diagram of the compositions of two analyzed amphibole grains according to the classification scheme of Leake (1978). Myrland sample ML-13B and Storvatnet sample SR-19 are from this report. Sample SK-1 is from the Skagen eclogite locality on Flakstadøy (Figure 3) described by Markl and Bucher (1997) and Steltenpohl et al. (2006).

	am-1		am-2				
Major oxide	Oxide wt. %	Norm. to 100 %	Oxide wt. %	Norm. to 100 %	atoms per formula unit		
					Element	am-1	am-2
SiO_2	42.53	45.28	41.15	41.82	Si	6.70	6.31
TiO_2	0.38	0.40	0.47	0.48	Ti	0.04	0.05
Al_2O_3	16.15	17.19	17.71	18.00	Al	3.00	3.20
MgO	10.77	11.47	9.98	10.14	Mg	2.53	2.28
FeO	14.25	15.17	14.08	14.31	Fe	1.88	1.81
CaO	7.68	8.18	12.24	12.44	Ca	1.30	2.01
MnO	0.13	0.14	0.17	0.18	Mn	0.02	0.02
K_2O	0.52	0.55	0.93	0.95	K	0.10	0.18
Na_2O	1.52	1.62	1.67	1.70	Na	0.46	0.50
F	0.00	0.00	0.00	0.00	F	0.00	0.00
sum	93.92	100.00	98.41	100.00	sum	16.04	16.37

Table 2: Microprobe data for amphiboles in sample ML-13B (Figure 8).

Bucher, 1997). Amphiboles are interpreted to be the second generation of retrogressed omphacite following the reactions Om → low-Na Cpx + Pc followed by low-Na Cpx → Am.

Plagioclase feldspar is the second most abundant mineral in the Myrland retro-eclogites. Under cross-polarized light, many of these plagioclase crystals show zones composed of a thick rim and a diffuse boundary with the core suggesting a gradual change in conditions during formation. The single microprobed feldspar grain from sample ML-13B (Table 3) is andesine ($An_{36.4}$). The retrogressive relationship Cpx + Qz → Pc is responsible for the abundance of plagioclase. Grains form as irregular to ovoid blebs within, or as a halo that surrounds amphibole (Figure 8). Markl and Bucher (1997) reintegrated original omphacite compositions (45% jadeite) from plagioclase and low-Na clinopyroxene symplectites based on the breakdown reaction Om → low-Na Cpx (Di) + Pc.

Remaining minerals in Myrland retro-eclogites are present in small amounts (<10% of the mode, visual estimation). Biotite forms pseudomorphs at the expense of amphibole and also occurs as euhedral crystals at discrete nucleation sites in association with other accessory minerals (Figures 6 and 12). Minerals that nucleate with biotite include muscovite (Figure 12), sphene, and epidote/clinozoisite. These aggregations of minerals are commonly surrounded by a halo of plagioclase and quartz, separating the nucleation zone from the amphibole (Figures 6, 8, and 12).

Major oxide	Oxide wt. %	Norm. to 100 %	Element	atoms per formula unit
SiO_2	58.27	57.77	Si	2.91
TiO_2	0.04	0.04	Ti	0.00
Al_2O_3	26.89	26.66	Al	1.58
MgO	0.00	0.00	Mg	0.00
FeO	0.01	0.01	Fe	0.00
MnO	0.09	0.09	Mn	0.00
CaO	7.91	7.84	Ca	0.42
K_2O	0.02	0.02	K	0.00
Na_2O	7.65	7.58	Na	0.74
BaO	0.00	0.00	Ba	0.00
sum	100.87	100.00	sum	5.66

Table 3: Microprobe data from plagioclase feldspar in sample ML-13B (Figure 8).

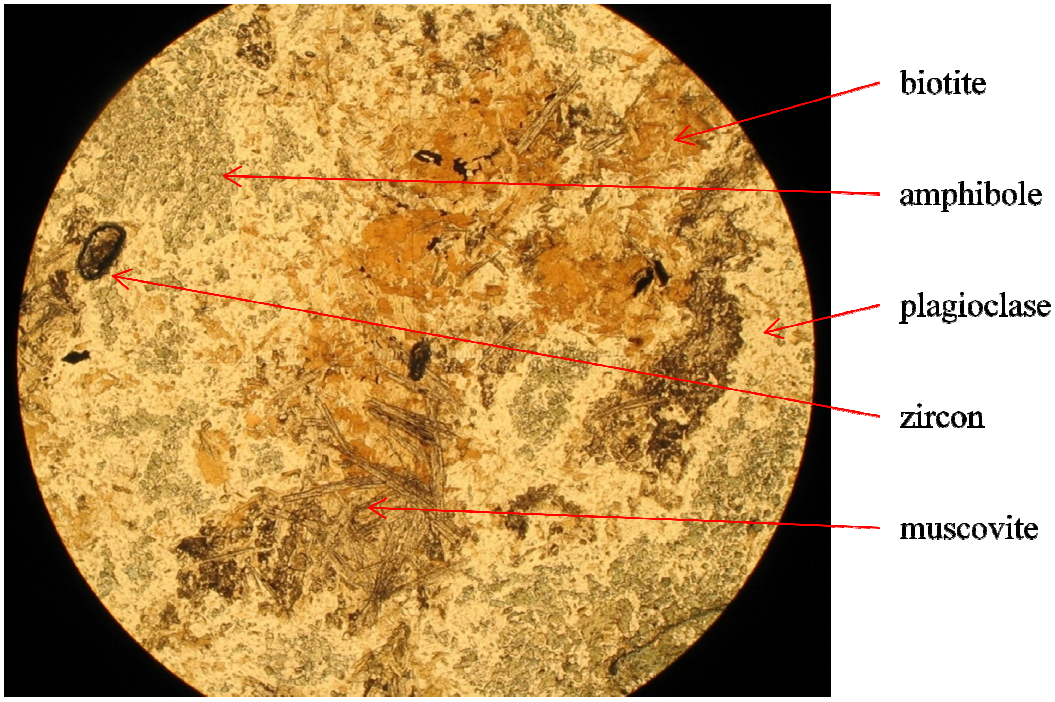

Figure 12: Photomicrograph of biotite and muscovite clusters within retrogressed eclogite. Note the irregular habit of biotite and the tabular habit of muscovite. Sample ML-13B. Plane-polarized light. FOV = 5 mm.

Amphibolite

Amphibolite is present between the interior retrograde eclogite lenses and the orthogneiss host rock (Figure 4). Amphibole, plagioclase, and biotite are the major rock-forming minerals. Garnet is abundant near the retro-eclogite, but the abundance decreases with distance from the retro-eclogite contact. Amphibolite lacks the symplectites characteristic of retro-eclogite. Thickness of the amphibolite is variable, ranging from centimeters to several meters. The transition from retrograded eclogite to amphibolite is gradual and the delineation of units is somewhat ambiguous. The distinction was made on the basis of rock color, structural features, and mineralogy. Whereas the retrograde eclogite was greenish-gray, the amphibolite is mostly black with a salt-and-pepper appearance, and only a faint dark-green tinge. In contrast with the retro-eclogite, amphibolite has well-developed foliations and lineations that parallel the retro-eclogite pod boundary. The strong foliation is defined by alternating bands of amphibole and plagioclase. Elongate biotite grains define a moderately developed mineral lineation that lies within the foliation plane.

Amphibole grains in amphibolite are small (<1 mm diameter), equigranular and polygonal to interlobate (scheme from Passchier and Trouw, 1998, p. 46, after Moore, 1970), constitute roughly 50-60% by volume (visual estimate) of the amphibolite, and are dark green to gray-green. The color is similar to the darkest-colored amphibole grains from the retro-eclogite. Grains are arranged in thin (1-5 mm thick) compositionally layered bands that alternate with bands composed mostly of plagioclase. At thin-section scale, amphibole bands within garnet-amphibolite pinch and swell, forming sigmoidal

shapes (Figure 13C). Bands within biotite-amphibolite, which are located farther from the retro-eclogite, are straight (Figure 13 A and B). The different banding styles are interpreted to have formed from recrystallization of single amphibole grains whose deformation intensity depended on distance from the eclogite pods. As the retro-eclogites are interpreted to have retained much of their competency during eclogite-facies deformation, the amphibolite immediately adjacent to the retro-eclogite (Figure 13C) experienced a lesser degree of deformation, thus retaining remnants of their eclogite textural heritage, than did the more distal amphibolite (Figure 13A and B).

Like amphibole, plagioclase grains are strain free, typically <1 mm in diameter, and are concentrated in compositional bands approximately 1-5 mm thick. Plagioclase accounts for roughly 40% of the rock (visual estimate). Twinned grains are common but not ubiquitous. Grain boundaries are straight to curvilinear.

Approximately 5-10% (visual estimate) of the rock is composed of brown biotite. Biotite grains define the foliation (along with amphibole and plagioclase bands) but do not preserve microstructural evidence for post-crystallization strain. Some grains are partially altered to chlorite. Biotite abundance decreases with proximity to retro-eclogite pods.

Accessory phases in the amphibolite are garnet and zoisite. Garnet increases in abundance proximal to eclogite. This increase occurs in conjunction with a decrease in

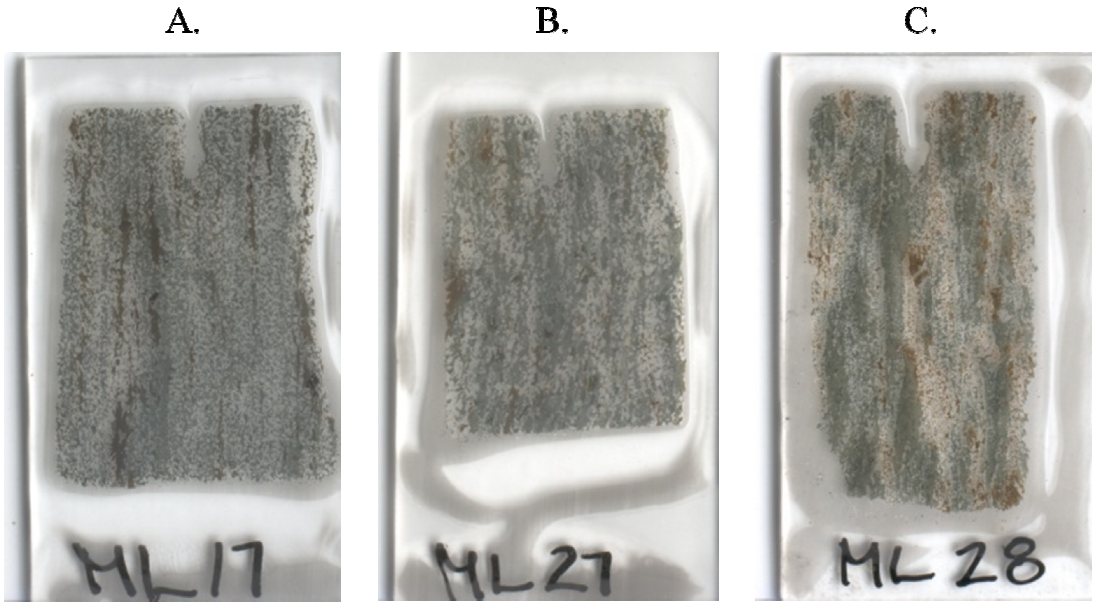

Figure 13: Scans of thin sections from amphibolite at the Myrland locality. Schistosity parallels long dimension. Short dimension is 2 cm. A) Biotite-amphibolite sample ML-17. B) Biotite-amphibolite sample ML-27. C) Garnet-amphibolite sample ML-28.

biotite abundance. The width of the garnet-bearing halo varies from tens of centimeters to meters. Garnet size and color are similar to those of garnets found within the eclogite lenses. Trace amounts of steel-blue zoisite are present in some samples.

Monzodioritic Orthogneiss

This unit was first described by Romey (1971), who identified it as "granulite-facies veined gneiss". The contact between this gneiss and mangerite to the south on Flakstadøy is reportedly gradational or finely interfingered (Romey, 1971). Although previous reports identified this unit as mangeritic (Markl and Bucher, 1997), during this study no high-pressure minerals (hypersthene) were observed in orthogneiss located proximal to retro-eclogite. Accordingly, the orthogneiss investigated herein is referred to as monzodiorite in order to reflect its composition (see below).

Orthogneiss at outcrop scale is light- to medium-gray and is dominated by coarse-grained plagioclase. Well developed, sub-vertical schistosity, defined by clots of fine- to medium-grained biotite and amphibole, is present throughout the exposed area. Progressive mylonitization of the orthogneiss as the amphibolite is approached results in schistosity intensification and grain size reduction, accompanied by change in rock color from gray to dark gray to black (Figure 14).

Plagioclase, K-feldspar, quartz, and biotite are the primary rock-forming minerals (Table 4). A large percentage of feldspar present in orthogneiss samples ML-35 and 38 is untwined, making it difficult to confidently differentiate between feldspar types using petrographic methods. Only a small amount of K-feldspar was identified positively,

Figure 14: Monzodioritic orthogneiss (right) darkens significantly as the amphibolite (far left) is approached. Field of view is ~4 m at bottom of photo. Location A on Figure 4.

	ML-38 (unsheared)		ML-35 (sheared)	
Phase	Count	Vol. %	Count	Vol. %
Pc	111	27.75	134	33.5
Kfs	4	1	7	1.75
Fsp	176	44	120	30
Qtz	41	10.25	15	3.75
Bt	43	10.75	91	22.75
Ep	9	2.25	22	5.5
Rt	1	0.25	1	0.25
Czo	3	0.75	4	1
Ttn	3	0.75	5	1.25
Am	5	1.25	0	0
Ser	3	0.75	0	0
Prt	1	0.25	0	0
Op	0	0	1	0.25
total	400	100	400	100

Table 4: Table of point count data for sheared and unsheared orthogneiss samples (n = 400 for each sample). Abbreviations after Siivola and Schmid (2007). Fsp denotes feldspar which could not be differentiated between Pc and Kfs using optical microscopy. (Refer to Figure 27 for sample locations.)

however, geochemical data indicate that K_2O comprises 2.94% - 3.34% of these rocks. It is, therefore, assumed that a significant fraction of the unidentified feldspar is K-feldspar. Other phases include epidote, rutile, clinozoisite, sphene, and dark-green amphibole. Amphibole is only present in minimally sheared rock and is observed to alter to biotite and quartz. Within sheared orthogneiss, plagioclase grains are twinned with curvilinear to wavy grain boundaries and abundant grain bulges and nucleation sites. Biotite grains are greenish-brown, aligned, and unbent. These same phases are present in unsheared orthogneiss; however, triple-point boundaries and straight grain edges dominate. Bulges or nucleations were not observed in unsheared orthogneiss grains.

Four samples submitted for geochemical analyses (Tables 5 and 6) have CIPW norms (Table 7) indicating monzodioritic compositions (Figure 15).

Felsic Injections

To the author's knowledge, felsic injections have not been previously described for any of the Lofoten eclogite localities. Romey (1971), who apparently was not aware of the presence of eclogites on Flakstadøy, described the host monzodioritic orthogneiss as "commonly veined". A sizeable volume of leucocratic injections (~15%, visually estimated from Figure 4) is, however, associated with the Myrland retro-eclogite occurrence. Felsic veins occur within the monzodioritic orthogneiss and are abundant throughout the retrograde eclogite and amphibolite zone. Veins within the retrograded eclogite lenses are tabular and planar and have sharp, high-angle bends, giving the

Major	Sheared Orthogneiss					Retro-eclogite	Felsic dike
Oxide	ML-35	ML-36	ML-35/36	ML-37	ML-38	ML-31	ML-42
SiO_2	58.20	57.10	57.05	57.00	57.50	48.10	76.00
Al_2O_3	18.10	17.65	17.83	18.00	18.00	16.90	13.65
Fe_2O_3	7.24	8.07	7.71	7.34	7.25	12.75	0.88
CaO	4.93	5.42	5.31	5.19	4.96	8.17	1.34
MgO	2.17	2.47	2.34	2.20	2.21	7.04	0.99
Na_2O	4.67	4.92	5.03	5.14	5.38	3.24	4.37
K_2O	3.38	2.99	3.11	3.23	2.96	1.28	1.56
Cr_2O_3	<0.01	<0.01	<0.01	<0.01	<0.01	<0.01	<0.01
TiO_2	0.92	1.01	0.97	0.93	0.79	1.19	0.10
MnO	0.15	0.17	0.16	0.15	0.15	0.18	0.01
P_2O_5	0.46	0.56	0.52	0.47	0.42	0.39	0.02
SrO	0.09	0.09	0.09	0.09	0.09	0.07	0.10
BaO	0.24	0.22	0.23	0.24	0.20	0.06	0.12
LOI	0.78	0.55	0.66	0.77	0.85	0.46	1.03
Total	101.33	101.22	100.99	100.75	100.76	99.80	100.17
Normalized to 100%							
SiO_2	57.44	56.41	56.49	56.58	57.07	48.20	75.87
Al_2O_3	17.86	17.44	17.65	17.87	17.86	16.93	13.63
Fe_2O_3	7.14	7.97	7.63	7.29	7.20	12.78	0.88
CaO	4.87	5.35	5.25	5.15	4.92	8.19	1.34
MgO	2.14	2.44	2.31	2.18	2.19	7.05	0.99
Na_2O	4.61	4.86	4.98	5.10	5.34	3.25	4.36
K_2O	3.34	2.95	3.08	3.21	2.94	1.28	1.56
Cr_2O_3	<0.01	<0.01	<0.01	<0.01	<0.01	<0.01	<0.01
TiO_2	0.91	1.00	0.96	0.92	0.78	1.19	0.10
MnO	0.15	0.17	0.16	0.15	0.15	0.18	0.01
P_2O_5	0.45	0.55	0.51	0.47	0.42	0.39	0.02
SrO	0.09	0.09	0.09	0.09	0.09	0.07	0.10
BaO	0.24	0.22	0.23	0.24	0.20	0.06	0.12
LOI	0.77	0.54	0.65	0.76	0.84	0.46	1.03
Total	100.00	100.00	100.00	100.00	100.00	100.00	100.00

Table 5: Geochemical major oxide weight percent data for samples collected from the Myrland shear zone, retro-eclogite, and felsic dike. Samples ML-35 and 36 were averaged as described in the text. See Figures 4, 18, and 27 for sample locations.

Trace	Sheared Orthogneiss					Retro-eclogite	Felsic dike
Element	ML-35	ML-36	ML-35/36	ML-37	ML-38	ML-31	ML-42
Ce	90.7	91.5	91.1	92.1	81.0	42.7	41.3
Dy	4.1	4.6	4.4	4.2	4.2	3.7	0.8
Er	2.1	2.5	2.3	2.1	2.2	2.2	0.1
Eu	2.1	2.1	2.1	2.1	2.0	1.6	0.2
Gd	6.5	7.2	6.9	6.8	6.3	4.7	1.8
Ho	0.4	0.5	0.5	0.4	0.4	0.7	<0.1
La	44.4	43.7	44.1	46.7	39.9	19.4	16.6
Lu	<0.1	<0.1	<0.1	<0.1	<0.1	0.2	<0.1
Nd	44.5	45.5	45.0	45.6	39.5	23.4	13.1
Pr	10.6	11.1	10.9	10.6	9.4	5.3	3.3
Sm	7.5	7.9	7.7	7.7	6.8	4.8	2.0
Tb	0.5	0.6	0.6	0.5	0.5	0.7	<0.1
Th	1.0	1.0	1.0	1.0	<1	1.0	15.0
Tm	<0.1	<0.1	<0.1	<0.1	<0.1	0.3	<0.1
U	0.6	0.8	0.7	0.7	0.9	0.8	6.6
Y	24.6	28.2	26.4	26.5	24.8	21.9	6.1
Yb	1.6	2.1	1.9	1.7	2.0	1.8	<0.1

Table 6: Geochemical trace element data (mg/kg) for samples collected from the Myrland shear zone, retro-eclogite, and felsic dike. Samples ML-35 and 36 were averaged as described in the text. See Figures 4, 18, and 27 for sample locations.

	Orthogneiss shear zone sample			Felsic dike
	ML-35/36	ML-37	ML-38	ML-42
Q	0.05	0.04	0.04	0.43
A	0.23	0.23	0.21	0.5
P	0.73	0.73	0.75	0.07
sum	1.01	1	1	1
CIPW norm values				
Qz	3.81	3.02	3.37	40.38
Co	0	0	0	2.39
Or	18.18	18.95	17.35	9.21
Ab	42.1	43.11	45.14	36.94
An	16.71	16.39	16.08	6.51
Di	4.7	4.77	4.37	0
Hy	3.56	3.21	3.42	2.46
Il	0.34	0.32	0.32	0.02
Hm	7.64	7.3	7.21	0.88
Ap	1.11	1.03	0.92	0.04

Table 7: CIPW norm values and data normalized for use on the Q-A-P-F diagram (Figure 15) for samples ML-35, 36, 37, 38, and 42 from the Myrland locality.

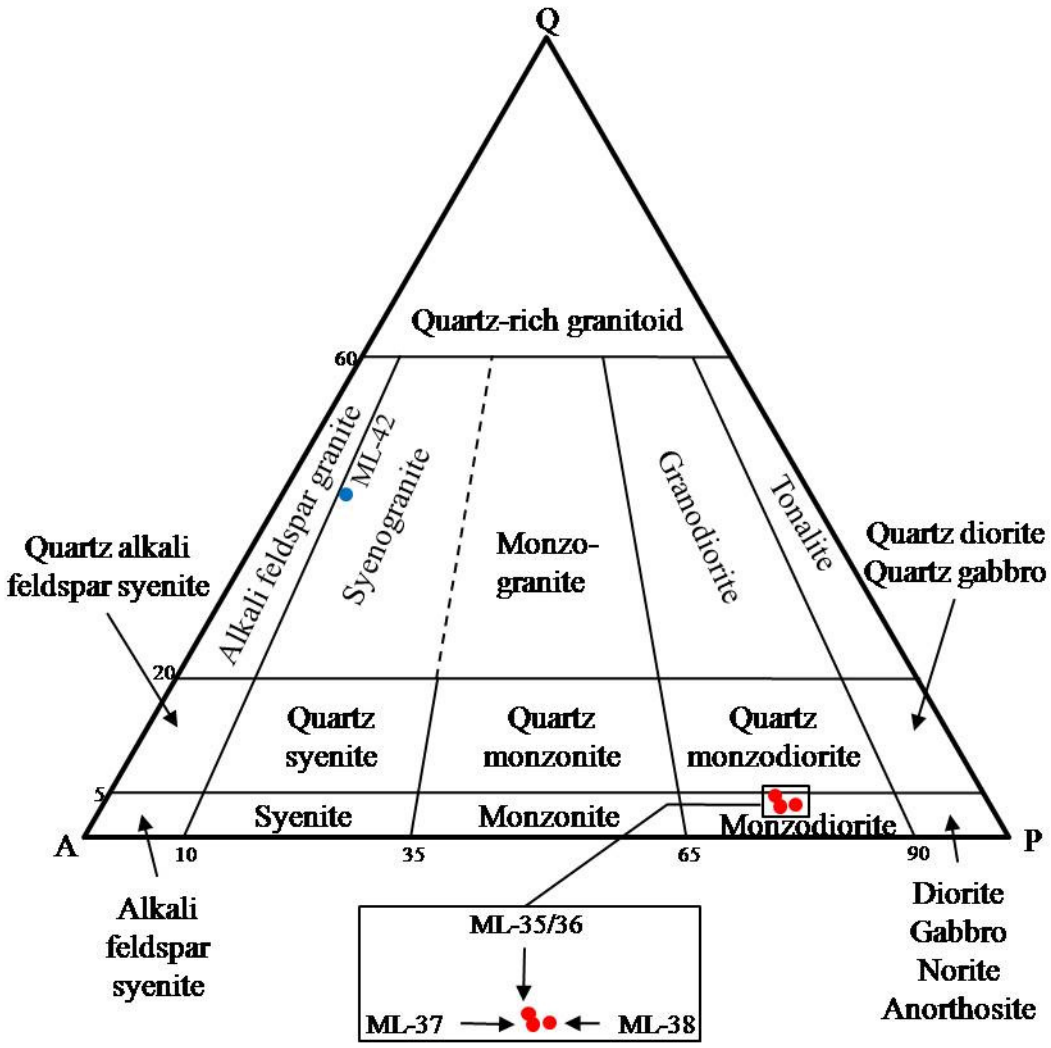

Figure 15: Upper half of the Q-A-P-F diagram (LeMaitre, 1989) on which the CIPW norm compositions of Myrland samples ML-35, 36, 37, 38 and 42 are plotted (Table 7).

appearance of having been injected into a brittle fracture network (see Figure 4, especially the easternmost lens). The volume of felsic material increases dramatically within the zone of amphibolite surrounding the retro-eclogite pods. Here the veins are highly contorted, wavy, folded, boudinaged, and necked (Figure 16). Felsic dikes within the orthogneiss occur as tabular veins that range from less than 1 centimeter to less than 2 meters in thickness. Some veins are cut by thin (2-4 cm thick), small displacement (<1 m) crystal-plastic shear zones (Figure 17). Bimodal grain size delineates two types of injections: either thin, fine-grained veins (Figure 18) or pegmatites (Figure 19).

Typical mineralogy of fine-grained veins is quartz, plagioclase ($An_{15.6}$, CIPW norm value), potassium feldspar, muscovite and biotite, with accessory clinozoisite, epidote, rutile, opaque minerals, zircon and xenotime. Quartz is present in a range of grain sizes. Most are small (1 mm) but many large (up to 2 cm long and 4 mm wide in the analyzed sample), tabular quartz grains are present. Larger quartz grains are aligned with the foliation and commonly fractured. Grain boundaries for the smaller quartz grains are curviplanar. Some plagioclase grains are twinned and/or zoned. Muscovite grains are slightly yellow-gold, up to several millimeters thick, rarely bent (as evidenced by undulatory extinction), and concentrated in bands easily visible to the naked eye. Biotite gives the rock a speckled appearance. Fine-grained veins have a strong foliation defined by white mica that always parallels the vein contact, which in turn generally parallel the retro-eclogite pod boundary. No lineation is evident. CIPW normative values (Table 7) obtained from whole-rock geochemical data (Table 5) indicate a syenogranitic composition (Figure 15).

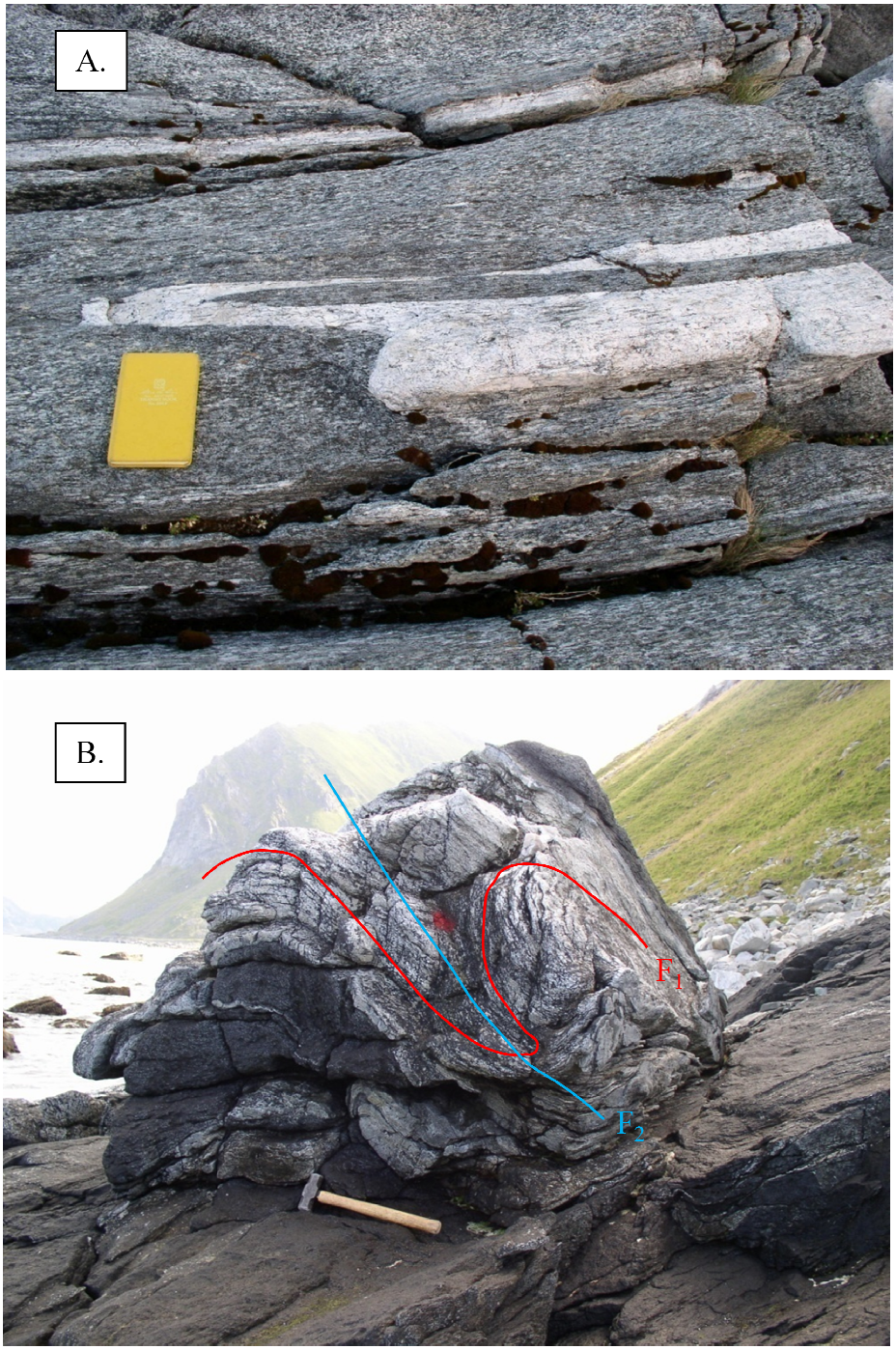

Figure 16: A. Isoclinally folded, sheared, and foliated felsic vein. Note axial planar foliation parallels that of country rock. B. Highly contorted and folded felsic vein. Early generation isoclines, F_1 (red), with axial-planar schistosity, are deformed by a later-phase fold, F_2 (blue), which has resulted in a Ramsay type III "fish hook" interference pattern. (Location C on Figure 4.)

Figure 17: Steeply dipping (to the left in photo), tops-north, distributed ductile shear zone cutting and displacing a felsic vein located ~4 m south of amphibolite/orthogneiss contact at Myrland. Shear zones are < 2 cm thick. View is to the west. Hammer is ~35 cm long.

Figure 18: Thin, fine-grained felsic vein at location B on Figure 4. See geochemistry sample ML-42 in Tables 5, 6, and 7, and in Figure 15. Sample AA03-3 was also sampled for U-Pb geochronology from this location. Hammer is ~35 cm long.

Figure 19: Pegmatitic boudin, ~90 cm long, at location A on Figure 4.

Where the injections are more voluminous, as in the eastern parts of the exposure and where they are boudinaged, pegmatite is the dominant type of injected material (Figures 4 and 19). Pegmatite mineralogy is simple but abundances are highly variable, ranging from ~100% quartz to plagioclase- and mica-rich varieties. Clear quartz grains in the pegmatites are up to several millimeters in diameter, equidimensional, and exhibit no discernible signs of deformation or preferred growth direction, implying crystallization from a molten state or a high degree of static annealing following deformation. Large (up to several cm), euhedral potassium feldspar, muscovite and/or biotite mica grains dominate in pegmatite boudins (Figure 19).

Structures

Structural Fabrics

Eclogites at Myrland are significant because they contain preserved fabrics from the eclogite-facies deformational event. All fabrics that recorded eclogite-facies deformation outside of the retro-eclogite pods have been totally recrystallized and obliterated by subsequent retrogression and deformation. Three phases of fabric development are recorded in rocks at Myrland.

The gneissosity, S_0, within the monzodioritic orthogneiss outside of its sheared boundary with the package of amphibolite and retro-eclogite clearly is a Proterozoic fabric. Since the research objectives of this study are focused on those fabrics within the eclogite/amphibolite package and adjacent country rocks that likely are Caledonian in age (Steltenpohl et al., 2003), the Proterozoic structures and fabrics were not analyzed.

Petrographic analysis of the retrograded eclogite reveals that much microstructural evidence for eclogite-facies shearing has been obliterated by amphibolite-facies retrogression. A weak S_1 foliation in the retro-eclogite pods is defined by delicately folded garnet and plagioclase ribbons (Figure 20) that are interpreted as a remnant of eclogite-facies deformation (D_1). This S_1 fabric has been transposed into the much more intensely developed S_2 foliation. Although eclogitic D_1 garnets may have survived, differentiating these from amphibolite-facies D_2 garnets has proven difficult. No other phases survived retrogression without recrystallization or neomineralization.

S_2 foliation is weakly- to moderately developed in the retro-eclogites but is also the predominant schistosity in the encapsulating amphibolites and along the sheared margins of the monzodioritic orthogneiss. Undeformed, dark-green clots of medium-grained amphibole (0.3 - 0.5 mm) and fine-grained plagioclase (< 0.3 mm) overprinting previously elongated minerals define S_2 in retro-eclogites (Figure 20). The individual amphibole crystals within these clots are significantly larger than the amphibole in the groundmass, has well-developed cleavage, and has characteristic second-order birefringence. Clots are interpreted to represent the recrystallized equivalent of sheared D_1 amphiboles and/or pyroxenes, which places D_2 as a post-eclogitic, amphibolite-facies event. Groundmass amphibole in retro-eclogites is very fine grained (<0.05 mm), anhedral, and has light green color and first-order to low second-order birefringence (anomalous birefringence is due to small crystal size and irregular grain edges). A few clusters of recrystallized grains in retro-eclogite appear to be ‘ghosts’ of

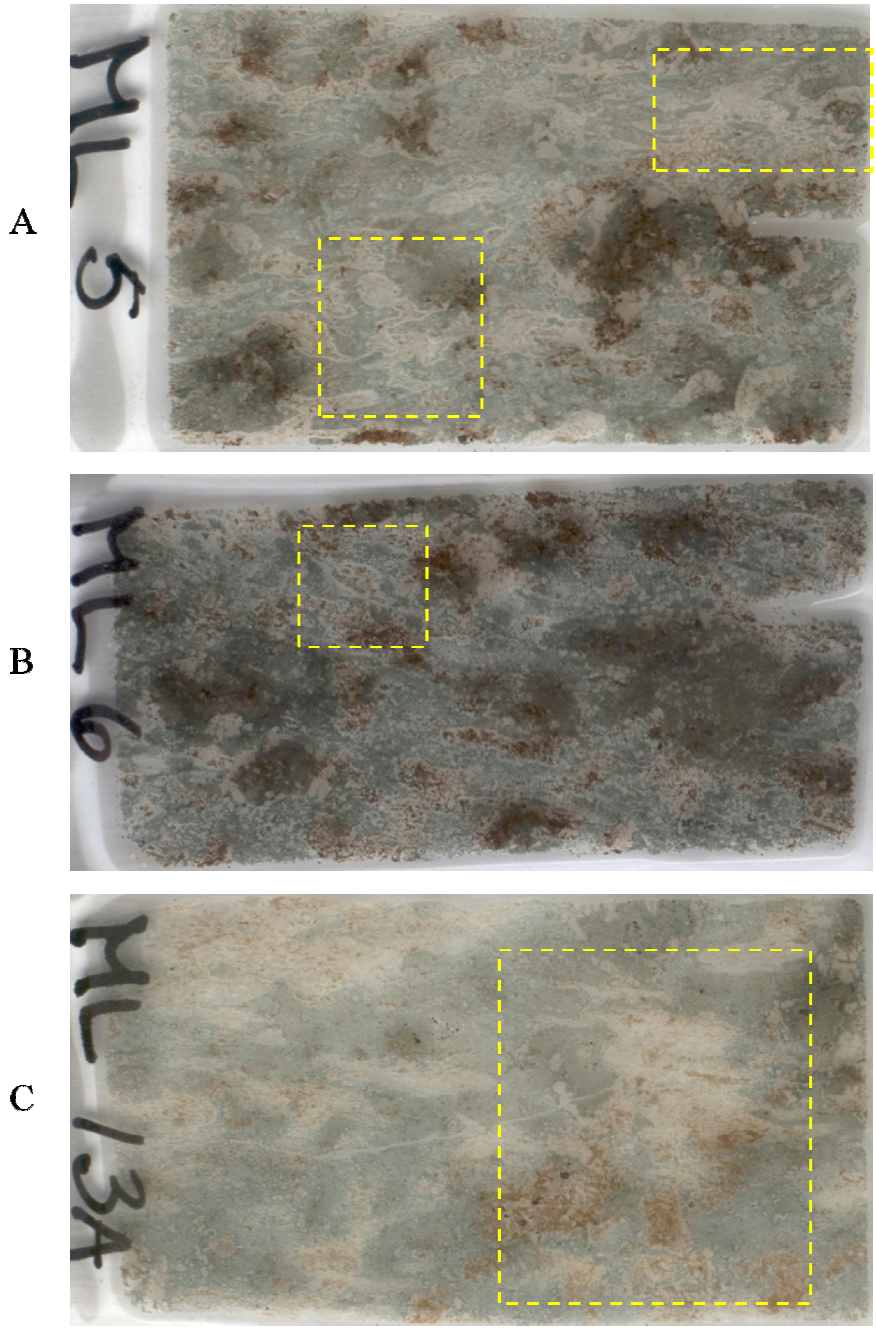

Figure 20: Thin section scans of retro-eclogite samples from the Myrland locality. All are cut parallel to elongation lineation and perpendicular to foliation. Schistosity, S_2, parallels long dimension of slides. Delicate dark and light banding, S_1, (yellow boxes) is clearly folded and transposed into the predominant schistosity, S_2. Phases visible are amphibole (dark and light green), garnet (red and pink), plagioclase (clear), and biotite (brown). A) Sample ML-5. B) Sample ML-6. C) Sample ML-13A.

porphyroclasts, some of which appear to be the remnants of sigma and/or delta clasts and microfolds (Figure 20). These ghost microstructures are parallel with S_2 and are, therefore, interpreted as D_2 products.

Deformation twins and abundant subgrains are found in plagioclase within retro-eclogite, likely recording the 'last gasp' of relatively low-temperature mylonitic deformation in the waning stages of amphibolite-facies overprint. Anhedral garnets of varying sizes within retro-eclogite show no evidence of internal deformation and the amphibole/plagioclase replacement of garnet retains the euhedral shape of the original garnet (Figure 7), supporting static conditions for retrograde metamorphism for some samples. Biotite and muscovite are likewise undeformed. The seriate and interlobate fabric (after Moore, 1970) of the retrograde eclogite is interpreted to be a function of static amphibolite-facies recrystallization.

D_2 structures are preserved in amphibolite primarily as foliation defined by bands of recrystallized amphibole and plagioclase and elongate biotite. Amphibole and biotite show no microstructural evidence of internal deformation but have a grain shape preferred orientation aligned with the S_2 foliation. Plagioclase subgrains and undulose extinction are common, indicating post-crystallization strain. Growth twins outnumber deformation twins by ~5:1 (determination according to Passchier and Trouw, 1998, p. 34).

D_1 and the resulting S_1 are interpreted as products of deformation under prograde, eclogite-facies metamorphism. D_2 clearly occurred under amphibolite-facies conditions,

although its transition from eclogite- to amphibolite-facies is difficult to discern. Static recrystallization under amphibolite-facies followed D_2 and partially destroyed S_2 fabrics.

Mesoscopic Structures

The Myrland locality can be described as a north-northwest trending ductile shear zone that affects the host monzodioritic orthogneiss and a package of four retrograde eclogite lenses within their encapsulating amphibolite. Amphibolite and retro-eclogite are affected by deformation in a drastically different manner than is the host rock. Each of these lithologies is characterized by distinct structures that reflect their different rheological properties. Neither the length nor the width of the shear zone is known, as its borders are mostly covered by rubble and project into the sea. Many millimeter- to centimeter-scale mylonite shear zones characterize the margins of the main shear zone in the orthogneiss host, commonly cross-cutting each other (Figure 21).

In map view, the retrograde eclogite lenses have a distinct lenticular shape (Figure 4). Several meters of topographic relief allow documentation of a minimum depth estimate (Figure 22). Combining a down-plunge projection of the lenses with the geometry seen in Figure 4 suggests that the retro-eclogites are necked or completely dismembered bodies stretched parallel to the elongation lineation measured in the rock (Figure 23).

The metamorphic foliation in the retro-eclogite lenses share a common strike direction, approximately N30°W, but some lenses have opposing dip directions (Figures 4 and 24). Northwest lenses dip ~50°SW whereas southeast lenses dip ~55°NE (Figures

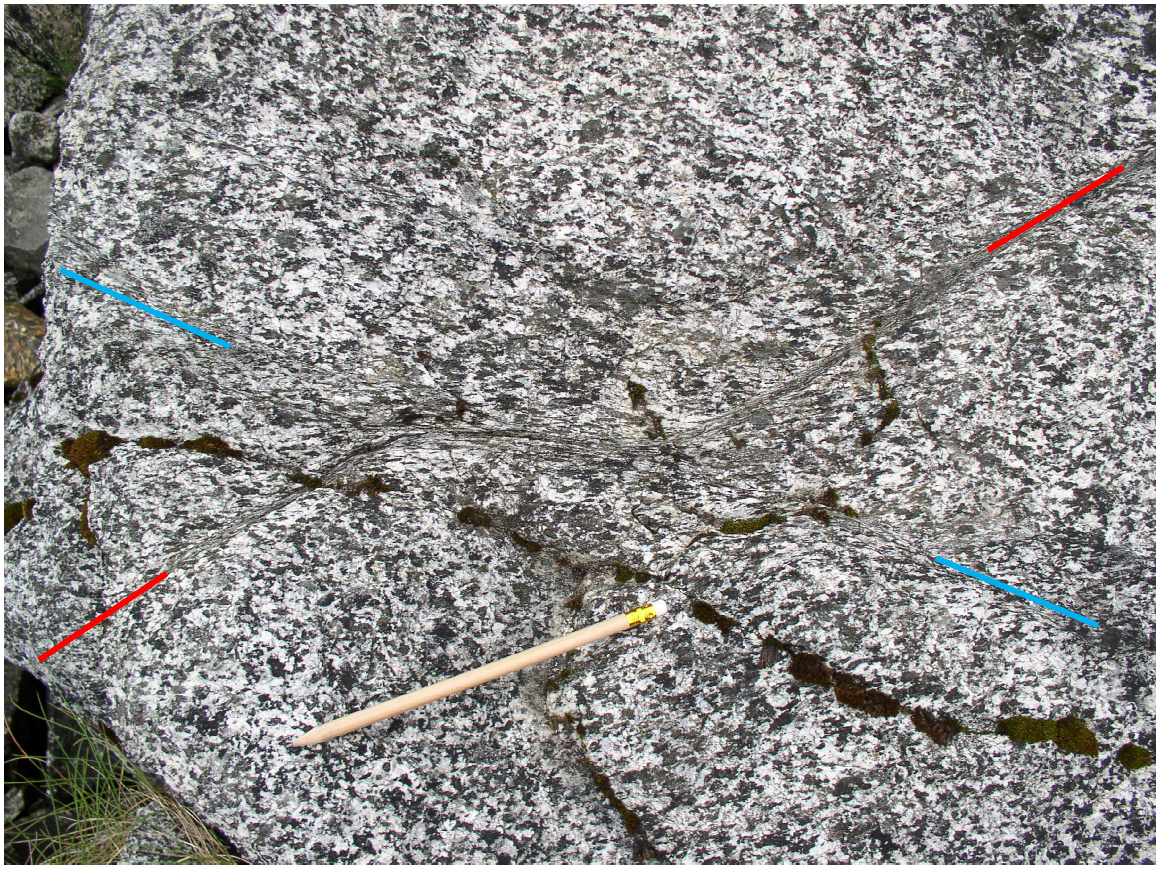

Figure 21: Thin (1-4 cm thick), cross-cutting mylonite shears along the margins of the Myrland eclogite zone, located several meters to the west of the area depicted in Figure 4. First shear zone (red) dips to the south with tops-down displacement. Second shear zone (blue) dips shallowly to the north with tops-north displacement. View is to the west.

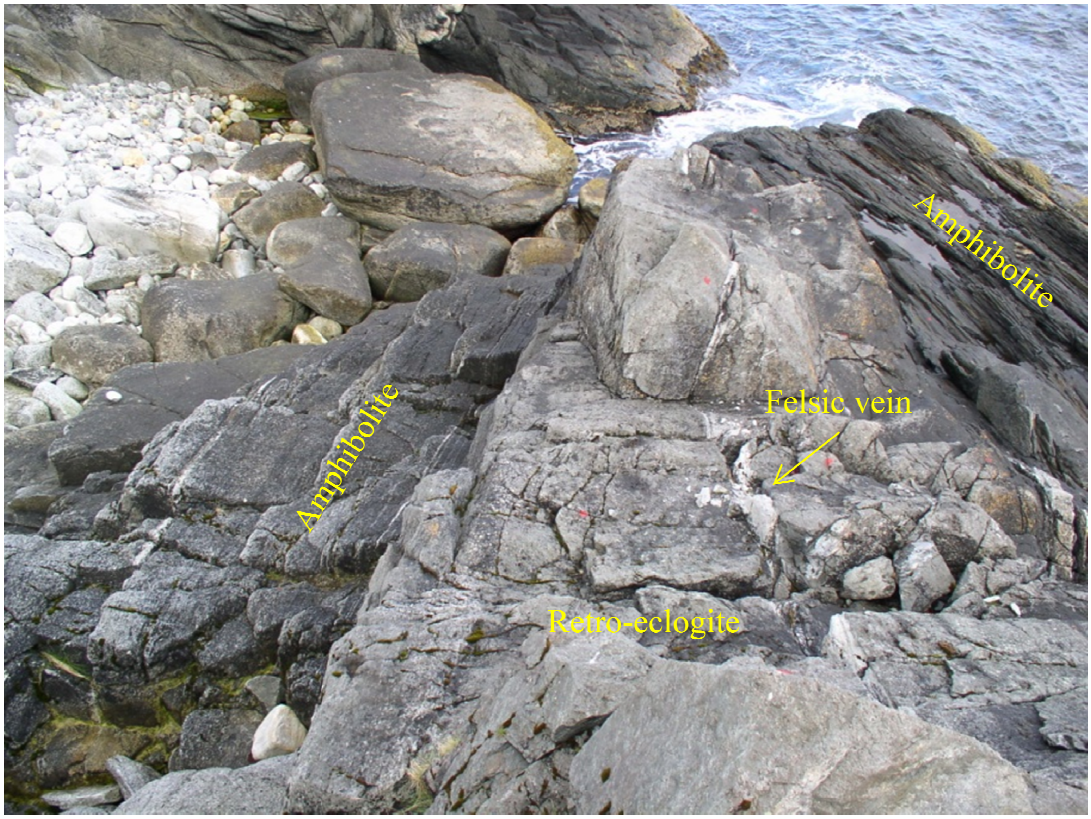

Figure 22: Nose of the northwest retro-eclogite lens at Myrland depicted in Figure 4 (Location B). Amphibolite foliation wraps around the lens. Felsic vein cuts through the center of the lens. View is to the northwest.

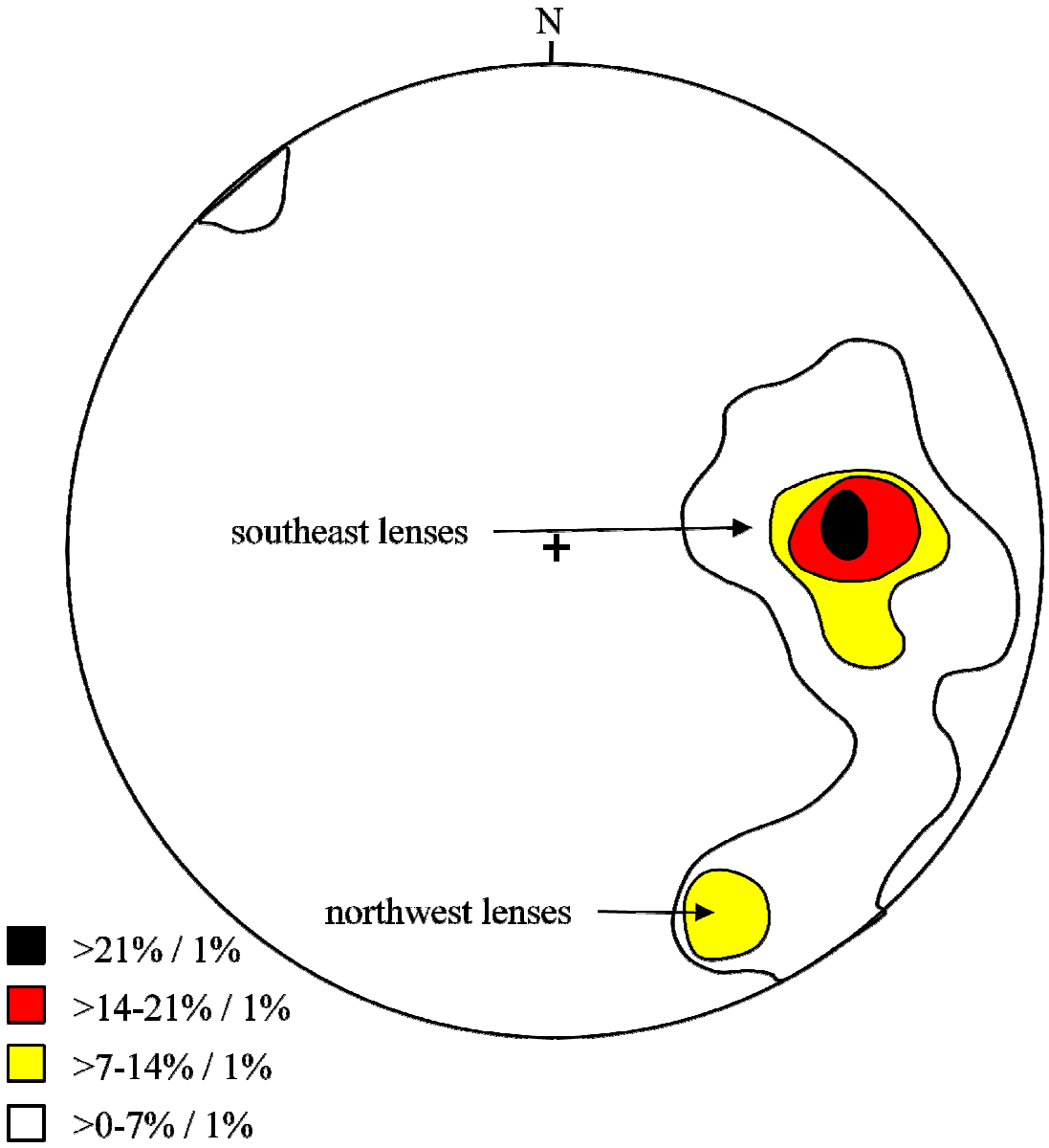

Figure 23: Lower-hemisphere stereographic contour plot of elongation lineations in retro-eclogite at the Myrland locality. Point maxima indicate lineations plunge moderately to the east and shallowly to the southeast. Legend denotes measurement density per 1% area. N = 31.

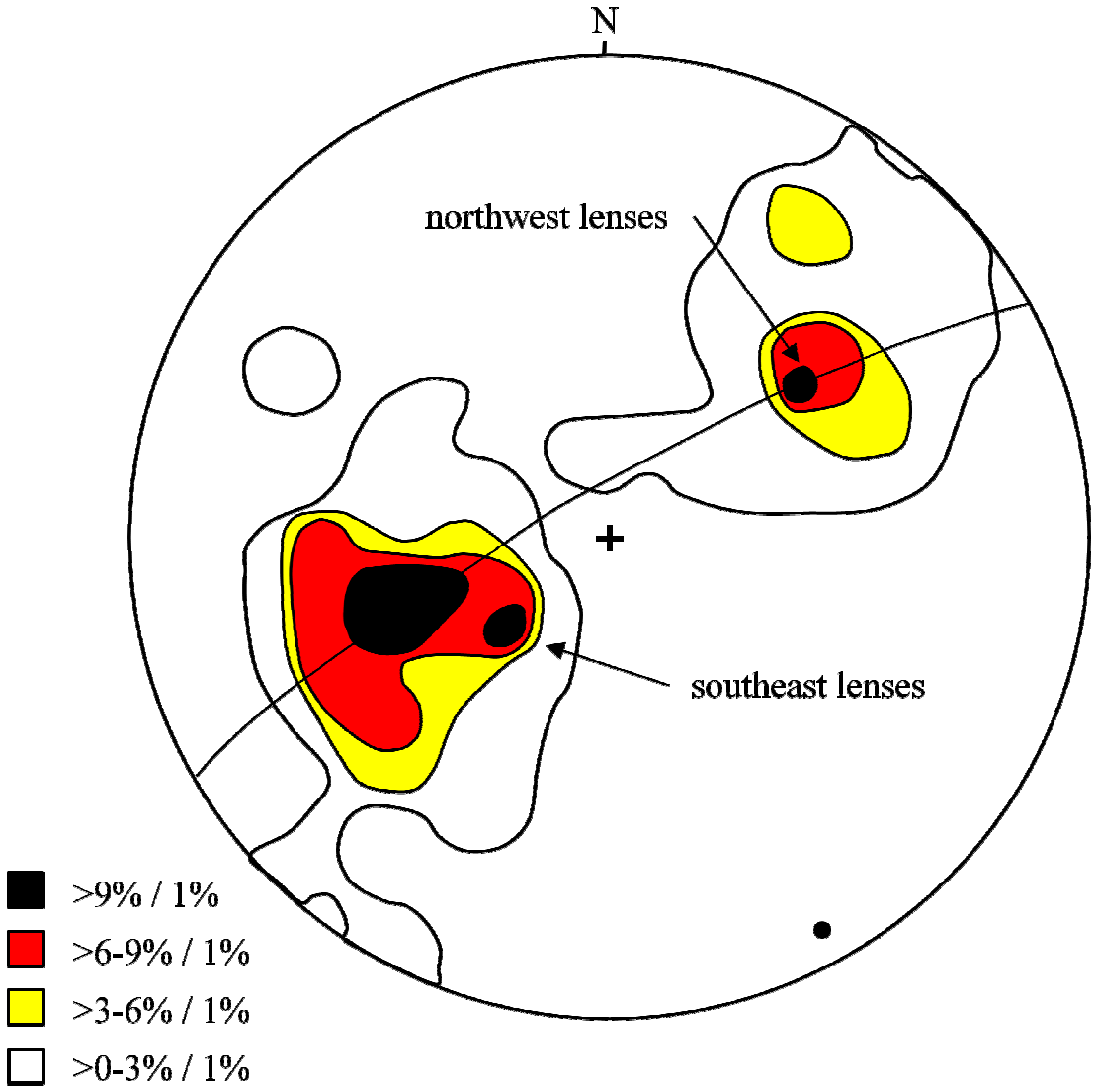

Figure 24: Lower-hemisphere stereographic contour plot of poles to foliations measured in retro-eclogite lenses at the Myrland locality. Point maxima are clustered in the northeast and southwest quadrants. β-axis (black dot) of visual best-fit great circle of poles to planes defined by the point maxima is oriented S28°E, 08°. Legend denotes measurement density per 1% area. N = 70.

4 and 24). Point maxima defined by poles to those foliations intersect with a β-axis oriented S28°E 08°; an interlimb angle of 104° is measured from the same geometric construction. Schistosity in amphibolite wraps around the retro-eclogite lenses (Figure 22) and also parallels the contact with the monzodioritic orthogneiss. Sheared amphibolite encapsulating the retrograde eclogite has acquired a much stronger foliation that generally strikes northwest and dips variably to the northeast and southwest (Figure 25). Comparison of Figures 4, 24, and 25 documents that foliations in the retrograde eclogite and amphibolite share a common strike direction, but the foliation of the northwest retrograde eclogite lenses dips in the opposite direction to the dominant foliation measured in the surrounding amphibolite. Although locally variable, the overall amphibolite foliation is oriented N30°W, 80°NE (Figure 25).

Weakly developed elongation lineations in retro-eclogite, defined by plagioclase and amphibole, plunge moderately to shallowly to the east in the southeast lenses and shallowly to the southeast in the northwest lenses (Figure 23). The difference in lineation orientations from the northwest and southeast exposures is appreciable, suggesting that the lineation has been reoriented together with the eclogite pod foliations. This interpretation is supported by the near-parallelism of the lineation with that defined by the intersection of the foliations (Figure 24). Amphibolite has a strong mineral lineation oriented S47°E, 25° that is defined by elongate biotite and clusters of small amphibole and plagioclase crystals (Figure 26). This lineation is consistent with those found in the

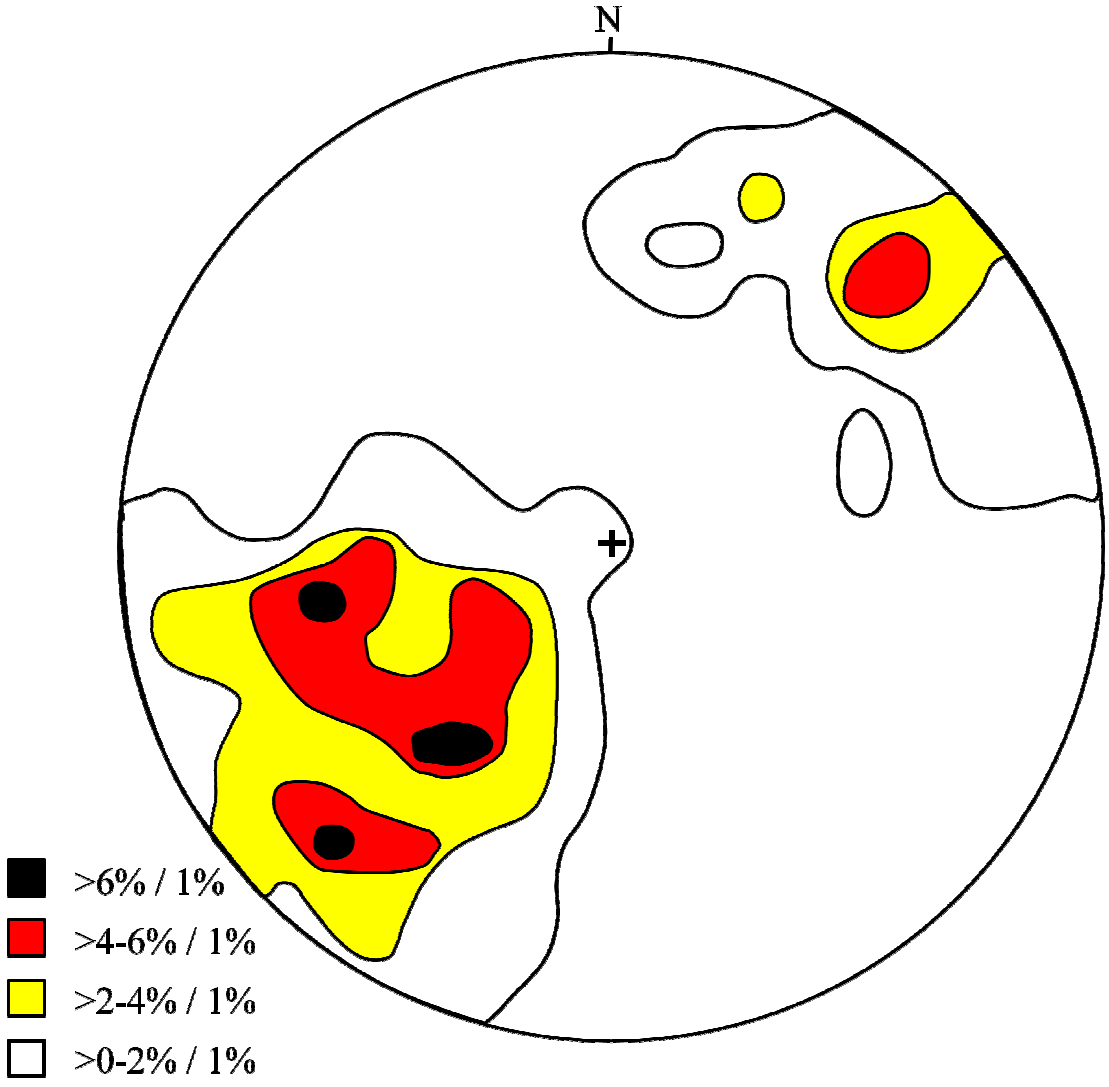

Figure 25: Lower-hemisphere stereographic contour plot of poles to schistosity in amphibolite at the Myrland locality. Point maxima are loosely concentrated in the southwestern quadrant. Legend denotes measurement density per 1% area. N = 150.

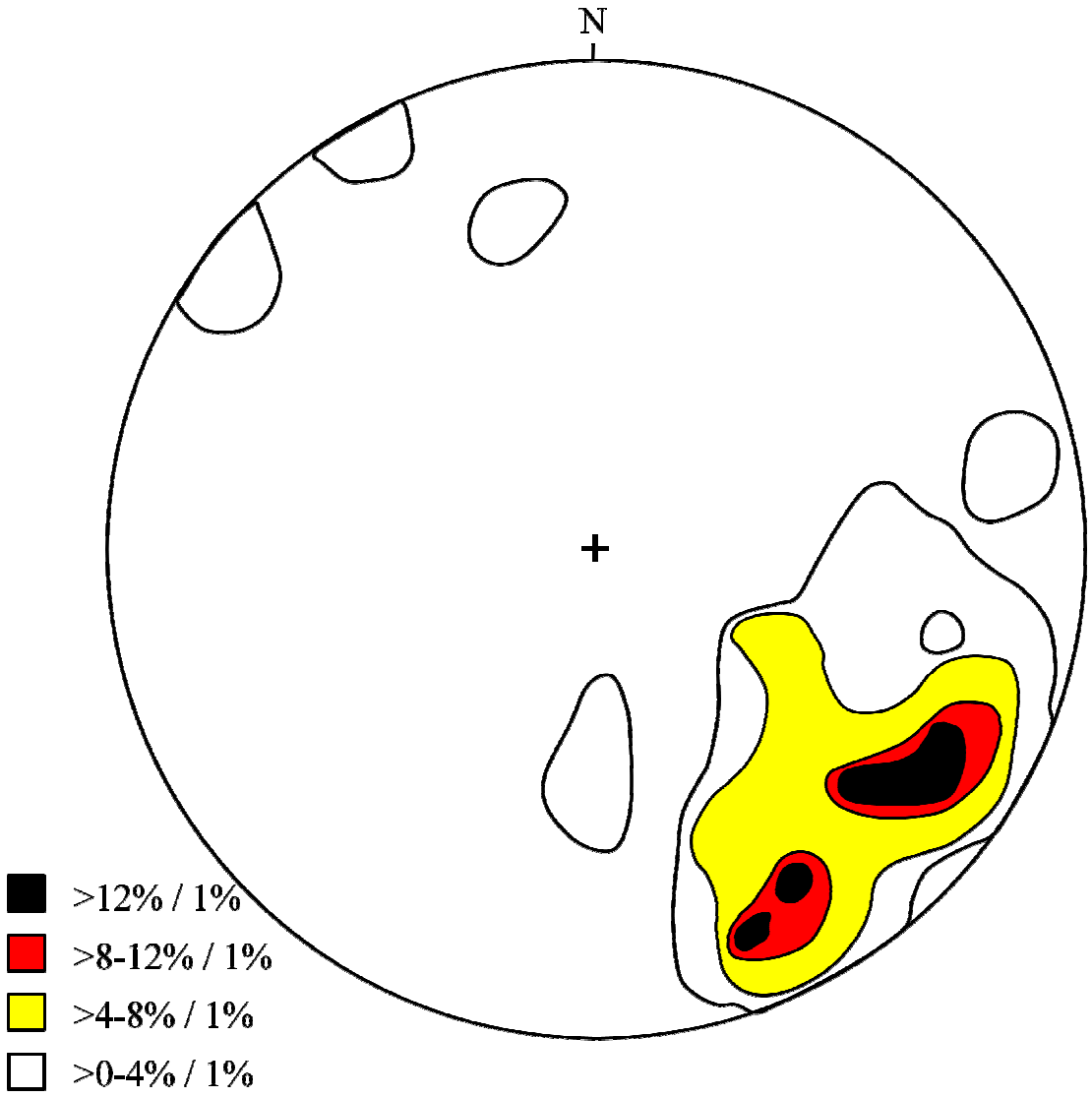

Figure 26: Lower-hemisphere stereographic contour plot of elongation and mineral lineations in amphibolite measured at the Myrland eclogite locality. Point maxima are concentrated in the southeast quadrant. Legend denotes measurement density per 1 % area. N = 63.

retrograded eclogite (cf., Figure 23). Shallowing of foliation dip within the southeastern lenses implies that the retro-eclogite cores may have been rotated with respect to the surrounding amphibolite as well as sheared during deformation.

In addition to this rotation, the retro-eclogite lenses also are folded and stretched in a direction perpendicular to the elongation lineation. This is consistent with the multiple phases of folds found to be restricted to the interior of the Myrland shear zone. These folds are all plastic styles, ranging from isoclinal to open, rarely displaying Ramsay type III interference patterns (Ramsay, 1962), and some have sheath-fold geometries (Figure 16). Fold axes generally are coaxial with the shallow, southeast-plunging elongation lineation. Figure 16b shows a well exposed, highly contorted and folded felsic vein. Early generation isoclines (F_1) with axial-planar schistosity are deformed by a later phase fold (F_2); resulting in type III "fish hook" interference patterns (Ramsay, 1962). Neither such styles nor intensity of folds were observed within the orthogneiss outside of the main shear zone. Orthogneiss-hosted felsic dikes are isoclinally folded, sheared, and foliated parallel to the isocline axial surface (Figure 16a).

Simple shear deformation zones are ubiquitous features in the monzodioritic orthogneiss at the Myrland locality (Figures 17 and 21). These are relatively small, crystal-plastic shears that cut the orthogneiss, felsic dikes, and other small shears. The shears are typically 1-3 cm wide and at least 1 m long, although discontinuous outcrop makes their absolute extent difficult to determine. Movement sense for individual shears is clearly marked by S-C composite fabrics and σ-clasts. In addition, these are classic Ramsay (1962) shears with foliation progressively developed and swept into the shear

zone from a non-foliated parent rock. Individual shears are randomly oriented and distributed, and show no obvious kinematic or geometric relationship. They displace felsic dikes (Figure 17) and also deflect, but do not truncate, other shears (Figure 21).

The most impressive structure at Myrland is a tremendous crystal-plastic shear zone, herein called the Myrland shear zone, where the monzodioritic orthogneiss is progressively mylonitized approaching the amphibolite contact, and ultimately reaches ultramylonite stage (Figure 27). Approximately 3 to 5 meters of thickness of orthogneiss is sheared along its northeast margin with the amphibolite contact. The Myrland shear zone is continuous northeastward across strike through the exposed amphibolite and retro-eclogite lenses and is submerged beneath the ocean. Northwestward, along strike, the shear zone projects beneath the sea and to the southeast it is covered by glacial sediments. The shear zone boundary within the orthogneiss is diffuse and the protomylonitic foliation parallels and grades into the gneissosity in the monzodioritic gneiss over a distance of ~4-5 m. Shear deformational fabric intensifies northward progressing from protomylonite through mylonite to ultramylonite before encountering the amphibolite (Figure 27).

Foliation within the Myrland shear zone strikes west-northwest and dips moderately to steeply to the northeast (Figure 28). Rare elongation lineations plunge shallowly to the east (Figure 28). Along eclogite pod boundaries the felsic veins are deflected in a dextral sense, consistent with the fold trains indicating overall right-lateral

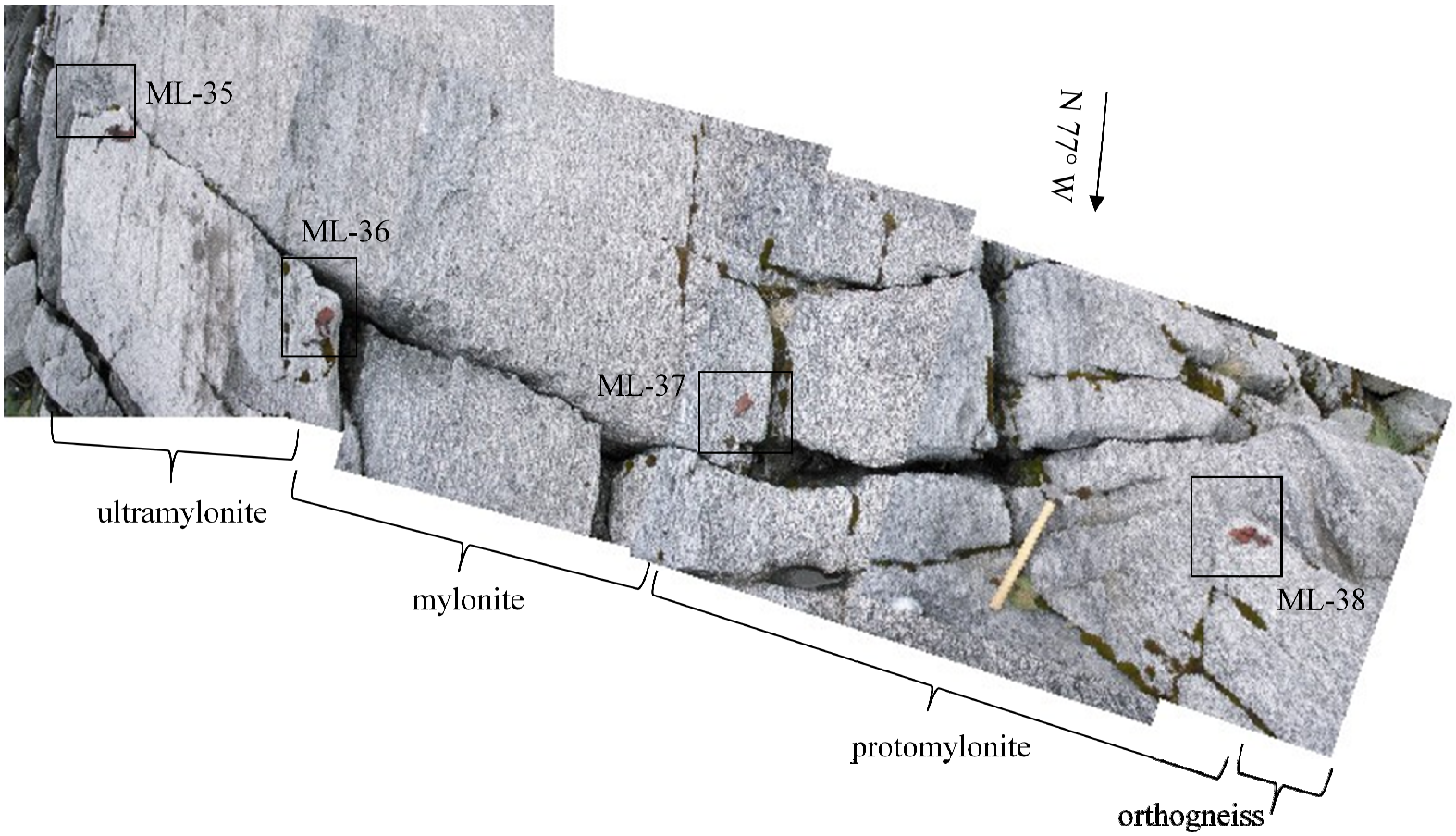

Figure 27: Photo mosaic that shows mylonite progression and geochemical sample locations from the Myrland shear zone. Hammer is ~35 cm long. View is vertical with mylonitic foliation oriented N~77°W, ~60°NE. Location is ~50 m northwest of the eclogite pods in Figure 4.

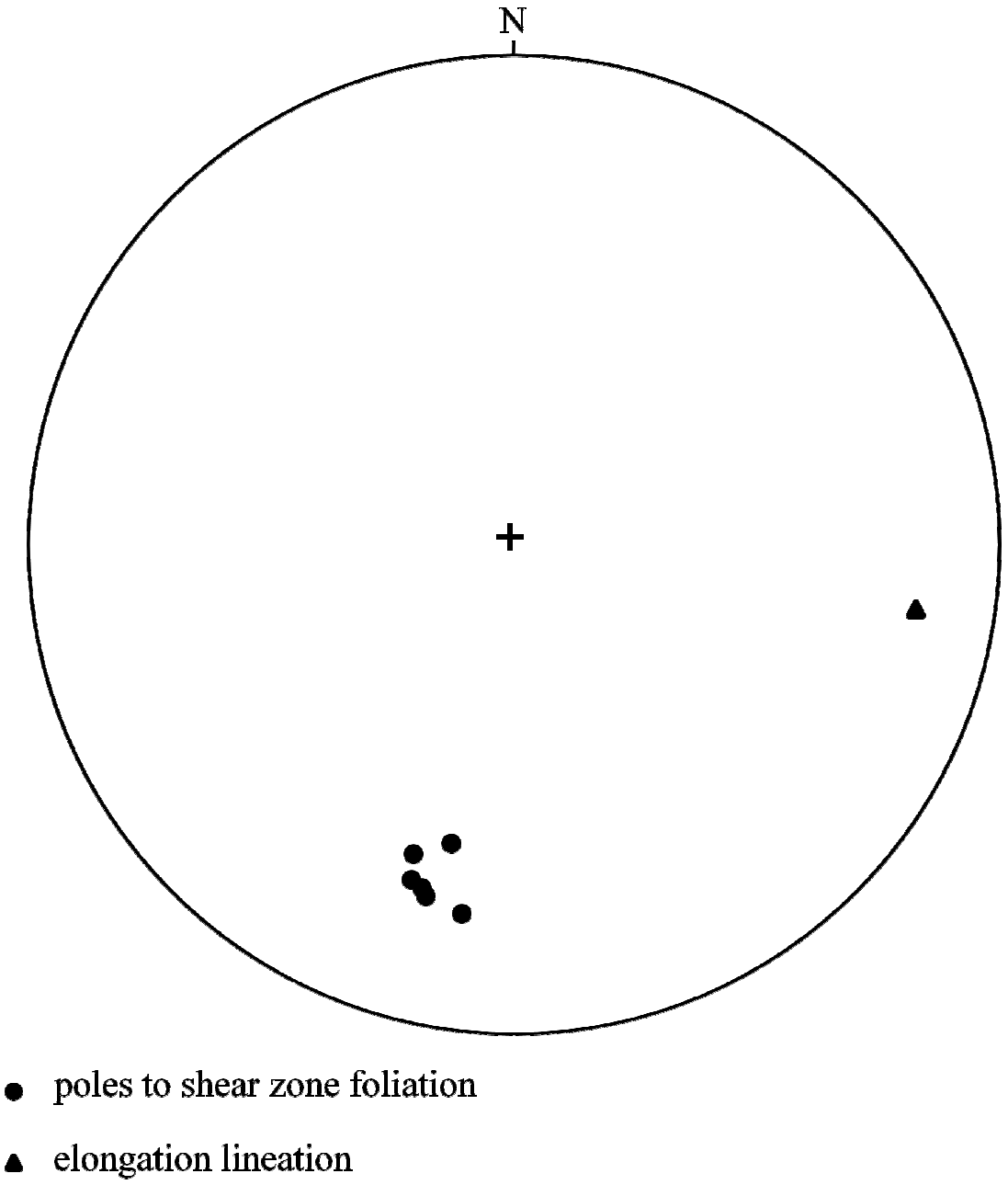

Figure 28: Lower-hemisphere stereographic projection of poles to Myrland shear zone mylonitic foliation (N = 6) and elongation lineation (N = 1).

shear sense (Figure 4). These observations, combined with the data in Figure 28, indicates that the Myrland shear zone is primarily a right-lateral, strike-slip shear zone with a lesser component of oblique reverse dip-slip displacement.

In minimally sheared orthogneiss (sample ML-38, Figure 27), plagioclase has abundant growth twins and straight to curvilinear grain edges that meet at triple-point boundaries, defining an equigranular, polygonal fabric. Average plagioclase grain size is 0.8 – 1.0 mm. Amphibole and biotite are undeformed but weakly aligned. Amphibole is arrested during decomposition to quartz and biotite. Epidote and titanite form at the expense of biotite, plagioclase, and opaques.

As mylonitization increases (samples ML-37 to ML-36), plagioclase average grain size decreases to 0.5 – 0.8 mm and the fabric defined by plagioclase grades to inequigranular-seriate and interlobate. Plagioclase grain bulges, nucleations, and growth twins are common, subgrains and deformation twins are present but rare. Evidence for plastic deformation was only observed in plagioclase. Amphibole is absent from ultramylonite (sample ML-35), presumably completely reacted to biotite, epidote, and quartz. Biotite is strongly aligned and is twice as abundant as in non-mylonitized orthogneiss (23% vs. 11%, Table 4). Epidote, altered from biotite, amphibole, and plagioclase, has also doubled its volume (5.5% vs. 2.25%, Table 4). These reactions appear to have followed $Am \rightarrow Bt + Qz$, followed by (or perhaps simultaneously with) $Pc + Bt + Qz \rightarrow Ep + Kfs$.

Increasing mylonitic fabric development and higher abundance of hydrous phases, including biotite and epidote, into the Myrland shear zone suggest fluid encroachment as

the controlling factor in shear formation. This fluid was likely derived externally, similar to that documented at Nusfjord (Kullerud, 1992, 1996; Kullerud and Erambert, 1999; Kullerud et al., 2001). The infiltration mechanism is not known at the time of this report.

The small shears discussed above are confined to the margins of the larger Myrland shear zone. Proximal location and cross-cutting relations indicate that these small shears formed broadly contemporaneous with the Myrland shear zone, likely in order to accommodate movements and volume change that occurred in the latter.

Mineral, chemical, and volume changes in the Myrland shear zone

The progressive shearing of the non-eclogitized orthogneiss into the Myrland shear zone presents itself to the investigation of mineralogical, chemical, and volume changes associated with its development. Four orthogneiss samples, ML-35 through ML-38, ranging from most strongly to least mylonitized, respectively, were collected for geochemical and density analysis (sample locations on Figure 27, geochemical data in Tables 5 and 6, density data in Table 8). One sample from the sheared mafic package, ML-31, was also collected for similar purposes (Tables 5, 6, and 8).

Density measurements for the samples increase with shearing intensity from 2.82 to 2.92 g/cm^3 (Table 8). Major oxide and trace element geochemical data for these samples are shown in Tables 5 and 6, respectively. Due to the identical density of samples ML-35 and 36, it was assumed that these two samples experienced the same degree of chemical alteration. Therefore, major oxide data for these two samples has been averaged in Table 5 and were used throughout this report. Data were scaled to

Sample	Density (g/cm^3)	Rock type or position in shear zone
ML-31	3.21	retro-eclogite
ML-35	2.92	ultramylonite
ML-36	2.92	ultramylonite near mylonite transition
ML-37	2.86	mylonite near protomylonite transition
ML-38	2.82	protomylonite near shear zone margin

Table 8: Measured densities of geochemical samples (location shown in Figure 27), plus a representative retrograde eclogite sample, ML-31.

100%. This data and Table 6 were used in generating Figure 29, which compares the oxide and trace element concentrations of the highly sheared composite sample ML-35/36 and the relatively unsheared sample ML-38. Major oxides are plotted by measured weight percent. Trace elements are plotted according to their measured concentration in parts per million (mg/kg). Cr_2O_3 was not present in measurable amounts in any sample and trace elements Ce, Er, La and Yb did not show any trend across the sample suite. These analyses, thus, were excluded from the diagram.

The best-fit isocon on Figure 29 was determined visually to be defined by CaO, K_2O, MgO, MnO, Fe_2O_3 and Y. This isocon has the equation $C^A=1.07C^O$; where C^A is final concentration (ultramylonitized rock) and C^O is original concentration (unsheared rock). This corresponds to a mass loss of 6.5% and a volume loss of 9% during shearing. An alternate isocon is defined by SiO_2 and Al_2O_3; these are near-colinear with the constant mass isocon. Mobilization and transportation of silica and alumina during shearing is considered more likely than enrichment in Ca, K, Mg, Mn, Fe, and Y, hence the choice of the best-fit isocon rather than the constant mass isocon. BaO, Sm, Ho, Pr and Nd lie on a common line with slope of 1.13. Trace element enrichment may indicate fluid migration through the sheared rocks. TiO_2 and P_2O_5 lie on one line and U and LOI on another, but these are suspected to be coincidence rather than indicative of geochemical coupling.

Comparing sheared rock to unsheared, concentration losses include silica (-6.9%), alumina (-11.3%), Na_2O (-10.8%), volatiles reported as LOI (-27.7%), and uranium (-26.9%). Gains include TiO_2 (+16.1%), P_2O_5 (+16.1%), Nd (+7.3%), and Pr (+10.8%).

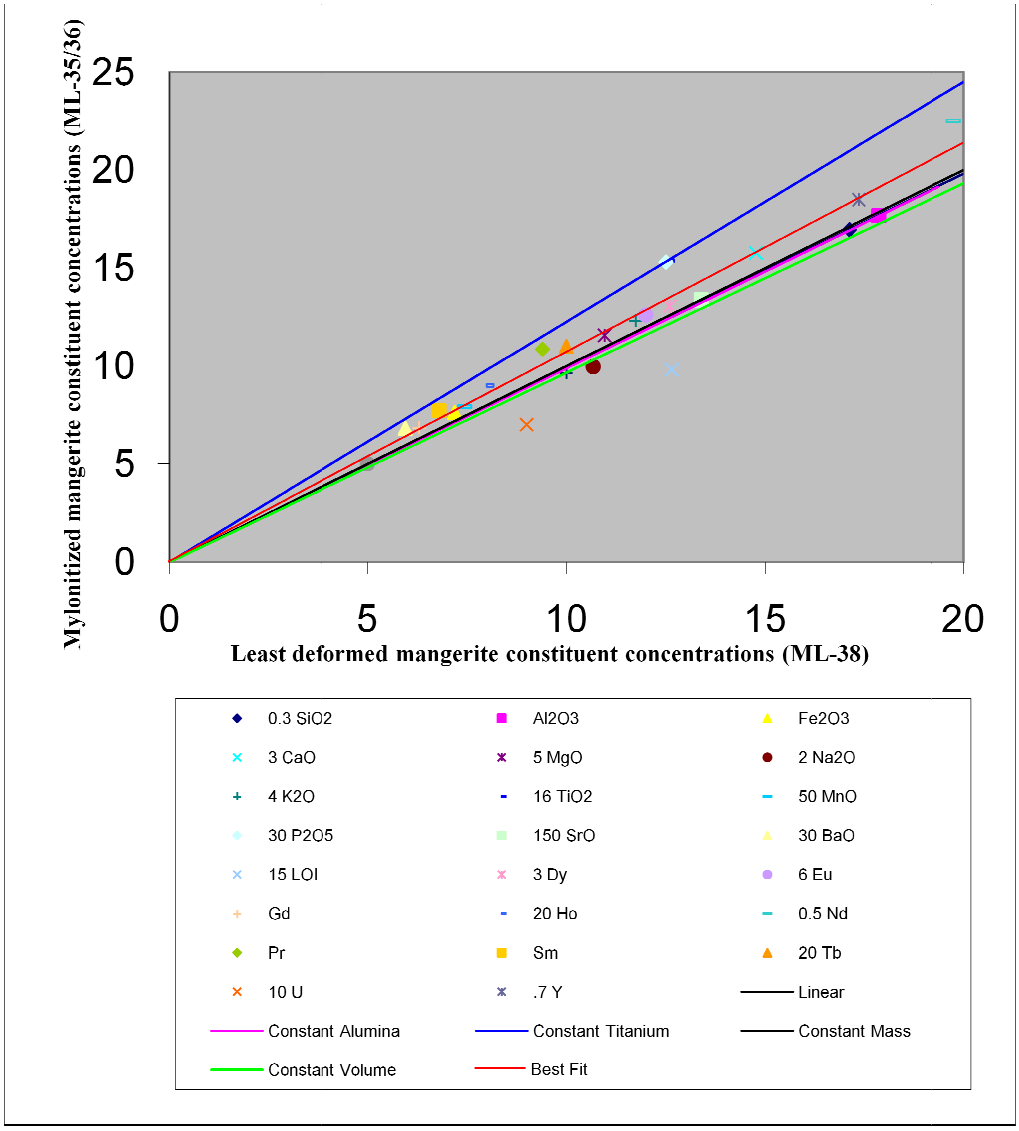

Figure 29: Isocon diagram comparing geochemical data for strongly sheared and relatively unsheared samples ML-35/36 and ML-38, respectively. Units are weight percent for oxides and mg/kg for trace elements. Concentrations are multiplied as shown, using methods reported by Grant (1986).

The estimated loss of silica and alumina is reflected in petrographic analysis (Table 4), which shows an overall 63% loss of free quartz and a 10% loss of feldspar in the shear zone. The decrease of twinned feldspar grains in the shear zone sample may reflect the increase in CaO and decrease in Na_2O, which may indicate a transition to calcic feldspars and the mobilization and removal of Na. Al_2O_3 also decreases in sheared rocks, which may contribute to a decrease in twinned feldspars. TiO_2 increases are reflected in the slight increases in sphene and opaque minerals. Fluid migration may be responsible for deposition or removal of trace elements in the same manner as the Cl-rich fluids, which infiltrated the Nusfjord locality (Kullerud, 1992, 1996; Kullerud and Erambert, 1999; Kullerud et al., 2001).

The "isocon" method also lends itself to exploring the formation of the eclogites and felsic injections. Two scenarios exist for eclogite protolith, a mafic xenolith or intrusion in the orthogneiss, or the separation of parent monzodioritic orthogneiss into concentrated felsic and mafic zones. If the eclogite formed from a mafic inclusion, as previous investigations have suggested for other Flakstadøy eclogites (Markl and Bucher, 1997; Kullerud et al., 2001) then the orthogneiss and eclogite would have no geochemical relationship. If, however, the eclogite formed from melanosomal material separated from the orthogneiss, then there should be a geochemical link. The comparison requires the assumption that mass was not gained or lost during the amphibolite-facies retrogression as the chemical composition of retrograded eclogite (amphibolite), not pristine eclogite, is compared to that of the orthogneiss and the felsic injection. The following analysis stemmed from field observations from the Storvatnet eclogite locality (described below)

that indicate mobilization of leucocratic material into felsic veins like those present at Myrland. Figure 30 compares the constituent concentrations of retrograde eclogite (sample ML-31) with those of orthogneiss. TiO_2, CaO, and Fe_2O3 define a weak linear relationship with a slope of 1.69. This corresponds to a proposed mass loss of 41% and a volume loss of 48% if eclogite formed from monzodioritic orthogneiss. SiO_2, Al_2O_3, MnO, P_2O_5, Na_2O, and K_2O would be depleted. Only Mg shows enrichment. Several other possible isocons exist but all have slopes less than 1.69. For the purposes of this model, the eclogite is considered to have formed due to depletion of felsic constituents rather that enrichment of mafic ones. Therefore, the selection of the isocon with the steeper slope is favored.

Comparison of felsic injection geochemical concentration data (sample ML-42) with the calculated mass lost in the hypothetical transition from monzodioritic orthogneiss (sample ML-38) to eclogite (sample ML-31) shows no indication that there is a geochemical relationship between the retrograde eclogite, felsic veins, and monzodioritic orthogneiss host rock. Calculations for this scenario are presented in Table 9. Based on these data and on field relationships, the conclusion is that the retrograde eclogite protolith was a mafic inclusion within the host orthogneiss.

It is still possible, however, to hypothesize that the felsic veins formed by mobilization of constituents from the orthogneiss, chemically independent of eclogite formation. If this is true, ultramylonitized orthogneiss (sample ML-35/36) would be depleted in felsic constituents relative to unsheared orthogneiss (sample ML-38). For this purpose Figure 29 serves as the comparison of ‘melanosome’ (sample ML-35/36) to

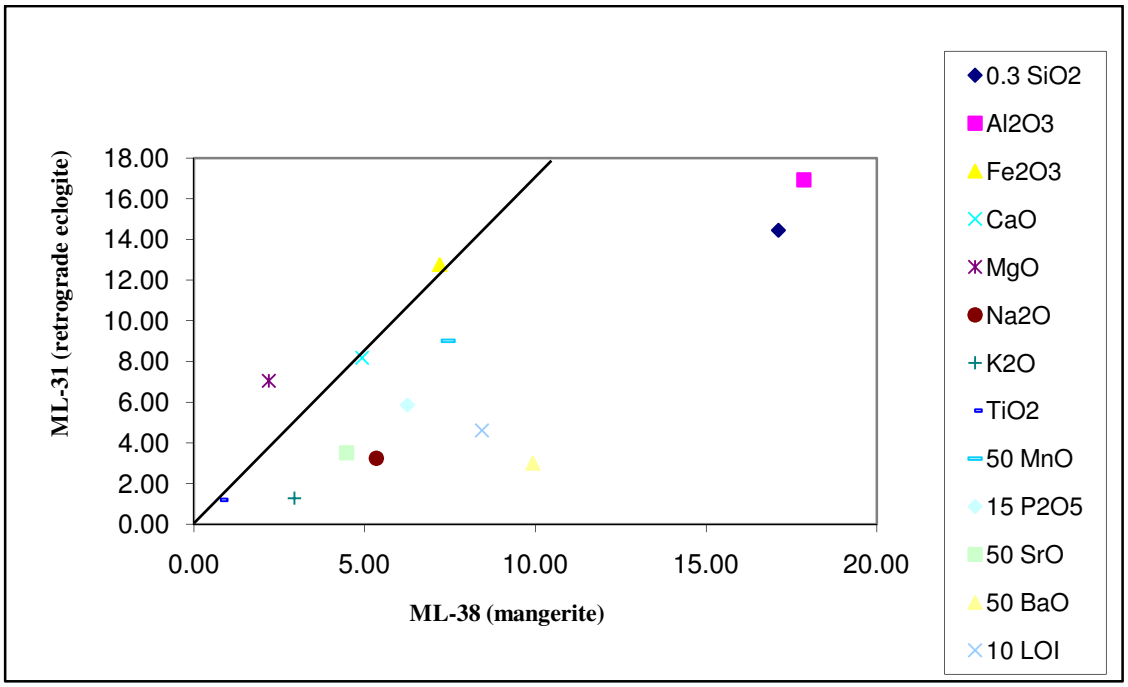

Figure 30: Isocon diagram comparing geochemical data from ML-31 (retrograded eclogite) and ML-38 (unsheared monzodioritic orthogneiss). Multiple possible isocon lines are possible. Only the isocon with the steepest slope is depicted.

Major Oxide	Wt % normalized to 100%					
	ML-31	ML-38	ML-42	A	B	C
SiO_2	48.18	57.07	75.87	27.53	29.53	68.91
Al_2O_3	16.93	17.86	13.63	9.67	8.19	19.11
Fe_2O_3	12.77	7.20	0.88	7.30	-0.10	-0.24
CaO	8.18	4.92	1.34	4.68	0.25	0.57
MgO	7.05	2.19	0.99	4.03	-1.84	-4.28
Na_2O	3.25	5.34	4.36	1.85	3.48	8.13
K_2O	1.28	2.94	1.56	0.73	2.20	5.14
Cr_2O_3	<0.01	<0.01	<0.01	<0.01	<0.01	<0.01
TiO_2	1.19	0.78	0.10	0.68	0.10	0.24
MnO	0.18	0.15	0.01	0.10	0.05	0.11
P_2O_5	0.39	0.42	0.02	0.22	0.19	0.45
SrO	0.07	0.09	0.10	0.04	0.05	0.11
BaO	0.06	0.20	0.12	0.03	0.16	0.38
LOI	0.46	0.84	1.03	0.26	0.58	1.35
Total	100.00	100.00	100.00	57.14	42.86	100.00

Column	Description
A	mass remaining in eclogite based on 100g orthogneiss protolith
B	mass forming felsic dike based on 100g orthogneiss protolith
C	felsic dike mass (B) recalculated to 100%

Table 9: Data for comparison of felsic injection with the calculated mass lost during the hypothetical transition from monzodioritic orthogneiss to eclogite.

'paleosome' (sample ML-38), revealing the mass flux during the hypothetical removal of felsic constituents. If the felsic dike was created from material lost by orthogneiss, constituent concentrations would lie along a line with a slope of 1 (y = x), however, comparison reveals no clear coupling relationships between any constituents. Data for this comparison is present in Table 10. This implies that either the veins were not derived from partial melting of the orthogneiss or that significant mobilization of all constituents took place.

Geochronology

A sample was taken from the felsic dike at location B in Figure 4 (see also Figure 18) within one of the retrograded eclogite lenses in order to constrain better the time of mangeritic intrusion, dike intrusion, eclogitization, and deformation. Sample AA03-3 is a fine grained, white syenogranite with a strongly developed foliation defined by mica grains aligned in rather distinct layers. Muscovite is of generally larger grain size and also dominates over brownish-green biotite. Quartz is the predominant mineral and it occurs as recrystallized quartz bands. Feldspar occurs as newly crystallized tiny grains, both K-feldspar and plagioclase. Felty green patches of feldspar alteration products are common. These patches contain muscovite as well as both clinozoisite laths and to a minor degree epidote. Rutile, opaque minerals, zircon and very rare xenotime constitute the accessory phases.

The zircon population of the sample is rather homogeneous and most grains are fractured but transparent. Size varies widely and color ranges from colorless to pink and

	Wt % normalized to 100%					
Oxide	ML-35/36	ML-38	ML-42	A	B	C
SiO_2	56.49	57.07	75.87	52.80	4.27	65.25
Al_2O_3	17.65	17.86	13.63	16.50	1.37	20.91
Fe_2O_3	7.63	7.20	0.88	7.13	0.06	0.99
CaO	5.25	4.92	1.34	4.91	0.01	0.20
MgO	2.31	2.19	0.99	2.16	0.03	0.49
Na_2O	4.98	5.34	4.36	4.66	0.68	10.46
K_2O	3.08	2.94	1.56	2.88	0.06	0.91
Cr_2O_3	<0.01	<0.01	<0.01	<0.01	<0.01	<0.01
TiO_2	0.96	0.78	0.10	0.90	-0.11	-1.74
MnO	0.16	0.15	0.01	0.15	0.00	0.01
P_2O_5	0.51	0.42	0.02	0.48	-0.06	-0.91
SrO	0.09	0.09	0.10	0.08	0.01	0.09
BaO	0.23	0.20	0.12	0.21	-0.01	-0.22
LOI	0.65	0.84	1.03	0.61	0.23	3.56
Total	100.00	100.00	100.00	93.46	6.54	100.00

Column	Description
A	mass remaining in sheared rock based on 100g orthogneiss (ML-38) protolith
B	mass forming felsic dike based on 100g orthogneiss (ML-38) protolith
C	felsic dike mass (B) recalculated to 100%

Table 10: Data for comparison of felsic injection with calculated mass lost in ultramylonitized relative to unsheared monzodioritic orthogneiss.

purplish-pink. Almost all grains are prismatic, with differing aspect ratios, although a few multifaceted grains occur. No obvious rims were observed. Xenotime is very rare, but the grains present are euhedral and have a grayish pink color. Ten zircon fractions and one xenotime crystal were analyzed, which ranged from single grains to multigrain fractions and fragments. In general the analyzed grains were free of inclusions, fractures and turbidity (further descriptive details in Table 11).

The country rock has an age of ca. 1800 Ma (Corfu, 2004b). The sampled pod of melt associated with the eclogites contains a population of inherited zircon, which all are discordant, variably between 1.5 and 22%. The upper intercepts and hence the ages of the xenocrystic zircon seem to range between 1780 and 1810 Ma, projecting the analyses individually. Due to the scatter of upper intercepts, a lower intercept, even if there is a common one is difficult to calculate and will thus have a large error. Despite those circumstances it is possible to calculate a speculative discordia line. A line including all ten analyses have an upper intercept at 1799 ± 11 Ma and a lower intercept at 485 ± 90 Ma (MSWD =18) (Figure 31). The statistics of this line is poor, which is dominantly due to the scatter of inheritance ages. The differing properties of individual fractions, such as common lead content or whether single- or multigrain fractions are analyzed are also of relevance. Such is for example the case with analysis C, which is 15 % discordant, but has a rather high common lead content (Table 11). Analyses B and J appear to have a slightly younger xenocrystic component than the other analyzed fractions. If those analyses are discarded in the calculation, an upper intercept is found at 1800 ± 5 Ma and the lower intercept at 478 ± 41 Ma (MSWD = 4) (Figure 31).

Fraction[a]	Weight (µg)	U (ppm)	Th/U[b]	Pb_{com}[c] (pg)	$^{206}Pb/^{204}Pb$[d]	$^{207}Pb/^{235}U$[e]	2 s (abs)	$^{206}Pb/^{238}U$[e]	2 s (abs)	r	$^{207}Pb/^{206}Pb$[e]	2 s (Ma)	Disc.[f] (%)
A- clabfr	7	763	0,29	5,2	18343	427,916	0,02401	0,28690	0,00159	0,987	1768,9	1,6	9,1
B- lpabfr	32	45	0,30	8,1	3493	472,100	0,01821	0,31409	0,00125	0,855	1783,0	3,8	1,4
C- sprclabfrS	8	365	0,24	52,5	915	373,397	0,01699	0,25816	0,00103	0,858	1712,6	4,3	15,2
D- lpabfr	19	284	0,27	8,0	12460	443,309	0,01079	0,29613	0,00065	0,959	1775,6	1,3	6,6
E- sclmfS	1	492	0,36	1,8	5063	448,683	0,01494	0,29982	0,00096	0,922	1775,0	2,4	5,4
F- clfrS	1	461	0,15	3,5	1950	333,813	0,01280	0,23363	0,00089	0,850	1690,1	3,8	22,1
G- stprclabS	4	491	0,23	2,1	16992	428,141	0,01224	0,28741	0,00081	0,913	1766,6	2,2	8,8
H- stprclabS	6	2456	0,23	15,6	17079	428,564	0,01298	0,28791	0,00085	0,943	1765,3	1,8	8,6
I- stprclabS	3	678	0,30	0,7	59527	463,677	0,02044	0,30776	0,00133	0,984	1787,3	1,4	3,7
J- sprab	1	375	0,29	0,8	8094	419,008	0,01638	0,28077	0,00110	0,932	1770,0	2,6	11,1
Xen- peuS	2	886	1,14	7,04	4256	985,501	0,03941	0,65904	0,00335	0,722	1773,6	6,4	-108,1

All analyses were corrected for blanks of 2 pg Pb and 0.1 pg U.

[a] cl- colourless, ab- abraded, fr- fragment(s), l- large, p- pink, s- small, pr- prismatic, S- single, mf- multifaceted, st- stubby, Xen-xenotime, eu-euhedral

[b] model value calculated using the 208Pb/206Pb ratio and the age of sample

[c] total common Pb (including initial common Pb of sample and analytical blank)

[d] corrected for spike contribution and fractionation

[e] corrected for spike, fractionation, blank and initial common lead

[f] degree of discordance

Table 11: Table containing details for grains analyzed for U/Pb dating.

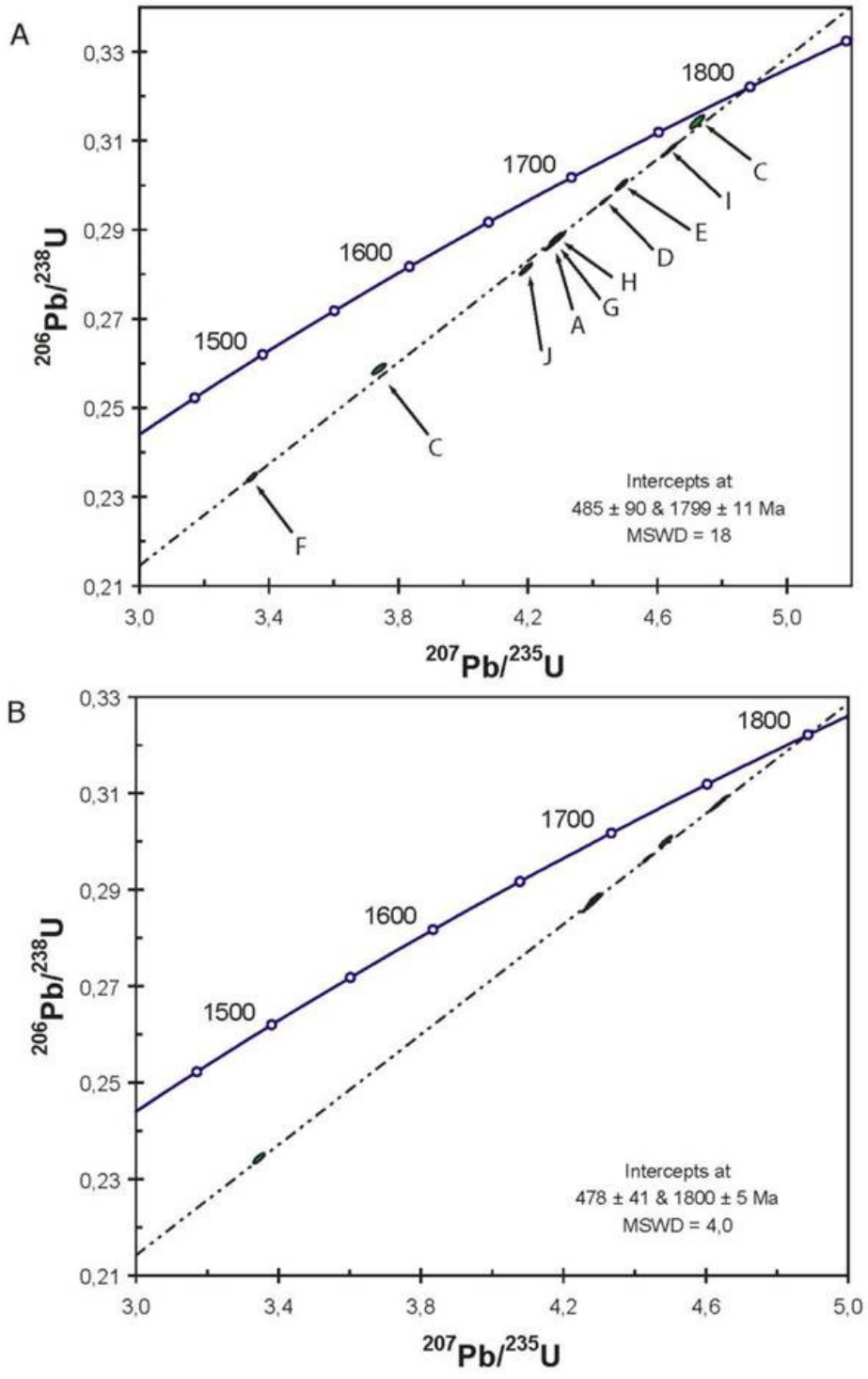

Figure 31: Upper discordia intercept for zircon grains.

Analysis F is the most discordant (22%). This analysis strongly guides the discordia towards the lower intercept. The analyzed fraction is a single colorless tip with average contents of U and Pb. However, in comparison with the other analyzed fractions, it has a conspicuously low Th/U. Varying Th/U ratios are often attributed to varying magmatic or metamorphic conditions during crystallization of different phases. Zircon formed under eclogite-facies conditions commonly have remarkably low Th/U ratio (e.g. Rubatto et al. 1999). The lower Th/U of analysis F may, therefore, indicate that a proportion of the analyzed zircon crystallized during metamorphic (i.e. eclogitic) conditions.

The xenotime analysis is very strongly reversely discordant due to anomalous behavior of the uranium. The cause of this is not known. This makes the data difficult to interpret and possibly the $^{207}Pb/^{206}Pb$ age is the most reliable estimate of the crystallization age of the xenotime. This age is 1774 ± 6 Ma (Figure 32) and this probably records the crystallization age of the vein as well. Xenocrystic xenotime has been documented by Viskupic and Hodges (2001), but this was in low-temperature anatectic melts and it is not certain that these conditions are comparable to the situation studied here. Furthermore, xenotime has not been documented anywhere else in the Lofoten Complex (Corfu, 2004b, Markl et al., 1998, Rehnström, 2003). It is, therefore, unlikely that the analyzed xenotime is inherited.

The 1800 ± 5 Ma date for intrusive crystallization of the felsic vein intruding eclogitized rocks at Myrland is compatible with previous reports (Griffin et al., 1978). The timing of eclogitization is less certain. Markl and Bucher (1997) assigned

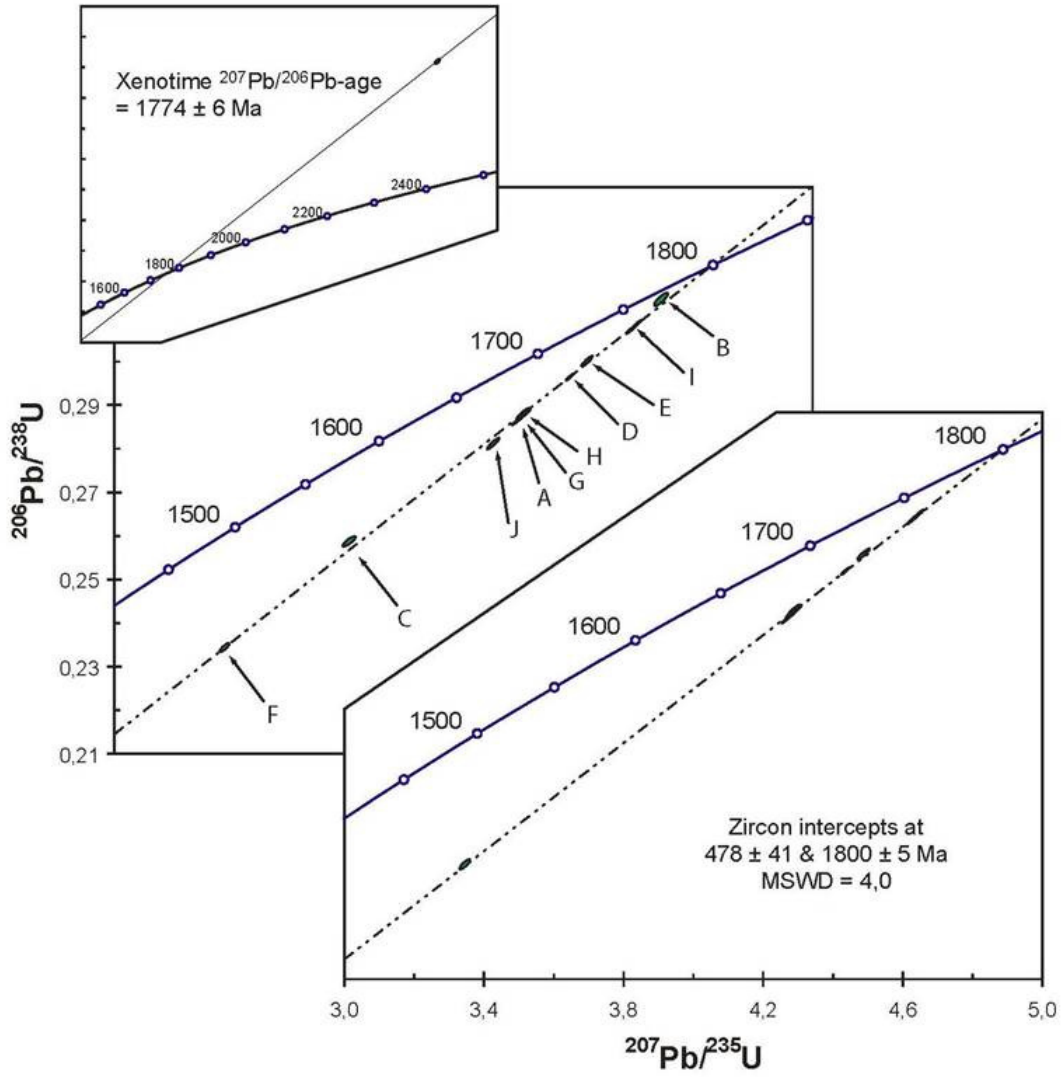

Figure 32: Upper discordia intercepts for zircon and xenotime grains.

eclogitization to the 1.1 Ga "Leknes Event" of Griffin et al. (1978), but subsequent studies have refuted this interpretation (Steltenpohl et al., 2003; this report). The lower intercept age of 478 ± 41 Ma, reported herein, records deep subduction of continental basement rocks. Recently, Corfu (2004a) reported U-Pb ages which place amphibolite-facies metamorphism and deformation of the Leknes Group between 461 and 469 Ma, which that author also interprets as the time of emplacement onto the Lofoten basement. Although not directly related to timing of eclogitization, these dates are compatible with deep crustal subduction at 478 Ma. Steltenpohl et al. (2004) reported a $^{40}Ar/^{39}Ar$ date of 433 ± 9 Ma for hornblende from the retrograde eclogite at Nusfjord that records cooling through the 500 °C isotherm during continued, slow exhumation.

Interpretations and Conclusions from the Myrland Investigation

Mafic enclaves of gabbroic composition were included in orthogneiss now exposed at the northern tip of Flakstadøy (Markl and Bucher, 1997), which was emplaced at 1800 ± 5 Ma. Both the orthogneiss and gabbro were cut by a syenogranitic dike at 1774 ± 6 Ma. Based on U-Pb dates obtained from mineral separates from this dike, eclogitization of the gabbroic inclusions is loosely constrained to 478 ± 41 Ma.

The package of monzodioritic orthogneiss host rock, amphibolite, and retrograde eclogite displays a sequence of pervasive but variable deformation intensity. D_1 deformation formed the S_1 foliation preserved in retro-eclogite, and is interpreted as synchronous with prograde eclogite-facies metamorphism. Retro-eclogite pod geometry and internal fabric, fabrics in amphibolite, and the Myrland shear zone and associated

smaller-scale shears are all interpreted as amphibolite-facies D_2 products. Any pre-existing foliation that may have existed in amphibolite or adjacent orthogneiss (S_0 and/or S_1) has been mostly obliterated.

During D_2 eclogite pods were progressively sheared from outside inward. Initial D_2 conditions were likely eclogitic allowing crystal-plastic fabrics to develop in the eclogite. Felsic dikes are weakly deformed within eclogite pods (note right-angle bends in Figure 4) but within amphibolite the dikes are severely plastically stretched and necked. This disparity requires injection of the felsic veins into a brittle stockwork prior to eclogitization and relatively brittle behavior of the pods after eclogitization. The eclogite cores were rigid and did not participate in D_2 shearing to the extent that the margins of the eclogite did. Somewhat analogous to a competent clast within a ductile shear zone, progressive shearing allowed the interior eclogite 'knockers' to be tumbled within the amphibolite, the latter being a more-retrograded version of the outer parts of the original eclogite. This accounts for the preserved garnet relics and limited development of plastic structures in the cores of the retro-eclogite lenses. The Myrland shear zone is a substantial D_2 structure that encapsulates the retro-eclogite pods. This steeply dipping, right-slip shear zone has a slip line that trends S 77° E and plunges shallowly, roughly parallel to the direction of emplacement of Caledonian allochthons onto the mainland. Anhedral, post-eclogitic amphibole replaces and preserves the characteristic shape of garnet, implying static conditions for the final phase of retrogression at Myrland (Figure 7).

NUSFJORD ECLOGITE LOCALITY

Overview

The Nusfjord eclogite locality is located less than one kilometer west of the small community of Nusfjord at the southern end of Flakstadøy (Figure 3; UTM: 33W, 430127 E, 7547640 N). The Nusfjord eclogites are an unusual style of 'shear zone' eclogites, and they contrast sharply with the pod-like occurrences described for Myrland and Storvatnet (see below). The Nusfjord locality was originally mapped by Romey (1971) and the eclogites were first described by Wade (1985). Further petrological and geochemical investigations on the eclogites are reported by Kullerud (1992, 1996), Markl and Bucher (1997, 1998), Kullerud and Erambert (1999), and Kullerud et al. (2001). No structural analysis is published leaving us with an incomplete understanding of how shear deformation accommodated eclogitization.

Kullerud et al. (2001) describe three shear zones at Nusfjord with varying degrees of eclogitization. During the present study a fourth eclogite shear zone was discovered (IV in Figure 33). Markl and Bucher (1997) state that one shear zone in this location is traceable over a distance greater than 2 kilometers, but this could not be verified during this investigation. Exposed shears ranged from ~75 meters to ~250 meters in strike length. The extent of the new shear zone is not known due to inaccessible cliff faces in

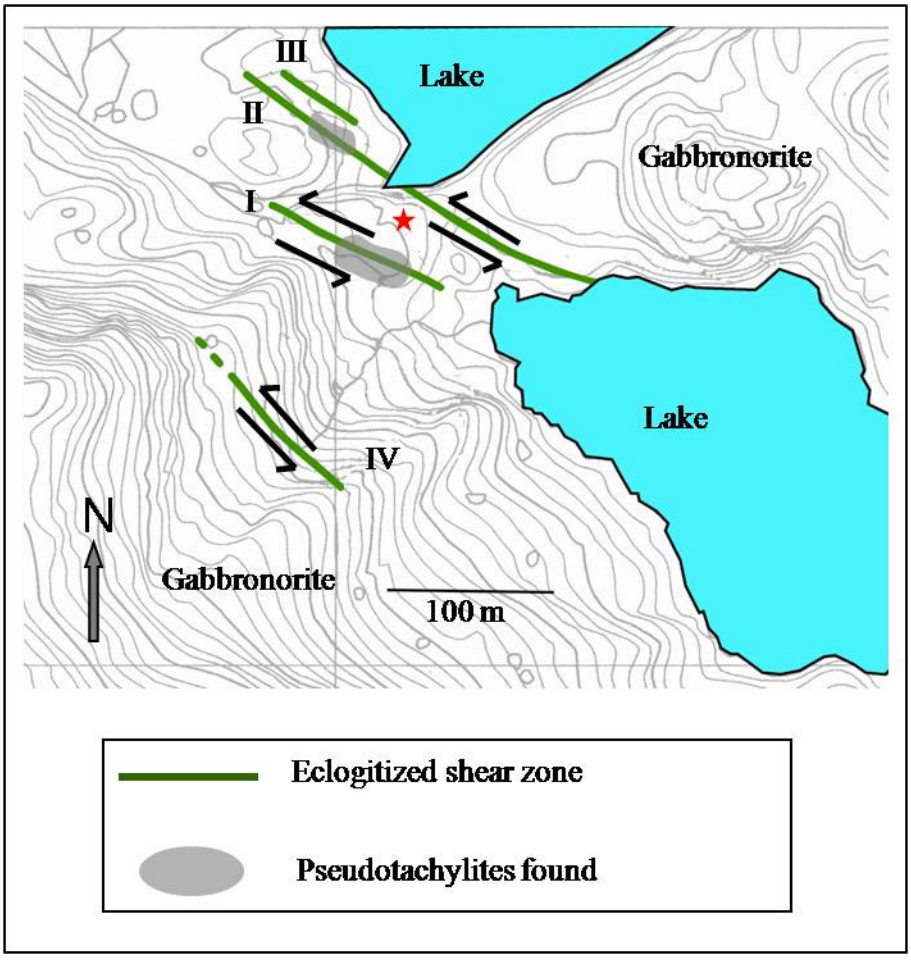

Figure 33: Geologic map of the Nusfjord eclogite locality. Shear zones are designated I-IV to be consistent with Kullerud et al. (2001). Topographic base map (1:5000) obtained from Statens Kartverk, Norway. UTM coordinates in text marked with red star.

that area, and the extent of shear zone (SZ) II is unknown due to erosion. All four shear zones are sub-parallel, sub-vertical, and trend northwest-southeast and each is documented herein to have left-lateral strike-slip displacements (Figure 33).

Three of the Nusfjord shear zones nucleated along mafic dikes that intruded the host gabbronorite. These dikes were determined by Flaat (1998, as quoted in Kullerud and Erambert, 1999) to be of basaltic composition. Shear zone I occurs in gabbronorite (Markl and Bucher, 1997). Shearing appears to be concentrated in the mafic rocks but also significantly deforms the gabbronorite in their immediate shoulders as well (Figure 34). A strong shear foliation and elongation lineation are found in both the eclogitized shears (Figure 35) and the gabbronorite shoulder rock. The transition from undeformed to strongly sheared gabbronorite is abrupt (Figure 34). Shearing intensity in shoulder rocks increases towards the center of the shear zone, and the shear foliation is progressively rotated into parallelism with the shear zone boundary (Figure 34).

Lithologic Units

Gabbronorite

Host rocks at Nusfjord are predominantly gray-brown, gabbronorite that comprises ~60% plagioclase, ortho- and clinopyroxene, biotite, and limonite set in an ophitic, sparsely porphyritic texture (Romey, 1971; Kullerud and Erambert, 1999; Kullerud et al., 2001). Individual plagioclase crystals reach up to 20 cm in length.

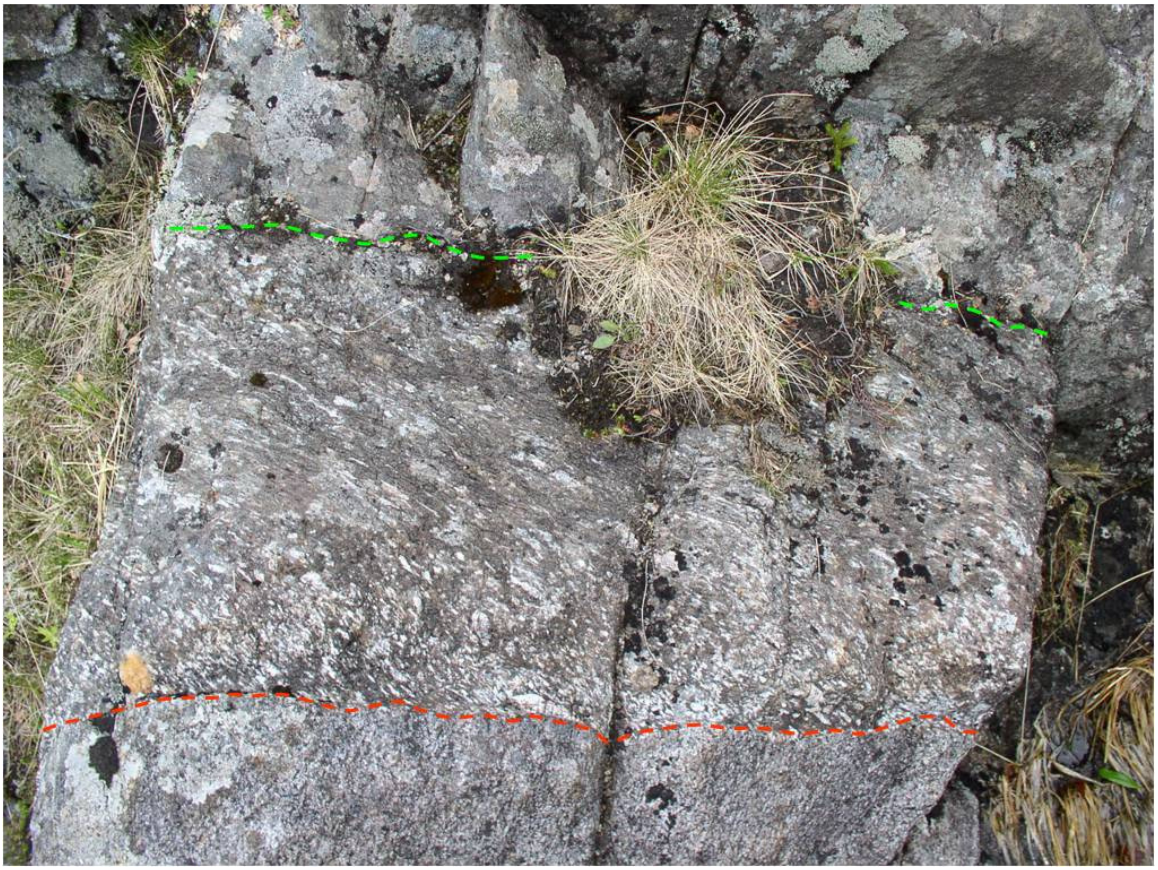

Figure 34: Photograph of the northern half of shear zone II. Retro-eclogite is at the top, deformed gabbronorite shoulder is in the center, and undeformed host gabbronorite is on the bottom. Red line is shear boundary in gabbronorite. Green line marks the gabbronorite-metabasalt contact. Notice the asymptotic shearing in the deformed shoulder, indicating left-slip displacement. Horizontal FOV = ~50 cm.

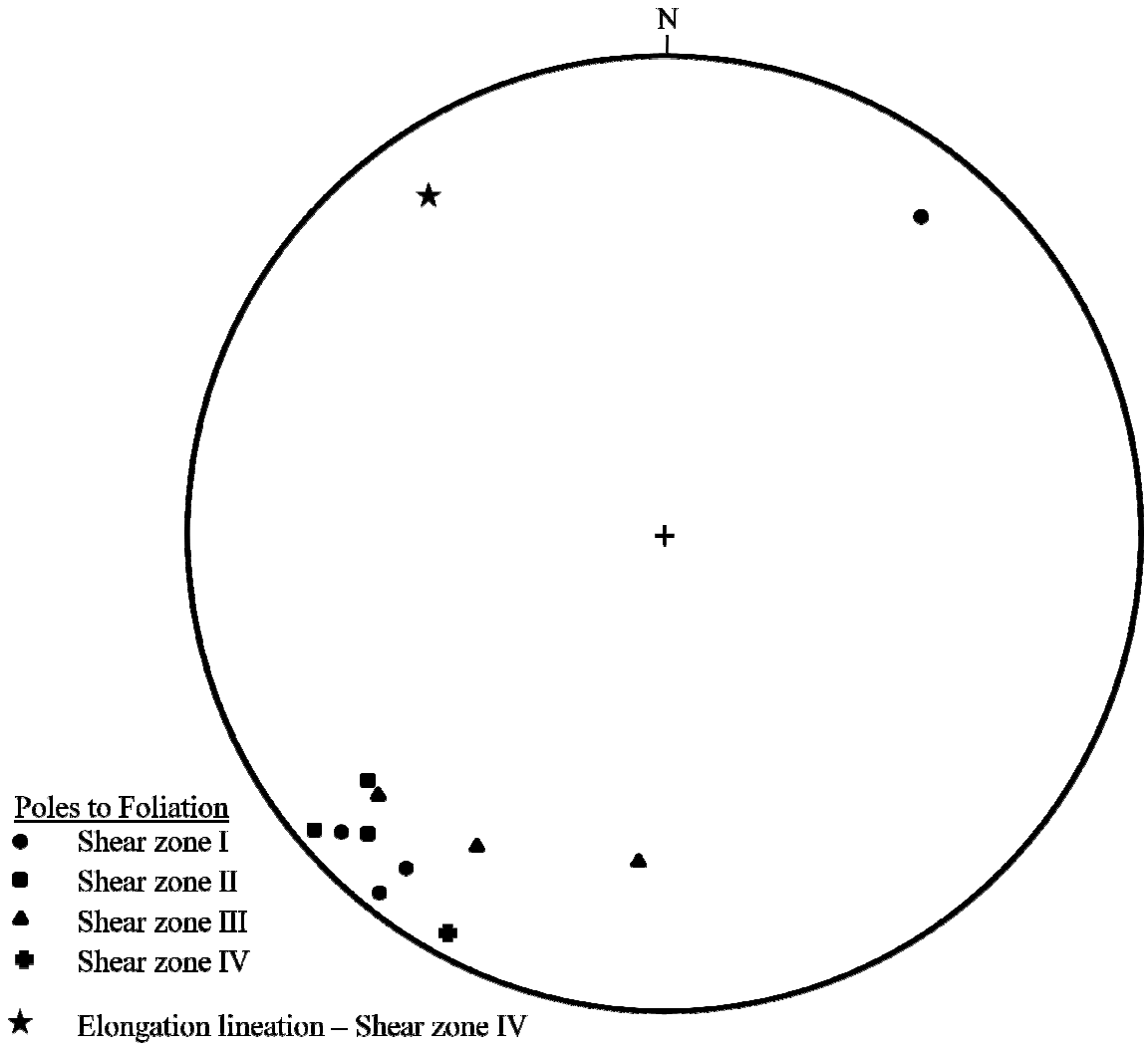

Figure 35: Lower-hemisphere stereographic projection of one elongation lineation and poles to eleven shear zone foliation measurements.

Basalt Injections

Flaat (1998) first described basalts at the Nusfjord locality. The basalts are dark-green to black, fine grained, and have preserved intrusive contacts with their host gabbronorite (Kullerud et al., 2001). Mineralogically, the basalt is comprised of both fine-grained and aggregated green amphibole and sub- to anhedral garnet set in a matrix of fine-grained amphibole and plagioclase (Kullerud et al., 2001). Rare igneous clinopyroxene crystals also exist (Kullerud et al., 2001).

Eclogite

Strongly foliated eclogite, formed from both a gabbronorite protolith (Markl and Bucher, 1997) and a basalt protolith (Flaat, 1998; Kullerud et al., 2001), occur in shear zones ranging from one to four meters in thickness. Host rock is strongly deformed adjacent to the eclogite, but a sharp boundary separates the two units. Eclogite is composed primarily of omphacite, garnet, and plagioclase, with abundant apatite (Kullerud et al., 2001). Kullerud et al. (2001) noted that plagioclase, as well as rutile and ilmenite, occur in textural equilibrium with omphacite and garnet. In addition to Markl and Bucher's (1997) observation of omphacite filled fractures in garnet, Kullerud et al. (2001) report that a later generation of omphacite cuts the omphacite-replacement assemblage garnet-plagioclase-amphibole.

Structures

Mesoscopic Structures

Variably retrograded eclogites occur in the four sub-parallel ductile shear zones at Nusfjord (Figure 33). Shear zones II, III, and IV nucleated along tabular mafic injections within massive gabbronorite (Figures 33 and 34), whereas shear zone I formed completely in gabbronorite (Markl and Bucher 1997; Kullerud et al., 2001). Both shoulders of shear zones II, III, and IV are well exposed. Only the northeastern side of shear zone I is exposed.

The Nusfjord eclogite shear zones are classic Ramsay and Allison (1979) ductile shear zones with planar folia, S_2, progressively developed along the shoulder rock and having been asymptotically swept into the zone in a left-lateral sense (Figure 34). The gabbronorite is generally massive, but in places contains a strong S_0 igneous flow foliation defined by aligned plagioclase crystals (Romey, 1971). Proterozoic metamorphic foliation is not present at Nusfjord. Shear zone boundaries consistently strike N 69° W and dip 47° NE (Figure 35). A well developed S-C composite foliation is observed in shear zones I, II and III (Figure 36 and 37). C-planes parallel the shear zone boundaries and the S-planes have an average N 34° W, 70° NE attitude, indicating left-slip movement (Figures 34, 36 and 37). Slip lines and principal stress axes were determined stereographically using three paired S-C plane measurements from shear zones I and III. Slip lines lie in the C-plane and are 90° from the intersection of the S and C planes (Berthé et al., 1979): σ_1 is normal to the average S plane; σ_2 is the intersection of the average S and C planes; σ_3 is normal to σ_1 and σ_2. The shear zone I slip line is

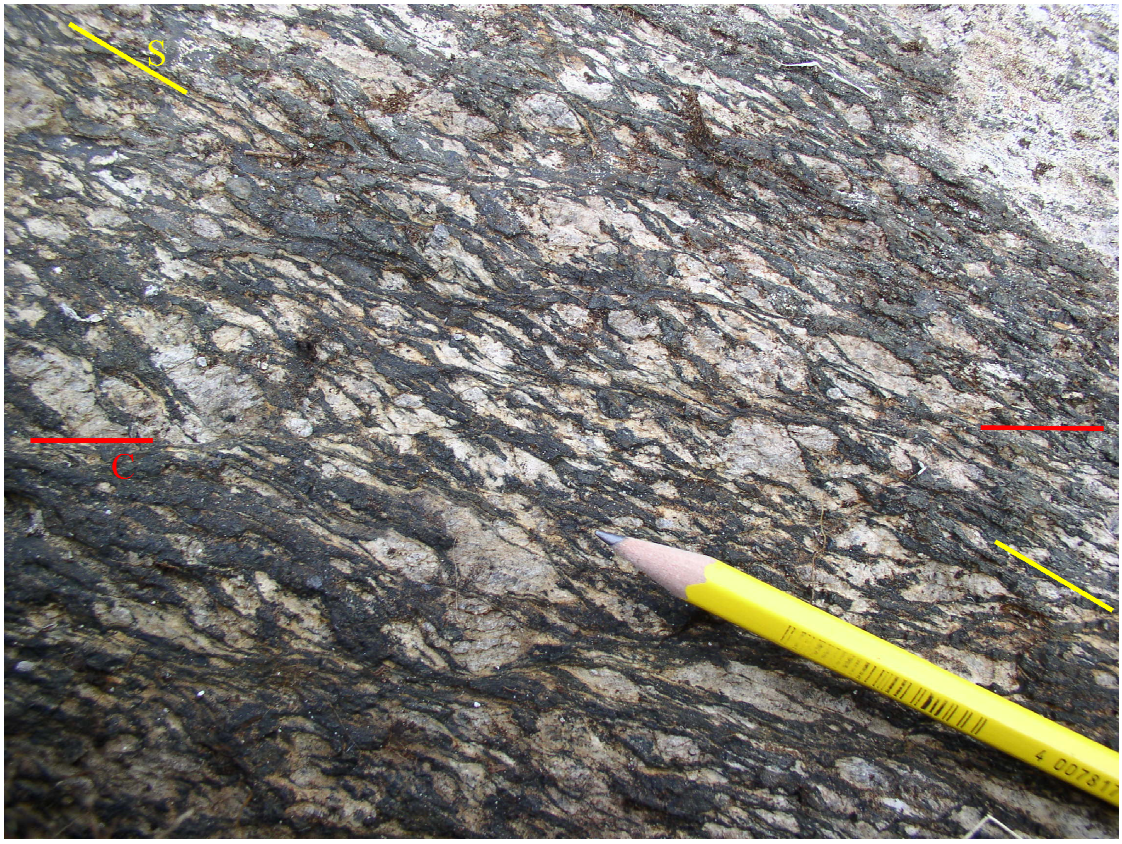

Figure 36: Photograph of paired S-C fabrics in the eclogitized shoulder of shear zone II. View is vertical. S-plane – yellow. C-plane – red.

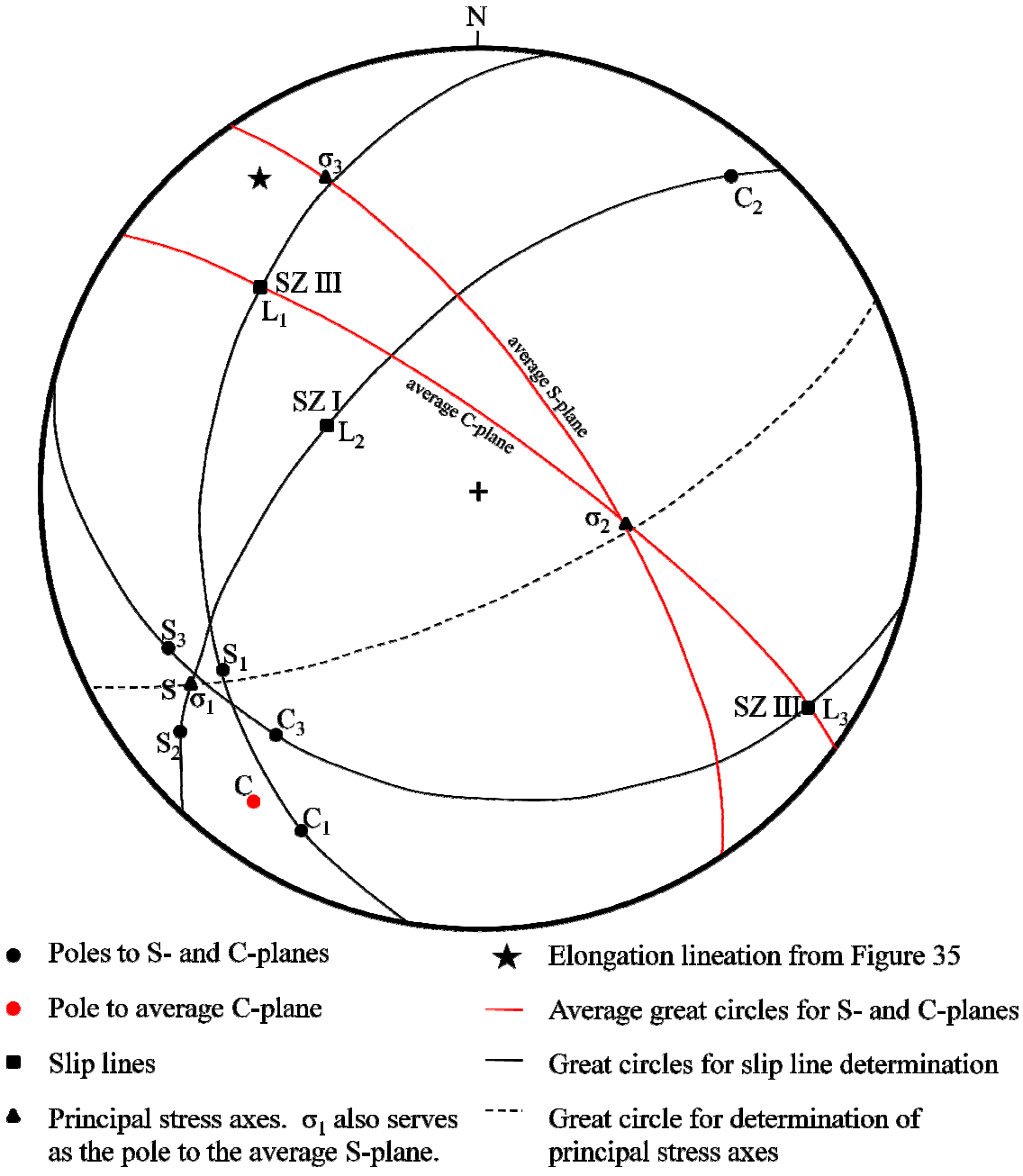

Figure 37: Lower-hemisphere stereographic projection of poles to S- and C-planes, slip lines, principal stress axes, and elongation lineation from the Nusfjord locality. Slip lines: SZ I – N 56° W, 58°; SZ III – N 53° W, 33°, and S 56° E, 11°. Principal stress axes: σ_1 = S 57° W, 20°; σ_2 = S 75° E, 61; σ_3 =N 26° W, 20°.

oriented N 65° W, 58°, whereas shear zone III slip lines are oriented N 53° W 33° and S 56° E 11° (Figure 37). Principal stress axes σ_1 and σ_3 are oriented S 57° W, 20° and N 26° W, 20°, respectively (Figure 37). The shallow (20°) inclination for slip indicates a minor normal component in the overall left-slip kinematic plan.

Ubiquitous feldspar ribbons within retro-eclogite have been deformed creating small-scale (<1 cm amplitude), intrafolial flow folds of the mylonitic foliation (S_2) (Figures 38 and 39). These trend S63°E and plunge steeply (81°) within the shear plane and show predominantly 'S' asymmetry, further supporting left-slip movement (Figure 38) Some of these folds, however, do not show a clear sense of shear (Figure 39). Folded feldspar ribbons give a minimum shortening of 62% based upon total ribbon length versus length parallel to shear direction. Asymmetric garnet and pyroxene porphyroclasts and strain shadows (Figures 40, 41, 42, and 43), broken and displaced grains (Figures 44 and 45), lattice-preferred orientations in feldspar ribbons (Figure 46), and composite foliations (Figure 36) all give consistent left-slip shear.

Similar to the Myrland locality, numerous, narrow (<7 cm but usually <2 cm wide) plastic shears conspicuously cut the gabbronorite country rock directly outside of the Nusfjord shear zones, but not the eclogitized shear zones themselves. These easily overlooked ductile shears appear to occur randomly. Sense of shear is generally easily determined, with strike slip movement predominating but generally with some component of oblique normal slip. Sub-equal numbers of sinistral and dextral shears

Figure 38: Photograph of a steeply plunging, intrafolial, ‘S’ fold of the mylonitic foliation from the southeastern portion of shear zone I. The white layer marking the fold is a feldspar ribbon.

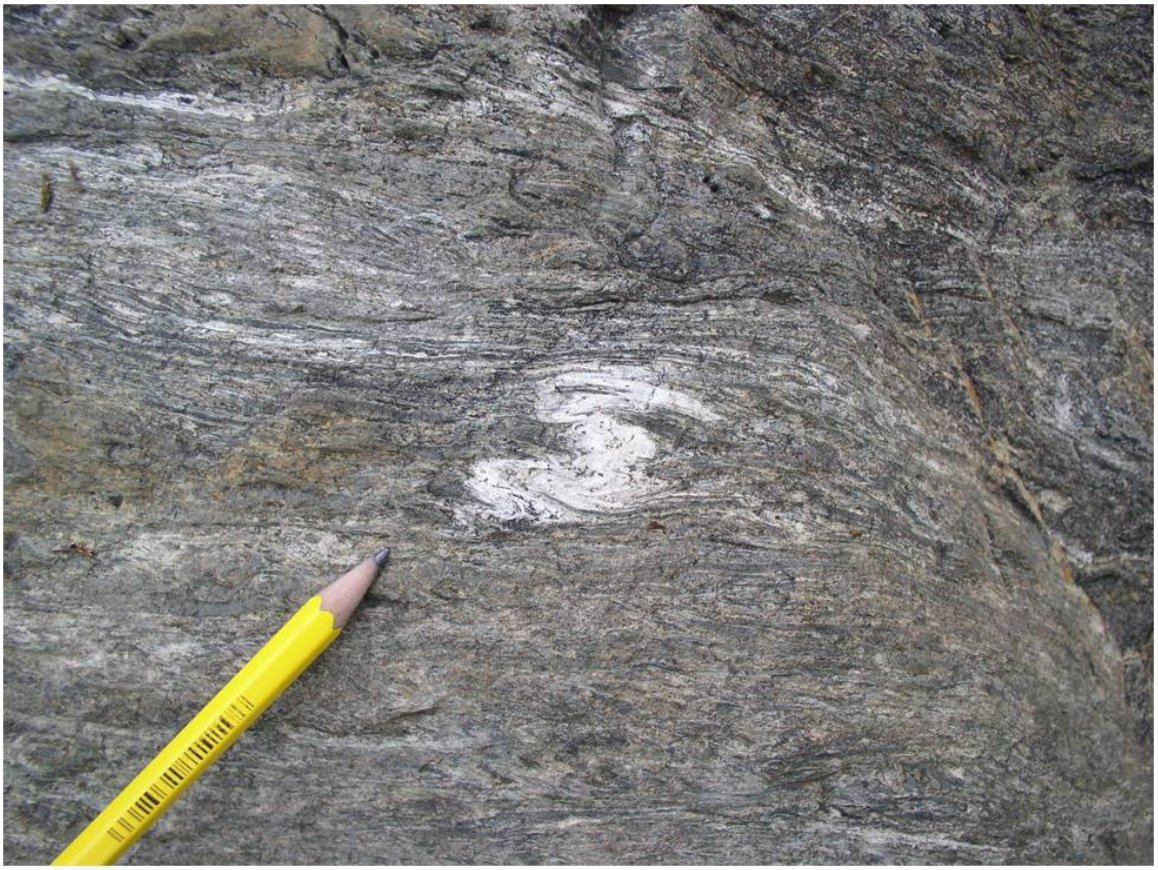

Figure 39: Photograph of steeply plunging, rootless fold of the mylonitic foliation within shear zone I that does not show a clear sense of shear. Other nearby folds, however, are asymmetric and clearly indicate left-slip vergence.

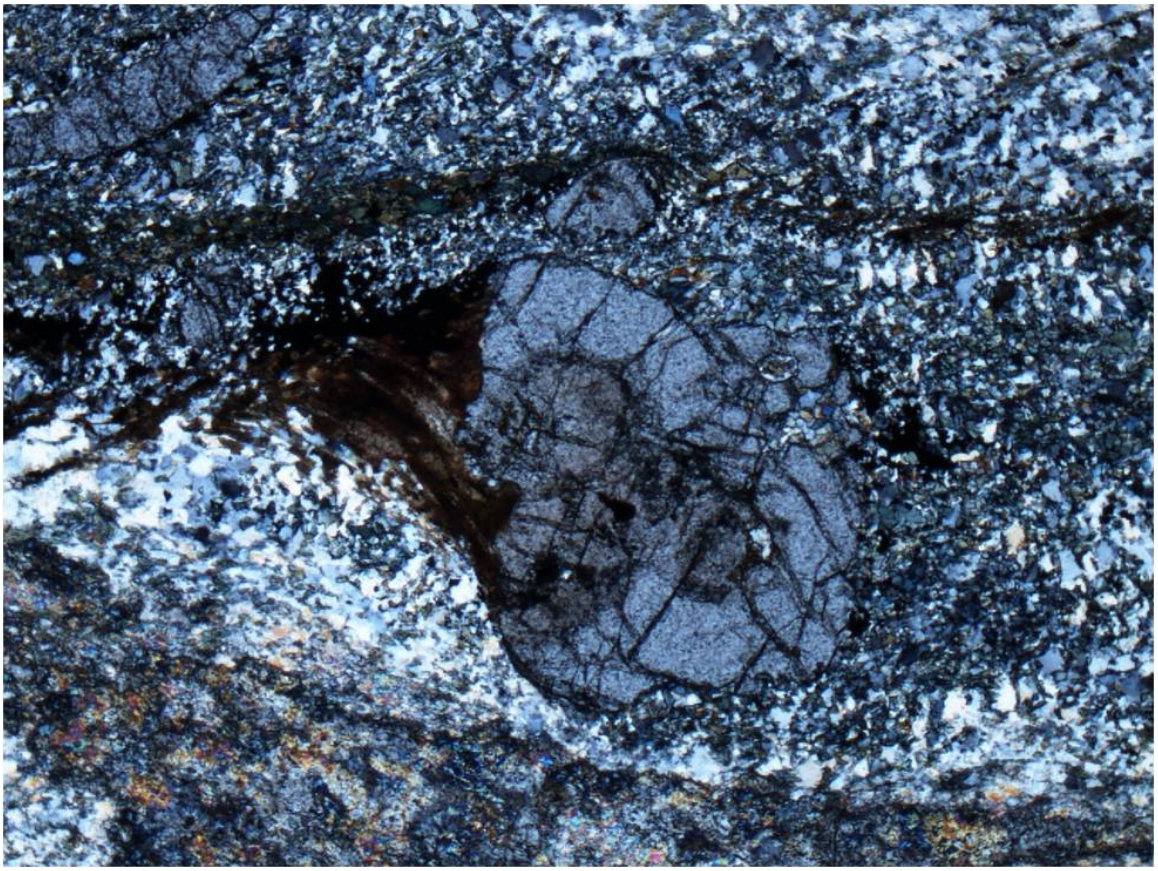

Figure 40: Photomicrograph of a tops-left, σ-type garnet porphyroclast from sample NFA-2 under cross-polarized light and a ¼ wave plate. Note the subtle color saturation difference. Crystal faces are moderately well preserved. Biotite in pressure shadow is a late retrogressive feature. Note also the amphibole tail in the lower right. Horizontal FOV = 2.1 mm.

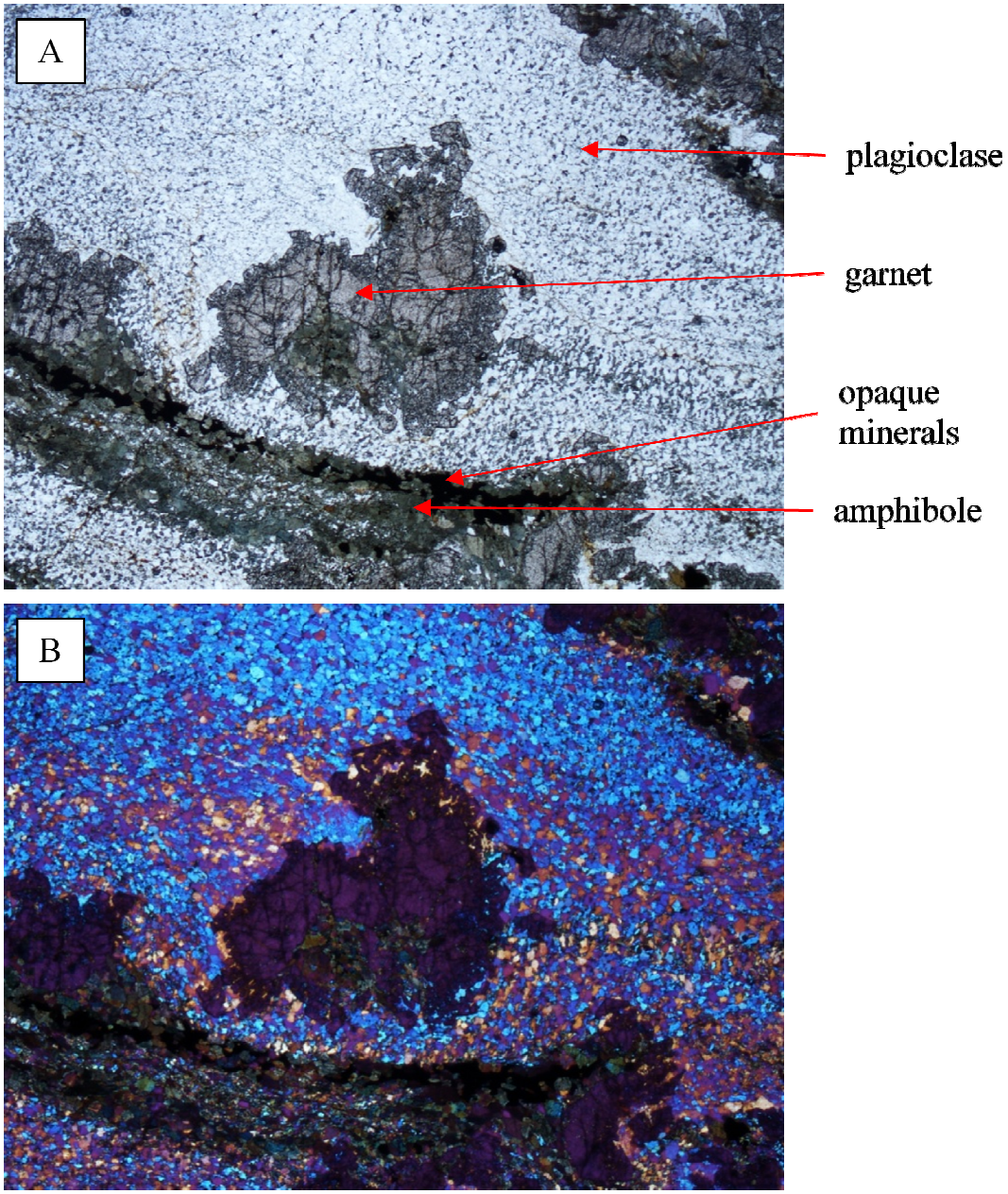

Figure 41: Photomicrograph of sample NFA-10. Weak LPO in plagioclase and strain shadow (upper left of garnet) indicate left-lateral shear sense. Horizontal FOV = 5.5 mm. A) Plane-polarized light. Euhedral 1st generation garnets with rim of 2nd generation growth. B) Cross-polarized light with the ¼ wave plate inserted. Plagioclase has a uniform LPO except in vicinity of the relict garnet clast.

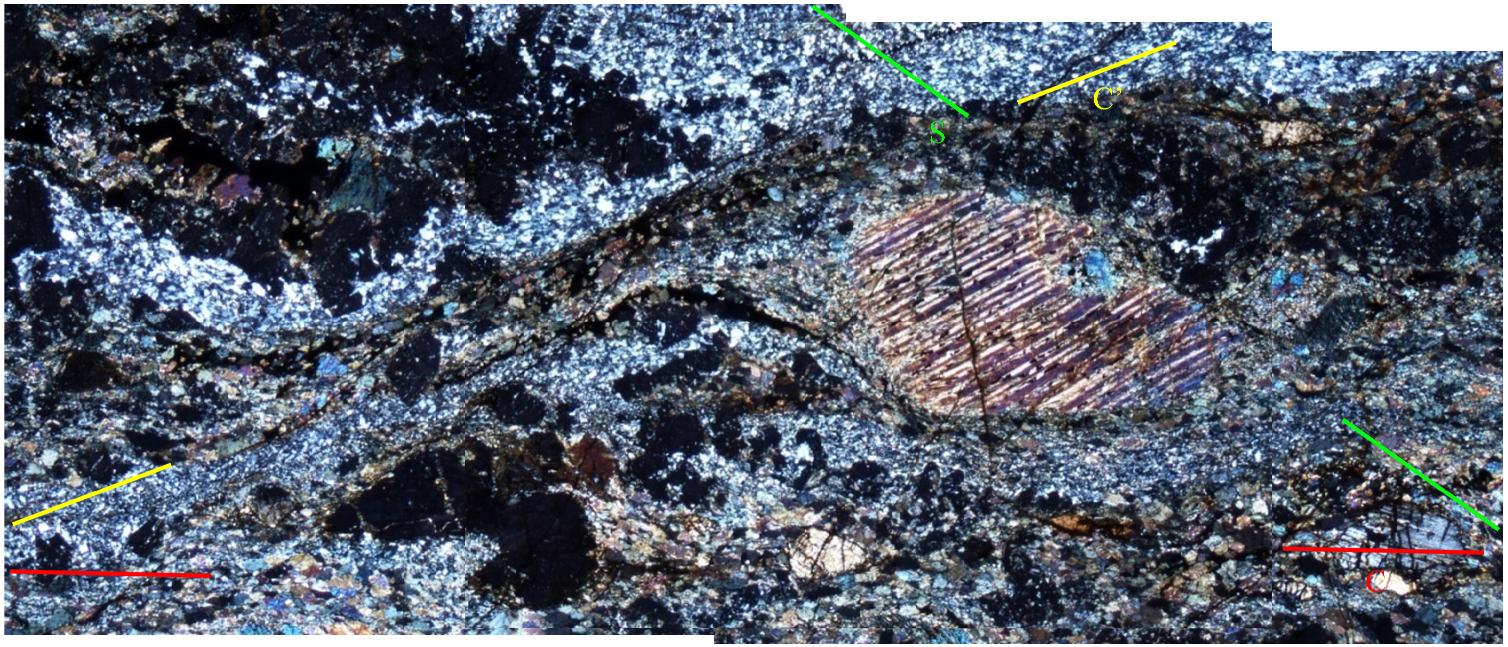

Figure 42: Photomicrograph of omphacite retrograded to diopside in sample NFA-8. Lamellar exsolution along twin planes with 1st order white and yellow birefringence are omphacite; those with 1st order blue and purple birefringence are diopside. Blue-grey bleb in the upper right of this pyroxene is plagioclase. S-plane – green. C-plane – red. C', or extensional shear band – yellow.

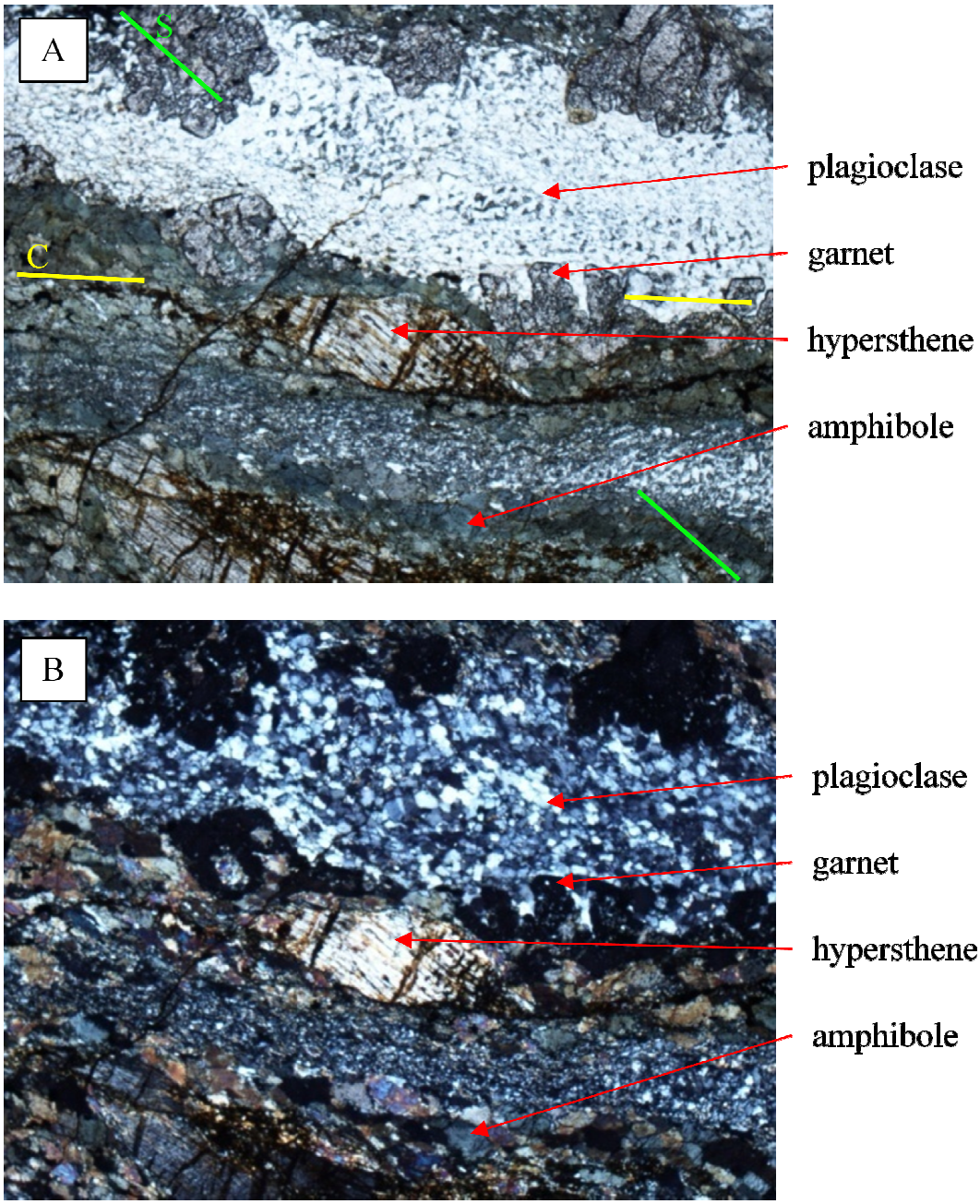

Figure 43: Photomicrograph of a hypersthene grain rotated sinistrally into the C-plane, consistent with LPO in plagioclase. A) Plane-polarized light. C-plane – yellow. S-plane – green. B) Cross-polarized light. Horizontal FOV = 2.75 mm.

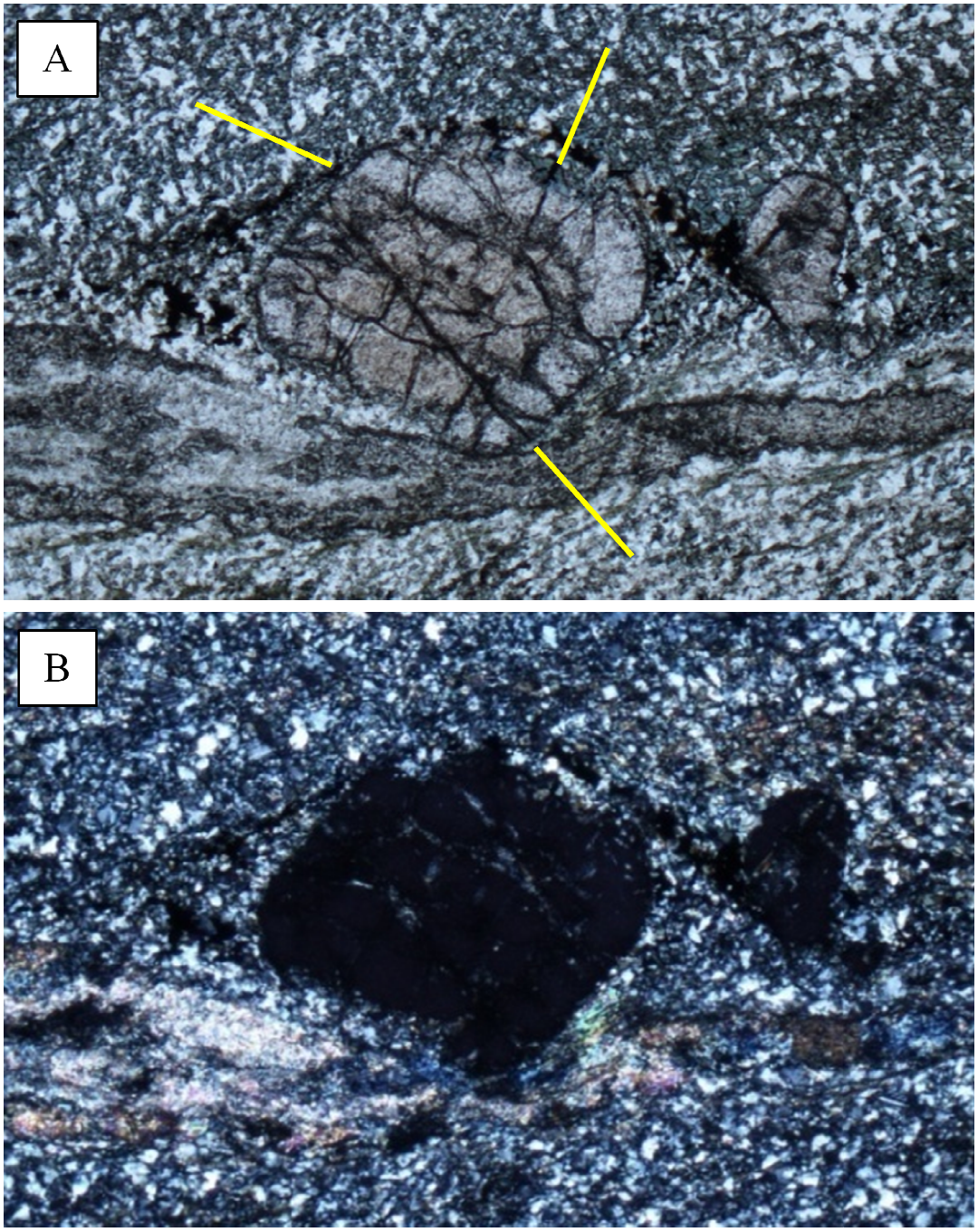

Figure 44: Photomicrograph of broken, displaced garnet in sample NFA-2. Sense of displacement (antithetic, tops-down to right) is consistent with overall left-slip kinematic plan. A rim of 2nd generation garnet surrounds both 1st generation cores. Fracture sets marked by yellow lines. A) Plane-polarized light. B) Cross-polarized light. Horizontal FOV = 5.5 mm.

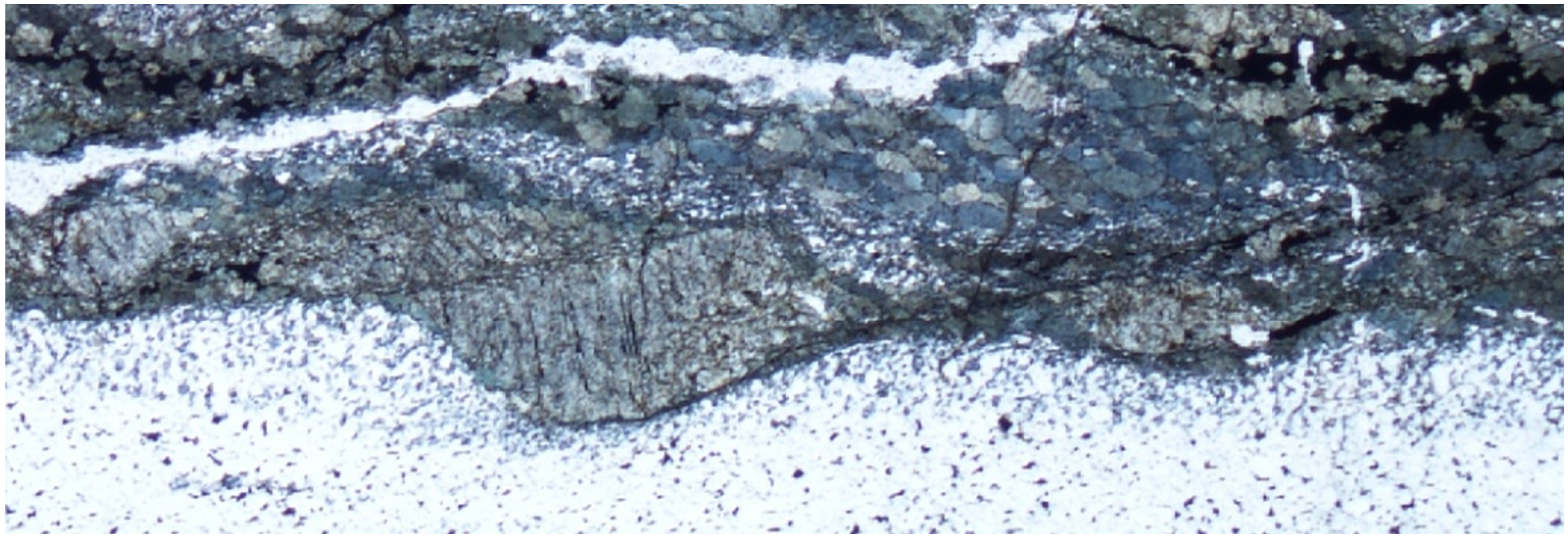

3 mm

Figure 45: Broken and displaced clinopyroxene grain from sample NFA-8. Grain is cut into three pieces. Sense of displacement (synthetic, tops-down the left) is consistent with overall left-slip kinematic plan. Plane-polarized light.

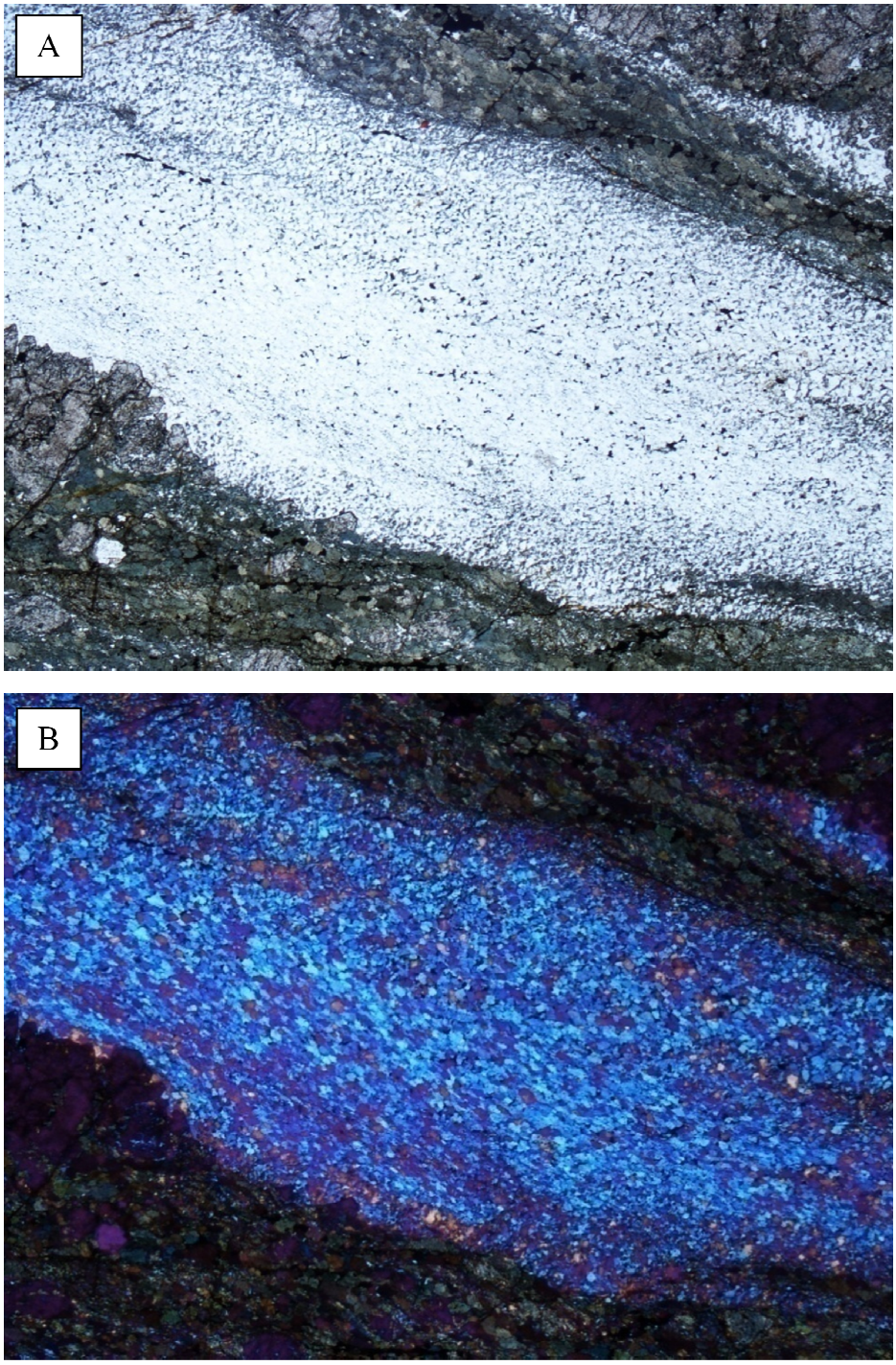

Figure 46: Photomicrograph of a part of a plagioclase ribbon from sample NFA-2. Note the preferred grain shape orientation and the strong LPO indicating left-slip shear. Horizontal FOV = 2.75 mm. A) Plane-polarized light. B) Cross-polarized light through a 1-wavelength plate.

were observed and they strike generally northwest and dip moderately to steeply toward the southwest. Slip lines, determined stereographically from paired S-C foliations, generally plunge moderately-to-shallowly toward the east and west.

The small-scale shear zones approach the larger eclogite-facies shear zones at a slight to moderate angle. Displacements along these shears are small because many terminations were observed. The most likely mechanism for small ductile shear zone formation appears to be fluids infiltrating along pre-existing brittle fractures causing hydrolytic weakening and allowing ductile deformation to occur (Segall and Simpson, 1986). The presence of stranded and mineralized cracks (Figure 47) is consistent with such an interpretation. Epidote-filled brittle fractures are commonplace throughout the Nusfjord area, documenting that fluids infiltrated the fracture network, although the relative timing of epidote deposition to plastic deformation and eclogite formation remains unknown. The random orientation of the small shears suggests that they did not form as a result of the regional stress field. Ductile deformation along these fractures and the small-scale shears is presumed to have accommodated volume reduction that occurred during the transition of basalt and gabbronorite to eclogite.

Steltenpohl et al. (2006) describe pseudotachylites associated with the Nusfjord eclogite shears (see Figure 33). These authors interpret the frictional melts to have formed slightly before or early during the formation of the eclogite shears, consistent with the observations herein. Since they contain the same retrograde assemblages

Figure 47: Parallel, stranded and mineralized fracture sets at Nusfjord.

observed in the eclogite shears they are interpreted as deep- to intermediate-level seismic faults. The pseudotachylites appear to parallel a set of brittle shears and fractures striking roughly N40°W and dipping moderately northeast to vertical.

Rheological Observations

Samples NFA-2, NFA-8, NFA-9, NFA-10, and NFA-17 were collected from SZ II (Figure 33), which is the longest and best exposed shear zone, for petrographic characterization of its rheological development. NFA-2 and NFA-17 were collected from the southeastern end of SZ II. NFA-9, 8, and 10 are a series of samples collected along a transect perpendicular to strike from the longitudinal shear zone center. Samples from the center of the shear zone have a preserved dynamic flow texture: ribbons of amphibole and plagioclase display a well-preserved mylonitic banding. S-C fabrics are not apparent in this zone. Samples from the more distal edges of the shear zone have preserved S-C fabrics (Figure 36). These observations indicate a higher degree of shear strain in the center of the shear zone (Ramsay and Graham, 1970; Berthé et al., 1979). For this study, all samples were oriented in the field and then cut perpendicular to foliation and parallel to elongation lineation. Below is a description of microstructural observations related to the rheology of individual phases from rocks in key positions within eclogite SZ II.

Amphibole observed at this locality has a variably saturated green to blue-green color. Grains are amoeboid with no euhedral grains observed. Amphibole is volumetrically the dominant mineral present but displays no post-crystalline deformational microstructures in thin section. Kullerud (1996) reported that although

retrogressive amphibole is Cl-free, amphiboles derived from host rocks (determined by their presence as garnet inclusions) contain remobilized crustal Cl (Markl et al., 1997). These observations detail the relative ages of amphibole growth as eclogitization within the shear zone was mediated by infiltration of a Cl- and H_20-bearing fluid (Kullerud, 1996; Kullerud et al., 2001). Figure 6 of Kullerud (1996) indicates that amphibole formed from host rocks tends to be of ferroan pargasitic to ferro-pargasite compositions and retrogressive amphiboles tend to be of edenitic, edenitic hornblende, ferroan pargasitic hornblende, and ferroan pargasite compositions (Leake, 1978). Markl and Bucher (1997) report chemical analyses of several amphibole grains from a partially retrogressed eclogite sample at Nusfjord that ranged from edenitic hornblende to ferroan pargasite and which clearly follow a linear trend on plots of $X_{(Mg)}$ v. Si (see Figure 11), likely a function of timing of their formation relative to eclogitization. It is notable that amphiboles from the Skagen, Storvatnet, and Myrland eclogite localities (Figures 3 and 11) all have similar compositions to the retrogressive amphiboles of Kullerud (1996).

Two distinct generations of garnet are present in the shear zone. These generations were determined by petrographic appearance; clear, inclusion-poor, euhedral garnets are assigned to the 2nd generation, whereas cloudy, inclusion-rich garnets with an eroded or deformed shape are assigned to the 1st generation. First generation garnets are likely relicts of eclogitization. Original grain shape and size are rarely preserved due to subsequent recrystallization.

In some cases, smaller 2nd generation garnets have replaced a single 1st generation garnet grain retaining the original outline, clearly indicating that the 2nd generation

garnets grew at the expense of the 1st. Broken and displaced garnets have 2nd generation overgrowths that completely engulf the 1st generation on both fragments, indicating 2nd generation growth after deformation had ceased (Figure 44). To the best of my knowledge, this observation has not previously been reported. The boundary between the two generations is especially evident under cross-polarized light using a ¼ wave plate (Figure 40).

Evidence for both brittle and plastic deformation of garnet within the shear zone was observed. Garnet 'stringers', similar to those described by Storey and Prior (2005), were observed in NFA-8, NFA-9, and NFA-10 (Figures 48 and 49). These stringers are composed of linear trains of small (0.1 - 0.5 mm), subhedral to euhedral, second generation garnets aligned parallel with the mylonitic foliation. Such trains are observed stretching from a larger aggregate of small garnets or a mixture of small garnets surrounding a degraded core of a larger (> 0.5 mm) first generation garnet. Second generation garnets defining the stringers have sharp, straight crystal edges in contact with plagioclase but are less crisply defined where adjacent to amphibole; these correspond to Morphology 4 garnets described by Storey and Prior (2005). According to Storey and Prior (2005), high-temperature (700 °C) deformation allows garnet to be dynamically recrystallized forming elongate bands, phi-clasts, and less commonly sigma clasts. Temperatures sufficient to deform garnet in this manner can be attained under amphibolite-facies, however, the presence of eclogites at Nusfjord and their textural relations suggest that early deformation of garnet occurred under eclogite-facies conditions. Other garnets in samples NFA-8 and 9 have an inclusion- rich, cloudy core

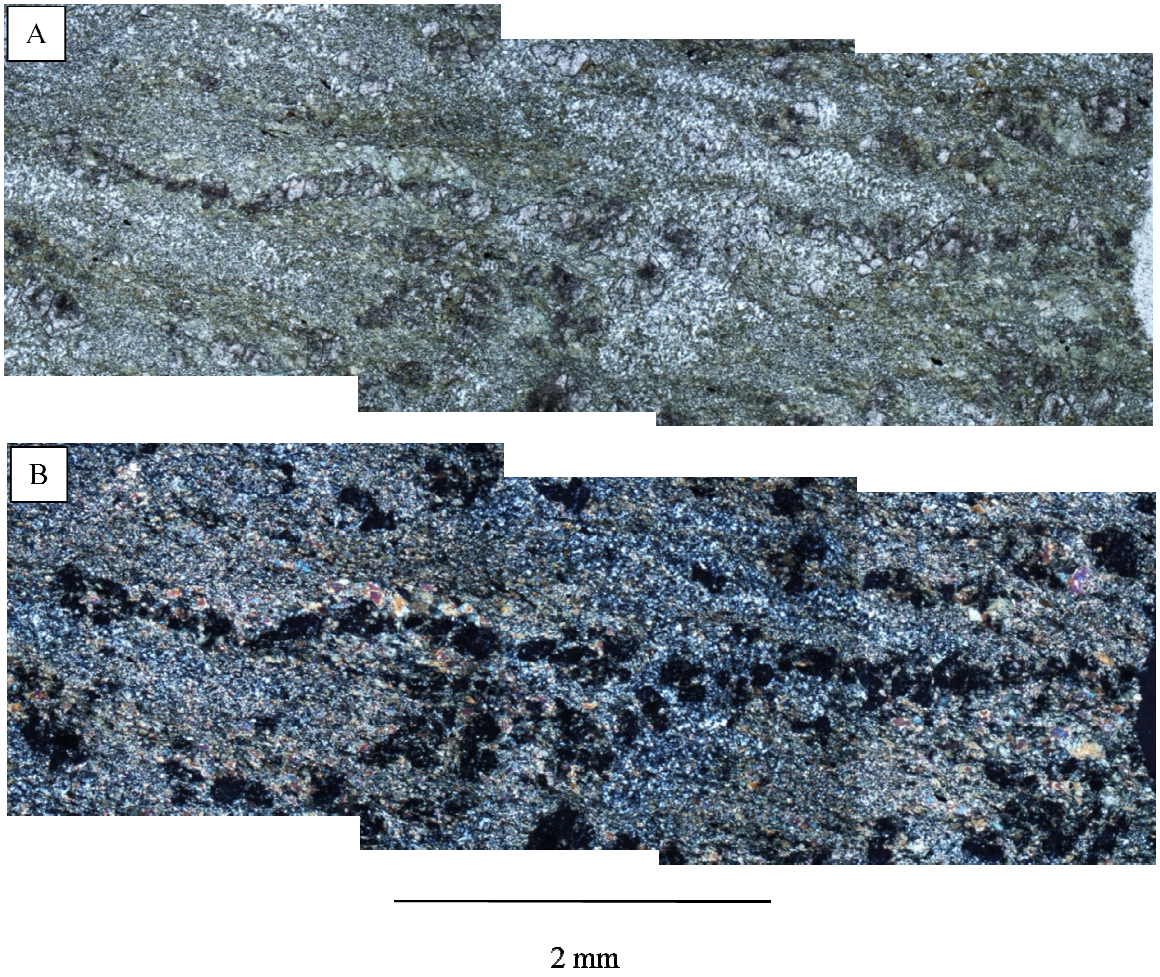

Figure 48: Photomicrograph mosaic of a garnet 'stringer' (train of black grains along the longitudinal center of mosaic B composed of small, 2nd generation euhedral garnet crystals recrystallized from plastically deformed 1st generation garnet. Stringers are oriented parallel with long direction of mosaic. A) Plane-polarized light. B) Cross-polarized light.

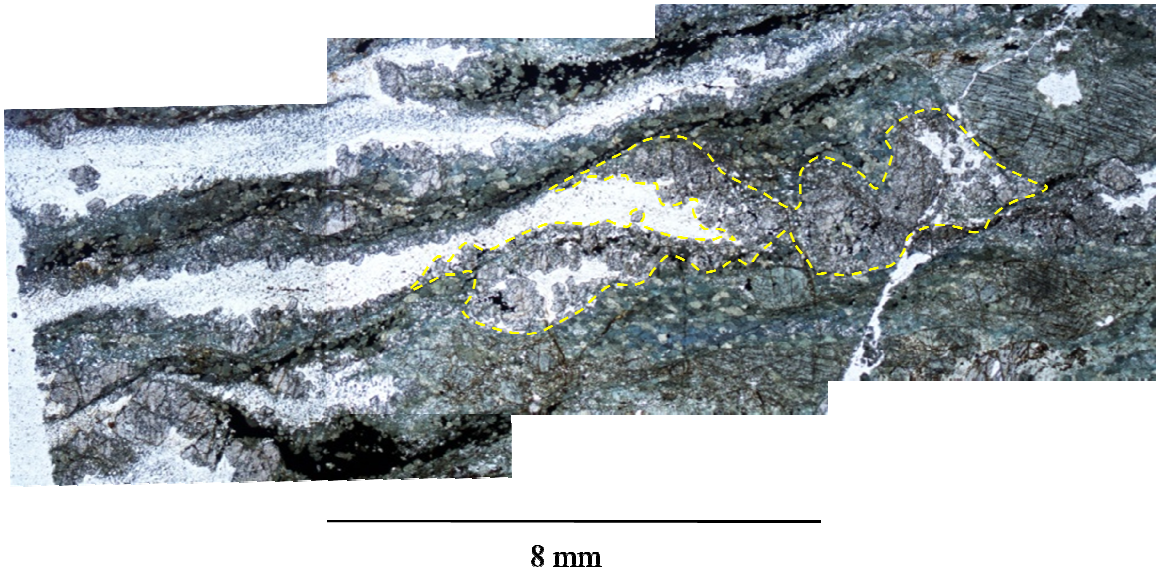

Figure 49: Photomicrograph mosaic of a garnet stringer in sample NFA-8. Stringer extends from garnet concentration (in yellow), interpreted to be a first generation garnet recrystallized and partially destroyed during retrogression. Second generation garnets are concentrated along the margins of plagioclase ribbons. Viewed under plane-polarized light.

and an inclusion-poor, clear rim with incomplete extinction (Figure 50). This may indicate incomplete replacement of 1st generation garnets with 2nd generation ones. Garnets in NFA-10, a sample from closer to the shear zone edge than NFA-8 and 9, commonly retain their original shape but still show 2nd generation growth (Figure 41).

Evidence of plastic deformation of garnet was not observed in eclogite shear zone samples NFA- 2 and 17; rather, they are fractured and displaced by synthetic microfaults (Brunel, 1986; Blumenfeld and Bouchez, 1988; as paraphrased in Passchier and Trouw, 1998) and rigidly rotated (Figures 44 and 51, respectively). Garnets in these samples have three well-developed fracture sets (Figures 40, 44, and 52). Two of these fracture sets cut cores and, where present, rims; the third set cuts only the rims. These sets are parallel in all garnet grains within a given thin section. Rotated garnets are sub- to well-rounded but do not show obvious evidence for internal plastic deformation. Amphibole and opaques wrap around these garnets, indicating that garnet clearly was a competent phase during deformation (Figure 51).

Brittle or plastic behavior of garnet appears to be dependent on position within the shear zone. The most plastically deformed garnets occur in the centers of shear zones whereas brittle, porphyroclastic garnet is progressively more prevalent toward the shear zone boundaries. These observations are consistent with the interpretation that fluid infiltration and mineral plasticity is most pronounced in the centers of the shear zones. Limited element mobility along grain edges, mechanical breakage, and/or rotational recrystallization are responsible for the rounded appearance of the garnets.

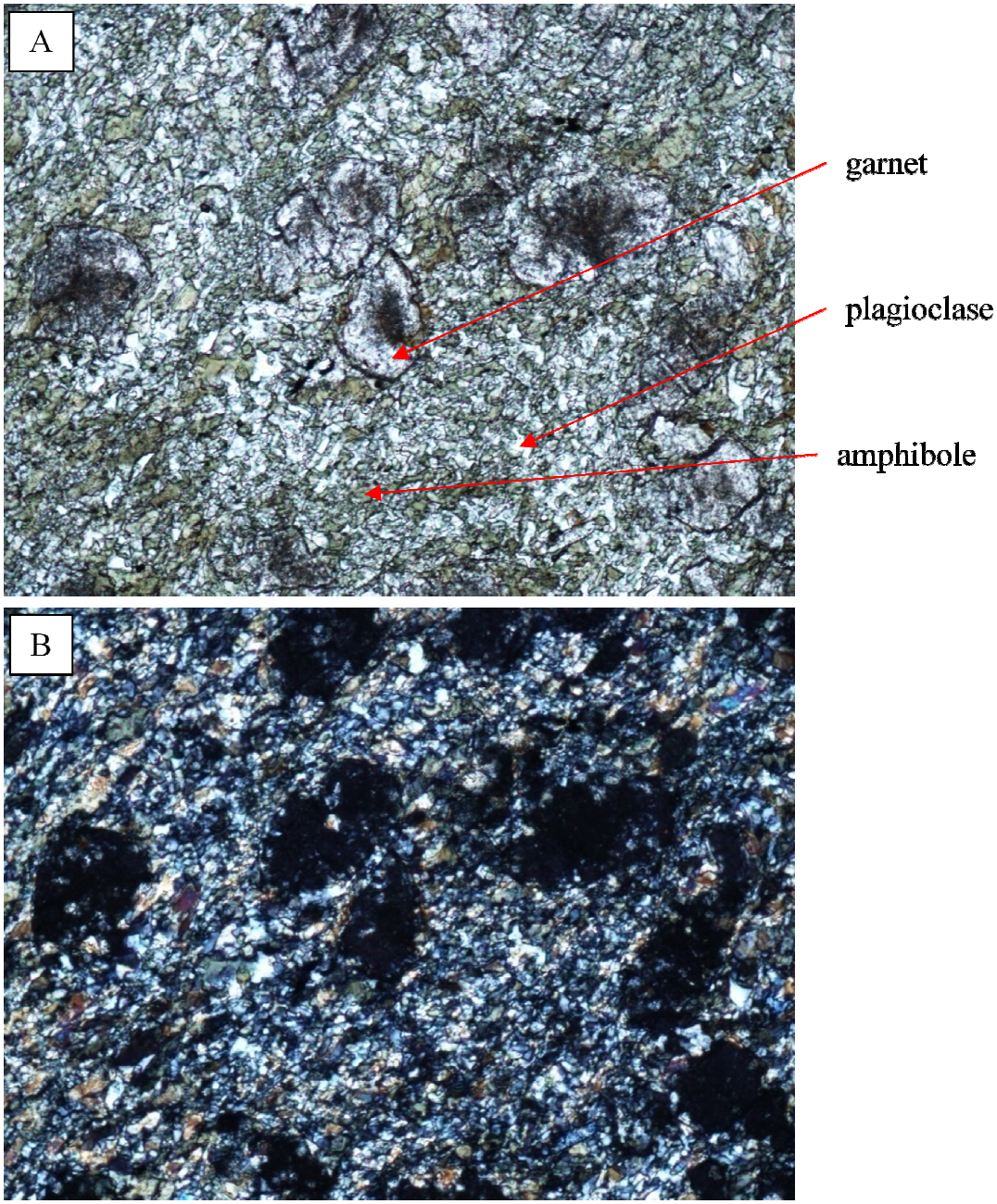

Figure 50: Photomicrograph of sample NFA-9 (shear zone interior). A) Plane-polarized light. Note cloudy core and clear rims of anhedral garnets. B) Cross-polarized light. Horizontal FOV = 2.75 mm.

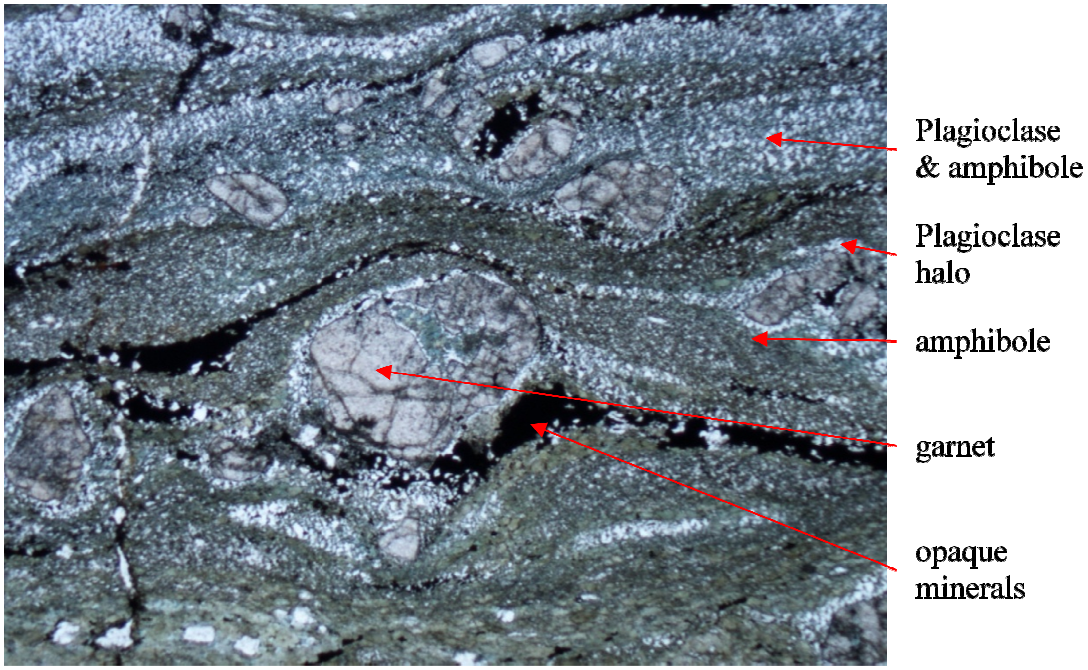

Figure 51: Photomicrograph of rotated garnet porphyroclasts from sample NFA-2. Viewed under plane-polarized light. Horizontal FOV = 5 mm.

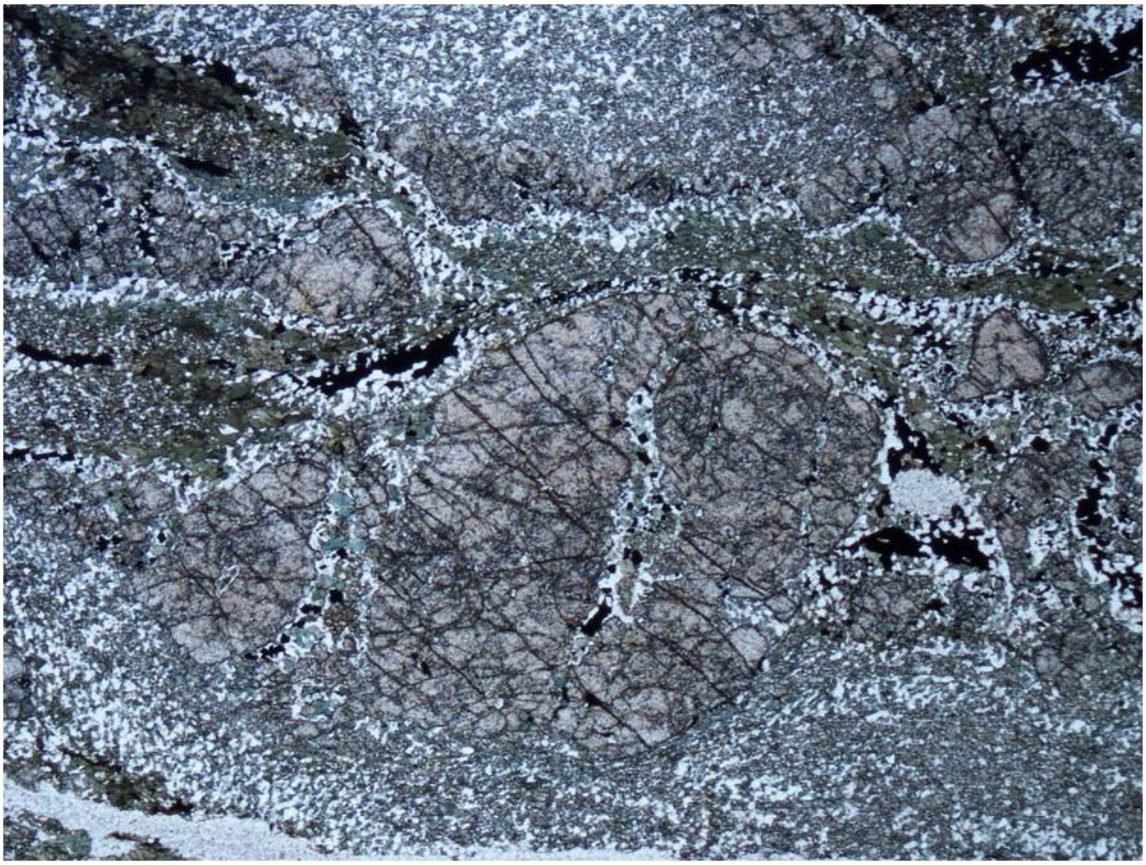

Figure 52: Photomicrograph of one well-developed and one poorly developed fracture set in a relict 1st generation garnet with no rim from sample NFA-17. The dominant fracture set is inclined moderately to the right; the subordinate set is inclined shallowly to the left. Plane-polarized light. Horizontal FOV = 5.5 mm.

Plagioclase occurs as highly elongated ribbons of small (~0.1 mm) recrystallized grains. The recrystallized grains have a strong LPO and preferred grain shape orientation (Figures 41 and 46). The fine but uniform grain size suggests that these grains formed due to dynamic recrystallization of large (>2 cm) plagioclase grains observed in the host country rocks. Large, primary plagioclase grains outside of the shear zone have similar LPO, grain size reduction, and preferred grain orientation along microfractures (Figure 53). Strain was clearly absorbed by the softer plagioclase grains forming the ribbons that wrap around garnet and pyroxene grains forming a 'lee' effect in the strain shadow (Figure 41). This phenomenon was also observed in plagioclase from the Storvatnet locality.

Omphacite, a characteristic eclogite-facies mineral, is rarely preserved in Nusfjord eclogite samples. Figure 54 shows an omphacite sigma-clast from sample NFA-10. Crystallization of this grain preceded mylonitization, which indicates eclogitization prior to shearing. Although primary omphacite grains are rare, retrogressive products are identifiable. Omphacite is replaced by clinopyroxene and a symplectic intergrowth of plagioclase and amphibole, which is interpreted as a further retrograded clinopyroxene. Sample NFA-8 contains several omphacite grains arrested during retrogressive metamorphism to form another clinopyroxene, likely diopside (Figures 42, 45, 55 and 56).

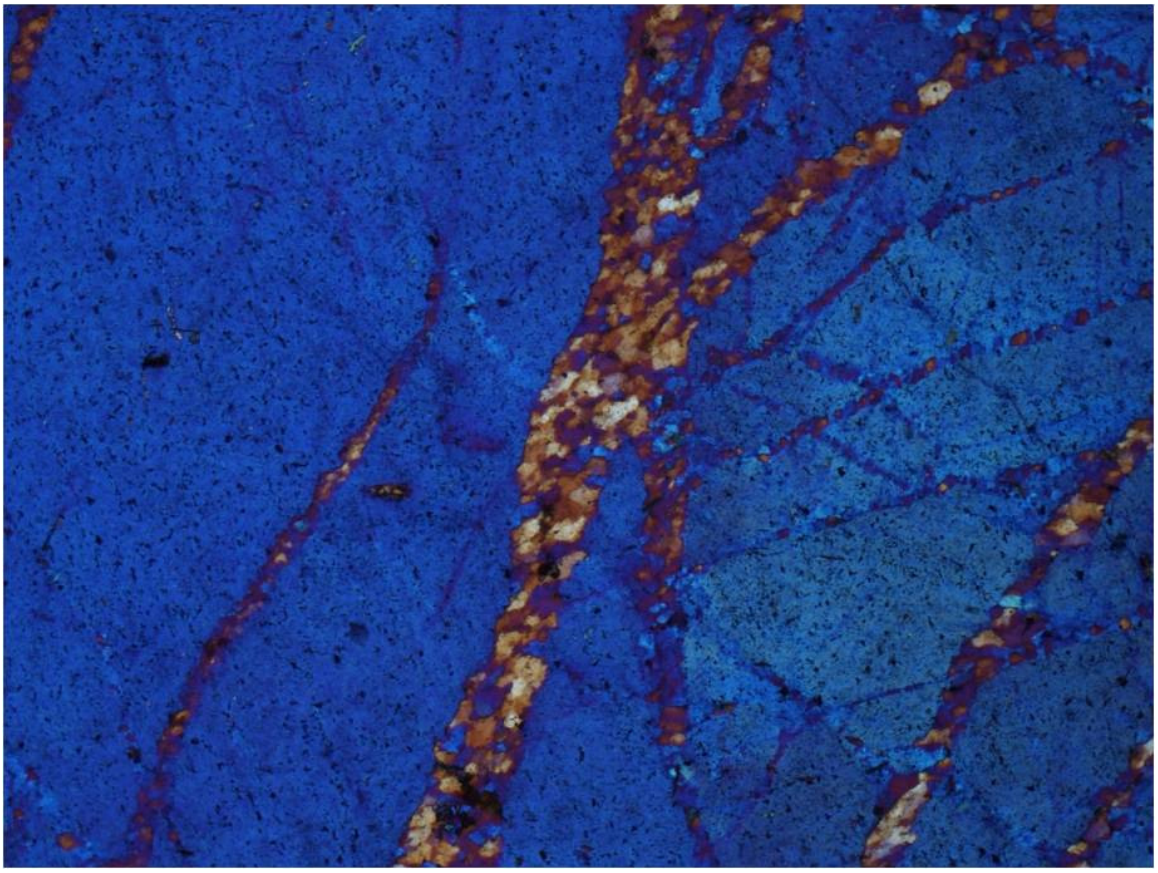

Figure 53: LPO, grain size reduction, and grain shape preferred orientation along fractures in a plagioclase grain from host rock sample NF-11 located near the eclogitized shear zones. Viewed under cross-polarized light with the ¼ wave plate inserted. Horizontal FOV = 2.75 mm.

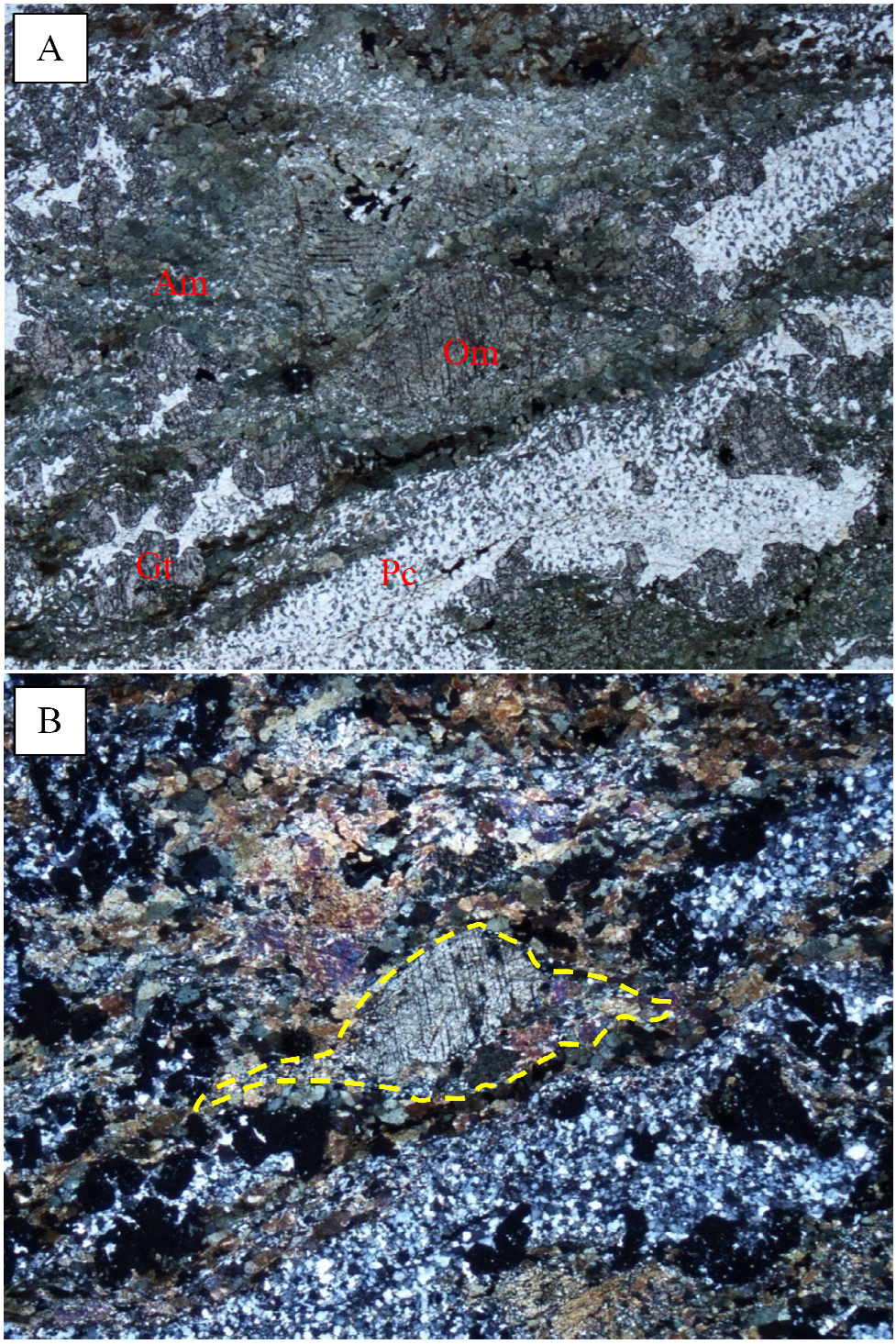

Figure 54: Primary eclogite-facies omphacite σ-clast in sample NFA-10. Lower third of grain is altered to amphibole. Horizontal FOV = 2.75 mm. A) Plane-polarized light. B) Cross-polarized light. Omphacite σ-clast outlined in yellow.

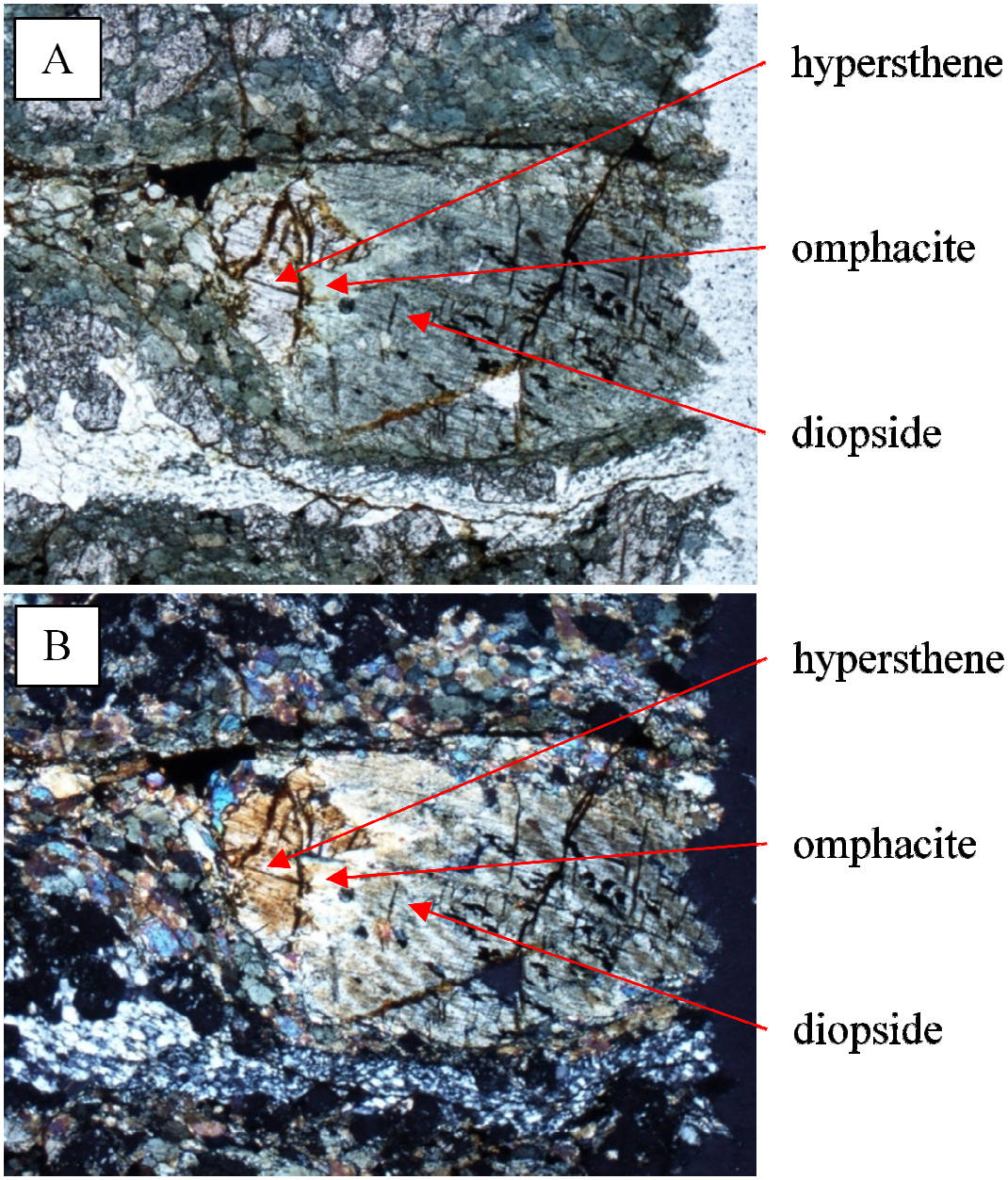

Figure 55: Breakdown of omphacite in sample NFA-8. Hypersthene is first replaced by omphacite, and followed by diopside. Horizontal FOV = 2.75 mm. A) Plane-polarized light. B) Cross-polarized light.

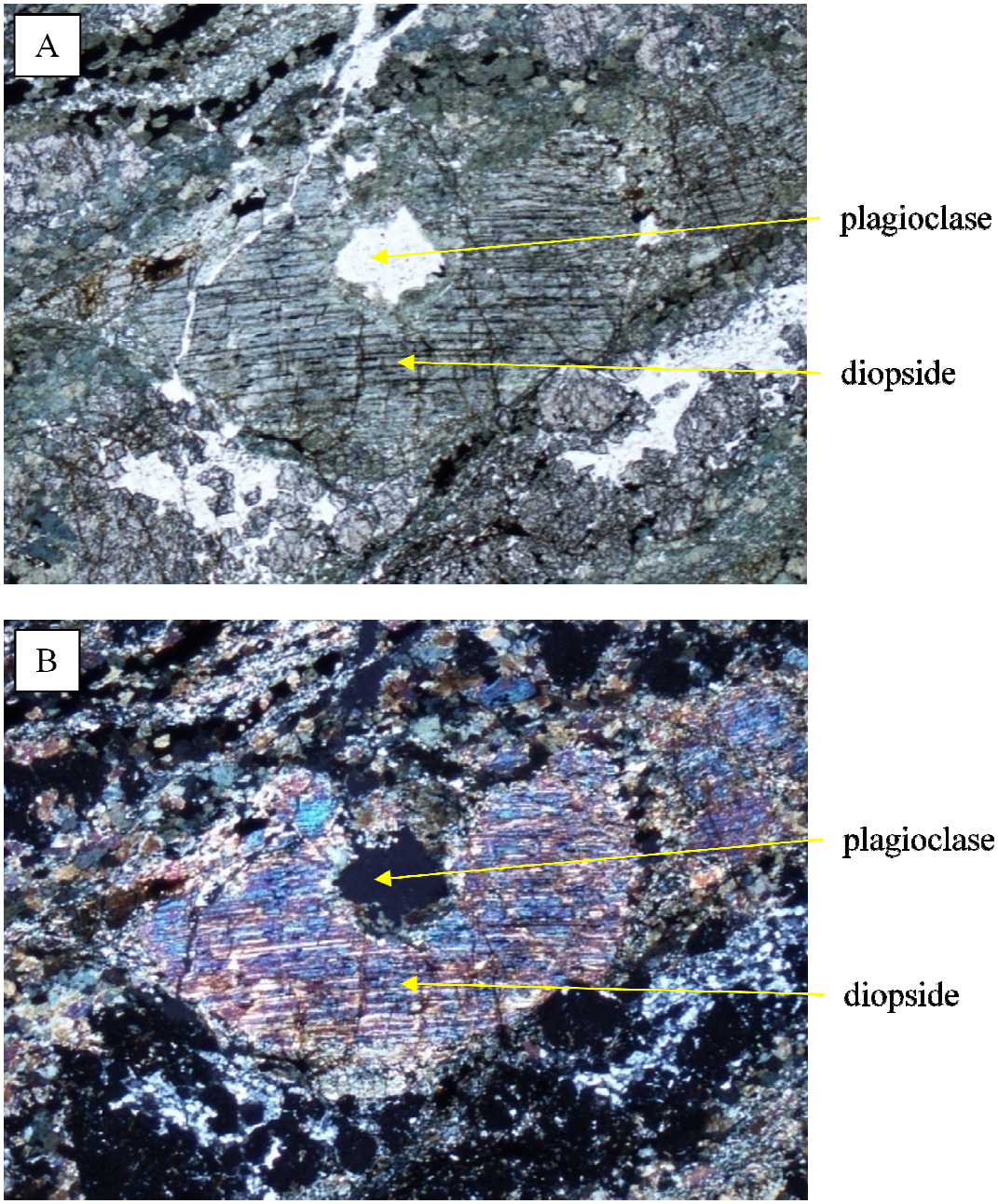

Figure 56: Near-complete replacement of omphacite by diopside and plagioclase in sample NFA-8. Omphacite is low-birefringence, sub-horizontally oriented lamellae in the diopside grain. Horizontal FOV = 2.75 mm. A) Plane-polarized light. B) Cross-polarized light.

Steltenpohl et al. (2006) also reported diopsidic to jadeitic compositions for grains interpreted as retrogressed omphacite in eclogite-facies pseudotachylites found at the Nusfjord locality. Na released from omphacite during this reaction is interpreted to have been accommodated by plagioclase formation.

Retrogression to diopside was accelerated along twin planes (Figures 42 and 56), indicative of slow exhumation (Anderson and Moecher, 2007), and follows the amphibolite-facies reaction Om → low-Na Cpx + Pc. Conversely, sample NFA-17 contains a symplectic mixture of plagioclase and amphibole (Figure 57), which is reported to indicate relatively rapid exhumation (Anderson and Moecher, 2007). Omphacite characteristically breaks down to plagioclase and diopside (Markl and Bucher, 1997; Steltenpohl et al., 2006). In this case, diopside is further retrogressed to green amphibole following low-Na Cpx → Am. The symplectite occurs along garnet rims and within garnet embayments. Markl and Bucher (1997) report reintegrated omphacite compositions based on low-Na clinopyroxene and plagioclase symplectites from Nusfjord to be similar to compositions preserved in omphacite from the Skagen eclogite locality (Figure 3).

Hypersthene, a high-pressure orthopyroxene, is found within the eclogite shear zones as remnants of the granulite-facies host rock and is variably replaced by omphacite, documenting eclogitization of the host gabbronorite within the eclogite shear zone shoulder (Figure 55). As hypersthene does not contain Na, and because the eclogitization

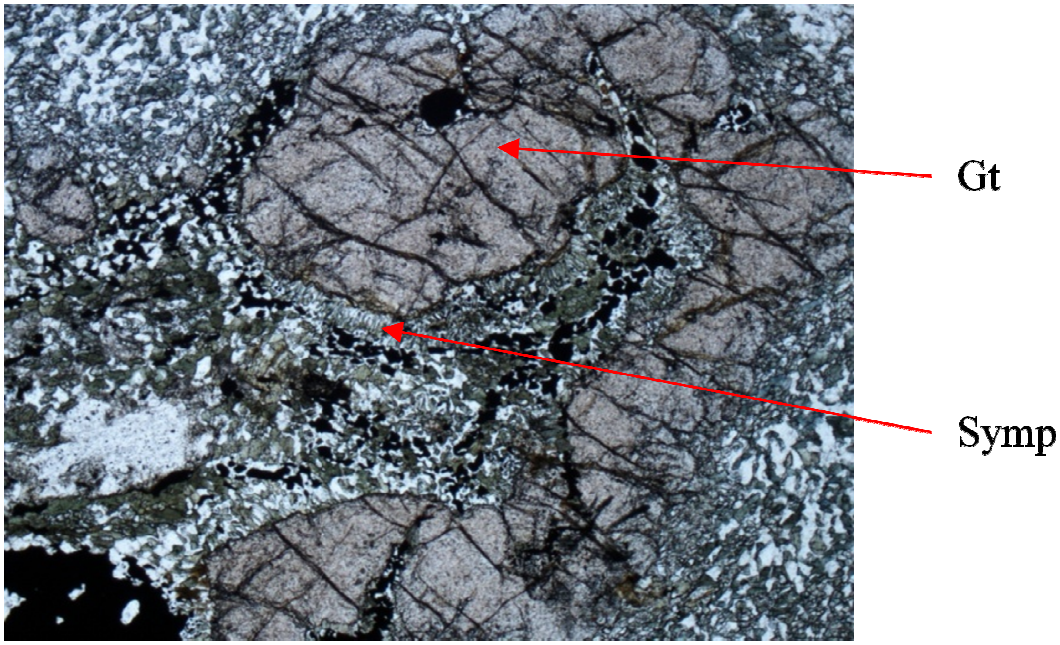

Figure 57: Photomicrograph of symplectic intergrowth (Symp) of plagioclase and amphibole within an embayment in garnet (Gt) in sample NFA-17. Viewed in plane-polarized light. Horizontal FOV = 2.75 mm.

reaction was isochemical (Markl and Bucher, 1997) with the exception of the addition of Cl, Ba, and H_2O (Markl et al., 1998; Kullerud et al., 2001), this reaction must have followed Hyp + Pc → Om.

Preserved hypersthene grains retained their competency and were rotated into the C-plane during shearing (Figure 43). Hypersthene preservation through eclogitization and subsequent amphibolitization can be attributed to its anhydrous state which must have retarded metamorphic development of omphacite. The arrested reaction series Hy → Om → Di can be seen in a single grain in Figure 55.

Zoisite (sample NFA-6A) is an accessory mineral in Flakstadøy eclogites (Markl and Bucher, 1997). Laths of zoisite in Nusfjord samples are aligned parallel with S-planes in the eclogite shears (Figure 58). Some zoisite grains have subgrain formation (Figure 59), indicating they formed prior to or during the shearing event. Kullerud et al. (2001) documented increasing amounts of clinozoisite in sheared shoulder rocks approaching the eclogite shear zone. In addition, Markl and Bucher (1997) report zoisite inclusions in garnet from Nusfjord eclogites, and amphibole-rimmed zoisite aggregates in eclogites from the Skagen locality. Observations presented here, combined with these previous observations, imply that zoisite is a primary eclogite-facies phase preserved through retrogression.

Interpretations and Conclusions from the Nusfjord Investigation

Tabular injections of basalt (Flaat, 1998) were injected into host gabbronorite prior to shearing and eclogitization (Kullerud, 2001). Gabbronorite and basalt were then

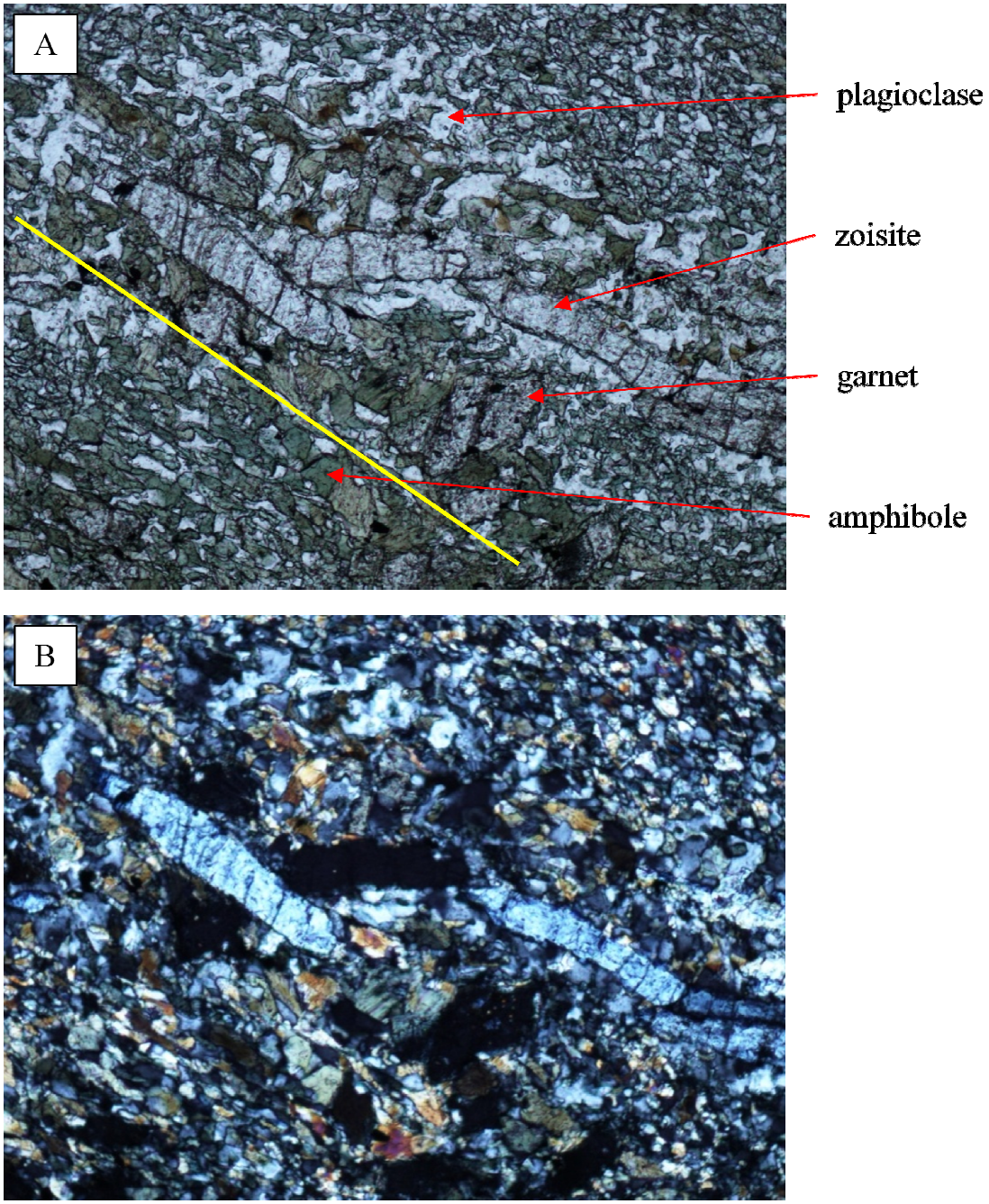

Figure 58: Zoisite in sample NFA-6A is aligned roughly parallel with the eclogite S-plane (yellow). Horizontal FOV = 2.75 mm. A) Plane-polarized light. B) Cross-polarized light.

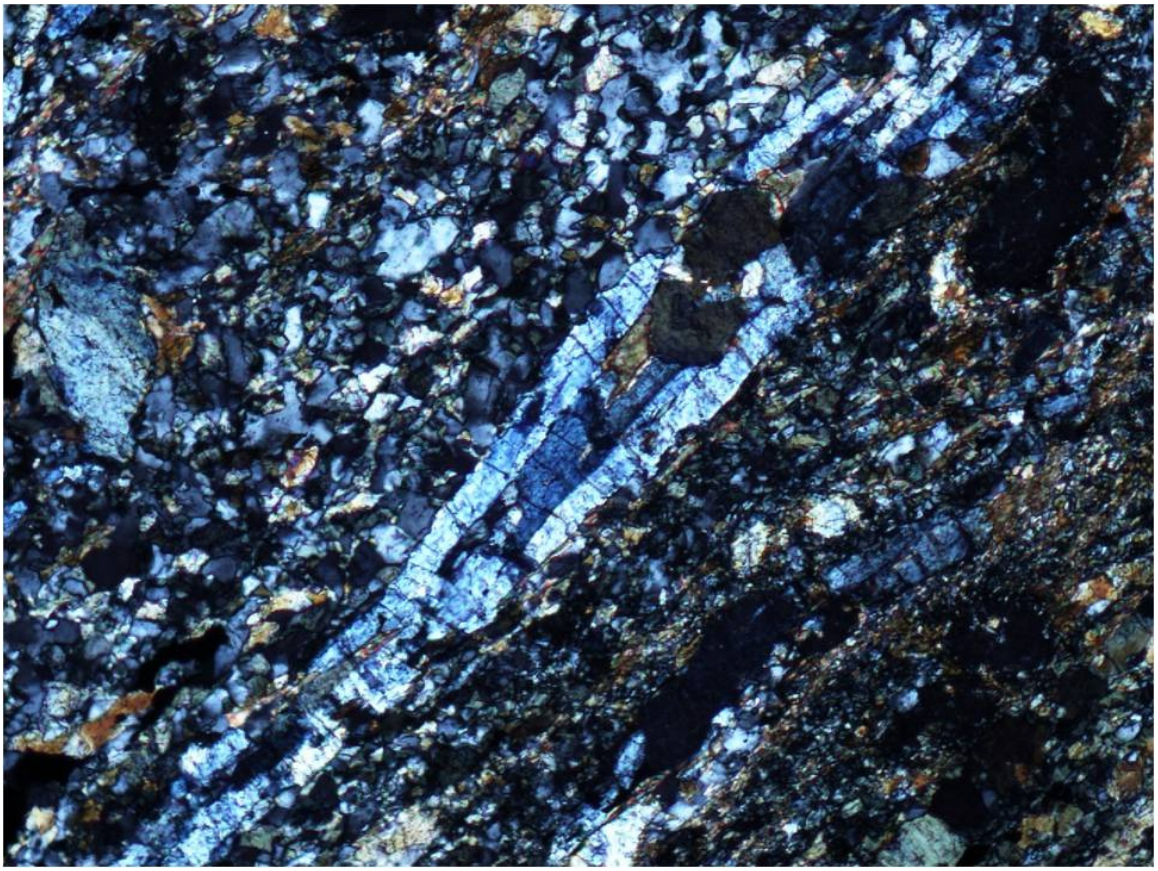

Figure 59: Photomicrograph of zoisite in sample NFA-6A. Subgrain formation indicates formation prior to or during shearing. Cross-polarized light. Horizontal FOV = 2.75 mm.

fractured, most likely during subduction under anhydrous conditions, creating a secondary porosity that allowed deep-crustal Cl- and H_20-rich fluids (Kullerud, 2001; Markl et al., 1998) to infiltrate. This fluid allowed eclogitic assemblages to form in both basalt and adjacent gabbronorite (Markl and Bucher, 1997; Steltenpohl et al., 2006). Left-lateral shearing along an average slip line N 53° W, 16 ° commenced after eclogitization began, as indicated by undeformed cores of omphacite σ-clasts. The rheological response to fluid-mediated weakening in this case was plastic deformation of eclogite and gabbronorite. Measurement of the original and final length of a folded mylonitic layer of plagioclase indicates that shearing resulted in local shortening of no less than 62% in SZ I, the thickest of the Nusfjord shear zones. Omphacite porphyroclasts have tails of amphibole and clinopyroxene (Figure 42) that indicate left-slip shearing took place under amphibolite-facies conditions as well.

Abundant thin (< 2 cm thick) ductile shear zones occur in the gabbronorite host rocks but not in the main eclogite shear zones. These likely formed to accommodate combined rotational displacements and volume decrease due to eclogitization within the shear zone. After eclogitization, the unit was subjected to pervasive amphibolite-facies retrogression that left only scattered remnants of the eclogite facies assemblages.

Markl and Bucher (1997) calculated minimum conditions of 680 °C and >15 kbar for eclogitization of rocks at Nusfjord. Kullerud (1995) reported garnet-biotite thermometry which suggested the mineral assemblage in the shear zone margins formed at >580 °C, herein interpreted to represent amphibolite-facies retrogressive conditions. Steltenpohl et al. (2003) reported a ~433 Ma closure date for a hornblende from a retro-

eclogite at Nusfjord, which records the date the rocks passed through the ~500 °C isotherm during exhumation. If it is assumed that Nusfjord rocks were subjected to eclogite-facies conditions simultaneously with Myrland rocks at ~478 Ma, then Nusfjord eclogites would have to cool through at least 180 °C over a time span of ~45 m.y., which equals a minimum average cooling rate of ~4 °C per million years. Disparate types of omphacite breakdown (symplectite vs. exsolution lamellae) imply differing uplift rates, interpreted to indicate that early exhumation proceeded more rapidly than the later stages.

STORVATNET ECLOGITE LOCALITY

Overview

Retro-eclogites occur near the north-south striking contact between anorthosite, to the east, and troctolite to the west at the Storvatnet retro-eclogite locality (Figure 3; UTM: 33W, 431291 E, 7550515 N). Of the three eclogite localities described herein, Storvatnet is the largest but, unfortunately, outcrops are highly weathered and mostly obscured. The Storvatnet locality, named for a nearby lake, occurs on the slope of a glacially carved valley that is mostly covered by vegetation, glacial till, and float from the ridge above, as well as blocks that clearly were derived from underlying eclogitized rocks. This is unfortunate because the Storvatnet locality has the most diverse lithologic assemblage of the three eclogitized areas investigated in this report. The geologic map of Storvatnet (Figure 60), thus, is an outcrop map interpreted to reveal several retro-eclogite pods encapsulated within the anorthosite and troctolite. Retro-eclogite pods range from a few meters in length and width to up to ~300 m in length by ~100 m width. Although the shape of these pods is not directly observable, they appear to be somewhat lenticular and not interconnected, following by analogy to the better exposed Myrland locality. Variable foliation dip is consistent with the interpretation of isolated pods. In general, the pod long axes appear to be oriented north to northwest, parallel with the strike of the foliation. These pods also contain variable amounts of sheared troctolite and garnet

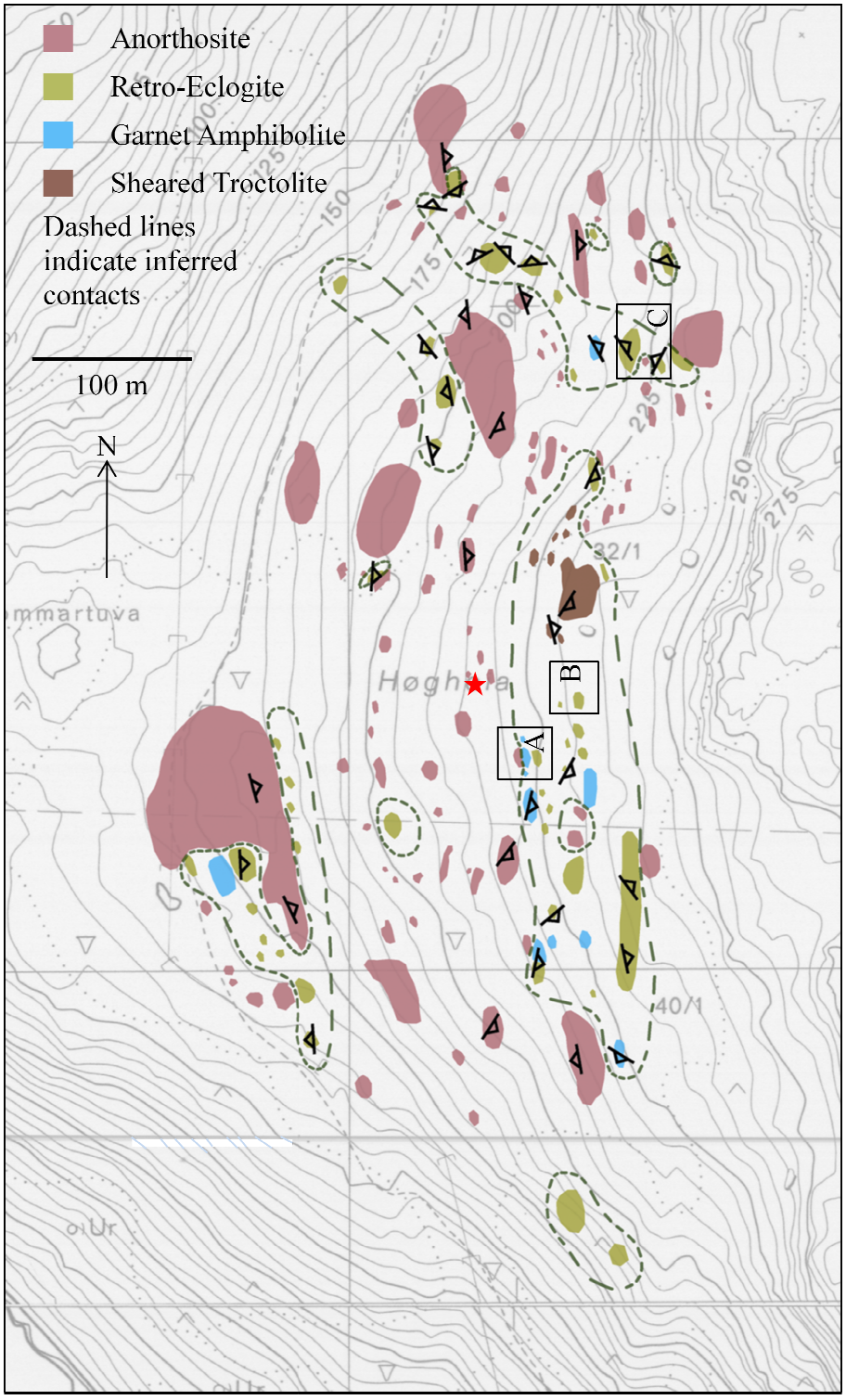

Figure 60: Geologic outcrop map of the Storvatnet eclogite locality created on a 1:5000 topographic base map (Statens Kartverk, Norway). A) Location of eclogite-derived leucocratic veins in Figure 74. B) Location of shear zone in Figure 79. C) Location of paired S-C planes from Figure 81. UTM coordinates in text marked by red star.

amphibolite, which Markl and Bucher (1997) interpreted to be eclogite protolith and retrograde eclogite, respectively. The contact between the country rock and eclogite was only preserved in one location, where it is gradational.

Lithologic Units

Anorthosite

The easternmost unit in the Flakstadøy Basic Complex (Romey, 1971) is anorthosite. Anorthosite outcrops over ~20 km^2, strikes north-northeast, and dips eastward. Plagioclase ($An_{50.5}$-$An_{57.5}$) constitutes between 75% and 98% of the rock. Mafic minerals (with the exception of olivine, which has a very low abundance) make up the balance. As a result, the area depicted as anorthosite in Figure 60 is actually composed of anorthositic norite, noritic anorthosite, and anorthosite. Large feldspar crystals are bent and/or granulated. In-situ plastic fabrics are only observed in shear zones directly proximal to eclogite, otherwise this unit is coarse-grained and massive. Many thin, late-stage mylonitic shears are present in the more plagioclase-rich zones of the anorthosite, similar to those observed at the Myrland and Nusfjord localities. Anorthositic mylonites were observed in locally-derived float blocks. This unit is interpreted to be an early cumulative deposit in the Flakstadøy Basic Complex batholith (Romey, 1971).

Troctolite

Markl and Bucher (1997) report that troctolite is the eclogite protolith at the Storvatnet locality. Weathering has colored these rocks noticeably redder than surrounding units. Mineralogy in the sheared troctolite at Storvatnet is roughly volumetrically equal plagioclase and pyroxene. Only one outcrop of troctolite was observed. This outcrop is located within an inferred eclogite pod (Figure 60) and has a crystal-plastic deformation foliation indicated by plagioclase ribbons and plastically necked pyroxenes. Elongation lineation was not measurable as this outcrop was flush with the ground surface. Despite having been sheared in proximity to observed retro-eclogite, troctolite at this outcrop lacks the garnet of the retro-eclogite. Layered units of troctolite dip predominantly to the east with minor fluctuations that dip westward (Romey, 1971). Troctolite in the Basic Complex generally has a well developed ophitic texture consisting of plagioclase, orthopyroxene, and olivine, which define rhythmically layered units with an average grain size of ~2 cm. Grain size in sheared troctolites is much smaller ($\leq$0.5 mm) indicating dynamic recrystallization, however, the outlines of the original grains are preserved.

Porphyritic Norite

Although anorthosite and troctolite are the predominant country rock units at Storvatnet, porphyritic norite was also observed ~800 m to the south of the eclogitized zone shown on Figure 60. Plagioclase phenocrysts are up to 20 cm long and range from euhedral and trapezoidal shaped to ellipsoidal. These phenocrysts occur in a dark,

aphanitic matrix composed of plagioclase, hypersthene, and ore minerals (Romey, 1971). Phenocrysts are arranged parallel, interpreted to be due to igneous flow. Only limited evidence for crystal-plastic deformation, including stretched grains and ribbons, are observed (Figure 61).

Retro-Eclogite

Retro-eclogite occurs as isolated pods contained within the anorthositic host rock. The retro-eclogites are characterized by red garnets (up to several cm in diameter), patches of green amphibole, and abundant white plagioclase. Although individual grain size is small, mineral types are commonly clustered, giving the rock a distinctive coarse-grained, green, red, and white appearance. Foliation is weakly developed in the retro-eclogite and elongation lineations are rarely observed.

Two distinct generations of amphibole are observed in the retro-eclogite. In Figure 62, the large amphibole grain is unusual in that is has a relatively large, tabular shape. This amphibole has a saturated green color near cleavage planes and a pale blue-green color in the core. It is surrounded by coarsely symplectic plagioclase and amphibole of a markedly darker green color. The large amphibole is, therefore, interpreted to be of an earlier generation, perhaps a preserved primary amphibole. First generation amphiboles are typically euhedral to subhedral, pleochroic (dark green to light green or colorless), and have low second-order birefringence. Fine-grained amphiboles are more prevalent. They occur as halos around primary amphibole and pyroxene, form dynamically recrystallized ribbons (Figures 63 and 64), and exist as

Figure 61: Porphyritic norite ~800 m from eclogitized zone. Light colored grains are plagioclase. Hammer is ~35 cm long.

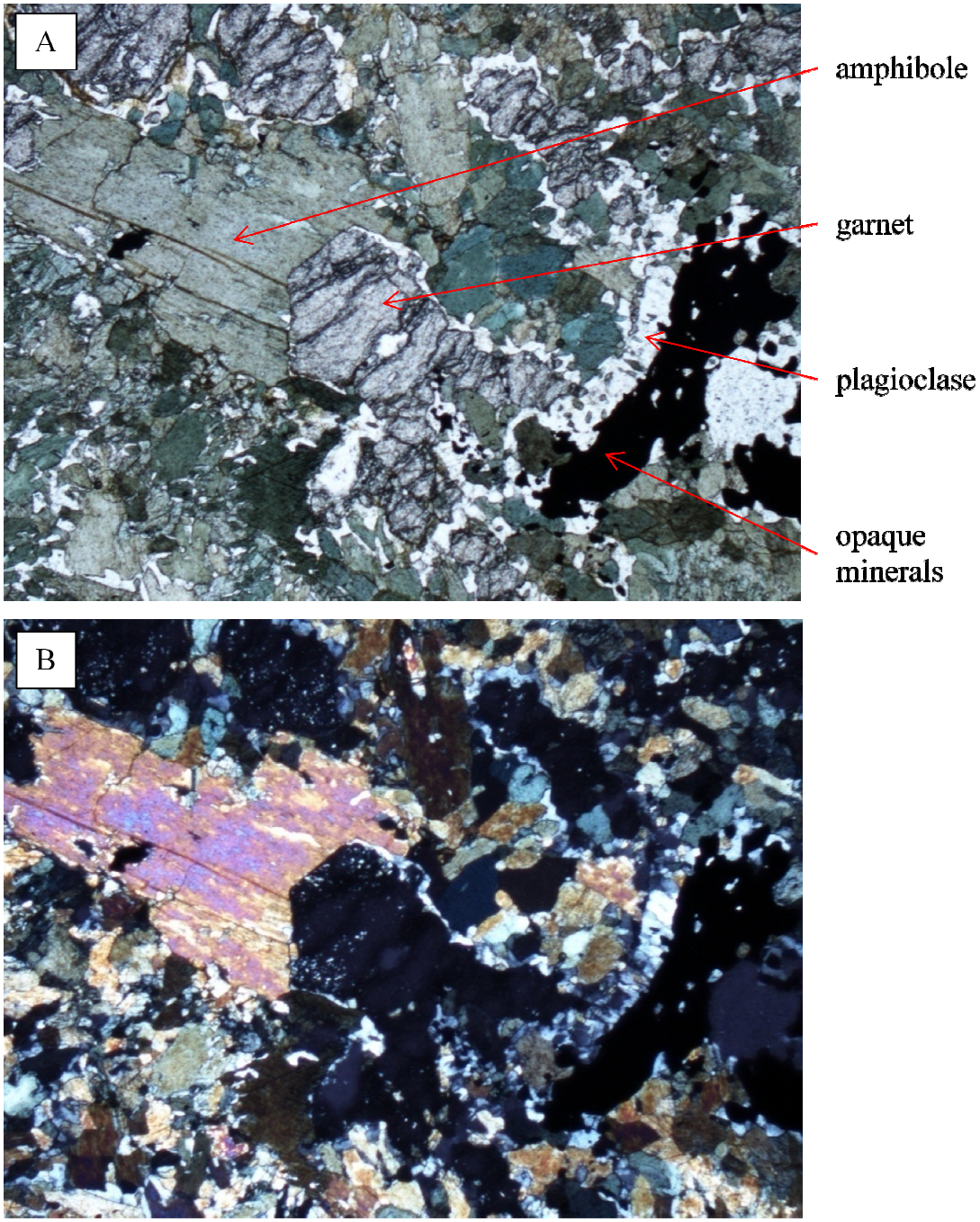

Figure 62: Photomicrograph of garnet crystal faces preserved along contact with amphibole in sample SR-24 from the Storvatnet locality. Horizontal FOV = 2.75 mm. A) Plane-polarized light. B) Cross-polarized light.

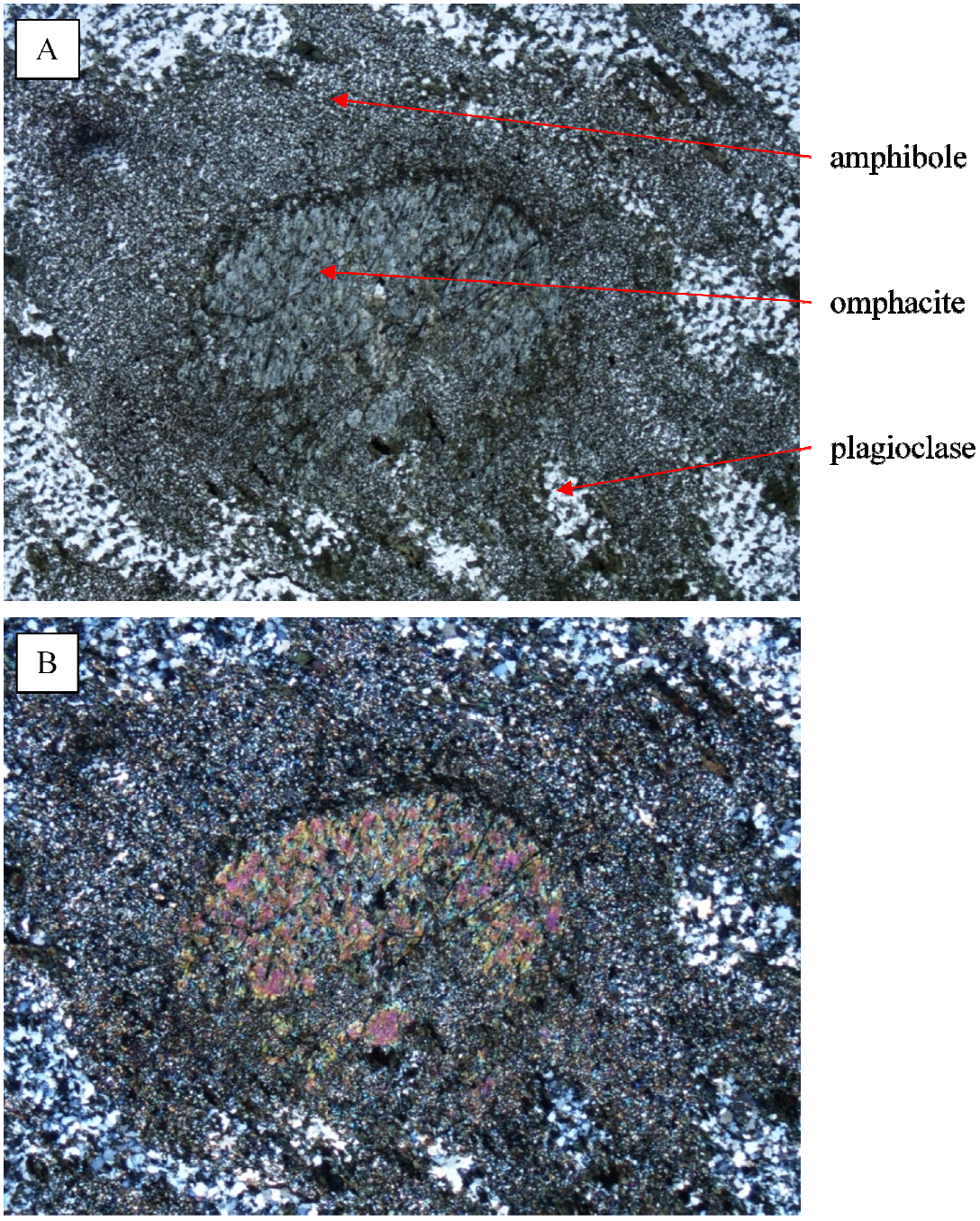

Figure 63: Mantle of fine grained amphibole (core-mantle structure) surrounding relict omphacite from sample SR-22. Note fairly high birefringence. A) Plane-polarized light. B) Cross-polarized light. Horizontal FOV = 5.5 mm.

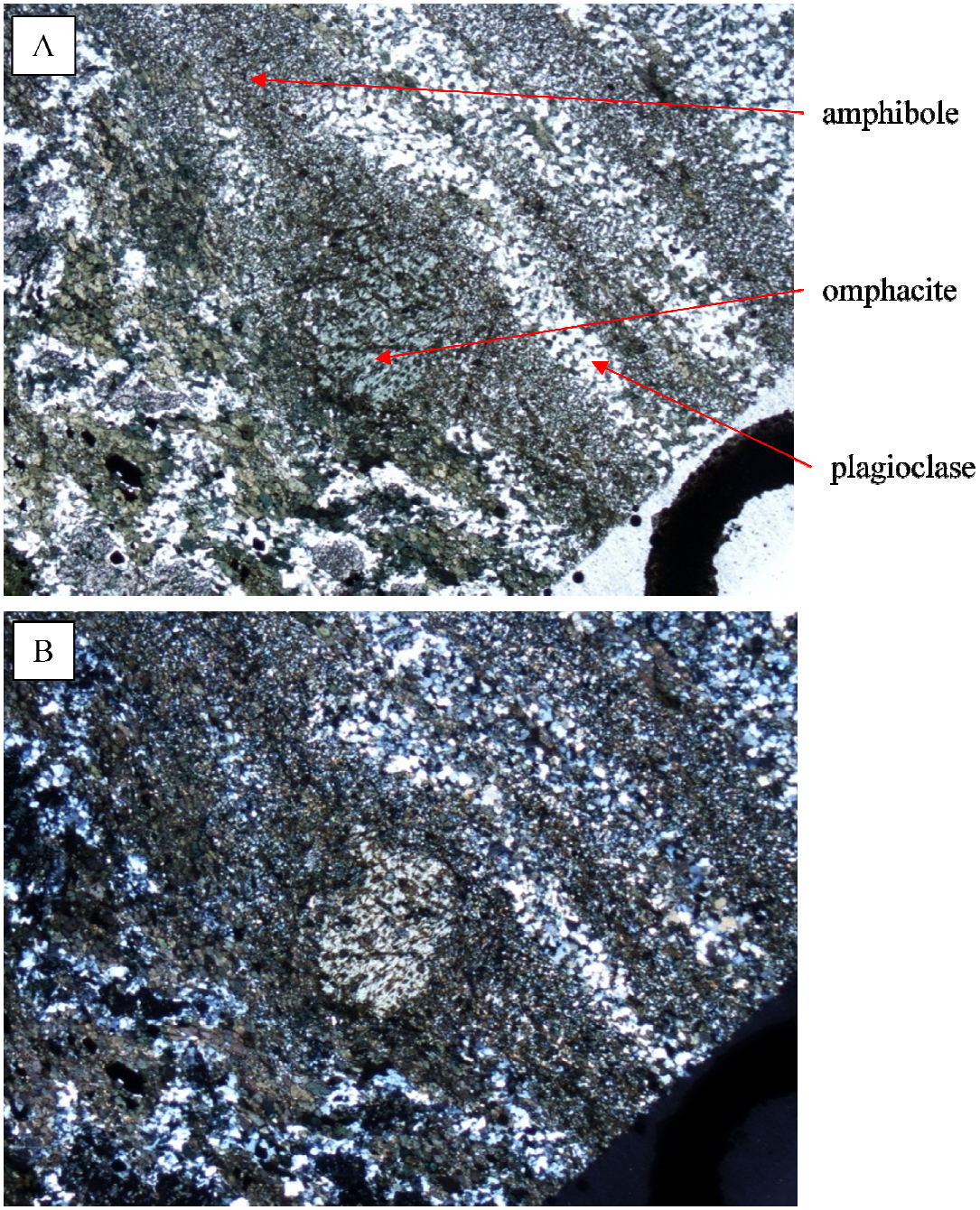

Figure 64: Relict omphacite theta clast surrounded by fine grained tails of dynamically recrystallized amphibole. Note low birefringence. Plagioclase and amphibole flow banding wraps around omphacite clast. Horizontal FOV = 5.5 mm.
A) Plane-polarized light. B) Cross-polarized light.

plagioclase/amphibole symplectite inclusions in large, primary garnets (Figure 65). Second generation amphiboles have a much smaller average grain size (~0.05 – 0.5 mm), are anhedral, non-pleochroic, and have low first-order birefringence, although the fine grain size may partly mask the latter two qualities. The halo and ribbon amphiboles are interpreted to be retrogressed primary amphibole grains, possibly sheared. The symplectites are interpreted to be the retrogressive product of omphacite inclusions in primary garnet.

Most of the plagioclase in Storvatnet area rocks appears to be a reaction product from the breakdown of primary eclogite-facies minerals, however, some primary plagioclase does exist. Primary plagioclase typically occurs in ribbons of very fine grains that define a flow texture (Figure 66). These plagioclase bands are the result of dynamic recrystallization from a larger parent plagioclase, likely derived through comminution of the porphyritic troctolite, the presumed eclogite protolith.

Rocks in the Storvatnet area contain two distinct garnet generations that are similar to those described from the Nusfjord area. First generation garnets are irregularly shaped grains that are usually full of inclusions. They appear highly degraded and only rarely preserve their original grain shape (Figure 67). The characteristic anhedral form of these garnets is interpreted to be a function of retrogression and/or neomineralization. First generation garnets have one well-developed fracture set and one lesser fracture set (Figure 68). Second generation garnets are optically clearer grains, commonly as haloes around agglomerations of other minerals (Figures 69 and 70) or as euhedral grains (Figure 62). Garnet haloes are radially fractured with some fractures continuous into the

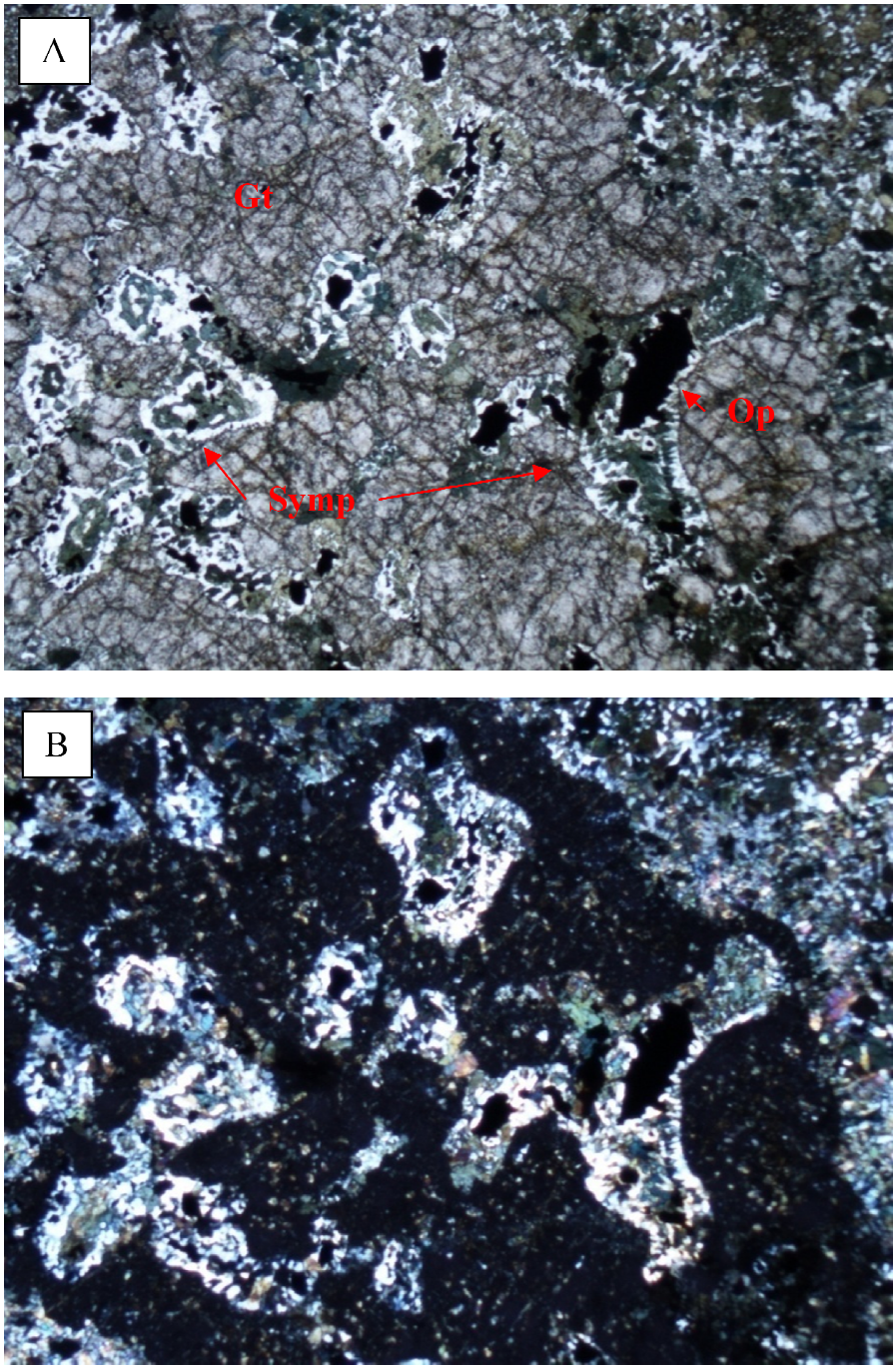

Figure 65: Photomicrograph of amphibole + plagioclase + opaques symplectite (Symp) formed from inclusions in garnet in Storvatnet area sample SVM-1. Gt = Garnet; Op = opaque minerals. Horizontal FOV = 2.75 mm. A) Plane-polarized light. B) Cross-polarized light.

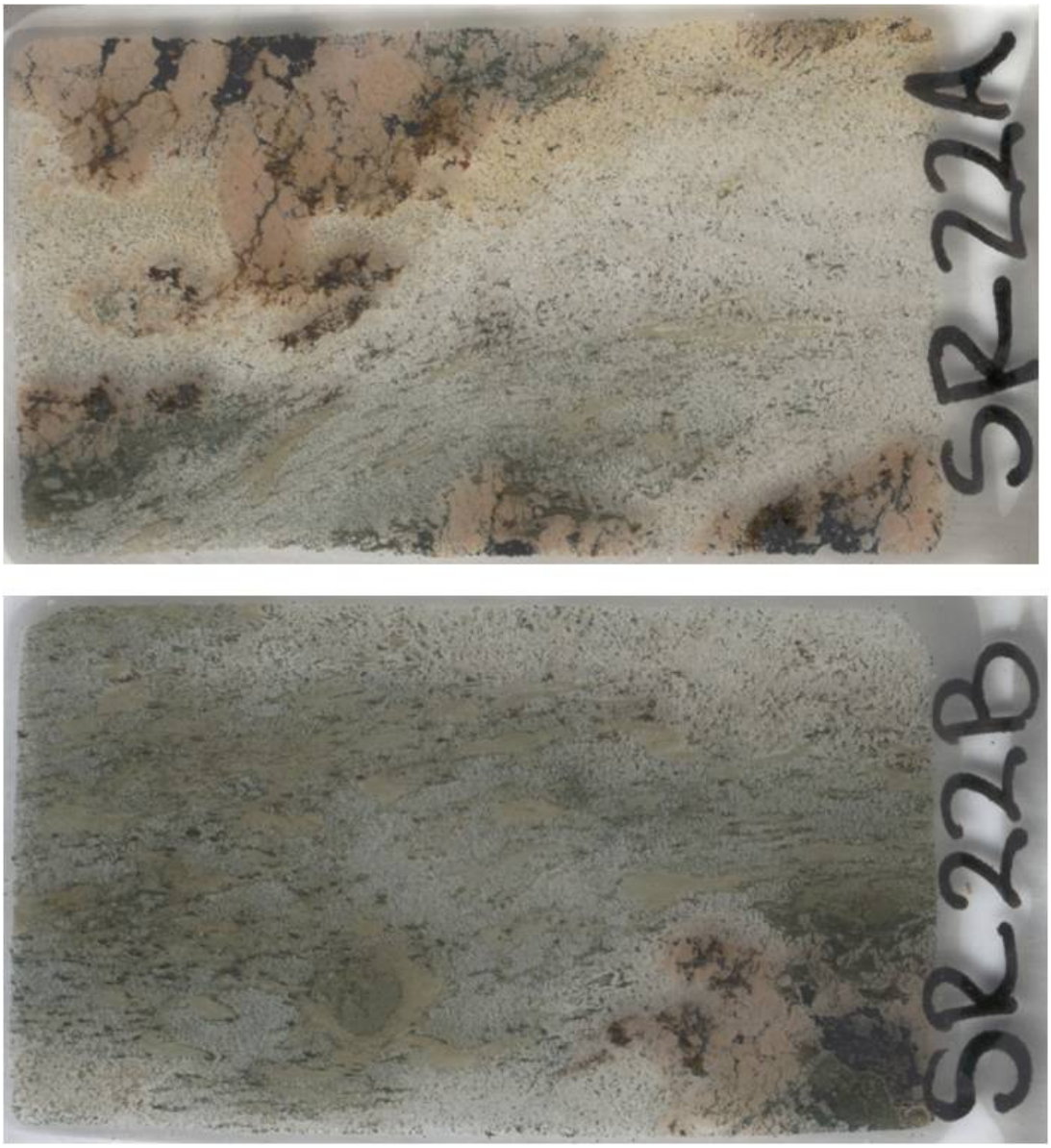

Figure 66: Scans of two thin sections from Storvatnet sample SR-22. Foliation was not clear, therefore, these two thin sections were cut perpendicular to each other and parallel to elongation lineation. Plastic flow structure wraps around undeformed, but retrograded garnet. The flow structure is defined predominantly by the fine grained, dynamically recrystallized plagioclase. Short dimension of slide is 2 cm.

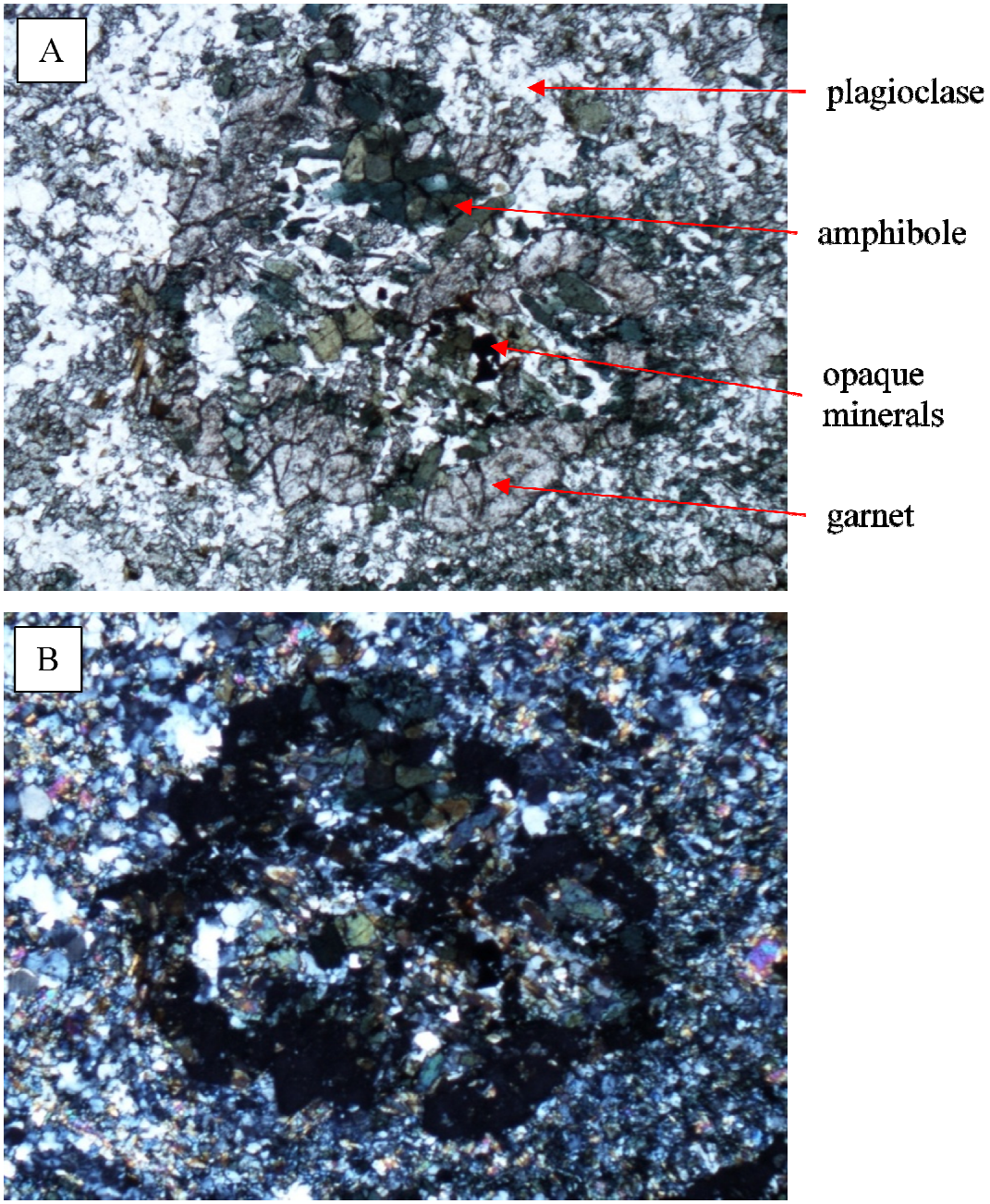

Figure 67: Photomicrograph of a highly degraded, inclusion filled, first generation garnet from Storvatnet area sample SR-21. Included material comprises amphibole, plagioclase, and opaque minerals. Horizontal FOV = 2.75 mm. A) Plane-polarized light. B) Cross-polarized light.

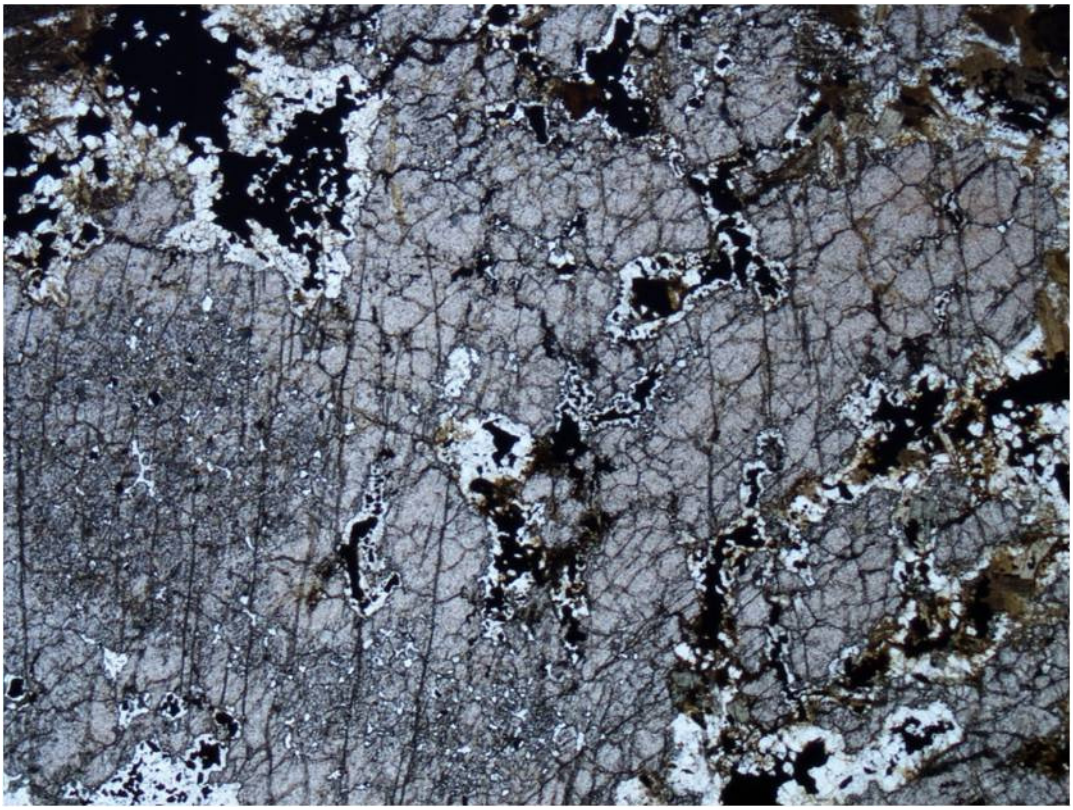

Figure 68: Photomicrograph of a first generation garnet from sample SR-22 with two fracture sets. The dominant fracture set is oriented roughly vertical in this photo. The subordinate set is oriented roughly 50 °Clockwise from vertical. Inclusions are opaques with plagioclase rims. Plane-polarized light. Horizontal FOV = 5.5 mm.

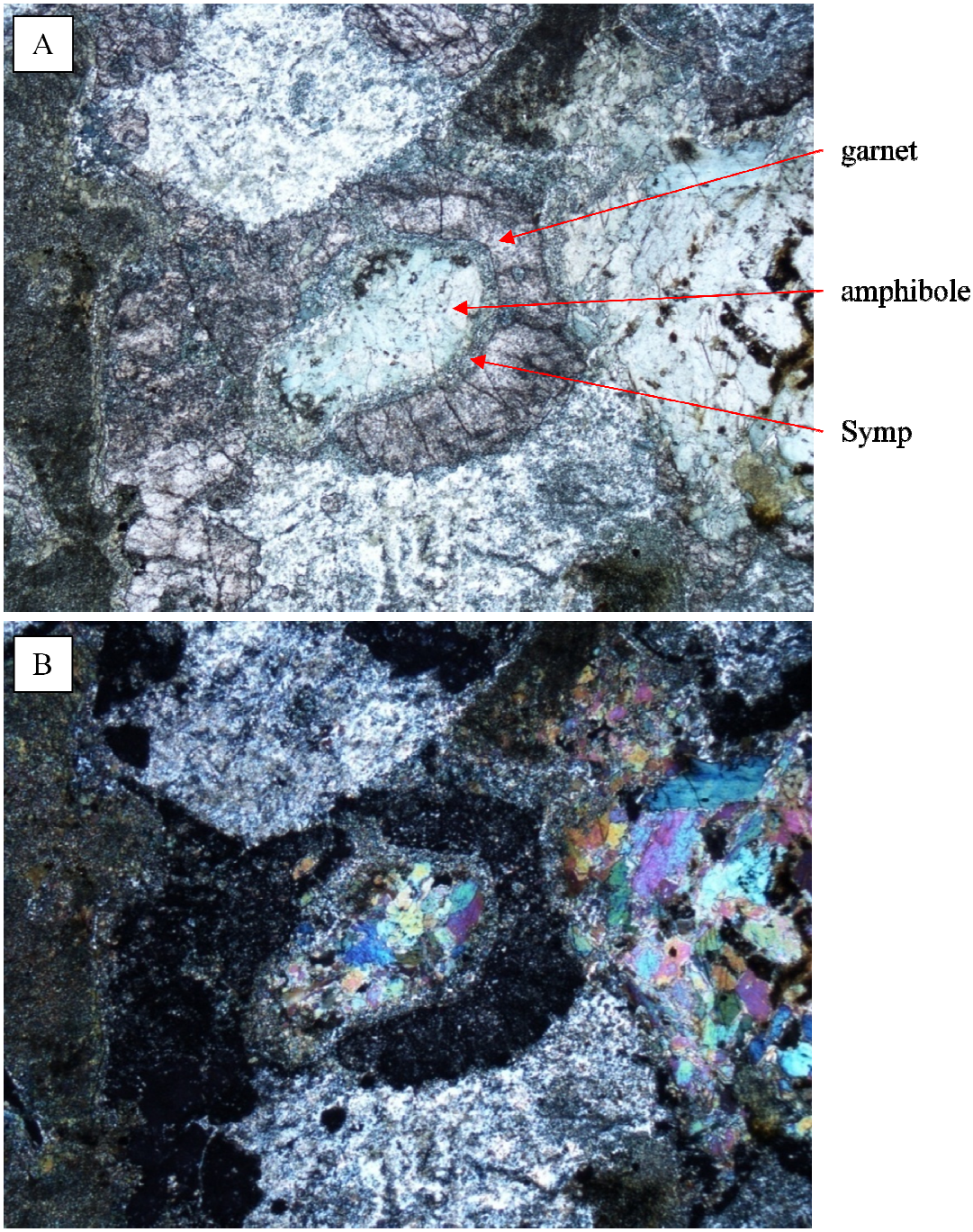

Figure 69: Garnet halo formed around amphibole grains. The garnet has numerous tiny inclusions and is radially fractured. Amphibole color is pale green-blue to clear. A thin corona of very fine-grained amphibole/plagioclase symplectite (Symp) exists between the garnet and the larger amphiboles. Horizontal FOV = 2.75 mm. A) Plane light. B) Cross-polarized light.

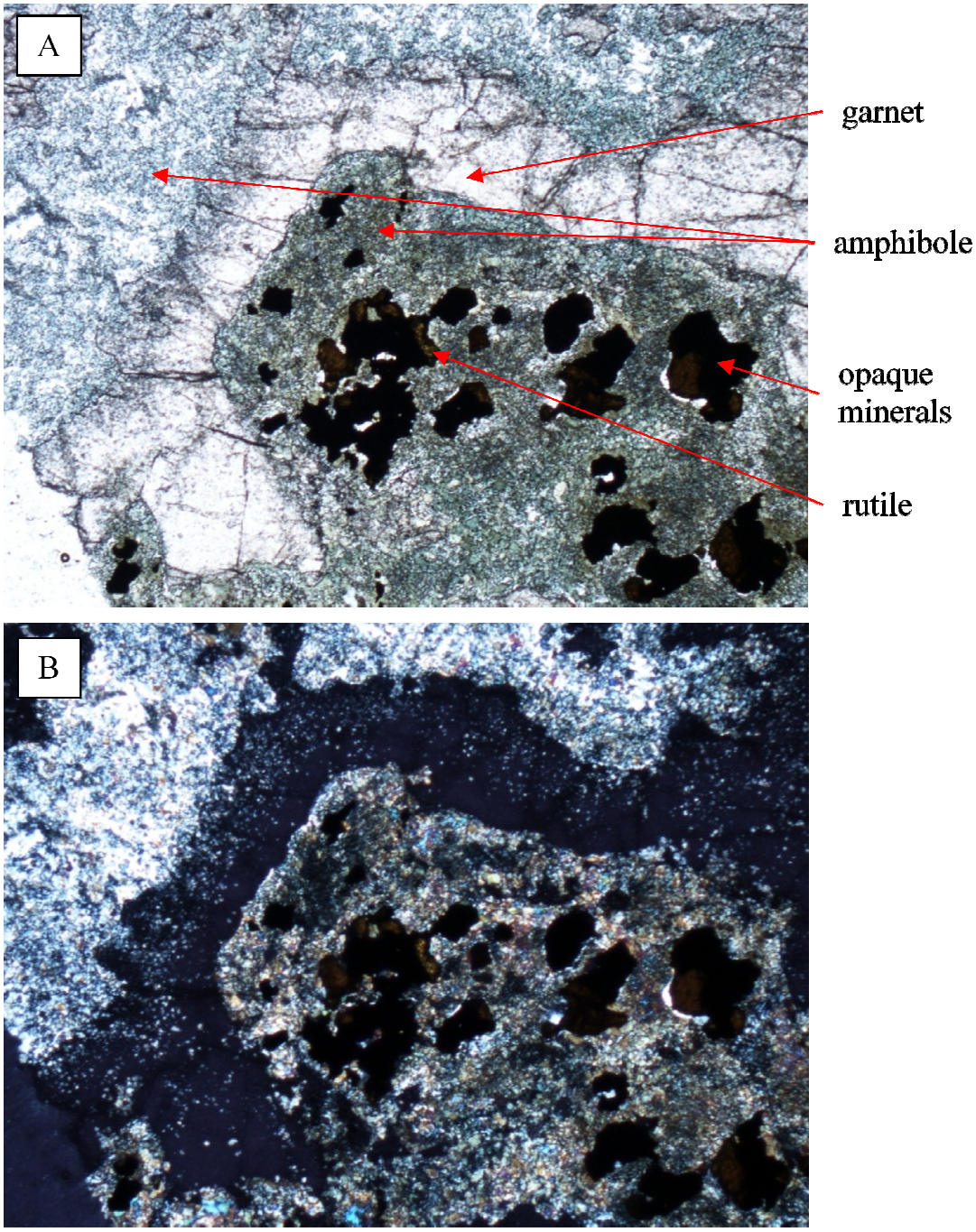

Figure 70: Photomicrograph of a garnet halo around fine grained amphibole, plagioclase, and opaque minerals. Note the inclusion density increasing outwards within the garnet rim. Horizontal FOV = 2.75 mm. A) Plane-polarized light. B) Cross-polarized light.

central material (Figure 69). Inclusion density in the haloes increases towards the outer rims (Figure 70). Outer edges of garnet rims are irregular whereas the inner edges are significantly straighter (Figure 70). Radially fractured haloes are not interpreted to record deformation but, rather, the result of volume changes due to retrogression.

The spatial association of the garnets with the amphibole and the euhedral nature of the garnets compared with the eroded texture of the amphiboles suggest that the garnets, and a small amount of plagioclase, formed at the expense of amphibole. Close inspection of Figure 62 reveals no amphibole embayments into the garnet and only minimal rim degradation. These might be expected had the amphibole formed subsequent to the garnet.

Aside from fractures, garnets from rocks in the Storvatnet area, regardless of generation, do not appear to be internally deformed. Other minerals, especially plagioclase, however, are finely recrystallized due to crystal-plastic deformation and wrap around the more competent garnets (Figure 66), indicating the garnets had grown before deformation was complete. Notably missing from Storvatnet retro-eclogites are dynamically recrystallized stringers or tails of garnet that are common at Nusfjord. Rather, garnet porphyroclasts at Storvatnet generally retain their round and dodecahedral form though mostly without crisp planar crystal faces (Figure 67). In other samples, particularly where plagioclase is not abundant, garnet has an amoeboid or 'reef' appearance, which also implies a relatively low degree of strain (Figure 71). The amoeboid and degraded garnets are interpreted to have grown first, prior to deformation.

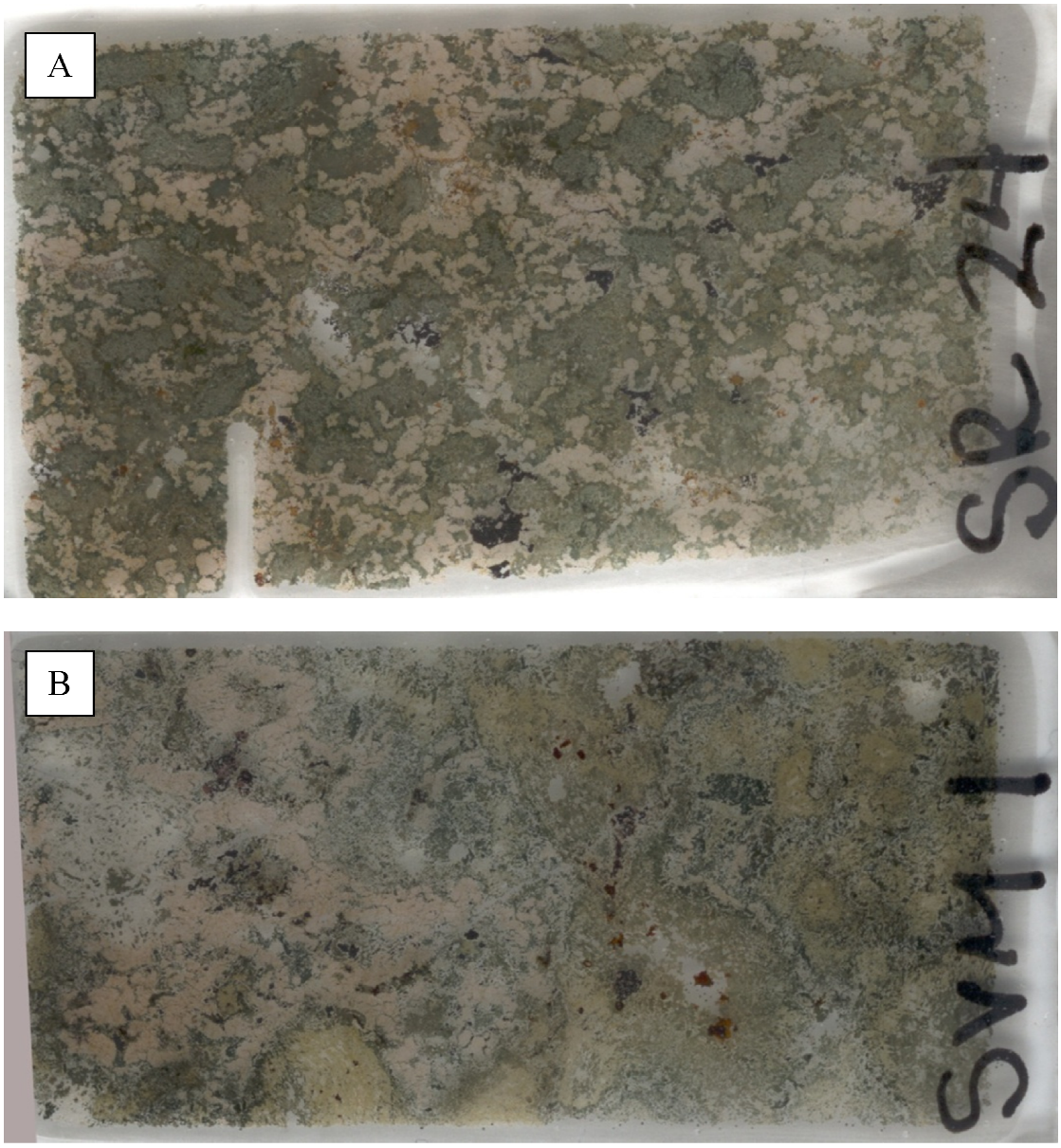

Figure 71: Scans of thin sections of retro-eclogite from the Storvatnet locality illustrating garnet in an amoeboid or 'reef' habit, which requires recrystallization after deformation. The paucity of plagioclase likely restricted dynamic flow in this rock. Short dimension of slide is 2 cm. A) Sample SR-24. B) Sample SVM-1.

Later, after deformation had ceased, the second, less abundant generation of garnet grew creating the haloes and euhedral grains. Amoeboid garnet symplectites and 'reef' structures are likely the result of exhumational processes.

Primary omphacite is only rarely preserved (e.g. sample SR-22B). These grains exist as degraded cores surrounded by fine grained amphibole with relatively minor Na. Omphacite grains were sheared progressively from the grain boundaries, forming core-mantle haloes (Figures 63 and 64), and documenting rotational recrystallization. These grains are interpreted to have been omphacite formed prior to shearing and amphibolite-facies retrogression. Omphacite was not observed in other samples, but characteristic omphacite retrogression products are common. Sample SVM-1 contains symplectic intergrowths of amphibole and plagioclase. These symplectites occur as both retrograded entire omphacite grains (Figure 72) and as rims on garnets and garnet inclusions (Figures 65 and 72). Previous studies of Flakstadøy eclogites have found omphacite formed as garnet inclusions and formed along cracks in garnets (Markl and Bucher, 1997). Like at Myrland and Nusfjord, omphacite at Storvatnet has broken down to symplectic intergrowths following the amphibolite-facies retrogressive reactions Om → low- or medium-Na Cpx + Pc and Cpx→Am.

Garnet-bearing Amphibolite

Garnet-bearing amphibolite is volumetrically small and, similar to the Myrland locality, is interpreted to be strongly retrogressed eclogite. In outcrop the rock is black with anastomose white bands. It occurs adjacent to retro-eclogite outcrops and is

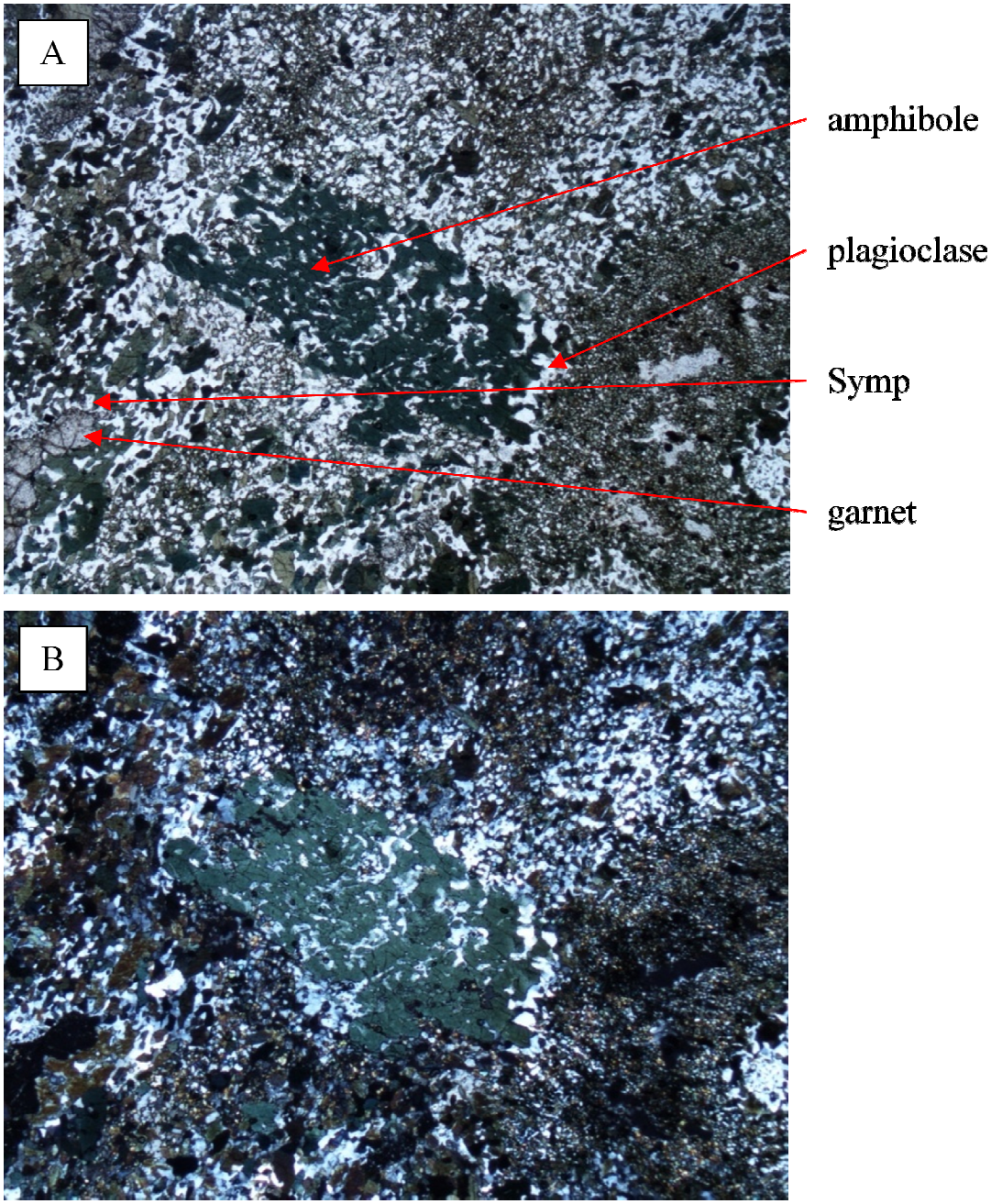

Figure 72: Photomicrograph of a pyroxene pseudomorph that has retained its original grain shape though it is now completely altered to amphibole and plagioclase. Note also the symplectite (Symp) rim around the garnet in the lower left corner. Horizontal FOV =2.75 mm. A) Plane-polarized light. B) Cross-polarized light.

included in the inferred retro-eclogite pods on Figure 60. Rare (< 1%), small (0.5 - 1 mm diameter), light red garnets are the only minerals readily identifiable to the naked eye. Mineralogy of amphibolite is predominantly fine- to medium-grained amphibole (≤ 2 mm, ~40%), fine-grained quartz (≤ 0.5 mm, ~30%), and plagioclase (~30%). Plagioclase forms thin (~3 mm width), irregular bands as well as equant grains. Evidence for crystal-plastic deformation was not observed in the amphibolite. Contacts with other rock types were not observed due to rubble and float cover.

Leucocratic Veins and Mobilized Rocks

Fine-grained, massive, leucocratic material was observed to form 'blebs' within, and to cut across retro-eclogite at the Storvatnet locality (Figures 73 and 74, location A on Figure 60). This material was observed mostly in float blocks of retro-eclogite, but was also observed within several in-situ retro-eclogite outcrops at the same location. The distribution of the blocks in combination with the outcrops implies a minimum area of injection and mobilized material of ~10 m^2. Mineralogy of this mobilized material is approximately 50% plagioclase, 30% muscovite, 20% zoisite, and trace biotite. Plagioclase crystals are 0.2 – 1.0 mm in diameter with curvilinear to lobate grain edges and commonly contain subgrains, nucleations, undulose extinction, and fractured grains. Large (≤ 5 mm) muscovite crystals form bands up to 2 cm long and 0.5 cm wide. Muscovite bands contain numerous inclusions of zoisite grains (up to 50% of the muscovite volume is zoisite). Zoisite crystals are aligned with each other and with the muscovite bands but not necessarily with individual muscovite crystals.

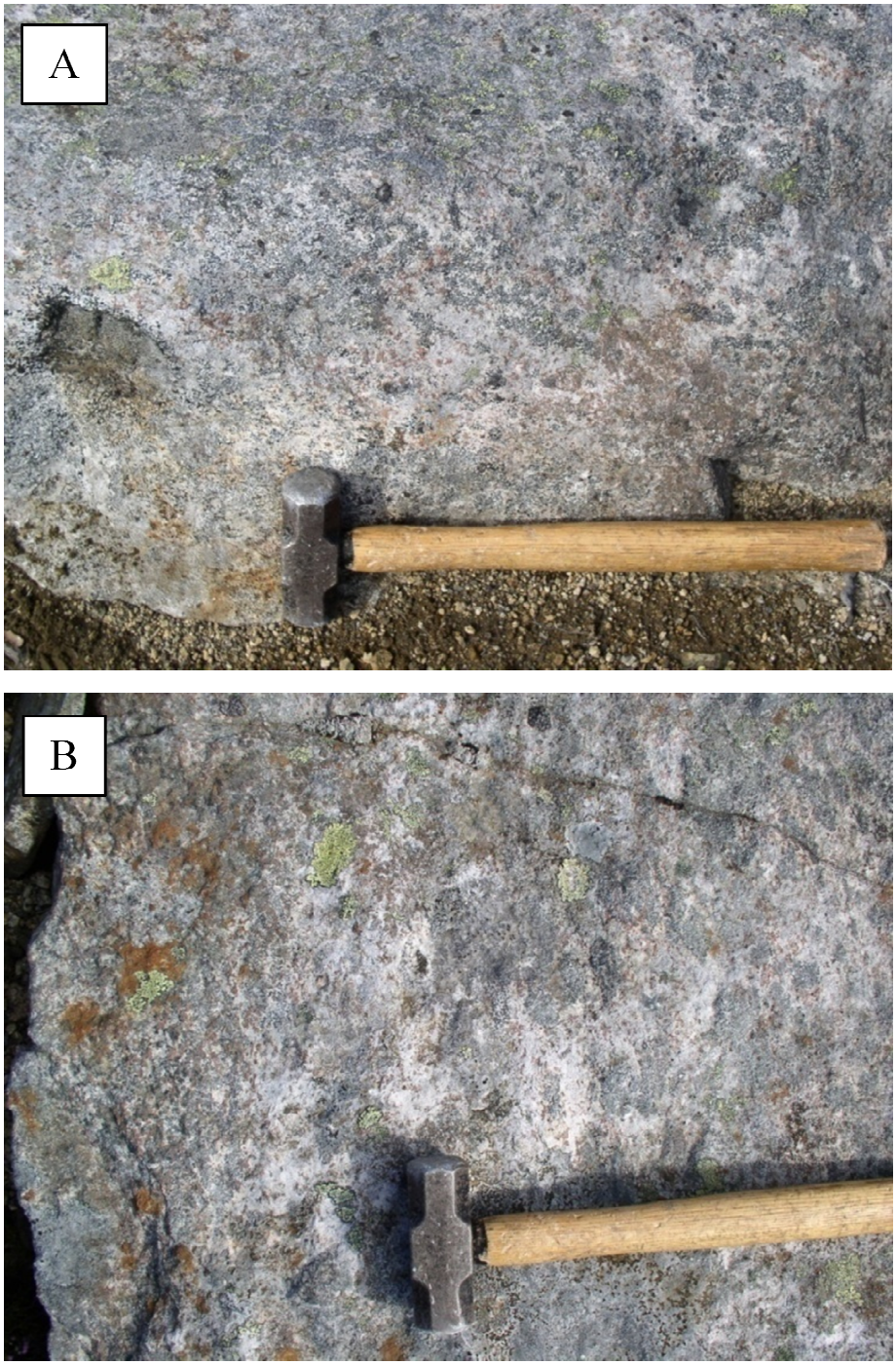

Figure 73: Diffuse, mobilized, monzodioritic to anorthositic ‘sweat out’ blebs within eclogite. Hammer is ~35 cm long. Hammer head is ~10 cm wide. A) Volume of mobilized material increases downwards in photograph. B) Mobilized material is roughly volumetrically equal to eclogite in this photograph.

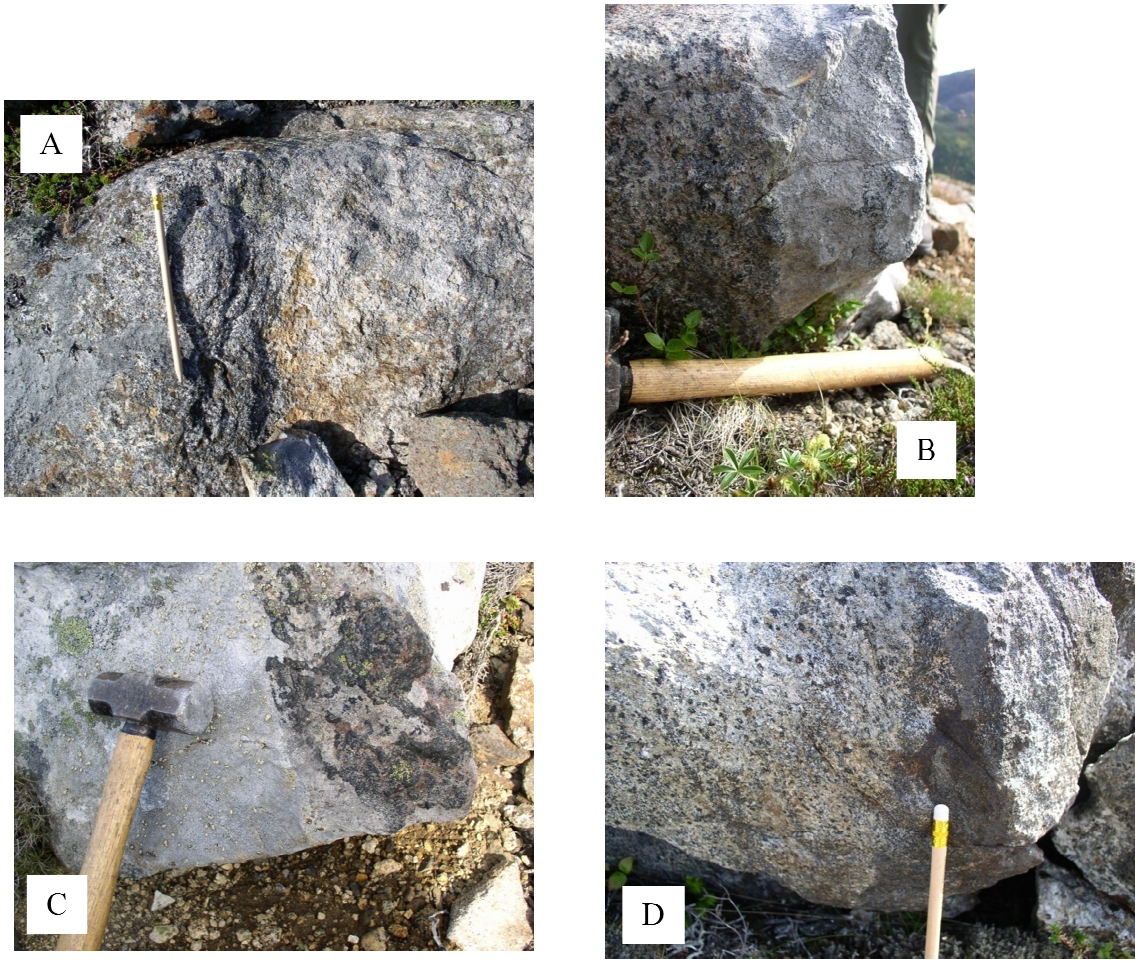

Figure 74: Photos depicting the contact between retro-eclogite and leucocratic injections. All were taken at location A on Figure 60 (samples SR-25 and SR-30). A) Retro-eclogite on left, injection on right. Contact is vertical and gradational over 1 - 2 cm. B) Retro-eclogite on left, injection on right. Contact is vertical and sharp. C) Injection on left, retro-eclogite on right. Contact is roughly vertical. Several small-scale off-shoot injections into retro-eclogite are present. D) Injection on left, retro-eclogite on right. Contact is vertical and sharp. Note the presence of biotite in the injection.

Whole rock geochemical data (Table 12) for samples SR-25 and SR-30 from mobilized material injections were used to calculate CIPW norm values (Table 13) that indicate monzo-dioritic and anorthositic compositions, respectively (Figure 75). These are interpreted to be eclogite-derived 'sweat-outs' (Figure 73) of minerals with low melting temperatures that coalesced into the *in-situ* injections in Figure 74. This process clearly post-dates eclogitization of the troctolite, but temperature and pressure conditions of this partial melting event and consequent injection of the veins are unknown at the time of this report. $^{40}Ar/^{39}Ar$ age dating of muscovite from sample SR-25 was being conducted by Dr. Willis Hames of Auburn University as this thesis was written.

Structures

The primary eclogite-facies assemblage of garnet-omphacite-rutile-magnetite is observed as scattered remnants within the amphibolite-facies fabrics preserved in Storvatnet rocks. Foliation and lineation data were measured in both anorthosite country rock and retro-eclogite lenses. Mylonitic foliation and elongation lineation in retro-eclogite is defined by dynamically recrystallized amphibole and plagioclase (Figures 63, 64 and 66). Omphacite grains with core-mantle structures (Figures 63), theta-clast omphacite grains (Figure 64), and plagioclase ribbons wrapping around large garnets (Figure 66) all indicate that eclogitization preceded shearing. Dynamically recrystallized amphibole has been found to form at temperatures ranging from 450 to ~640 °C (Biermann and van Roermund, 1983; Cumbest et al., 1989; Cao et al., 2007). Ribbons of dynamically recrystallized amphibole and omphacite theta-clast tails composed of

Major Oxide	Weight %		Recalculated to 100%	
	SR-25	SR-30	SR-25	SR-30
SiO_2	53.6	55.7	53.33	55.42
Al_2O_3	26	26	25.87	25.87
Fe_2O_3	3.3	1.67	3.28	1.66
CaO	7.44	8.59	7.40	8.55
MgO	0.38	0.18	0.38	0.18
Na_2O	4.47	5.87	4.45	5.84
K_2O	2.52	0.88	2.51	0.88
Cr_2O_3	<0.01	<0.01	<0.01	<0.01
TiO_2	0.27	0.18	0.27	0.18
MnO	0.02	0.01	0.02	0.01
P_2O_5	0.01	0.06	0.01	0.06
SrO	0.24	0.22	0.24	0.22
BaO	0.18	0.08	0.18	0.08
LOI	1.83	0.93	1.82	0.93
Total	100.5	100.5	100.00	100.00

Trace Element	Concentration (ppm)	
	SR-25	SR-30
Ce	4.4	4.7
Dy	<0.1	<0.1
Er	<0.1	<0.1
Eu	0.5	0.1
Gd	<0.1	<0.1
Ho	<0.1	<0.1
La	2.8	2.8
Lu	<0.1	<0.1
Nd	1.4	1.5
Pr	<0.1	<0.1
Sm	<0.1	<0.1
Tb	<0.1	<0.1
Th	<1	<1
Tm	<0.1	<0.1
U	<0.5	<0.5
Y	0.6	0.5
Yb	<0.1	<0.1

Table 12: Major oxide weight percent and trace element geochemical data for samples SR-25 and SR-30, collected from the eclogite partial-melt injections shown in Figure 74.

	CIPW norm	
Mineral	SR-25	SR-30
Qz	1.48	0
Co	2.41	0
Or	14.82	5.19
Ab	37.62	49.06
An	36.62	41.76
Ne	0	0.17
Di	0	0.18
Hy	0.94	0
Il	0.04	0.02
Hm	3.29	1.66
Ap	0.02	0.13

Table 13: CIPW norm data for eclogite-derived leucocratic injections at the Storvatnet locality.

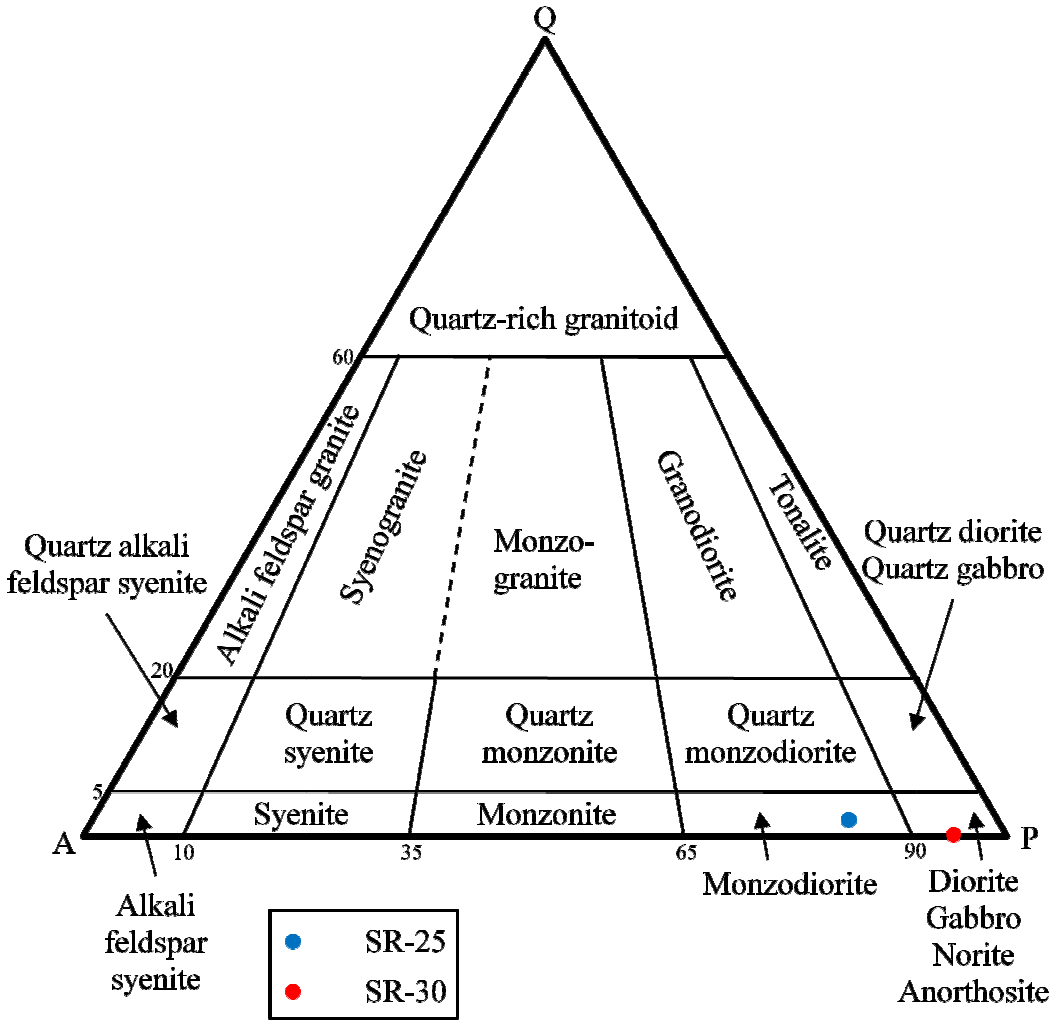

Figure 75: Upper half of a Q-A-P-F diagram (LeMaitre, 1989) on which the CIPW norm composition of Storvatnet samples SR-25 and SR-30 are plotted.

amphibole indicate that shearing took place under amphibolite-facies conditions. This interpretation is supported by the fact that garnet shows no evidence of internal deformation. Any eclogite-facies deformational fabrics that may have been present have been obliterated. Shear foliation was only apparent in country rocks adjacent to retro-eclogite pods, where a weak foliation is defined by plagioclase crystals stretched parallel to the pod boundary. Extensive weathering and poor exposure precluded observation of any lineations in the anorthosite marginal to the retro-eclogite lenses.

Mylonitic foliation in retro-eclogite strikes northward and dips eastward with the average orientation N 12° E, 44° SE (Figures 60, 76, and 77). Foliation orientation is variable in the northernmost exposures, which may indicate dependence on position within the eclogite body. This might be expected because the margins of the competent lens will naturally be the zone of most intense deformation and will parallel the deformation vector outside the lens. Rare elongation lineations weakly congregate around S 05° E, 45° in the stereographic projection in Figure 78.

A well-exposed crystal-plastic shear zone (Figure 79) oriented N 31° E, 41° SE (Figure 80) was observed at location B on Figure 60. This shear zone has a minimum strike length of 3 meters and a minimum thickness of 0.5 meters (determined by outcrop size). Elongation lineations measured in this shear zone trend due south and plunge at 23°. Stereographic reconstruction, using the changing attitudes of S-planes as they are swept into the C-plane, yields the slip line S 16° W, 13°, consistent with elongation lineations located both at this outcrop and throughout the Storvatnet locality (Figure 80). Predominantly left-lateral strike-slip motion with a minor reverse component is indicated.

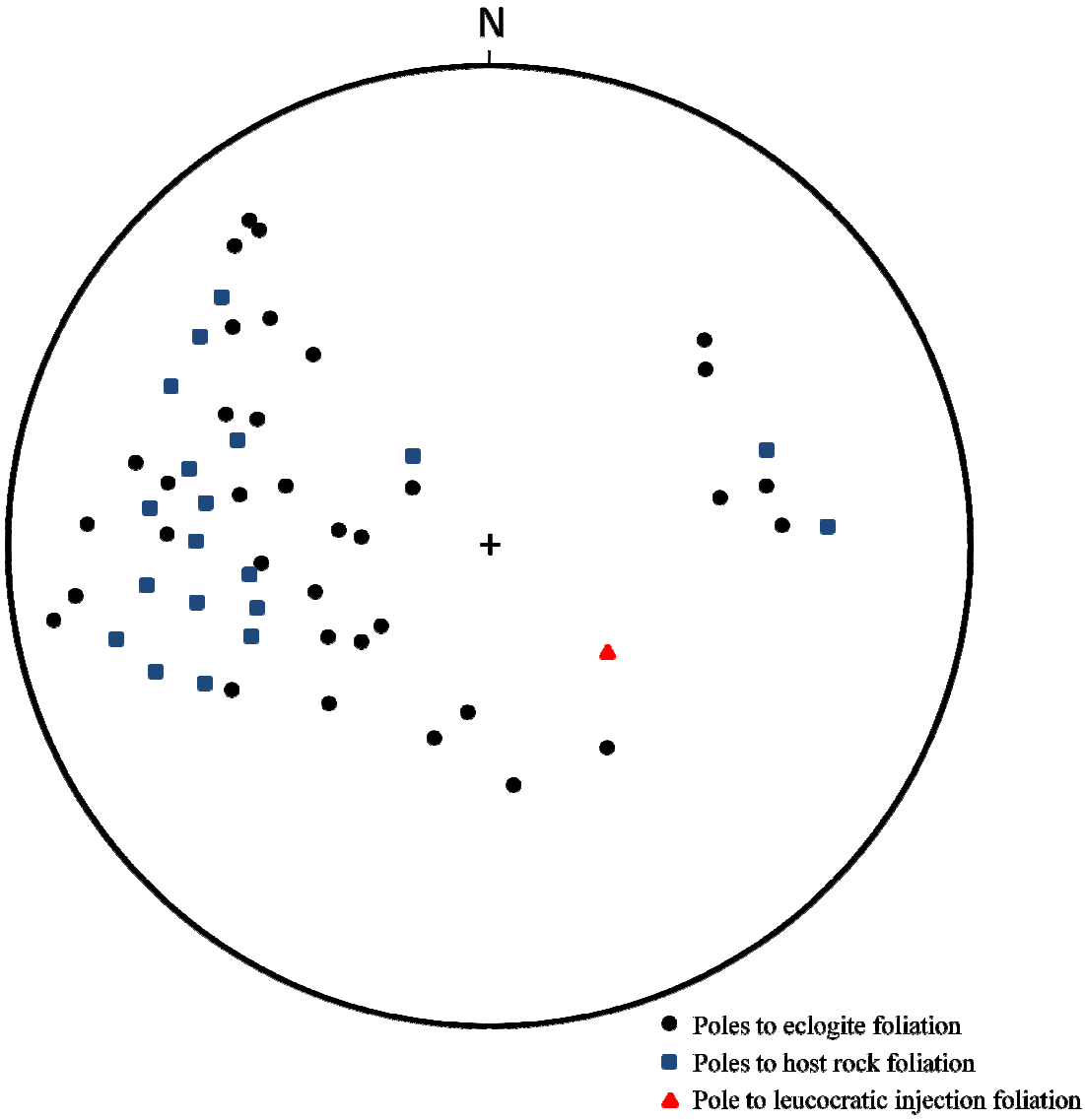

Figure 76: Lower-hemisphere stereographic projection of poles to foliation in retro-eclogite, anorthositic country rocks, and anorthositic and monzo-dioritic injections. Data are clustered mostly in the western and northwestern quadrants, and to a lesser extent in the northeastern quadrant. N = 55.

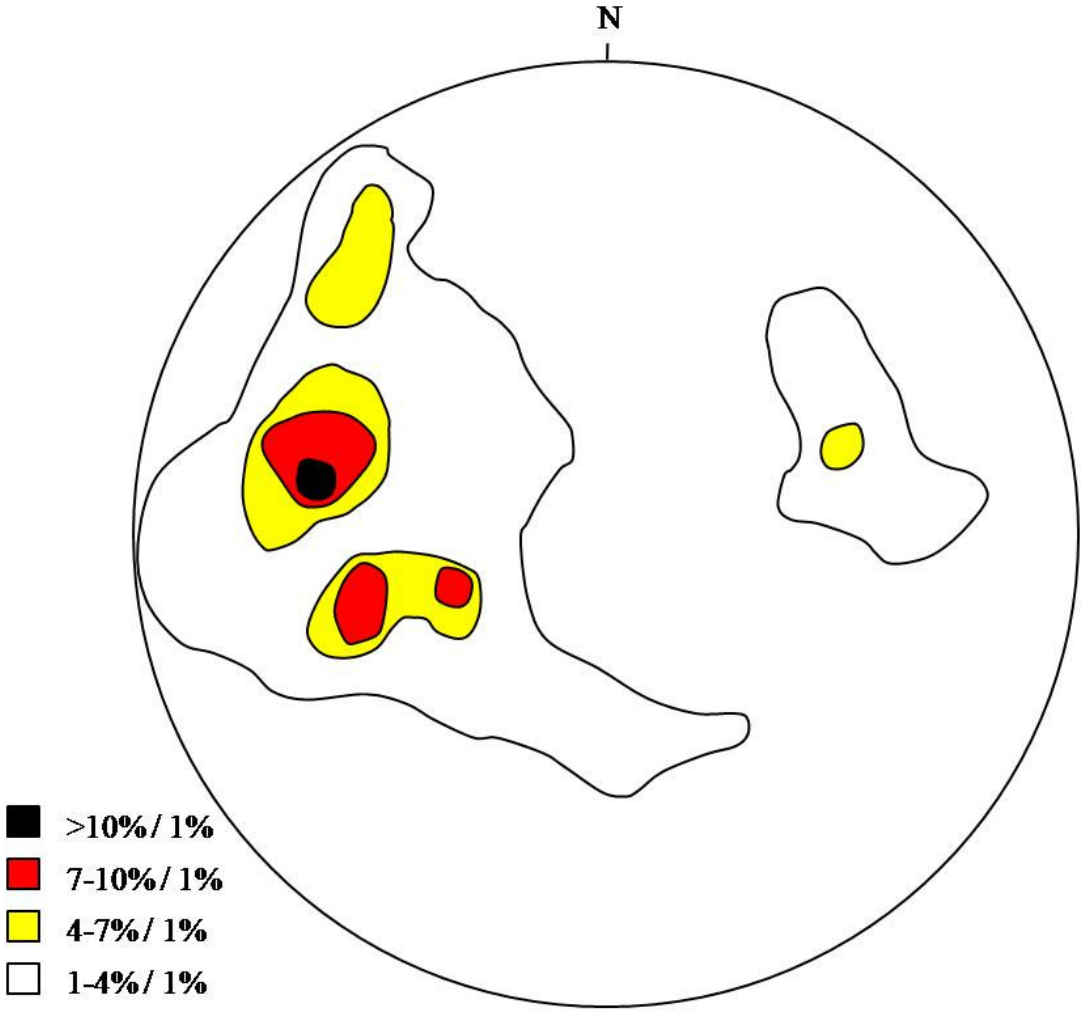

Figure 77: Lower-hemisphere contour diagram of foliation data in Figure 76. Point maximum is located at N79°W, 38°, which indicates an average foliation plane at N12°E, 44°SE. Legend denotes measurement density per 1 % area. N = 55.

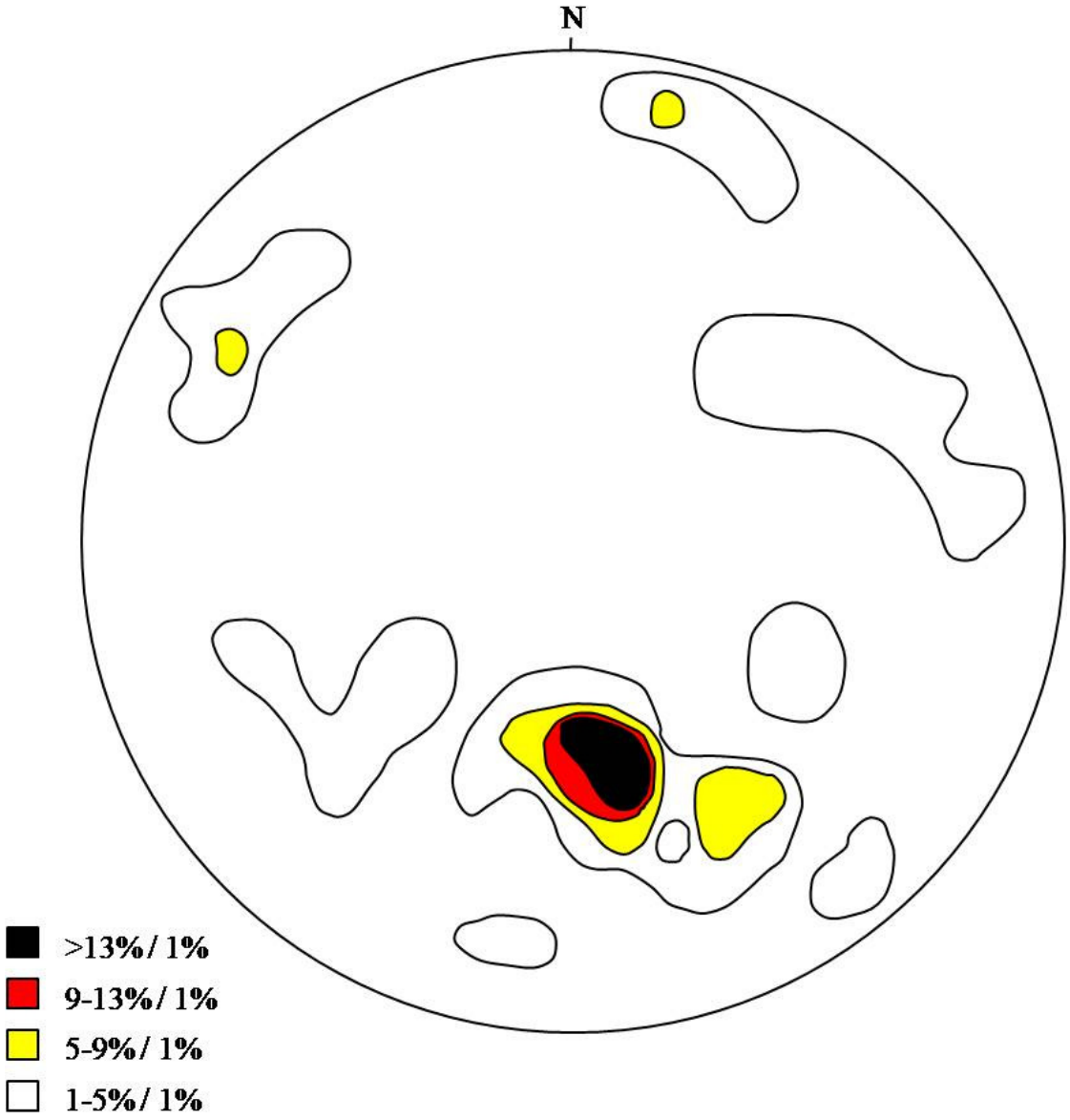

Figure 78: Lower-hemisphere stereographic projection of contoured elongation lineations in retro-eclogite at the Storvatnet locality. The maximum is located at S05°E, 45°. Legend denotes measurement density per 1 % area. N = 28.

Figure 79: Tops-northeast, plastic shear in eclogite observed at Storvatnet (location B on Figure 60). Movement sense is left-lateral with a minor reverse component. View is to the east. Note fabric swept up from the shear to the upper left. White blebs in this fabric are elongated plagioclase clusters. Hammer head is ~10 cm wide.

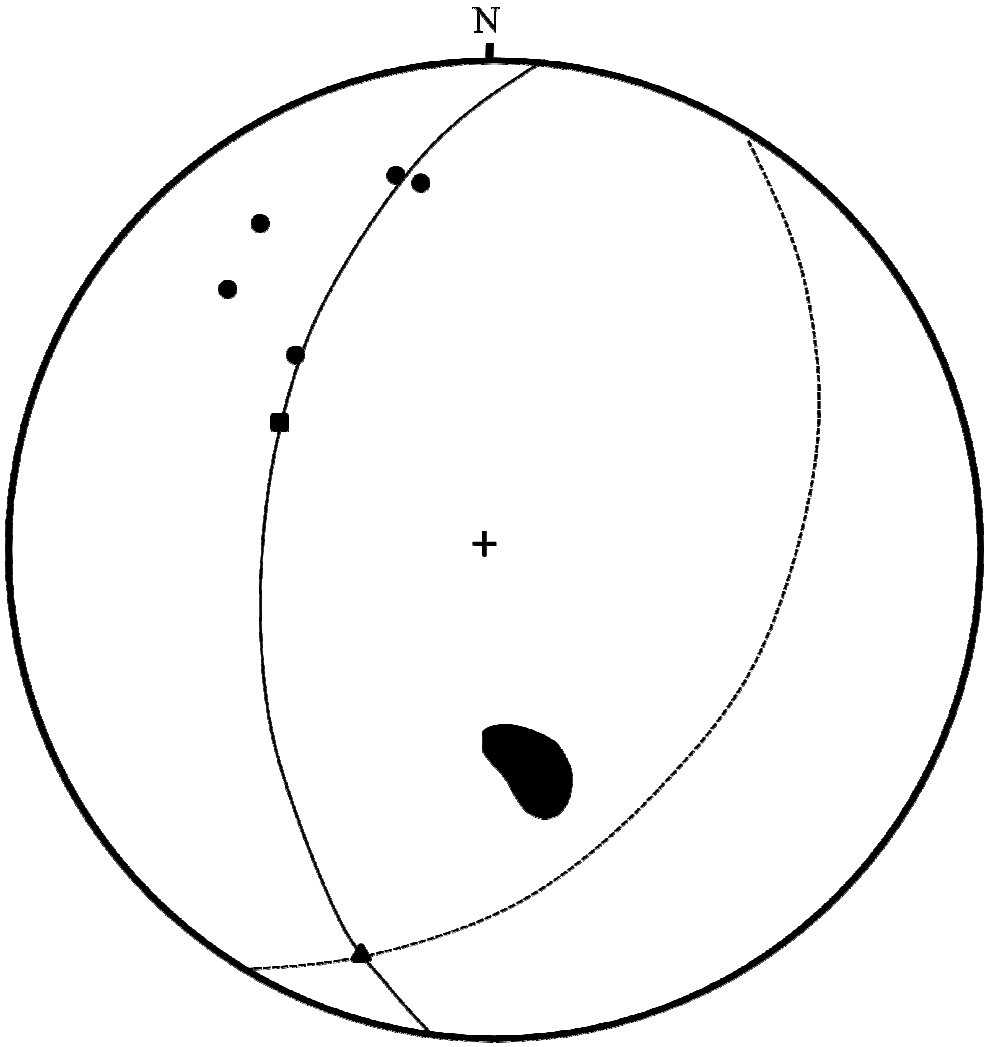

Figure 80: Lower-hemisphere stereographic reconstruction for the slip line at the shear zone observed at location B on Figure 60 (see text). The slip line is oriented S16°W, 13°, which generally agrees with the measured elongation lineations.

Three paired S-C planes, defined by plagioclase ribbons in retro-eclogite, were measured at location C on Figure 60. Slip lines geometrically constrained from these S-C planes are oriented S77°E, 12°, N77°E, 14°, and N90°E, 14°, indicating predominantly right-lateral strike-slip movement with a minor normal component (Figure 81).

The geometrically constrained slip lines at location C (Figure 60) differ from the main concentration of measured elongation lineations. This might reflect that the retro-eclogite pods at Storvatnet are competent bodies that have been independently rotated, similar to those at the Myrland eclogite locality. Storvatnet lacks a single pervasive, encapsulating shear zone such as the Myrland shear zone, but the former clearly is cut by individual shear zones that are similar in scale and appearance to those at Nusfjord. The C-planes depicted in Figures 80 and 81 are compatible with the interpretation that they formed as conjugate shears. Stereographic reconstruction using conjugate C-planes with σ_1 as the acute bisectrix, σ_2 as the intersection of the C-planes, and σ_3 as the obtuse bisectrix yields principal stress directions for σ_1, σ_2, and σ_3 of N22°W, 01°, N69°E, 28°, and S68°W, 60°, respectively. Rocks in the Storvatnet area, thus, were subjected to principal stress (σ_1) oriented northwest/southeast, resulting in coaxial shear along shallowly to moderately plunging, south-southwest and east oriented slip lines (Figure 82).

Blocks of mylonitized anorthosite containing isoclinal folds of the mylonitic foliation were observed at several locations between 200 m and 800 m to the south of the eclogite locality at Storvatnet (Figure 83). These blocks are >80% plagioclase with the remainder comprising sheared ribbons of mafic minerals. No garnet or other phases

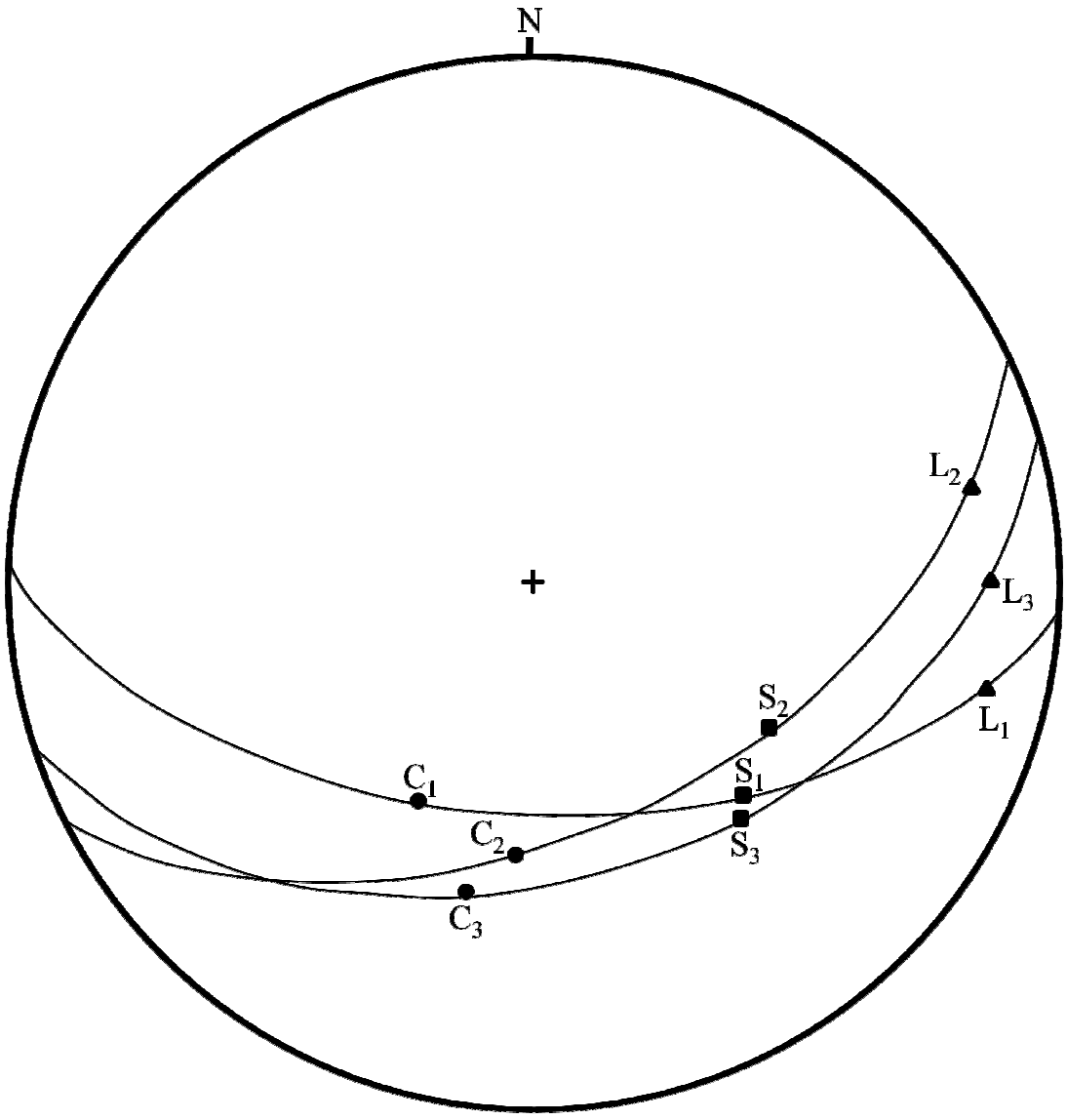

Figure 81: Lower-hemisphere stereographic reconstruction of slip lines from three paired S-C planes measured at location C on Figure 60. Slip lines are oriented S77°E, 12°, N77°E, 14°, and N90°E, 14°.

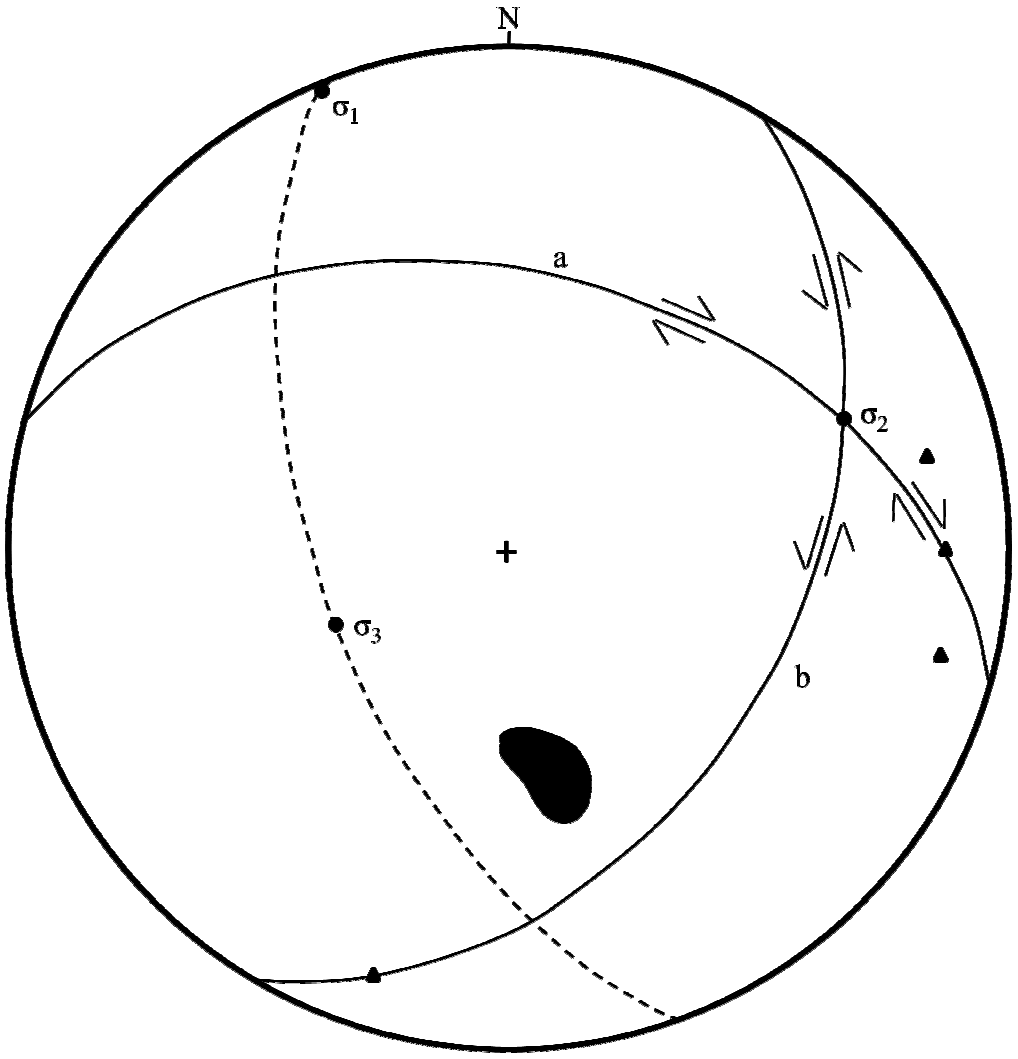

Figure 82: Lower-hemisphere stereographic reconstruction of principal stress axes based on conjugate shear fracture criteria. Orientations for principal stress axes are: σ_1 = N22°W, 01°; σ_2 = N69°E, 28°; and σ_3 = S68°W, 60°. Elongation lineations in retro-eclogite from Figure 78 and slip lines determined in Figures 80 and 81 are also presented for comparison. Arrows indicate relative movement sense. (a) right-lateral strike-slip movement with minor normal component. (b) left-lateral strike-slip movement with minor reverse component.

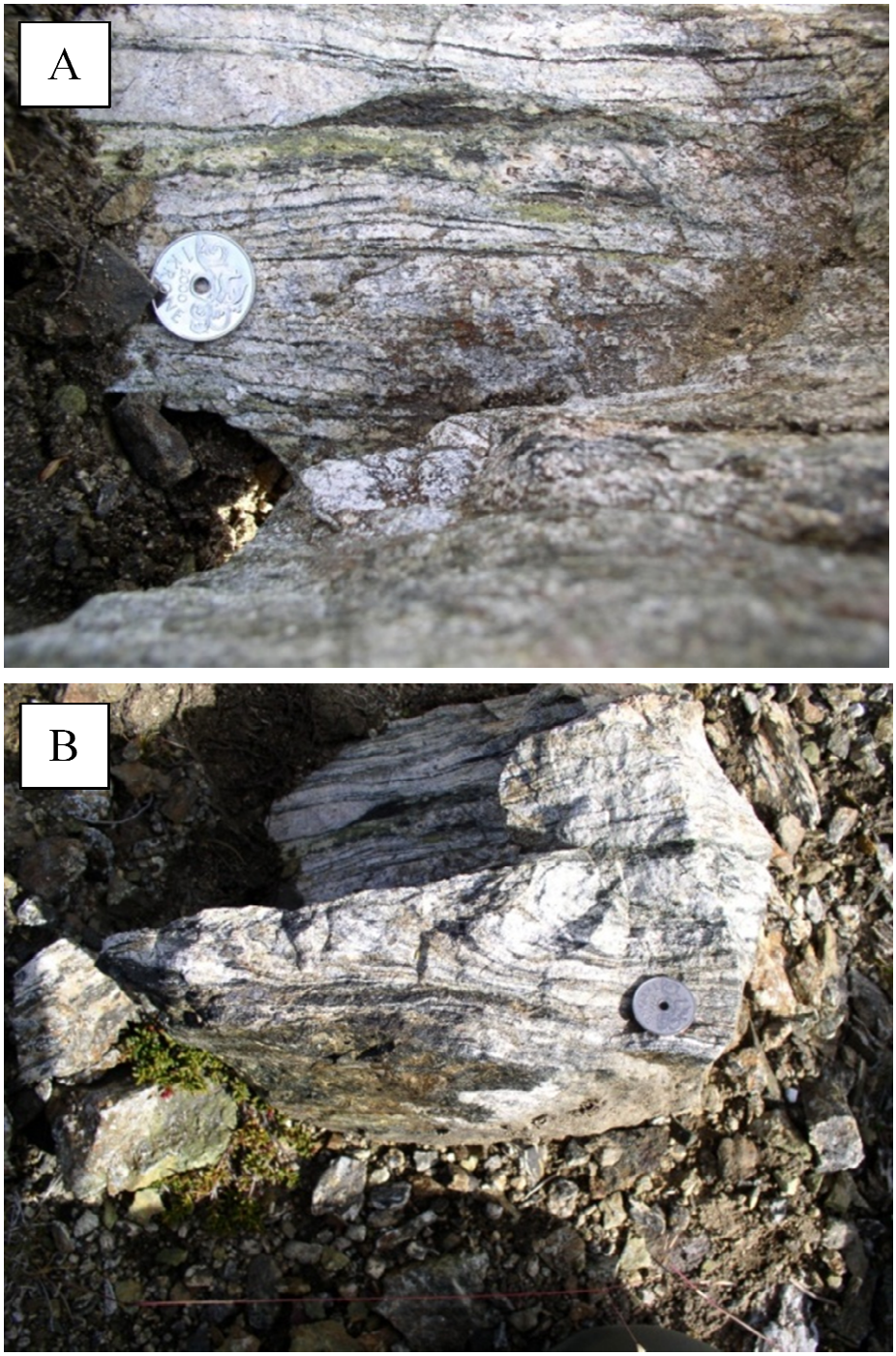

Figure 83: Strongly mylonitized and folded anorthosite in float blocks found at the southeastern corner of the Storvatnet eclogite locality depicted in Figure 60. Folds are defined by mylonitic foliation. Coins are ~2 cm in diameter. A) Ultramylonite with sheath fold geometries. B) Tight to isoclinal, intrafolial folds.

indicative of eclogitization were observed. These blocks could have been derived from the southern extension of the shear zone observed at the Storvatnet retro-eclogite locality.

Brittle fractures are conspicuous structures in Storvatnet country rock outcrops (Figure 84), but were not observed in retro-eclogite pods. Weathering clearly accentuates these structures. Striae or other features that might provide evidence for shearing were not observed on the surfaces of the fracture planes; they all appear to be simple Mode I opening joints (McKenzie and Brune, 1972; Sibson, 1975). Vein fillings in the immediate area of the Storvatnet eclogite area were not observed. Perhaps this was due to poor nature of the exposure because abundant epidote-filled fractures were observed within a 1 km radius to the east and northeast. Fractures are oriented in all directions, but the dominant set dips moderately to the southeast (Figure 85). These opening-type fractures are interpreted as pressure-release joints due to erosional unroofing.

Interpretations and conclusions from the Storvatnet investigation

Deformation in the Storvatnet locality was accommodated by plastic shearing of anorthosite around the more competent eclogite pods in a manner similar to boudin formation. Strain was accommodated within eclogite mainly by dynamic recrystallization of plagioclase, documenting that this was the weak phase controlling plastic deformation. The feldspar brittle/ductile transition is known to occur at ~500 °C in the presence of water (Gapais, 1989). Since eclogitization in rocks at Flakstadøy requires the addition of fluids, it follows that plastic deformation would occur in the surrounding anorthosite as well as eclogite-hosted plagioclase. The Storvatnet eclogite

Figure 84: Brittle structures at Storvatnet most likely are pressure-release joints. Three sets, representative of dominant brittle sets in this area, are visible here. View is to the east. Hammer is ~35 cm long. Set (1) Moderately inclined to the right of the photo. This is the dominant set in the Storvatnet area, corresponding to the point maximum shown in the northwestern quadrant of Figure 85. Set (2) Moderately inclined to the left of the photo. Set (3) Sub-horizontally oriented. The orientation of sets 2 and 3 is variable across the mapped area resulting in poles to fractures being spread across all areas except the southeast quadrant of Figure 85.

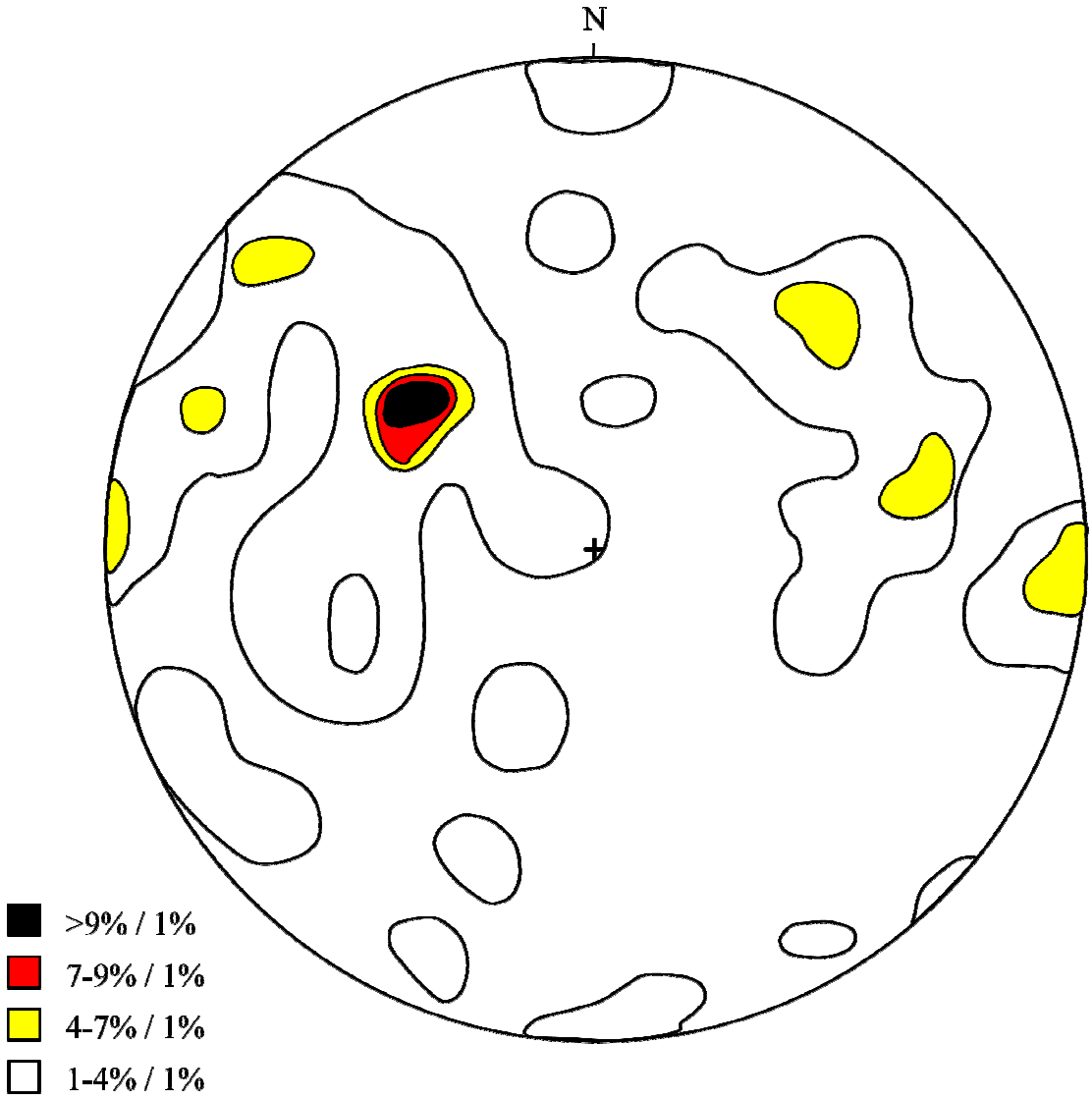

Figure 85: Lower-hemisphere contour diagram of poles to brittle fractures. A point maximum is located at N52°W 50°, indicating that the dominant brittle fracture set is oriented N38°E, 40°SE. Subordinate fracture sets loosely congregate in the northwest and northeast quadrants. Legend denotes measurement density per 1 % area. N = 63.

locality, thus, appears to be something of a poorly exposed and preserved analogue to the Myrland eclogite-lens occurrence. Individual shear zones, however, indicate similarities with Nusfjord eclogites as well.

Garnet, and to a lesser extent omphacite, were the load-bearing phases during deformation of the lower crustal rocks exposed at Storvatnet (Austrheim et al., 1996, Trepmann and Stockhert, 2002). Na-bearing pyroxene is significantly weaker than Na-free pyroxene (Zhang et al., 2006), such as common granulite-facies pyroxenes (hypersthene), and is therefore not expected to be resistant to crystal-plastic deformation. Omphacite is more chemically degraded than garnet in Storvatnet retro-eclogites, implying reaction softening of the former, yet also survived as porphyroclasts in some rocks.

Petrological observations from Storvatnet allow inferences to be made regarding the relative timing of eclogitization and deformation. Dynamic flow banding, defined by ribbons of dynamically recrystallized plagioclase and amphibole, wraps around earlier-formed omphacite grain cores (Figures 63 and 64) that are not internally deformed. Likewise, dynamically recrystallized plagioclase ribbons wrap around undeformed garnet (Figure 66). This implies that eclogite-facies conditions existed prior to commencement of dynamic recrystallization of plagioclase and amphibole. Omphacite is known to deform plastically at temperatures as low as 550 °C (Buatier et al., 1991). Dynamically recrystallized porphyroclast tails and core-mantle structures composed of amphibole that emanate from relict omphacite grains imply that shearing took place under upper amphibolite-facies conditions.

Several observations imply that the retro-eclogites at Storvatnet were not significantly reoriented during exhumation. Symplectite breakdown of omphacite, which is abundant in Storvatnet retro-eclogites, implies relatively rapid uplift. 'Reef' type garnet coronas imply static conditions for at least the final phase of amphibolite-facies retrogression. No evidence for wholesale rotation of individual lenses was detected. The preserved near-vertical orientation of σ_3 determined for the shear zones is consistent with unmolested vertical uplift and, therefore, is interpreted to represent overburden pressure.

If the retro-eclogites at Storvatnet are not appreciably reoriented then the pattern for lower-crustal deformation appears to be strike-slip with a general sub-horizontal, north-northwest/south-southeast trend for σ_1. This orientation for σ_1 is compatible with the well established orientation for Caledonian thrusting on the mainland. Subsequent exhumation is interpreted to have followed a near-vertical path although rotation about a vertical axis is possible. Monzodioritic veins and sweat-outs are interpreted to have been derived from decompression melting of the eclogite during exhumation. Finally, as these crustal rocks approached the Earth's surface, they were fractured and jointed by the release of overburden pressure.

DISCUSSION AND CONCLUSIONS

The three retro-eclogite localities on Flakstadøy discussed herein each occurs in different intrusive host units and can be categorized into two structurally controlled styles that are rheological inverses of one another, eclogite lenses and eclogite shears. Lenses of eclogite at Myrland and Storvatnet were competent bodies relative to their softer host rocks within which they were 'tumbled' during shearing. Eclogite in shear zones at Nusfjord, on the other hand, require that eclogite was the weak unit, serving as the locus of crystal-plastic deformation. Some retro-eclogite lenses at Storvatnet are strongly sheared, similar to Nusfjord retro-eclogites, but most are only weakly foliated, as at Myrland. Myrland and Nusfjord eclogites, therefore, function as end members of a competent-to-weak continuum, with Storvatnet eclogites located between them. The proximity of these different deformational styles suggests factors other than lithology alone are responsible for shear zone formation in the lower crust.

Although previous workers referred to the Myrland and Storvatnet occurrences as 'eclogite shear zones' (Markl and Bucher, 1997), the present investigation did not reveal any evidence documenting that shearing actually occurred under eclogite-facies conditions. Rather, these eclogites first formed from gabbroic or troctolitic enclaves within monzodioritic and anorthositic host rocks and then later the eclogites were stretched into lenses or pods by amphibolite-facies shear zones that overprinted and largely obliterated the eclogite-facies assemblages. Such eclogite occurrences are not

unusual and are reported in many of Earth's eroded mountain cores. Examples are from the Greenland (Brueckner et al., 1998; Buchanan et al., 2007) and Norwegian Caledonides (Griffin and Brueckner, 1980, 1985; Griffin et al., 1985), the Alps (Droop et al., 1990), and the southern Appalachians (Adams et al., 1995; Stewart and Miller, 2001).

The Nusfjord locality, on the other hand, contains true eclogite-facies shear zones in the strictest sense, and these are very rare occurrences. At Nusfjord, granulite-facies assemblages in the host gabbronorite were transformed into eclogite-facies assemblages only within the shear zones. Crystal-plastic deformation of garnet implies deformation at temperatures greater than 700 °C (Storey and Prior, 2005), consistent with the temperature estimates for the peak of eclogite-facies metamorphism (Markl and Bucher, 1997). The breakdown of hypersthene (+ plagioclase) to omphacite in the shoulders of the shear zones is a signature of fluid-mediated eclogitization reported for the type eclogite shear zones in the Bergen Arcs (Austrheim and Griffin, 1985; Austrheim, 1987; Boundy et al., 1992). Field relations of eclogite-facies pseudotachylites associated with the Nusfjord shear zones also require simple shearing under eclogite-facies conditions (Steltenpohl et al., 2006). Amphibole σ-clast tails extending from retrograded omphacite grains indicate that strains resulting in the Nusfjord eclogite shears continued under upper amphibolite-facies conditions as the rocks began their initial ascent to the Earth's surface.

Despite the rheological differences between these eclogite occurrences, several lines of reasoning indicate that they are genetically related to one another. First, all three retro-eclogite occurrences discussed herein strike north-south to northwest-southeast and display predominantly strike-slip motion. The σ_2 axis for eclogites from Nusfjord and

Storvatnet are near-parallel; σ_1 for both occurrences are roughly orthogonal. Although principal stress axes were not determined for the shear zone at the Myrland locality, non-coaxial shear and shallowly to moderately southeast-plunging elongation lineations imply northwest-southeast oriented σ_1 within a similar-striking plane and a vertical σ_2. Second, the structural styles and fluid-mediated development of the Flakstadøy eclogites are similar to those for Caledonian eclogites in the Bergen Arcs (Austrheim, 1987; Boundy et al., 1992) and the Western Gneiss Region (Anderson and Jamtveit, 1990). Third, U-Pb geochronology reported herein supports that the eclogites are Caledonian features rather than Proterozoic ones as was previously thought (Wade, 1985; Kullerud, 1995, 1996; Markl and Bucher, 1997; Kullerud and Erambert, 1999; Kullerud et al., 2001). Despite their similarities, however, no evidence was found to suggest that these three investigated eclogite occurrences are physically connectible.

In summary, tectonic development of the eclogites began as deep-crustal, granulite-facies, anhydrous rocks hosting mafic enclaves and dikes were subducted at ~478 Ma during an early phase of Caledonian Orogeny. Eclogitization is interpreted to have occurred simultaneously at the three localities discussed in this report. Conditions for eclogitization of rocks at Flakstadøy are estimated at 680°-780 °C and 11-15 kbar (Markl and Bucher, 1997). During subduction, aqueous fluids infiltrated brittle fractures at Nusfjord and allowed eclogitization and crystal-plastic deformation to proceed (Kullerud, 1996; Markl and Bucher, 1997; Kullerud and Erambert, 1999; Kullerud et al., 2001; Steltenpohl et al., 2006). Fluids are necessary for eclogitization of mafic rocks at Myrland and Storvatnet as well (Markl and Bucher, 1997), but the method of infiltration

was not detected in the present study due to the strong structural and metamorphic overprint. Thrust-emplacement of nearby Leknes Group rocks between 469 and 461 Ma (Corfu, 2004a) implies continued subduction (i.e., residence in the lower to lower-mid crust) for a minimum 17 m.y.

The timing of uplift initiation and passage into the middle crust for Flakstadøy eclogites is unclear. Isothermal decompression of the eclogites from 15-11 kbar took place under isothermal conditions at ~700 °C (Markl and Bucher, 1997), representing the retrogressive transition from eclogite- to amphibolite-facies. Metasomatic mobilization of the eclogites likely occurred at this point, forming the monzodioritic and anorthositic sweat-out veins at Storvatnet. The eclogites passed through 500 °C at 433 Ma, based on $^{40}Ar/^{39}Ar$ dating of hornblende from a retrograde eclogite at Nusfjord (Steltenpohl et al., 2003). Since plasticity in feldspar sets in at approximately 500 °C (Gapais, 1989), this date places a lower constraint on amphibolite-facies shear zone formation and indicates an average cooling rate of ~4°-6 °C/m.y. However, isothermal decompression from 15 to 11 kbar, corresponding to roughly 11 km of continental crust, must have occurred relatively rapidly in order to accommodate a temperature drop of ≥ 200 °C in 45 m.y. This is supported by the observations of omphacite breaking down via symplectite formation and also by formation of exsolution lamellae, which are indicative of rapid and slow exhumation, respectively (Markl and Bucher, 1997; Anderson and Moecher, 2007). It is probable that the amphibolite-facies shear zones on Flakstadøy formed during or soon after this period of rapid uplift, which is compatible with delamination of buoyant

crust during continued Caledonian contraction. This hypothesis is further supported by stress orientations at the Storvatnet locality, where contraction continued during retrogression (i.e., after subduction ceased and uplift had begun).

The Lofoten block is known to have experienced a pulse of uplift during the Early Devonian (~390-405 Ma: Coker et al., 1995; Steltenpohl et al., 2004). Final uplift of the eclogites into the upper crust is recorded by $^{40}Ar/^{39}Ar$ age dates for muscovites from throughout Lofoten that gradually young from northeast to southwest from ~360 Ma on Vestvågøy (Klein, 1997) to ~271 Ma on Værøy (Mooney, 1997; see Figure 2 in Steltenpohl et al., 2004). This systematic age distribution implies that the eclogites began passing through the ~350 °C isotherm during Early Carboniferous and then were rapidly uplifted during the Early Permian pulse documented by Steltenpohl et al. (2004). The Flakstadøy eclogites, therefore, resided in the middle- to lower-upper crust for approximately 101 to 190 m.y. (following the 461 Ma thrust-emplacement and amphibolite-facies metamorphism of the Leknes Group [Corfu, 2004a; Key et al., 2007]). This long period residence, which post-dates phenomenal rates of rapid Devonian extension throughout western Norway, facilitated the high degree of retrogression relative to eclogites from the Bergen Arcs and the Western Gneiss Region.

REFERENCES

Adams, M., Stewart, K., Trupe, C., and Willard, R., 1995, Tectonic significance of high-pressure metamorphic rocks and dextral strike-slip faulting along the Taconic suture, in Hibbard, J., van Staal, C., and Cawood, P., eds., Current Perspectives in the Appalachian-Caledonian Orogen: Geological Association of Canada, Special paper 41, p. 21-42.

Anderson, T., and Jamtveit, B., 1990, Uplift of deep crust during orogenic extensional collapse: A model based on field studies in the Sogn-Sunnfjord region of western Norway: Tectonics, v. 9, p. 1097-1112.

Anderson, E., and Moecher, D., 1997, Omphacite breakdown reactions and relation to eclogite exhumation rates: Contributions to Mineralogy and Petrology, v. 154, p. 253-277.

Austrheim, H., 1987, Eclogitisation of lower crustal granulites by fluid migration through shear zones: Earth and Planetary Sciences Letters, v. 81, p. 221-232.

Austrheim, H., Erambert, M., and Boundy, T., 1996, Garnets recording deep crustal earthquakes: Earth and Planetary Science Letters, v. 139, p. 223-238.

Austrheim, H., and Griffin, 1985, Shear deformation and eclogite formation within granulite-facies anorthosites of the Bergen Arcs, western Norway: Chemical Geology, v. 50, p. 267-281.

Bartley, J. M., 1982a, Limited basement involvement in Caledonian deformation, Hinnøy, North Norway, and tectonic implications: Tectonophysics, v. 83, p. 185-203.

Bartley, J. M., 1984, Caledonian structural geology and tectonics of east Hinnøy, north Norway: Norsk Geologisk Tidsskrift, v. 396, p. 1-24.

Berthé, D., Choukroune, P., and Jegouzo, P., 1979, Orthogneiss, mylonite and non coaxial deformation of granites: the example of the South Armorican Shear Zone: Journal of Structural Geology, v. 1, p. 31-42.

Biermann, C., and van Roermund, H., 1983, Defect structures in naturally deformed clinoamphiboles – a TEM study: Tectonophysics, v. 95, p. 267-278.

Blumenfeld, P., and Bouchez, J. L., 1988, Shear sense criteria in granite and migmatite deformed in the magmatic and solid states: Journal of Structural Geology, v. 10, p. 361-372.

Boundy, T. M., Fountain, D., M., and Austrheim, H., 1992, Structural development and petrofabrics of eclogite facies shear zones, Bergen Arcs, western Norway: implications for deep crustal deformational processes: Journal of Metamorphic Geology, v. 10, p. 127-146.

Brueckner, H., Gilotti, J., and Nutman, A., 1998, Caledonian eclogite-facies metamorphism of Early Proterozoic protoliths from the north-east Greenland eclogite province: Contributions to Mineralogy and Petrology, v. 130, p. 103-120.

Brunel, M., 1986, Ductile thrusting in the Himalayas: shear sense criteria and stretching lineations: Tectonics, v. 5, p. 247-265.

Buatier, M., van Roermund, H., Drury, M., and Lardeaux, J., 1991, Deformation and recrystallization mechanisms in naturally deformed omphacites from the Sesia-Lanzo zone; geophysical consequences: Tectonophysics, v. 195, p. 11-27.

Buchanan, J., Augland, L., Steltenpohl, M., and Andresen, A., 2007, Structural and petrologic framework of a Caledonian eclogite terrane within southern Liverpool Land, east Greenland: Geological Society of America Abstracts with Programs, v. 39, p. 231.

Cao, S., Liu, J., and Hu, L., 2007, Micro-and submicrostructural evidence for high-temperature brittle-ductile transition deformation of hornblende: case study of high-grade mylonites from Diancangshan, western Yunnan: Science in China Series D: Earth Sciences, v. 50, p. 1459-1470.

Coker, J., Steltenpohl, M., Andresen, A., and Kunk, M., 1995, An $^{40}Ar/^{39}Ar$ thermochronology of the Ofoten-Troms region: Implications for terrane amalgamation and extensional collapse of the northern Scandinavian Caledonides: Tectonics, v. 14, p. 435-447.

Corfu, F., 2004a, U-Pb geochronology of the Leknes Group: an exotic Early Caledonian metasedimentary assemblage stranded on Lofoten basement, northern Norway: Journal of the Geological Society of London, v. 161, p. 619-627.

Corfu, F., 2004b, U-Pb Age, setting and tectonic significance of the anorthosite-mangerite-charnockite-granite suite, Lofoten-Vesterålen, Norway: Journal of Petrology, v. 45, p. 1799-1819.

Corfu, F., and Noble, S. R., 1992, Genesis of the southern Abitibi greenstone belt, Superior Province, Canada: evidence from zircon Hf isotope analyses using a single filament technique: Geochimica et Cosmochimica Acta, v. 56, p. 2081-2097.

Corfu, F., and Stone, D., 1998, The significance of titanite and apatite U-Pb ages: constraints for the port-magmatic thermal-hydrothermal evolution of a batholithic complex, Berens River area, northwestern Superior Province: Geochimica et Cosmochimica Acta, v. 62, p. 2979-2995.

Cumbest, R., Drury, M., van Roermund, H., and Simpson, C., 1989, Dynamic recrystallization and chemical evolution of clinoamphiboles from Senja, Norway: Contributions to Mineralogy and Petrology, v. 101, p. 339-349.

Droop, G., Lombado, B., and Pognate, U., 1990, Formation and distribution of eclogite facies rocks in the Alps: in Carswell, D., ed., Eclogite facies rocks, Blackie, Glasgow, p. 225-229.

Flaat, K., 1998, Element mobilization and fluid-rock interactions during the formation of lower-crustal shear zones at Flakstadøy, Lofoten [Cand. Scient. Thesis]: Tromsø, Norway, University of Tromsø.

Gapais, D., 1989, Shear structures within deformed granites: mechanical and thermal indicators: Geology, v. 17, p. 1144-1147.

Grant, J., 1986, The isocon diagram - a simple solution to Gresens' equation for metasomatic alteration: Economic Geology, v. 81, p. 1976-1982.

Griffin, W. and Brueckner, H., 1980, Caledonian Sm-Nd ages and a crustal origin of Norwegian eclogites: Chemical Geology, v. 285, p. 315-321.

Griffin W., and Brueckner, H., 1985, REE, Rb-Sr and Sm-Nd studies of Norwegian eclogites: Chemical Geology, v. 52, p. 249-271.

Griffin, W. L., and Taylor, P. N., 1978, Geology and age relations on Værøy, Lofoten, north Norway: Norges Geologiske Undersøkesle, v. 338, p. 71-82.

Griffin, W., Austrheim, H., Brastad, K., Bryhni, I., Krill, A., Krogh, E., Mørk, M., Qvale, H., and Tørudbakken, B., 1985, High-pressure metamorphism in the Scandinavian Caledonides: in Gee, D., and Sturt, B., eds., The Caledonide Orogen-Scandinavia and related areas, J. Wiley & Sons, Chichester, p. 783-801.

Griffin, W. L., Taylor, P. N., Hakkinen, J. W., Heier, K. S., Iden, I. K., Krogh, E. J., Malm, O., Olsen, K. I., Ormassen, D. E., and Tveten, E., 1978, Archean and Proterozoic crustal evolution of Lofoten-Vesterålen, north Norway: Journal of the Geological Society of London, v. 135, p. 629-647.

Hakkinen, J. W., 1977, Structural geology and metamorphic history of western Hinnøy and adjacent parts of eastern Hinnøy, North Norway [Ph.D. Thesis]: Houston, Texas, Rice University, 161 p.

Hodges, K.V., Bartley, J.M., and Burchfiel, B.C., 1982, Structural evolution of an A-type subduction zone, Lofoten Rombak area, northern Scandinavian Caledonides: Tectonics, v. 1, p. 441–462.

Key, T., Steltenpohl, M., Hames, W., Ball, J., and Andresen, A., 2007, Reconciling metamorphic timing between Precambrian basement and Caledonian

allochthonous cover in the Lofoten Terrane, north Norway: Geological Society of America Abstracts with Programs, v. 39, p. 229.

Klein, A. C., 1997, Geology of the Leknes Group and underlying basement in west-central Vestvågøy, north Norway: M.S. Thesis, Auburn University, Auburn, Alabama, 171 p.

Klein, A. C., Steltenpohl, M. G., Hames, W. E., and Andresen, A., 1999, Ductile and brittle extension in the southern Lofoten archipelago, north Norway: implications for differences in tectonic style along an ancient collisional margin: American Journal of Science, v. 299, p. 69-89.

Krogh, T. E., 1973, A low contamination method for hydrothermal decomposition of zircon and extraction of U and Pb for isotopic age determinations: Geochimica et Cosmochimica Acta, v. 37, p. 485-494.

Krogh, T. E., 1982, Improved accuracy of U-Pb zircon ages by the creation of more concordant systems using an air abrasion technique: Geochimica et Cosmochimica Acta, v. 46, p. 637-649.

Kullerud, K., 1992, Metamorphism and fluid-rock interaction in shear zones within the Flakstadøy basic complex, Lofoten, northern Norway [Unpublished Ph.D. dissertation]: Oslo, Norway, University of Oslo, 151 p.

Kullerud, K., 1995, Chlorine, titanium, and barium-rich biotites: factors controlling biotite composition and implications for garnet-biotite geothermometry: Contributions to Mineralogy and Petrology, v. 120, p. 42-59.

Kullerud, K., 1996, Chlorine-rich amphiboles: interplay between amphibole composition and an evolving fluid: European Journal of Mineralogy, v. 8, p. 355-370.

Kullerud, K., and Erambert, M., 1999, Cl-scapolite, Cl-amphibole, and plagioclase equilibria in ductile shear zones at Nusfjord, Lofoten, Norway: implications for fluid compositional evolution during fluid-mineral interaction in the deep crust: Geochimica et Cosmochimica Acta, v. 63, p. 3829-3844.

Kullerud, K., Flaat, K., and Davidsen, B., 2001, High-pressure fluid-rock reactions involving Cl-bearing fluids in lower-crustal ductile shear zones of the Flakstadøy Basic Complex, Lofoten, Norway: Journal of Petrology, v. 42, p. 1349-1372.

Leake, B. E., 1978, Nomenclature of amphiboles: American Mineralogist, v. 63, p. 1023-1052.

LeMaitre, R. W., ed., 1989, A Classification of Igneous Rocks and a Glossary of Terms: Blackwell Publishers, Oxford, England.

Ludwig, K. R., 1999, Using Isoplot/Ex Version 2.01, A Geochronological Toolkit for Microsoft Excel: Berkeley Geochronology Center Special Publication 1a, 47 p.

Markl, G., and Bucher, K., 1997, Proterozoic eclogites from the Lofoten Islands, northern Norway: Lithos, v. 42, p. 15–35.

Markl, G., and Bucher, K., 1998, Composition of fluids in the lower crust inferred from metamorphic salt in lower crustal rocks: Nature, v. 391, p. 781–783.

Markl, G., Frost, B.R. and Bucher, K. 1998: The origin of anorthosites and related rocks from the Lofoten Islands, northern Norway: I. Calculation of parental liquid compositions for anorthosites: Journal of Petrology, v. 39, *p.* 1425-1452.

Markl, G., Musashi, M., and Bucher, K., 1997, Chlorine stable isotope composition of granulites from Lofoten, Norway: Implications for the Cl isotopic composition and for the source of Cl enrichment in the lower crust: Earth and Planetary Science Letters, v. 150, p. 95-102.

McKenzie, D., and Brune, J. N., 1972, Melting on fault planes during large earthquakes: Royal Astronomical Society Geophysical Journal, v. 29, p. 65-78.

Mooney, L.J., 1997, Structural and lithologic investigation of Værøy, Lofoten, north Norway and regional study of Caledonian metamorphism: M.S. thesis, Auburn University, Auburn, Alabama, 108 p.

Moore, A. C., 1970, Descriptive terms for the textures of rocks in granulite facies terranes: Lithos, v. 3, p. 123-127.

Olesen, O., Torsvik, T. H., Tveten, E., Zwann, K. B., Loseth, H., and Henningsen, T., 1997, Basement structure of the continental margin in the Lofoten-Lopphavet area, northern Norway: constraints from potential field data, on-land structural mapping and palaeomagnetic data: Norsk Geologisk Tidsskrift, v. 77, p. 15-30.

Passchier, C. W., and Trouw, R. A. J., 1998, Microtectonics: Springer-Verlag Publishers, Berlin, Germany, 289 p.

Ramsay, J. G., 1962, Interference patterns produced by the superposition of folds of similar types: Journal of Geology, v. 70, p. 466-481.

Ramsay, R. G., and Allison, I., 1979, Structural analysis of shear zones in an alpinised Hycernian granite (Maggia Lappen, Pennine zone, central Alps): Schweizerische mineralogische und petrographische Mitteilurgen, v. 59, p. 251-279.

Ramsay, R., and Graham, R., 1970, Strain variation in shear belts: Canadian Journal of Earth Sciences, v. 7, p. 786-813.

Rehnström, E., 2003. Tectonic implications of geochronological and petrological from the Tielma Magmatic Complex, northern Swedish Caledonides: Norwegian Journal of Geology, v. 83, p. 243-257.

Romey, W., 1971, Basic igneous complex, mangerite, and high grade gneisses of Flakstadøy, Lofoten, Norway: I. Field relations and speculations on origins: Norsk Geologisk Tidsskrift, v. 51, p. 33-61.

Rubatto, D., Gebauer, D., and Compagnoni, R., 1999, Dating of eclogite-facies zircons: the age of Alpine metamorphism in the Sesia-Lanzo Zone (Western Alps): Earth and Planetary Science Letters, v. 167, p. 141-158.

Segall, P., and Simpson, C., 1986, Nucleation of ductile shear zones on dilatant fractures: Geology, v. 14, p. 56-59.

Sibson, R., 1975, Generation of pseudotachylite by ancient seismic faulting: Royal Astronomical Society Geophysical Journal, v.43, p. 775-794.

Siivola, J., and Schmid, R., 2007, A systematic nomenclature for metamorphic rocks: 12. List of mineral abbreviations. Recommendations by the IUGS Subcommission on the Systematics of Metamorphic Rocks. *Recommendations*, web version of 01.02.2007. Located at http://www.bgs.ac.uk/SCMR/docs/papers/paper_12.pdf.

Stacey, J., and Kramers, J., 1975, Approximation of terrestrial lead isotope evolution by a two-stage model: Earth and Planetary Science Letters, v. 34, p. 207-226.

Steltenpohl, M., Kassos, G., and Andresen, A., 2006, Retrograded eclogite-facies pseudotachylites as deep-crustal paleoseismic faults within continental basement of Lofoten, north Norway: Geosphere, v. 2, p. 61-72.

Steltenpohl, M., Hames, W.E., and Andresen, A., 2004, The Silurian to Permian history of a metamorphic core complex in Lofoten, northern Scandinavian Caledonides: Tectonics, v. 23, p. 1-23.

Steltenpohl, M., Hames, W., Andresen, A., Markl, G., 2003, A new Caledonian eclogite province in Norway and potential Laurentian (Taconic) and Baltic links: Geology, v. 31, p. 985-988.

Stewart, K., and Miller, B., 2001, The tectonic implications of 460 Ma eclogite along the Taconian suture in the eastern Blue Ridge of North Carolina: Geological Society of America Abstracts with Programs, v. 33, p. A-65.

Streckeisen, A. L., 1974, Classification and nomenclature of plutonic rocks: Recommendations of the IUGS Subcommittee on the systematics of igneous rocks: Geologische Rundschau, Internationale Zeitschrift fur Geologie, Stuttgart, v. 63, p. 773-785.

Storey, C. D., and Prior, D.J., 2005, Plastic deformation and recrystallization of garnet: a mechanism to facilitate diffusion creep: Journal of Petrology, v. 46, p. 2593-2613.

Talwani, M., and Eldholm, O., 1977, Evolution of the Norwegian-Greenland Sea: Bulletin of the Geological Society of America, v. 88, p. 969-999.

Trepman, C. A., and Stockhert, B., 2002, Cataclastic deformation of garnet: a record of synseismic loading and postseismic creep: Journal of Structural Geology, v. 24, p. 1845-1856.

Tull, J. F., 1977, Geology and structure of Vestvågøy, Lofoten, north Norway: Norges Geologiske Undersøkelse, v. 333, 59 p.

Tull, J.F., 1978, Geology and structure of Vestvågøy, Lofoten, north Norway: Norges Geologiske Undersøkelse, v. 42, 109 p.

Viskupic, K., Hodges, K. V., 2001, Monazite-xenotime thermochronometry; methodology and an example from the Nepalese Himalaya: Contributions to Mineralogy and Petrology, v. 141, 233-247.

Wade, S.J.R., 1985, Radiogenic isotope studies of crust-forming processes in the Lofoten-Vesterålen province of north Norway [Unpublished Ph.D. dissertation]: Oxford, England, Oxford University, 281 p.

Zhang, J., Green, H., Bozhilov, K., 2006, Rheology of omphacite at high temperature and pressure and significance of its lattice preferred orientations: Earth and Planetary Science Letters, v. 246, p. 432-443.